[redacted]

ORNL
MASTER COPY

[redacted]

ORNL-1658
Progress
17A

DECLASSIFIED

Per Letter Instructions Of
Tid-1148
E. Bonney
For: N. T. Bray, Supervisor
Laboratory Records Dept.
ORNL

LABORATORY RECORDS

Inv 56

HOMOGENEOUS REACTOR PROJECT

QUARTERLY PROGRESS REPORT

FOR PERIOD ENDING OCTOBER 31, 1953

CLASSIFICATION CANCELLED
DATE JUL 13 1979 (DOE Review Order)
R. S. Baker
DECLASSIFICATION OFFICER
OAK RIDGE NATIONAL LABORATORY
AUTHORITY DELEGATED BY ERDA 8-15-77

THIS DOCUMENT WAS PROPERLY DECLASSIFIED
AND IS EXEMPT FROM DOE 1979 REVIEW ORDER
PER DOE LETTER, 10-16-79, R.T. DUFF, OOC
P. S. BAKER, ORNL/CO J.S. 12/22/80
INITIALS DATE

OAK RIDGE NATIONAL LABORATORY
OPERATED BY
CARBIDE AND CARBON CHEMICALS COMPANY
A DIVISION OF UNION CARBIDE AND CARBON CORPORATION
UCC
POST OFFICE BOX P
OAK RIDGE, TENNESSEE

[redacted]

[redacted]

[redacted]

Copy 17A

ORNL-1658

[redacted] consists of 150 pages. [redacted]

Contract No. W-7405-eng-26

HOMOGENEOUS REACTOR PROJECT

QUARTERLY PROGRESS REPORT

For Period Ending October 31, 1953

Project Director – J. A. Swartout
Engineering – J. A. Lane
Chemistry – S. C. Lind, C. H. Secoy
Corrosion – E. G. Bohlmann
Chemical Technology – F. L. Culler, F. R. Bruce

Compiled by W. E. Thompson

DATE ISSUED

FEB 11 1954

OAK RIDGE NATIONAL LABORATORY
Operated By
CARBIDE AND CARBON CHEMICALS COMPANY
A Division of Union Carbide and Carbon Corporation
Post Office Box P
Oak Ridge, Tennessee

[redacted]

[redacted]

INTERNAL DISTRIBUTION

1. C. E. Center
2. Biology Library
3. Health Physics Library
4. Mathematics Library
5-6. Reactor Experimental Engineering Library
7-9. Central Research Library
10-16. Laboratory Records Dept.
17. Laboratory Records, ORNL R.C.
18-19. ANP Reports Office
20. R. [redacted]
21. S. [redacted]
22. W. [redacted]
23. E. [redacted]
24. E. [redacted]
25. G. [redacted]
26. W. [redacted] (Consultant)
27. R. [redacted]
28. R. [redacted]
29. F. [redacted]
30. A. D. Callihan
31. D. W. Cardwell
32. G. H. Cartledge
33. [redacted] Clewett
34. [redacted] Cole
35. [redacted] Cowen
36. [redacted] Culler
37. [redacted]
38. [redacted] (K-25)
39. [redacted] English
40. [redacted]
41. [redacted]
42. [redacted]
43. [redacted]
44. [redacted]
45. [redacted]
46. [redacted]
47. [redacted]
48. [redacted]
49. [redacted]
50. A. Hollaender
51. A. S. Householder
52. G. R. Jenkins (C&CCC, South Charleston)
53. G. H. Jenks
54. R. W. Johnson
55. C. P. Keim
56. M. T. Kelley
57. E. M. King
58. A. S. Kitzes
59. J. A. Lane
60. [redacted] E. Larson
61. [redacted] C. Lind
62. [redacted] S. Livingston
63. [redacted] N. Lyon
64. [redacted] Marshall
65. H. F. McDuffie
66. J. R. McWherter
67. E. C. Miller
68. K. Z. Morgan
69. E. J. Murphy
70. J. P. Murray (Y-12)
71. L. R. Quarles
72. P. M. Reyling
73. W. L. Ross
74. [redacted] P. Sanders
75. [redacted] Savage
76. [redacted] Secoy
77. [redacted]
78. [redacted]
79. [redacted]
80. I. Spiewak
81. C. D. Susano
82. J. A. Swartout
83. E. H. Taylor
84. W. E. Thompson
85. M. Tobias
86. [redacted] Visner
87. [redacted] P. Walker
88. [redacted] Weinberg
89. [redacted]
90. [redacted] (Consultant)
91. C. E. [redacted]
92. F. C. [redacted]
93. F. C. Zapp
94. P. C. Zmola
95. G. C. Williams
96. J. C. Wilson

[redacted]

[redacted]

EXTERNAL DISTRIBUTION

97. AF Plant Representative, Burbank
98. AF Plant Representative, Seattle
99. AF Plant Representative, Wood-Ridge
100. ANP Project Office, Fort Worth
101-111. Argonne National Laboratory
112. Armed Forces Special Weapons Project (Sandia)
113. Armed Forces Special Weapons Project, Washington
114-118. Atomic Energy Commission, Washington
119. Battelle Memorial Institute
120-122. Brookhaven National Laboratory
123. Bureau of Ships
124-125. California Research and Development Company
126-131. Carbide and Carbon Chemicals Company (Y-12 Plant)
132. Chicago Patent Group
133. Chief of Naval Research
134. Commonwealth Edison Company
135. Department of the Navy – Op-362
136. Detroit Edison Company
137-141. duPont Company, Augusta
142. duPont Company, Wilmington
143. Foster Wheeler Corporation
144-146. General Electric Company (ANPP)
147-150. General Electric Company, Richland
151. Hanford Operations Office
152. Iowa State College
153-156. Knolls Atomic Power Laboratory
157-158. Los Alamos Scientific Laboratory
159. Massachusetts Institute of Technology (Kaufmann)
160. Monsanto Chemical Company
161. Mound Laboratory
162. National Advisory Committee for Aeronautics, Cleveland
163. National Advisory Committee for Aeronautics, Washington
164. Naval Research Laboratory
165-166. New York Operations Office
167-168. North American Aviation, Inc.
169. Nuclear Development Associates, Inc.
[redacted]. Patent Branch, Washington
171-177. Phillips Petroleum Company
178. Powerplant Laboratory (NAPC)
179. Pratt and Whitney Aircraft Division (Fox Project)
180. Rand Corporation
181. San Francisco Operations Office
182. Sylvania Electric Products
183. USAF Headquarters
184. U. S. Naval Radiological Defense Laboratory
185-186. University of California Radiation Laboratory, Berkeley
187-188. University of California Radiation Laboratory, Livermore
189. Walter Kidde Nuclear Laboratories, Inc.
190-195. Westinghouse Electric Corporation
196-210. Technical Information Service, Oak Ridge

[redacted]

[redacted]

Reports previously issued in this series are as follows:

ORNL-527	Date Issued, December 28, 1949
ORNL-630	Period Ending February 28, 1950
ORNL-730	Feasibility Report – Date Issued, July 6, 1950
ORNL-826	Period Ending August 31, 1950
ORNL-925	Period Ending November 30, 1950
ORNL-990	Period Ending February 28, 1951
ORNL-1057	Period Ending May 15, 1951
ORNL-1121	Period Ending August 15, 1951
ORNL-1221	Period Ending November 15, 1951
ORNL-1280	Period Ending March 15, 1952
ORNL-1318	Period Ending July 1, 1952
ORNL-1424	Period Ending October 1, 1952
ORNL-1478	Period Ending January 1, 1953
ORNL-1554	Period Ending March 31, 1953
ORNL-1605	Period Ending July 31, 1953

[redacted]

[redacted]

SUMMARY

PART I

HOMOGENEOUS REACTOR EXPERIMENT

During this quarter, the HRE accumulated approximately 40 Mwh of operating time over a period of several hundred hours, and 35 nuclear kinetic experiments were carried out for studying the inherent stability of the reactor. Various methods of increasing reactivity were used, including control rods, reflector level, fuel concentration, and rapid heat withdrawal. In the most severe experiment, the reactor was cooled suddenly and the reactivity was increased at the rate of 0.8%/sec from a power level of 20 watts. The reactor responded as smoothly as was predicted; the power rose of a peak of 11 megawatts in 1 sec, and in the next 0.1 sec it declined to the 1.5 megawatts demanded from continuous cooling. The shortest period observed was 0.034 sec, corresponding to a reactivity of *0.3% above prompt critical.* A preliminary analysis of the data indicates reasonable agreement with the predicted behavior. The successful demonstration of inherent stability even for excess reactivity above the delayed neutron contribution has permitted the simplification of the reactor-control circuits.

Corrosion data were accumulated during two natural-uranium runs made prior to the power operation. The initial corrosion rate during these runs was about 9 mpy and steadily decreased to a rate of 1 to 2 mpy at the end of 85 hr of operation at 200°C. In the enriched uranium runs, a similar decrease in the corrosion rate was experienced. For the first 20 hr at 200°C and 100 kw, the rate was 40 mpy. Following this period, the reactor dump line was found to be plugged, although the plug apparently dissolved or decomposed after three days. Later, during an operating period of 67 hr at 200°C and a power level of 500 to 1000 kw, the general corrosion rate for the system was measured at about 3 mpy. (It should be noted that the average corrosion rate during the total time of HRE operation is about 1 mpy.)

After the above period of high-level operation, it was found necessary to clean the steam-side surfaces of the main heat exchanger tubes in order to improve heat transfer and to permit operation at full power (1000 kw). During this period, it was also necessary to repair a burned-out lead wire at the highly radioactive fuel-circulating pump.

PART II

BOILING REACTOR RESEARCH

Experiments have shown that the oxygen formed in a boiling homogeneous reactor by fission-recoil decomposition of the water will not maintain a high enough concentration in the solution to stabilize uranyl sulfate in contact with stainless steel at 250°C.

A series of experiments with Supo at Los Alamos has provided a large quantity of data which are still being analyzed.

A method has been found for correlating gas-rise data from a wide variety of bubbling gas-water systems. From this correlation it appears that the diameter of the container is one of the important variables in controlling the rate at which a gas rises through a liquid. In some cases, the gas was found to pass through the liquid (slip velocity) at speeds of more than 35 fps, and it appears that even higher slip velocities are possible.

PART III

GENERAL HOMOGENEOUS REACTOR STUDIES

Intermediate-Scale Homogeneous Reactor Design

The major effort of the ISHR Design Group has been devoted to studying larger aqueous homogeneous reactors for producing central-station power. The basic power plant is one which will produce approximately 300 megawatts of electricity. The effect of reducing the power output to 100 megawatts or of increasing it to 600 megawatts was also investigated. The power plant that is based on two-region reactors contains three reactors, each operated at a total power of 450 megawatts with about 100 megawatts of net electrical output. Each reactor consists of a 6-ft-dia, spherical core operated at a power of 320 megawatts (100 kw/liter) and surrounded by a 2-ft-thick blanket which is operated at a power of 130 megawatts (11 kw/liter). Under equilibrium conditions at 250°C, the core solution contains 1.3 g of U^{233} and approximately 5 g of total uranium – U^{233}, U^{234}, U^{235}, and U^{236} – as uranyl sulfate dissolved in D_2O. A 50% increase in uranium concentration is required for operation at 300°C.

The one-region reactor station contains a single reactor operating at 1350 megawatts total power to

[redacted]

produce approximately 300 megawatts of electricity. A thorium oxide–uranium oxide slurry containing 200 g of thorium per liter and 3.6 g of U^{233} per liter at 250°C, or 3.9 g of U^{233} per liter at 300°C, is considered as the fuel in a 15-ft-dia, spherical pressure vessel.

Costs of electrical power produced by means of a central power station utilizing each type of reactor have been computed for reactors operating at 250 and at 300°C. The total power cost, including fixed charges on chemical plants, is estimated to be 7.1 mills/kw-hr for 250°C operation, as compared with 6.6 mills/kw-hr for electric power from a reactor operating at 300°C. Comparable costs for a one-region reactor were estimated to be 7.3 mills/kw-hr for operation at 250°C and 6.8 mills/kw-hr for operation at 300°C.

Engineering Development

Components for ISHR. A full-scale model of the ISHR core was tested with water, and it appears to be satisfactory. A vaned elbow was tested by using water, and it was found that the pressure drop was low and that the flow distribution was uniform. Two-phase flow tests showed that the Martinelli correlation held quite well in straight runs of pipe, only. Plans for high-pressure testing of recombiners and entrainment separators are described.

Bids for large components for ISHR that cover covering design, development, and fabrication have been received from various manufacturers.

Miscellaneous Development. Weld quality has been developed sufficiently to permit the start of work on the 4000-gpm loop. An automatic tube welder has been developed by Linde Air Products Company, and preliminary bearing tests have been started at Worthington Corporation.

A small ¼-hp vane pump is being tested for its suitability for pumping radioactive gases.

Controls and Instrumentation

Process instrumentation required for the in-pile corrosion test loop has been planned, and the instruments have been obtained or placed on order. Design of the instrument panels has been completed, and one set of panels has been constructed.

Instrumentation for another test loop designed to utilize the Allis-Chalmers canned-rotor pump incorporates a novel interlock panel on the panel board. All protective interlock switch contacts which were provided to actuate arrangements or to shut down equipment were wired to the interlock panel and connected to jacks. Between each pair of jacks a pilot light was installed to indicate the open or closed position of these contacts. If the operator needs to bypass any safety circuit temporily, a "jumper" may be plugged into the jacks corresponding to that interlock. The presence of the jumper is obvious at all times on the front of the panel board, and the pilot light indicates the position of the "jumpered" contacts.

Other instrumentation has been provided routinely as needed to enable suitable data to be taken in the various experimental tests.

Corrosion

A continuous run (B-26) of 4500 hr duration was terminated during this quarter. The operating conditions were 250°C, a solution containing 5 g of uranium per liter with 0.005 *M* H_2SO_4, and 500 to 1500 ppm O_2. The generalized corrosion rate based on Ni analyses was 0.05 mpy, and the weight-loss data obtained from the specimens exposed during the run confirmed this result. The run was terminated by decision, not necessity, and the loop was dismantled. Examination of the loop and pump gave no indication that the run could not have continued indefinitely.

The titanium loop has been put back in operation after a period of inactivity caused by a shortage of titanium impellers. Three additional titanium impellers are being fabricated. The titanium loop is being used for examining the corrosion resistance of titanium and zirconium alloys in the absence of the iron and chromium oxide film which coats these materials when they are exposed in a stainless steel loop.

Further studies on the effect of added sulfuric acid on the corrosion of 300-series stainless steels by uranyl sulfate solutions have been completed. The primary effect of the added acid is to lower the "critical velocity."

Temperature studies have shown that little protection is afforded by the oxide films formed on the 300-series stainless steels exposed to uranyl sulfate solutions in the temperature range below 250°C. As the temperature is raised to 300°C, however, a more resistant film or coating may be indicated by the fact that the critical velocity increases.

Preliminary studies with a taper coupon specimen holder designed for use in the in-pile loop

indicate very good correlation with results obtained with the standard-taper coupon holder used in out-of-pile studies.

Initial tests on in-pile loop components have indicated various changes which are being incorporated in new designs now largely in fabrication. Some difficulty with wear on the thrust face of the Graphitar bearing in the ORNL pump has been encountered, but it is hoped that a change in placement of a machine relief groove will eliminate this difficulty. Present plans call for completion of construction and preliminary operation of the mock-up during the next quarter.

Metallurgy

Efforts to study the feasibility of producing crack-free, fully austenitic welds in type 347 stainless steels and to examine the phase relationships in these welds by metallographic means have emphasized the difficulty of obtaining completely ferrite-free welds by the use of commercial grades of materials. Crack-free welds were produced, but in each case the resultant weld did contain a small amount of ferrite.

Impact tests on control specimens of Zircalloy II (zirconium with 1½% tin and fractional percentages of iron, nickel, and chromium) indicate that the material is relatively notch-sensitive below about 50 to 100°C (under conditions of preparation and test) but that the impact resistance of the notched-bar specimens increased quite rapidly with increase in testing temperatures. This work is preliminary to an investigation of the effects of composition, heat treatment, and exposure to corrosion environments on this temperature-sensitive, notch-brittle behavior, which is an important factor in the design of homogeneous reactor components operating under stress and temperature. Studies of the fracture behavior of titanium and zirconium and their alloys, by use of a modified notched-bar, slow-bend test, are also being made.

Continued work on the formation of corrosion-protective films on austenitic stainless steels by selective oxidation in moist hydrogen at elevated temperatures has indicated that the films contain spinels which are high in chromium and manganese but are relatively low in iron and nickel, together with possibly some silica. The composition of the films is related to the temperature of formation, and work is continuing on a small scale to evaluate the relative protection offered by films of different composition and to establish optimum conditions for film preparation.

The effects of plastic deformation and subsequent heat treatment on the stress-corrosion cracking of austenitic stainless steels are being investigated to provide criteria of specifications for compositions, forming, and heat treatment of heat-exchanger components. The results thus far are by no means conclusive, but they do indicate the perplexity of the problem and the need for further investigation.

Aqueous Solution and Radiation Chemistry

Continued study of certain regions of the four-component system, UO_3-NiO-SO_3-H_2O, has disclosed several new solid compounds, some of which have been identified. The solubility of UO_3 in uranyl sulfate solutions of varying concentration at temperatures of 25, 100, 175, and 250°C, respectively, is reported. The 25°C isotherm for the system UO_2SO_4-$NiSO_4$-H_2O (stoichiometric compositions only) is presented, although all of the solid-phase compounds have not been identified.

An exploratory study of the effect of adding nitric acid to solutions of thorium nitrate on the hydrolysis of thorium nitrate and the resulting hydrolytic precipitation has been completed. The first mole of excess nitric acid markedly elevates the temperature at which precipitation occurs, further acid additions being decreasingly effective.

The solubility of tungstic acid in uranyl sulfate solutions containing 30 and 300 g of uranium per liter and in a uranyl fluoride solution containing 300 g of uranium per liter has been measured from room temperature to 290°C. The purpose of the investigation was to ascertain the permissible effective concentration of tungstic acid in an evaluation of its effectiveness as a corrosion inhibitor. Static and dynamic corrosion tests on type 347 stainless steel, in which uranyl sulfate solutions containing both 30 and 300 g of uranium per liter were used, indicate a marked decrease in corrosion rate.

Measurements of the vapor pressures of uranyl sulfate solutions at various concentrations and from 25 to 100°C have been completed, and the stoichiometric mean ionic molal activity coefficients have been calculated and are reported.

New data on the rate of decomposition of peroxide in uranyl sulfate and uranyl perchlorate solutions at varying acidities and ionic strengths

[redacted]

support the hypothesis of two decomposition paths being available. In the absence of excess hydrogen ion, the principal peroxide species appears to be UO_4, which decomposes to yield UO_3 and O_2. In the presence of a large excess of acid, hydrogen peroxide becomes the principal peroxide species, and the route of decomposition proceeds through it. Efforts to calculate the sulfate complexing of the uranium by comparing the kinetic data from sulfate solutions with those from perchlorate solutions have failed largely because of uncertainty in activity coefficients for H^+ and UO_2^{++} under the experimental conditions.

An extension of the kinetic studies of the effect of cupric ion catalysis of the hydrogen-oxygen recombination reaction has more firmly established the dependence on copper concentration and temperature. A few measurements, made with deuterium instead of hydrogen, indicate that the reaction is about 60% as fast with deuterium as with hydrogen.

A continuation of the static tests of the effects of reactor radiation on corrosion has involved tests on type 347 stainless steel and on titanium. In addition, several out-of-pile tests have been completed. A test on type 347 stainless steel at a power density of 2.1 kw/liter shows no significant departure from zero-power tests and indicates no appreciable radiation effect. A test at 4 kw/liter showed behavior similar to that of previous tests at 6 kw/liter, thus indicating a marked radiation effect. A more detailed analysis of the data is given in the report.

Blanket Systems

The status of various blanket systems, proposed for use in connection with aqueous homogeneous reactors, has recently been reviewed.[1] Recommendation has been made that the circulating thorium oxide slurry be evaluated thoroughly as the most promising alternative, with a boiling slurry as the next best possibility. The circulating slurry appeared to be most promising because of the following reasons.

1. Slurries of the desired thorium concentration can be formed by straight-forward chemical engineering processes.
2. These slurries can be circulated at high temperatures, apparently without abrasion except in regions of extremely high velocity.
3. Development of a suitable pumping system appears to be feasible.
4. These slurries appear to have low settling rates and are easily redispersed.
5. Power removal can be accomplished by circulation through an external heat exchanger. (Power removal from a boiling slurry is of less certain feasibility and would probably require entrainment separators inside the main pressure shell.)
6. Continuous mixing in the slurry will permit long operation of a blanket without buildup of undesirably high unproductive neutron absorption near the core.
7. Processing of slurries presents no intrinsic difficulties which cannot be dealt with by standard chemical engineering techniques.

Subsequent work during the quarter, as reported below, has continued to support interest in the circulating slurry, has somewhat discouraged consideration of the boiling slurry, and has introduced consideration of an aqueous fluidized bed of thorium oxide granules.

Laboratory investigation of the effect of calcination temperature on the properties of thoria produced by the thermal decomposition of thorium oxalate at 300, 500, 700, and 900°C has shown that as the temperature of calcination was increased (1) the average particle size as measured by the optical microscope increased only slightly from less than 2μ at 300°C to 5μ at 900°C; (2) the abrasiveness of slurries prepared from these materials, as measured by a jet-impingement test, increased markedly; (3) the x-ray diffraction patterns became sharper; (4) the surface area decreased from 43.87 m^2/g for the 300°C material to 1.83 m^2/g for the 900°C oxide; and (5) the densities of the oxide residues increased from 8.07 g/cc at 300°C to 9.64 g/cc at 900°C. Prolonged heating in water (600 hr) at 250°C did not change the abrasiveness of thorium oxide prepared by the calcination of thorium oxalate at 500°C, but it markedly decreased the abrasiveness of Ames oxide which is prepared from oxalate by calcination at 650°C.

The results of optical and electron microscope particle-size measurements of the various thorium oxide slurry preparations used in the laboratory abrasion tests support the conclusion that the method of preparation and the relative crystallinity

[1] H. F. McDuffie to J. A. Swartout, *Status of Thorium Blanket Development*, ORNL CF-53-8-95 (Aug. 14, 1953).

[redacted]

[redacted]

are more important than particle size in determining relative abrasiveness.

Circulation of thorium oxide slurries, containing up to 300 g of thorium per liter at 250°C, for periods of time up to 255 hr in stainless steel loops has produced results which support an optimistic view. Erosive attack was observed only at points where the velocity was 80 fps or greater. Slurries of Ames oxide were pumped without evidence of sedimentation or caking. The solids appear to be easily redispersed after shutdown, and any agglomerations appear to be broken up into smaller individual particles during circulation. Continuous lubrication of the Graphitar bearings of the Westinghouse 100A pump, using water condensate from the pressurizer, resulted in essentially no wear on these bearings.

Emphasis at the present time is focused on the development of slurries having satisfactory engineering properties, and studies of the effects of reactor radiation upon thorium oxide slurries have been initiated.

Physical Studies of Uranium Slurries

It has been found that $(UO_2)_3(PO_4)_2$, when added to a slurry of $UO_3 \cdot H_2O$ in water, tends to reduce the caking of oxide in a circulating system at 250°C. Modifications of previous circulating loops have been found which also reduce the caking of $UO_3 \cdot H_2O$ from water slurries.

Abrasion in circulating ThO_2 slurries has been found to be much less severe in most parts of a circulating system than at points of high velocity such as the outer rim of the pump impeller, the throat of the orifice, and the wear rings of the pump.

Chemical Processing

An adsorption process capable of removing rare-earth fission products from the fuel solution of a two-region breeder reactor has been developed and tested on a laboratory scale. This process would consist in passing fuel solution through a column packed with granules of calcium fluoride to remove the rare-earth fission products. This column operating at 100°C will remove more than 90% of the rare earths from the fuel solution by forming insoluble rare-earth fluorides which remain in the adsorption column.

A calcium fluoride column designed to process a 320-megawatt reactor core would contain 2 kg of calcium fluoride for one day of operation and would process about 1300 g of U^{233} per day. The most attractive design for such a column consists of a CaF_2 bed which may be slurried out along with the insoluble fission-product fluorides after use. The amount of U^{233} lost in this procedure would amount to less than 0.01% of the uranium processed.

After passing through the calcium fluoride column, the fuel solution will contain about 300 ppm of both fluoride and calcium. The calcium concentration is reduced to 20 ppm by heating the fuel solution to 270 to 300°C in a second column containing solid calcium sulfate, and the fluoride concentration can be reduced to less than 100 ppm by the addition of thorium sulfate to precipitate thorium tetrafluoride.

Of the alternate inorganic adsorbents tested, only titanite (calcium titano silicate) appeared to be attractive. This mineral in its natural form has the disadvantage that it removes significant amounts of uranium from solution in addition to the rare earths.

[redacted]

[redacted]

[redacted]

CONTENTS

SUMMARY v

PART I. HOMOGENEOUS REACTOR EXPERIMENT

HOMOGENEOUS REACTOR EXPERIMENT 3
Status of the HRE 3
Operations with natural uranium 3
Low-power operation 3
Corrosion rate at 250°C 3
Plugged dump line 3
Uranium peroxide formation 4
Corrosion at 1000 kw 4
Low heat transfer in the fuel heat exchanger 4
Kinetic Experiments 5
Normal reactivity controls 5
Rapid heat extraction from heat exchanger 6
Sudden cooling of core 6
Discussion of results 7

PART II. BOILING REACTOR RESEARCH

BOILING REACTOR RESEARCH 13
Chemical Stability of Boiling UO_2SO_4 Solution in Stainless Steel 13
Nuclear Stability of Boiling Homogeneous Reactors 14
Steam Removal from Boiling Reactors 15

PART III. GENERAL HOMOGENEOUS REACTOR STUDIES

INTERMEDIATE-SCALE HOMOGENEOUS REACTOR DESIGN 21
Aqueous Homogeneous Reactors for Central Station Power 21
Basis for Power Study 21
Two-Region Reactor Station 21
One-Region Reactor Station 25
Fuel Processing 27
Cost of Power 27
Two-region reactor stations 27
One-region reactor stations 29
Stress Analysis of Core Tank 30

ENGINEERING DEVELOPMENT 32
Components for the ISHR 32
Full-scale core model 32
Vaned elbows 32
Gas separators 32
High-pressure catalytic recombiner 32
Entrainment separators 33
Bids for large components for the ISHR 35
Miscellaneous Development 35
4000-gpm loop 35
Automatic tube welding 36
Worthington Corporation pump development 36
HRE off-gas pump 36

[redacted]

[redacted]

CONTROLS AND INSTRUMENTATION 39
In-Pile Corrosion Loop 39
Allis-Chalmers Pump Test Loop 39
ISHR Control Valves 39
Conductivity Transient-Measuring System for Flow Studies 39
Preliminary Salt Loop Mockup Instrumentation 41
Experimental Stress Analysis of ISHR Core Tank 41

CORROSION 42
Dynamic Corrosion Tests 42
Pump loop operation and maintenance 42
Titanium loop 44
HRE mockup 44
Westinghouse model 100-A pumps 45
Loop test results 45
General corrosion rates 45
Corrosion testing with dilute uranyl sulfate solutions 56
Effect of acid on corrosion by 0.02 M uranyl sulfate 57
Effect of time, velocity, and uranium concentration at 250°C 58
Effect of temperature and oxygen concentration 59
Other experiments 63
Decontamination 63
Scale stability 63
In-pile loop corrosion specimens 65
Discussion 66
Small-Scale Dynamic Corrosion Program 67
In-Pile Loop 67
Operating methods and equipment 67
Neutron shutter 67
Leak detection 68
Solution sampling 68
Revision of draining equipment 69
Neutron flux in hole HB-4 69
Status of design and construction 70
Loop package 70
Development and design 70
ORNL small pump 74
Static Corrosion Studies 74
Corrosion of type V2B stainless steel 74
Corrosion of Colmonoy 6 75

METALLURGY 76
Welding of Austenitic Stainless Steels 76
Fracture Behavior of Titanium and Zirconium 76
Properties of Titanium and Zirconium Alloys 77
Commercial-purity titanium 77
Zirconium-aluminum system 77
Zirconium-tin alloys 77
Selective Oxidation of Austenitic Stainless Steels 79
Stress Corrosion Cracking of Type 347 Stainless Steel 84

[redacted]

[redacted]

AQUEOUS SOLUTION AND RADIATION CHEMISTRY 87
The System UO_3-NiO-SO_3-H_2O 87
The System UO_3-SO_3-H_2O Above 300°C 90
A Preliminary Exploration of the $Th(NO_3)_4$-HNO_3-H_2O System at Elevated Temperature 93
Solubility of Tungstic Acid in UO_2SO_4 and UO_2F_2 – Corrosion Inhibition 96
Estimation of Activity Coefficients of UO_2SO_4 Solutions from Vapor-Pressure Measurements 99
Decomposition of Peroxide in Uranyl Salt Solutions 100
Mechanism of the Hydrogen-Oxygen Recombination Reaction in Solutions 105
Homogeneous Reactor Solutions Under Irradiation 108

RELATED CHEMISTRY RESEARCH 112
Chemistry of Corrosion 112

BLANKET SYSTEMS 113
Thorium Oxide Chemistry 113
Thermal decomposition of thorium oxalate 113
Reaction between thorium oxide and water at 250°C 114
Hydrolytic decomposition of thorium oxalate 115
Laboratory Studies of the Properties of Thorium Oxide Preparations 115
Engineering Studies of Circulating Thorium Oxide Slurries 118
Pumping studies at room temperature 118
Pumping studies at elevated temperatures 118
Boiling Slurries 124
Fluidized Solid Blanket Bed 125
Thorium Nitrate Solutions 126
Present Program 126

PHYSICAL STUDIES OF URANIUM SLURRIES 127
Alternative Uranium Slurries 129
Uranyl Phosphate, $(UO_2)_3(PO_4)\cdot 4H_2O$ 129
Discussion of Run S-36 130
Discussion of Run S-38 130
Discussion of Run S-39 131

CHEMICAL PROCESSING 132
Calcium Fluoride Processing for Two-Region Breeder Reactor 132
Capacity of calcium fluoride 132
Control of $CaSO_4$ concentration 133
Removal of fluoride from calcium fluoride-treated uranyl sulfate solutions 134
Process equipment design 134
Summary of Chemical Process Development by the Vitro Corporation of America 135

[redacted]

[redacted]

Part I

HOMOGENEOUS REACTOR EXPERIMENT

[redacted]

HRP QUARTERLY PROGRESS REPORT

HOMOGENEOUS REACTOR EXPERIMENT

S. E. Beall, Section Chief

S. Visner, Experimental Physics Group Leader

E. L. Compere, Reactor Chemistry Consultant[1]

J. J. Hairston J. W. Hill, Jr. T. H. Thomas
Operations Group Leaders

D. I. Eissenberg S. I. Kaplan
V. K. Paré P. M. Wood
Reactor Engineers

T. E. Haynes J. A. Watts W. B. Krick
A. L. Johnson G. H. Johnstone J. D. Jones
Technicians

STATUS OF THE HRE

Operations with Natural Uranium

Installation of a new pulsafeeder fuel-feed pump was completed early in the quarter, and a natural uranium run was begun for the purposes of demonstrating a material balance, ensuring removal of any contaminating ions present, and providing a corrosion base line at 200°C. The run was discontinued after 34 hr because of trouble with a check valve in the pulsafeeder pump. After the valve was repaired, a second natural uranium run was made in the period from August 12 to 15. Successful material balances were demonstrated in both runs, and the 200°C corrosion base line was found to be about 1 to 2 mpy after 63 hr of operation.

Low-Power Operation

During removal of the natural uranium, it was necessary to repair both shim and safety rods. With both rods operating properly, the reactor was filled with enriched uranyl sulfate solution and was run at 10 kw on August 29 and 30 while air activity samples were collected as a leak test. No leakage was detected.

Corrosion Rate at 250°C

Although earlier plans for a measure of the effect of high-level radiation on corrosion had included an extended operation at 200°C, recent data from loop experiments indicated superior corrosion resistance at 250°C. For this reason, the corrosion-run conditions were revised to give a core-outlet temperature of 250°C. In order to achieve this temperature, it was necessary to supply heat by maintaining the reactor power level at 100 kw. It was planned to operate later at 1 megawatt and to compare results under these two conditions. Shortly after 250°C at 100 kw was reached, a hot dump occurred. The fuel was reconcentrated and the run was resumed. The corrosion rate was about 40 mpy, and approximately 40 g of nickel was picked up by the fuel solution.

Samples were isolated from the high-pressure system at 4-hr intervals and were removed after cooling for various periods. Low analytical values for uranium were found for those samples remaining in the sampler for only a short cooling time, and it was speculated that some uranium precipitate (possibly the peroxide) may have formed as the solution was cooled below 100°C, settled out, and then slowly redissolved or decomposed.

Plugged Dump Line

On September 10 a scram signal of undetermined origin actuated the fuel-dump circuit, but it was learned that the reactor core could not be emptied because of a plugged fuel-dump line.

Although the reflector had been emptied by the scram, the reactivity value of the reflector is only

[1]On loan from Chemistry Division.

8% *k*, which is equivalent to a drop in fuel temperature of approximately 60°C. This means that the reactor would have become critical again at 190°C unless the fuel could be dumped, diluted, or heated. However, the temperature was prevented from going below 200°C by heating with plant steam, and dilution was effected intermittently until the concentration was sufficiently low to make further heating unnecessary.

Over a period of 48 hr, all attempts to unplug the dump line were unsuccessful, even at pressures as high as 1400 psi. However, after leaving the line undisturbed over the next 36 hr, a normal dump was observed.

The plugging of the dump line may have been caused by uranium peroxide from the sampler, hydrolytically precipitated uranium trioxide, corrosion scale broken loose by the earlier hot dump, or corrosion products and uranium dioxide possibly produced in the normally stagnant dump line where the solution is depleted of oxygen. The evidence is not sufficient for distinguishing between these possibilities for plugging the dump line, and, of course, more than one effect may have occurred at the same time.

It was noted that the pH of the fuel solution was 2.1 to 2.5 (theory 2.5) during the run, and this may possibly indicate a small precipitation of uranium oxide. Immediately after the dump line opened, the pH of the diluted fuel was 2.4 to 2.5, and one week later it was 3.29 (theory 2.8). This large change is consistent with the alkaline effect of the nickel picked up from corrosion and of the redissolving of a uranium oxide precipitate if the precipitate was present. In order to lower the pH to the theoretical value of 2.8, H_2SO_4 was added to the fuel solution. After another 40 hr of operation, during which the pH again rose above 3.0, it was necessary to make another H_2SO_4 addition.

Uranium Peroxide Formation

After the dump line was unplugged, the reactor was again taken critical at 100°C on September 19, 1953, and it was operated at a power level which later proved to be 70 kw to permit measurements for fuel inventory purposes. A voluminous gray precipitate, which proved to be 70% uranium peroxide and 30% Fe, Cr, and Ni oxides, was observed in a fuel sample. Another sample taken after 2 hr of operation at 100 to 120°C and zero power indicated that the uranium peroxide precipitate had been decomposed satisfactorily.

The appearance and dissolution of the uranium peroxide precipitate substantiate the predictions of Secoy, Silverman, McDuffie, and Watson.[2]

Corrosion at 1000 kw

A 67-hr period of operation at power ensued, of which about 35 to 40 hr were at 1000 kw. A spurious scram signal due to an instrument tube failure caused a 200°C dump on October 9, 1953.

The general corrosion rate for the system from the beginning of the kinetic runs and throughout the high-power operation at 200°C was about 3 mpy, with values ranging from 0 to 11 mpy.

Increasingly high levels of radioactivity were encountered during this period; over 100 r/hr at 1 ft was observed for a ½-ml sample of fuel. The ordinary Beckman "one-drop" glass electrode became useless for reading pH on such samples because it gave high and erratic readings. Useful results were obtained by diluting the samples 20 to 1, observing the pH on the meter in the regular way, and correcting for dilution. In the future, it is planned to use the expendable capillary-glass electrodes which were developed by the Analytical Chemistry Division for very radioactive samples.

Low Heat Transfer in Fuel Heat Exchanger

The reactor was again brought to power at about 1000 kw on October 13; however, during this period the heat-transfer coefficients at the main fuel heat exchanger gradually diminished. Previous measurements of the over-all heat-transfer coefficient had provided evidence that the normal coefficient was 1000 to 1200 Btu/hr·ft^2·°F. Heat-transfer data taken during several days of the high-power run above showed that the coefficient steadily decreased from a value of approximately 1000 to approximately 570; then, during the following 8 hr, it suddenly decreased to a value below 100. This low value reduced the heat extraction from the reactor, and thus the power level was reduced to approximately 300 kw.

While an attempt was being made to determine the cause of the sudden change in the heat-transfer coefficient, operations were terminated by

[2] C. H. Secoy to S. E. Beall, Jan. 23, 1953 (private communication); M. D. Silverman, G. M. Watson, and H. F. McDuffie, *The Radiation Chemistry of Aqueous Reactor Solutions. II. The Decomposition of Hydrogen Peroxide in Aqueous Homogeneous Reactor Systems*, ORNL CF-53-4-294; M. D. Silverman, G. M. Watson, and H. F. McDuffie, *Reactor Science and Technology* 3, No. 3, TID-2010, p. 43 (Sept. 1953).

an electrical failure of the fuel-circulating pump. The cause of the failure was a terminal burnout at the highly radioactive circulating pump, and several days were required to shield the pump and to install a new wire. Upon resumption of operation, the heat-transfer coefficient was again measured at about 50. Treatment of the steam-side tube surfaces with 5% trisodium phosphate solution successfully removed the heat-transfer resistance and resulted in improving the over-all coefficient to its old value of approximately 1000. Samples of the cleaning solution indicated that the fouling was a result of the accumulation of oil and rust on the outer surfaces of the tubes.

KINETIC EXPERIMENTS

Toward the end of the quarter, a series of nuclear kinetic experiments was performed on the HRE to obtain information useful for evaluating the safety of the reactor when it was subjected to rapid increases in reactivity and for checking theoretical safety calculations. A preliminary analysis of the results indicates good agreement with the predicted behavior, and it verifies that the reactor is capable of safely absorbing the largest reactivities that can be introduced, even those in excess of the delayed neutron contribution. Although the power level rises to a peak value for each reactivity excursion, in some cases several times higher than the rated power, the power decreases rapidly to an equilibrium value because of the large negative temperature coefficient. The potential danger to the reactor from such a reactivity "accident" lies not in the increase in temperature, which is only about 10°C for each per cent of reactivity introduced, but in the transient pressure in the core caused by sudden expansion of the fuel solution. This pressure depends on the inertial and frictional forces in the relief pipe to the pressurizer, and although it has not been measured, it can be calculated in a straightforward manner. While it has been estimated that a pulse power of 500 megawatts would be required to generate a dangerous core pressure in the HRE, the highest pulse power reached in the kinetic experiments was only 11 megawatts.

It is impossible to introduce step increases in reactivity into the reactor; therefore a number of experiments were performed which involved linear increases in reactivity. The program started with the mildest experiments, in which the reactivity was introduced at approximately 0.001 %/sec, and progressed to the more severe, in which the reactivity introduction was at the rate of 0.8 %/second. The reactivity exceeded prompt critical in the latter cases. The starting power level ranged between 1 watt and 20 kilowatts. Since more time is available for the accumulation of excess reactivity before the reactor reaches a power level at which the heating introduces a negative coefficient, the lower initial power for a given rate of reactivity increase leads to a more severe test. Thus, for any constant rate of introduction of reactivity, there is an equivalent power such that the reactivity rate is given by the product of the equivalent power, the temperature coefficient of reactivity, and the reciprocal heat capacity of the core. Therefore each series of experiments started with the highest practical operating power and decreased to the lowest practical power. The experiments are listed in Table 1, along with the manner in which reactivity was introduced and the test conditions which are described below. The detailed program for the kinetic experiments and the theoretical predictions are given in a memorandum.[3]

Normal Reactivity Controls

The reactor power and temperature were first adjusted to the desired initial values. For this group of experiments, 1 through 9, the reactivity was increased by means of the usual reactor-control mechanisms which included raising the reflector at a pumping speed of up to 2.4 gpm, concentrating the fuel solution by evaporating water at rates of up to 0.75 kg/min, and simultaneously raising the reflector and shim rod. The power level rose, at a period which became steadily shorter as the excess reactivity in the reactor increased, until the equivalent power was reached at which the excess reactivity reached its maximum. The power went through a peak which removed the accumulated reactivity by heat generation, and then it decayed to the equivalent power which is sufficient to compensate for the reactivity being added and to the heat losses from the reactor. The introduction of reactivity was

[3] V. K. Paré and S. Visner, *Experimental Program for HRE at High Power, Part II: Kinetic Experiments*, ORNL CF-53-10-73 (Oct. 1, 1953).

stopped at this point, and the reactor power automatically adjusted itself to match the heat losses.

The reactivity rates attained by this method were from 0.001 to 0.008 %/sec, and they yielded reactor periods as short as 1.5 sec and peak powers as high as 153 kw.

Rapid Heat Extraction from Heat Exchanger

A more drastic series of tests, 12 through 18, was carried out which entailed rapid increases in the rate of heat removal from the main heat exchanger while the fuel circulating pump was running. Reactivity was introduced at rates of up to 0.07 %/sec, thus causing the reactor to behave very much as it did in the preceding experiments. However, the pile periods were as short as 0.29 sec, and the peak powers reached 665 kw. It was not feasible to attain faster reactivity rates by this method since the designated reactivity is approached with a relaxation time of 6 sec, which, in order to keep the experiment meaningful, must be kept small in comparison with the time required to reach the equilibrium power.

Sudden Cooling of Core

Finally, to obtain the most drastic tests of the inherent stability of the reactor, an unusual set of conditions was achieved whereby the reactor core was suddenly cooled. This cooling was accomplished by stopping the fuel circulating pump, cooling the main heat exchanger while the core temperature was maintained relatively constant, and then restarting the pump. In this way, the protective effect of the large heat capacity of the heat-exchanger water was circumvented and rates of reactivity introduction up to 0.8 %/sec were achieved. Periods as short as 34 msec and peak powers as high as 11 megawatts were observed.

The behavior of the reactor power in experiments 25 and 26 is shown in Fig. 1 as measured with a Brush recorder at a speed of 5 fps. For experiment 26, the behavior below 100 kw could not be measured because the amplifiers for the recorder were not sufficiently fast. Therefore the behavior in this region was inferred from experiment 25 and is represented by the broken portion of the curve. With the reflector at 200°C and the fuel circulating at 185°C, the reactor power was first adjusted to the desired initial values, 19 kw for experiment 25 and 14 watts for experiment 26. The main circulating pump was

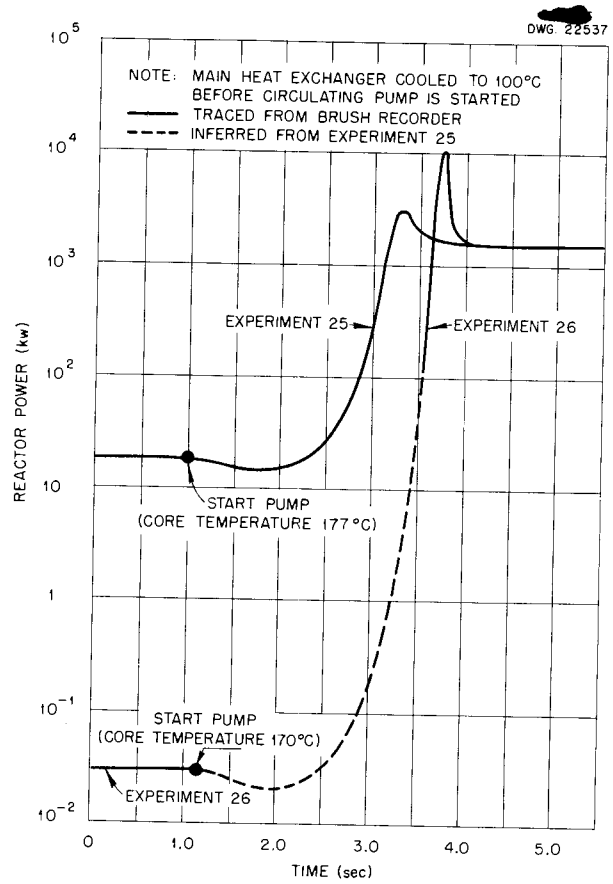

Fig. 1. Power Response of HRE During Reactivity Increase of 0.8%/sec.

then stopped, and the steam valve from the fuel heat exchanger was opened completely for 5 min, thus reducing the temperature in the heat exchanger to 100°C. Meanwhile, the reactor power was kept constant by lowering the reflector level to compensate both for the augmented delayed neutron fraction and for minor cooling of the fuel. Thus, for experiment 25, the reflector was lowered the equivalent of 0.88 % in reactivity, and it is inferred from this that the core temperature had decreased to 177°C by the time the circulating pump was restarted.

Similarly, for experiment 26, the corresponding inferred temperature was 170°C. For the difference in temperature between core and heat exchanger of about 75°C, the power demand on the core or equivalent power is approximately 1.6 megawatts, which is equal to a linear reactivity increase of approximately 0.8 %/second. However, during approximately the first second, while

the pump is accelerating, the fuel entering the core is that which has been residing in the pipes and in the pump and which, consequently, has not cooled so much as the heat exchanger. Therefore during the first second there is in effect a reactivity rate of increase which is of relatively small magnitude and which just compensates for the decrease in reactivity that occurs when the pump is started and is due to some loss of delayed neutrons on circulation. The planned rate of reactivity increase effectively starts when the power has returned to its initial value, and this takes place 1.3 sec after the pump is started.

From this point on, the response of the reactor is similar to that observed for the earlier two sets of experiments. For experiment 25, the shortest pile period, which occurs at 2.10 sec, indicates a peak excess reactivity of 0.61 % and a calculated rate of 0.76 %/second. For experiment 26, the shortest period, which is found at 2.65 sec, indicates a reactivity of 0.80 % and a calculated rate of 0.67 %/second. This is in reasonable agreement, in view of the approximations made, with the rate of 0.80 %/sec estimated from the initial temperature conditions. The equilibrium power of 1500 kw, which was attained in both experiments following the peak power, is also in good agreement with the power demand which is estimated to have decayed during this time from its initial value of 1600 kw to a value of 1400 kw.

It is noteworthy that the power peak of 11,000 kw in experiment 27, although 11 times higher than the rated reactor power, is safe since its duration is only of the order of 0.1 sec and the excess gas and integrated radiation through the shield are negligible. The inferred peak pressure associated with this peak power is 5 psi, which is indeed small compared with the 2000 psi which would be required to burst the core tank.

Discussion of Results

The results obtained in the kinetic experiments are summarized in Table 1, along with the predictions from theory. It is expected that the numbers presented will be modified somewhat after a more thorough analysis is completed; however, the basic trends are believed to be well enough established and of sufficient interest to justify publication at this time.

For each experiment, the minimum period was determined by measuring the slope of the steepest portion of the Brush recorder trace of the power, and the period was converted to reactivity by an in-hour curve. [Note: A period observed while the reactivity is changing is not in general the stable period associated with the instantaneous reactivity; the discrepancy increases with the rate of change of reactivity and the importance of the delayed neutrons. Thus the observed minimum period is a good measure of the maximum reactivity during the excursion when the reactivity is changing slowly or when it is above prompt critical where the delayed neutrons are unimportant. An in-hour curve was constructed for the HRE (with the fuel circulating) to cover the range of periods encountered in the kinetic experiments by adjusting the delayed neutron fractions to fit the observed relationship between stable period and excess reactivity for periods longer than 10 sec, and by taking the value of the prompt neutron generation time as 1.0×10^{-4} second. The total delay fraction from this in-hour curve fit turned out to be 0.51 % as compared with the 0.60 % inferred from the difference in reactivity between the reactor when circulating and when static.]

The rate of introduction of reactivity was determined by means that were appropriate to each experiment. In experiments 1 to 9, it was obtained from the known calibrations of the control system. For experiments 12 to 18, the rate of reactivity increase was obtained from the rate of cooling of the reactor core. This cooling rate can be easily inferred from the fuel-circulating flow, the heat capacities of the core and heat exchanger, and the rate of heat withdrawal from the heat exchanger as indicated by the equilibrium reactor power after the excursion. In this group of experiments, the time spent between the start and the power peak was at least 30 sec, which is long compared with the previously mentioned 6-sec time constant for establishing the equilibrium power demand on the core.

For experiments 21 through 36, in which the reactivity was introduced by restarting the fuel-circulating pump after the heat exchanger had been cooled, the rate of reactivity increase shown in the table is the quotient of the peak reactivity obtained from the observed minimum period and

the time during which the reactivity was introduced. As was explained earlier, for the first 1.3 sec after starting the pump, a much smaller reactivity increase rate was in effect which just compensated for the reactivity decrease due to the loss of delayed neutrons. This time interval is then subtracted from the time which elapsed between starting the circulating pump and the instant of maximum reactivity.

The methods of predicting the peak power, minimum period, and peak pressure for a given rate of introduction of reactivity and initial power have been described previously.[4] Since the power rises very rapidly from the equivalent power to the peak, the reactivity added during this time is negligibly small and the behavior during the peak can be analyzed as though a reactivity step of a magnitude given by the maximum excess reactivity had been introduced. In this manner, the peak excess reactivity has been calculated for each observed peak power and listed in Table 1 for comparison with the reactivity inferred from the minimum period. A graphical comparison is available in Fig. 2, where peak excess reactivity is plotted against observed peak power. The theoretical curve was calculated with reactor constants appropriate to 200°C operation, whereas the experiments were performed over a range of temperatures. Agreement appears to be good only for the higher reactivities above prompt critical, which indicates that the accuracy of the calculations is poor when delayed neutrons are important.

In order to compare the observed peak power with that predicted for the particular initial power and rate of reactivity increase, the calculated peak power is also given in the table. The experimental peak powers are plotted in Fig. 3 as a function of the reactivity rate, and the initial power is indicated adjacent to each point to permit comparison with the theoretical curves. No comparison was made for experiments 1 to 9 because the times required were large enough for there to be appreciable heat loss to the reflector as the core heated up to compensate for the reactivity introduction. This cooling may be considered either as an additional introduction of reactivity or as an increase in the heat capacity of the core.

For experiments whose predicted power peaks are above 2500 kw, the observed peaks are all less than those calculated, averaging about 23% lower. This is well within the probable accuracy of the approximate calculations. For smaller power excursions, the observed peaks are all higher by factors averaging about 2.1 than those predicted; the discrepancies apparently increase as the peak power decreases. This is another indication that the calculations lose accuracy with the increasing importance of delayed neutrons. Fortunately, the predictions are most accurate and tend to be conservative for the most extreme experiments.

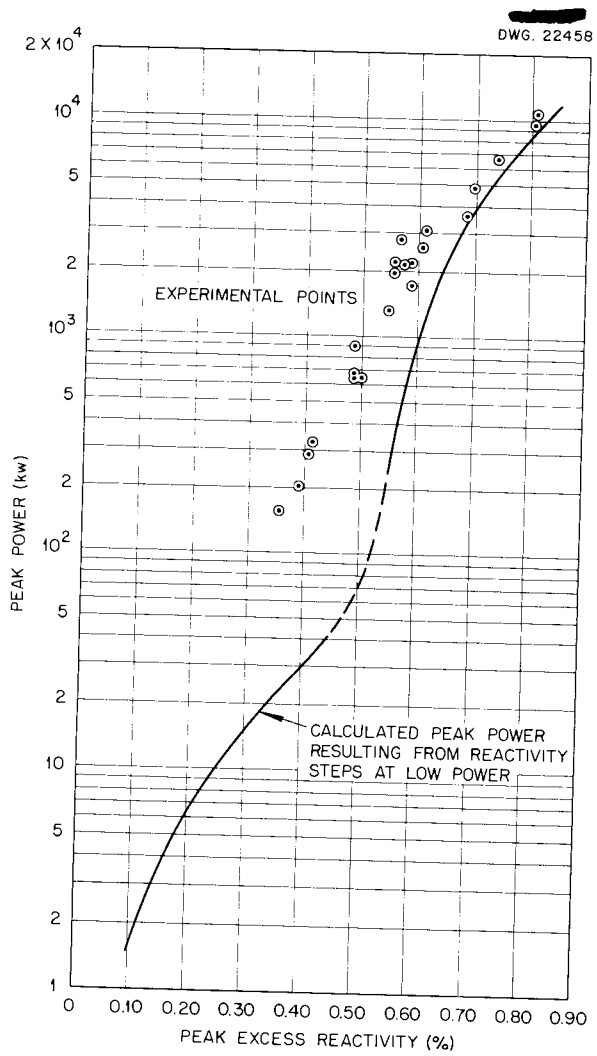

Fig. 2. Observed Peak Power vs. Peak Reactivity for HRE.

[4] S. Visner and V. Paré, *HRP Quar. Prog. Rep. July 31, 1953*, ORNL-1605, p. 8.

TABLE 1. RESULTS OF KINETIC EXPERIMENTS ON HRE

EXPERIMENT NUMBER	METHOD OF INCREASING REACTIVITY	RATE OF INCREASE OF REACTIVITY (%/sec)	INITIAL POWER (kw)	PEAK POWER (kw)		OBSERVED MINIMUM PERIOD (sec)	PEAK EXCESS REACTIVITY, $\Delta k/k$ (%)		TIME SPENT TO REACH MAXIMUM REACTIVITY (sec)
				Predicted	Observed		Calculated to Give Observed Peak Power	Corresponding to Observed Minimum Period	
1	Raise reflector 1.13 gpm	0.0015	1.0		22.5	34	0.280	0.104	120
2	Raise reflector 0.92 gpm	0.0012	0.010		37.5	13.6	0.351	0.166	165
3	Raise reflector 2.37 gpm	0.0032	0.0001		110	6.5	0.482	0.228	220
4	Concentrate fuel 0.40 kg condensate/min	0.0019	1.1		31	34.8	0.313	0.102	360
5	Concentrate fuel 0.50 kg condensate/min	0.0024	0.010		54	12.6	0.395	0.172	400
6	Concentrote fuel 0.75 kg condensate/min	0.0047	0.00005		93	2.23	0.518	0.325	500
9	Raise shim rod reflector 2.53 gpm	0.0076	0.001		144	1.45	0.537	0.364	115
12	Open steam valve with fuel-circulating pump running	0.018	0.0032	83	153	1.58	0.539	0.357	92
13	Open steam valve with fuel-circulating pump running	0.024	0.0033	115	201	1.07	0.547	0.389	78
14	Open steam valve with fuel-circulating pump running	0.030	0.0030	191	282	0.869	0.552	0.404	61
15	Open steam valve with fuel-circulating pump running	0.034	0.0049	229	323	0.788	0.556	0.411	55
16	Open steam valve with fuel-circulating pump running	0.068	0.0053	1,000	633	0.243	0.580	0.499	33
17	Open steam valve with fuel-circulating pump running	0.065	0.0049	1,000	665	0.291	0.581	0.485	39
18	Open steam valve with fuel-circulating pump running	0.065	0.0067	851	625	0.292	0.579	0.485	31
21	Cool main heat exchanger and start fuel-circulating pump	0.16	10.7	439	889	0.290	0.591	0.486	3.1*
22	Cool main heat exchanger and start fuel-circulating pump	0.16	0.080	1,850	2,170	0.096	0.644	0.585	3.7*
23	Cool main heat exchanger and start fuel-circulating pump	0.38	9.8	1,460	2,190	0.124	0.644	0.557	1.46*
24	Cool main heat exchanger and start fuel-circulating pump	0.51	0.030	8,890	6,540	0.042	0.752	0.738	1.46*
25	Cool main heat exchanger and start fuel-circulating pump	0.76	19	3,260	3,060	0.0851	0.670	0.609	0.80*
26	Cool main heat exchanger and start fuel-circulating pump	0.67	0.014	13,100	9,490	0.0345	0.803	0.802	1.35*
27	Cool main heat exchanger and start fuel-circulating pump	0.73	0.028	13,500	10,800	0.0340	0.817	0.806	1.10*
28	Cool main heat exchanger and start fuel-circulating pump	0.22	7.6	736	1,300	0.142	0.613	0.545	2.45*
29	Cool main heat exchanger and start fuel-circulating pump	0.30	0.019	4,980	4,800	0.051	0.716	0.696	2.34*
30	Cool main heat exchanger and start fuel-circulating pump	0.26	12.1	804	1,940	0.125	0.638	0.557	2.18*
32	Cool main heat exchanger and start fuel-circulating pump	0.22	20.3	589	2,780	0.116	0.670	0.564	2.58*
33	Cool main heat exchanger and start fuel-circulating pump	0.23	0.76	1,750	2,120	0.109	0.646	0.571	2.46*
34	Cool main heat exchanger and start fuel-circulating pump	0.34	1.14	2,690	1,700	0.096	0.630	0.585	1.74*
35	Cool main heat exchanger and start fuel-circulating pump	0.46	2.1	3,470	2,540	0.087	0.659	0.603	2.60*
36	Cool main heat exchanger and start fuel-circulating pump	0.32	0.017	5,450	3,560	0.055	0.682	0.682	2.14*

*The total time from the instant the circulating pump is turned on is 1.3 sec greater.

In several of the more severe cooling experiments, there is some evidence of small oscillations in the power as it decays from the peak to the equilibrium value determined by the power demand. The period of the oscillations is approximately 20 sec, and it has not been determined as yet whether the cause is nuclear or mechanical, as, for instance, a temporary variation in heat transfer or some temporary instability of the gas letdown system from the core.

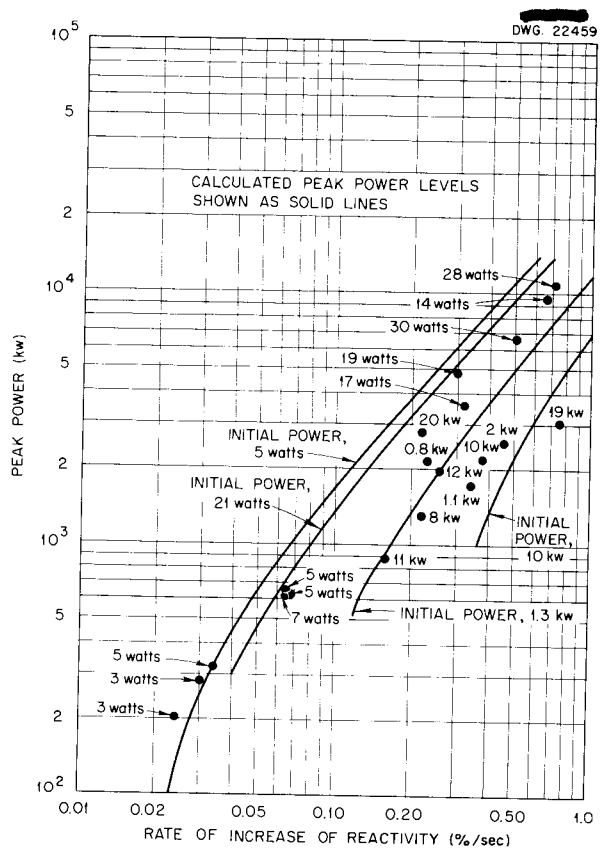

Fig. 3. Peak Power in HRE as Function of Rates of Reactivity for Various Initial Powers.

Part II

BOILING REACTOR RESEARCH

BOILING REACTOR RESEARCH

R. N. Lyon, Section Chief

CHEMICAL STABILITY OF BOILING UO_2SO_4 SOLUTION IN STAINLESS STEEL

C. G. Lawson

It has previously been known that stainless steel will reduce uranyl sulfate solution at 250°C in the absence of other oxidizing agents. A concentration of 50 ppm or more of dissolved oxygen has been found to prevent reduction of the uranium salt; however, in a boiling system it is apparently impractical to maintain an oxygen concentration greater than the steady-state concentration which occurs when fission causes water to decompose to hydrogen and oxygen. If fission produces all the heat for boiling, the equilibrium oxygen concentration will be essentially independent of power level, since both the water decomposition rate and the heat formation rates will be proportional to the power level. At 250°C this equilibrium oxygen concentration would be approximately 6 ppm (7.5 ppm when measured at 25°C). The equilibrium concentration will decrease with decreasing temperature because of the lower pressures and lower oxygen solubility. (A minimum in the latter occurs just above 100°C.)

In order to determine the effectiveness of these low oxygen concentrations in preventing the reduction of uranyl sulfate, a test bomb was set up with a means for bubbling oxygenated steam through the bomb contents. The temperature of the bomb, the oxygen concentration in the steam, and the pressure of the steam could all be controlled.

Details of the procedure and equipment will be listed in a forthcoming report. A flowsheet of the equipment is shown in Fig. 4.

Seven test runs were made, the results of which are listed in Table 2. In all cases the initial U-to-SO_4 ratio was 1.01. The oxygen concentration at 250°C was calculated from the partial pressure in the steam and the Henry's law constant reported in BMI-T-25[1] and was then referred to 25°C.

The runs are listed in order of increasing oxygen concentration rather than in chronological order. It will be seen that the U-to-SO_4 ratio decreased with decreasing oxygen below 30 ppm of oxygen. This is also shown in Fig. 5 where the per cent uranium precipitated is plotted vs. the oxygen concentration. It will also be observed that the

[1] H. A. Pray, C. E. Schweickert, and B. H. Minnich, *The Solubility of Hydrogen, Oxygen, Nitrogen, and Helium in Water at Elevated Temperatures*, BMI-T-25 (May 15, 1950).

TABLE 2. RESULTS OF LOW-OXYGEN-CONCENTRATION STABILITY TESTS

OXYGEN PRESSURE (psia)	RUN NUMBER	OXYGEN CONCENTRATION REFERRED TO 25°C (ppm)	FINAL* U-to-SO_4 RATIO	FINAL** URANIUM CONCENTRATION REFERRED TO 25°C (mg/ml)	FINAL pH
1	SS-7	5	0.87	53.3	1.2
1.8	SS-6	9	0.945	47.3	1.5
4.0	SS-8	20	0.975	102.0	1.7
5.0	SS-9	25	0.99	55.5	1.9
6.0	SS-5	30	1.01	106.0	2.2
8.0	SS-10	30	1.02	76.9	2.5
8.0	SS-4	40	1.01	63.7	2.4

*Initial U-to-SO_4 ratio was 1.01.

**Initial uranium concentration was 60 g/liter. Final concentration varied because of random dilution and concentration during test.

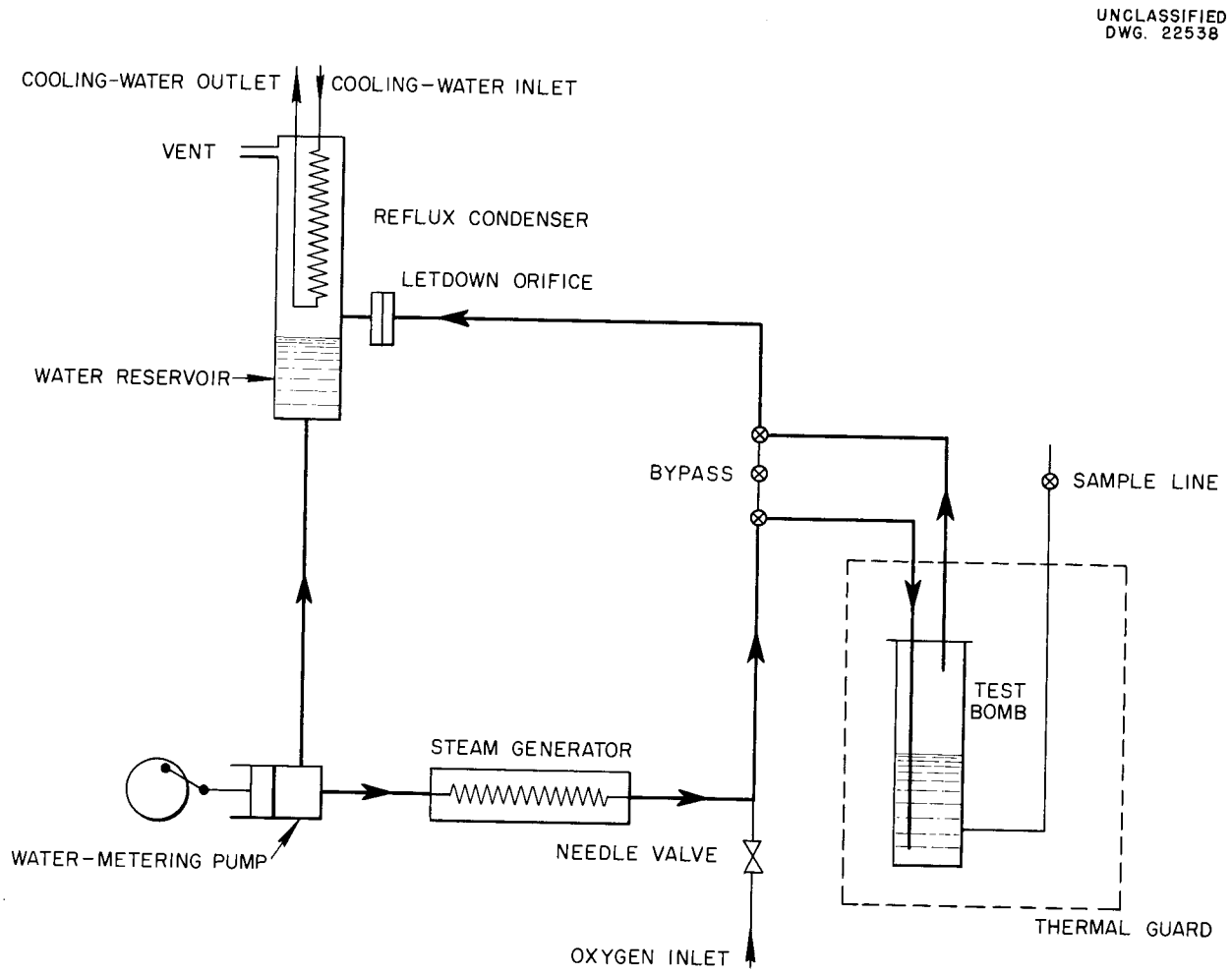

Fig. 4. Flow Diagram of Apparatus Used in Low-Oxygen-Concentration Stability Tests.

pH was lowered by the lower oxygen concentrations.

From these results it is concluded that one of the following steps would have to be taken in a boiling homogeneous reactor:

1. avoid the use of stainless steel in contact with the fuel solution at elevated temperatures,
2. use a less corrosive fuel – e.g., a slurry,
3. add some soluble, nonvolatile oxidizing agent to the system.

NUCLEAR STABILITY OF BOILING HOMOGENEOUS REACTORS

P. R. Kasten
R. J. Goldstein
D. G. Thomas
W. P. Walker
D. S. Toomb

Early this quarter, a group from ORNL, in cooperation with Omega Site personnel at Los Alamos, performed a series of stability tests on the Supo reactor under both boiling and nonboiling conditions. A preliminary report on these tests is currently in preparation.

The experiments consisted of suddenly removing a boron containing rod from the reactor core while the reactor was at some predetermined power level. The rod position with time and the reactor neutron flux were simultaneously recorded. From this information and a calibration of the rod with respect to position, it appears that a variety of reactor properties can be computed that include the delay in the formation of steam and gas bubbles, the prompt generation time, the percentage of delayed-neutron emitters lost up the stack, and, from rod insertion experiments, the rate at which bubbles rise to the surface of the reacting solution.

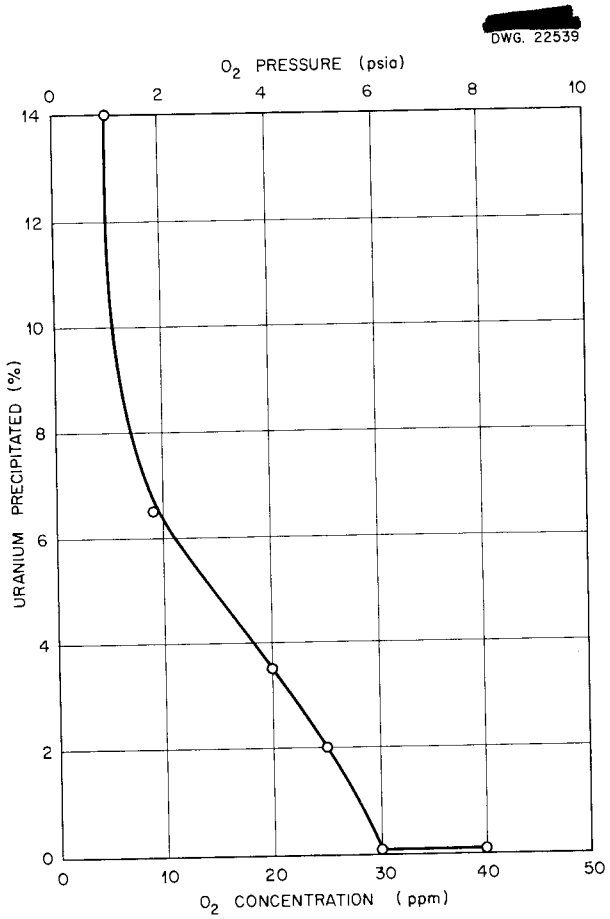

Fig. 5. Per Cent Uranium Precipitated vs. Oxygen Concentration During 24-hr Test.

It was found that the reactor compensated for the sudden introduction of reactivity more rapidly when it was initially boiling than when it was not initially boiling. In nonboiling cases, the higher the initial power level, the more quickly the reactor compensated for reactivity increase and the less the total energy release during the power surge. It appears from this fact that at the higher power levels, the bubbles of decomposition gas are more effective in stabilizing the nonboiling reactor than is the temperature coefficient.

In general, the reactor demonstrated no characteristics which would raise serious doubts as to the stability of a boiling homogeneous reactor, and in spite of minor fluctuations in power level, it appeared even more stable in a gross sense than did the reactor under nonboiling conditions. It should be pointed out, however, that the steady-state power fluctuations increased with power level and that the maximum power removed by boiling was only about 3 to 4 kw.

STEAM REMOVAL FROM BOILING REACTORS

R. V. Bailey[2] H. A. MacColl
W. S. Brown M. Richardson
P. C. Zmola

In the work on steam removal from boiling reactors, experimental results have been obtained from a total of seven systems. In three of the systems, volume boiling was produced by electrical-resistance heating of the liquid, and in the remaining four systems, volume boiling was simulated by bubbling air through the liquid. A brief description and the approximate range of operation for each of the systems are given in Table 3.

It has been possible to correlate the results from all these experiments on a single plot that is shown in Fig. 6 by casting the data into the form

$$\frac{DG}{\mu}\,\frac{1}{Z^{1/2}} = F(\bar{f}) \,, \tag{1}$$

where D is the hydraulic diameter of the system, G is the mass velocity of the vapor based on the entire cross-sectional area of the test region, μ is the dynamic viscosity of the vapor, Z is the active height of the boiling region, and $\bar{f}$ is the average vapor fraction of the boiling region. At low pressures and hence over the range of experimental work reported here, $\bar{f}$ is identical with the somewhat more significant parameter previously reported,[3]

$$1 - \frac{\bar{\rho}}{\rho_l} \,.$$

Data from the 6 × 6 in. natural-vapor-rise system and the $1\frac{1}{4} \times 4$ in. circulating system (I-A and I-C in Table 3) are represented by the dashed curve. Results from the 6 × 6 in., the 24 in., and the 69-in. air-water systems (II-B, II-C, and II-D in Table 3) are represented by the solid curve. The small-diameter natural-rise systems (I-B and II-A in Table 3) exhibited a "slugging" flow in

[2]Consultant, Tulane University.

[3]R. V. Bailey and P. C. Zmola, *A Preliminary Investigation of Power Removal from a Boiling Reactor*, ORNL CF-53-11-145 (Nov. 1, 1953).

TABLE 3. SUMMARY OF EXPERIMENTAL SYSTEMS OPERATED IN POWER-REMOVAL STUDIES

DESCRIPTION OF SYSTEM		APPROXIMATE RANGE OF OPERATION								
Test Section Size	Flow Arrangement	Active Boiling Height (ft)	Power Density (kw/l)	Mass Velocity of Vapor or Gas (lb/hr·ft²)	Total Pressure (atm)	Mean Density Decrease of Vapor Fraction, $\bar{f}$	Density Distribution Measured	Temperature Distribution Measured	Approximate Number of Runs	Remarks
I. Volume-boiling experiments with electrical-resistance heating of liquid										
A. 6 × 6 in. cross section; 4 ft high	Natural vapor rise	0.4 to 3.7	to 9	to 1380	1	0.08 to 0.63	Yes	Yes	135	
B. 1¼ × 4 in. cross section; 4 ft high	Natural vapor rise	1.3 to 3.2	to 9	to 4630	1 to 3	0.34 to 0.68	Yes	Yes	15	Slugging flow
C. 1¼ × 4 in. cross section; 4 ft high	Natural circulation	0.6 to 4	to 14	to 5420	0.1 to 2	0.24 to 0.61*	Yes	Yes	15	
II. Air-water experiments										
A. 4 in. dia; 4 ft high	Natural vapor rise	0.9 to 3.3		to 3200	1 to 2.7	0.18 to 0.65	No		80	Slugging flow
B. 6 × 6 in. cross section; 4 ft high	Natural vapor rise	0.5 to 3		to 1890	1	0.17 to 0.66	No		50	
C. 24 in. dia; 5 ft high	Natural vapor rise	1.2 to 4.2		to 364	1 to 3	0.10 to 0.47	No		40	
D. 69 in. dia; 12 ft high	Natural vapor rise	3.7 to 8.7		to 62	1	0.10 to 0.41	No		15	

*Based on active boiling height.

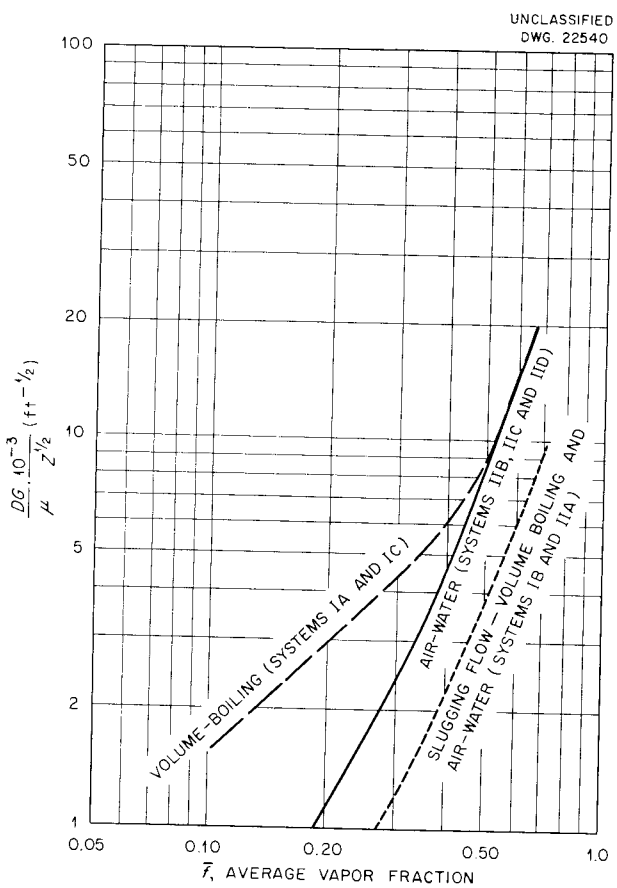

Fig. 6. Comparison of Data from Volume-Boiling and Air-Water Experiments.

which pockets of gas or vapor of a size comparable to the diameter of the test sections formed and rose with an irregular motion. The data from these systems are represented by the dotted curve. Individual points are not shown since the three curves are based on a total of about 350 runs.

Although the power density, P, does not appear explicitly in Eq. 1, as represented graphically in Fig. 6, G/Z is proportional to the power density so that

$$\frac{DG}{\mu} \frac{1}{Z^{1/2}} \sim PDZ^{1/2} . \tag{2}$$

The difference between the values of the ordinate for low vapor fraction in the volume-boiling and air-water systems appears to be due to the manner in which the air is introduced in the latter. In the air-water system, all the air is introduced at the bottom and it traverses the entire height of the test region. In the volume-boiling systems, vapor generation is distributed with preferential generation in the upper region of the test section at low power densities. At higher vapor fractions, the curves become confluent as the region of maximum energy generation moves downward in the volume-heated systems.[4]

[4]This can be inferred from the change in density distribution with increased power density. See, for example, W. S. Brown, H. A. MacColl, M. Richardson, and P. C. Zmola, *HRP Quar. Prog. Rep. March 31, 1953*, ORNL-1554, p. 25, Fig. 14.

For volume-heated systems, the power density is directly proportional to the average vapor fraction up to vapor fractions of approximately 30%. The power density becomes more strongly dependent upon the vapor fractions at higher vapor fractions; for example, the power density at 50% vapor varies as the 2.5 power of the average vapor fraction.

In small natural-rise systems, "slugging" flow occurs and has the effect of increasing the operating vapor fraction for a given power level. The slope of the curve for slugging flow remains the same as that for nonslugging flow when the data are plotted as in Fig. 6.

The influence of pertinent variables on power removal appears to be as follows:

Height. For a given operating average vapor fraction, the power density varies inversely as the square root of the height. This is perhaps the most definite conclusion that can be drawn from this work, and it is supported by calculations based on a number of analytical models[5] and by the experimental results. The experimental work included heights from 0.4 to 8.7 feet.

Diameter. For a given operating average vapor fraction, the power density varies inversely with the diameter. The experiments covered the range $0.16 < D < 5.8$ feet. Qualitatively, it appears that increasing the diameter permits increased eddying and internal recirculation which impede the vapor removal. To date it has not been possible to support this hypothesis by calculation. The effect of diameter will be checked by further experiments in which egg-crate baffles will be installed in the 69-in.-dia air tank.

Viscosity. There is insufficient experimental information for determining the role of viscosity in power removal, but it is included in the correlating expression on the basis of plausibility. The use of the viscosity of the gas or vapor in the correlation brings the volume-boiling and air-water systems into slightly better agreement and it remains consistent with the taking of G as the mass velocity of the gas or vapor. The viscosity of the liquid could have been used; in fact, it would be expected that the viscosities of both the liquid and the gas should enter into the correlation, perhaps in some more subtle manner.

[5]R. V. Bailey, W. S. Brown, H. A. MacColl, M. Richardson, and P. C. Zmola, *HRP Quar. Prog. Rep. July 31, 1953*, ORNL-1605, p. 22, Eq. 1.

Vapor-Slip Velocity. The vapor-slip velocity is defined as difference between the mean velocity of the vapor and the mean velocity of the liquid. During the search for an explanation for the fact that the results of both the natural-vapor-rise and natural-circulation volume-boiling systems coincide when plotted as in Fig. 6, it appeared that they could coincide only if the ordered motion of the liquid in the natural-circulation case was small relative to the vapor velocity. Accordingly, a low-pressure-drop flowmeter was installed in the downcomer of the $1\frac{1}{4} \times 4$ in. natural-circulation system so that the velocities of both the liquid and vapor leaving the test section could be calculated. A plot of these velocities against the power density, based on the active boiling height, is shown in Fig. 7. In fact, it can be seen that the vapor velocity is large compared with the liquid velocity, hence the agreement with the natural-vapor-rise system.

Pressure. The effect of operating pressure on power removal is intimately associated with the slip velocity. Although the amount and the range of the data obtained at other than atmospheric

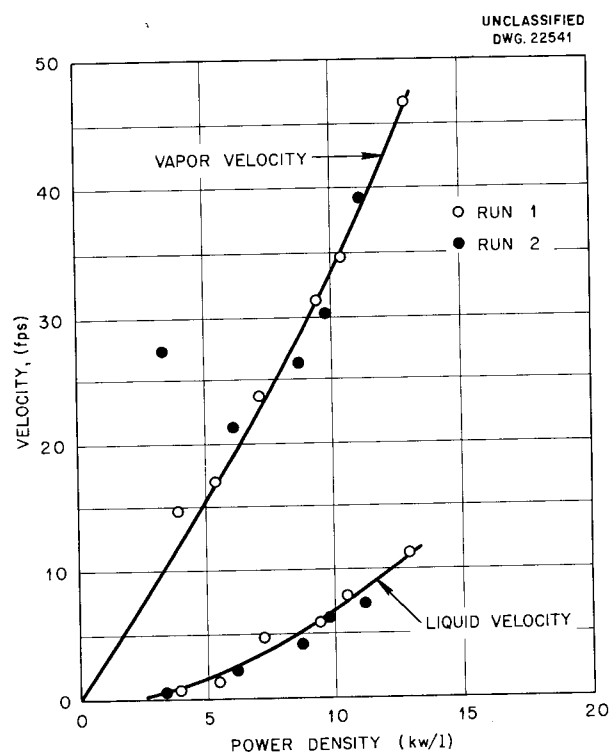

Fig. 7. Liquid and Vapor Velocities at Test-Section Exit in $1\frac{1}{4} \times 4$ in. Circulating System.

pressure in these experiments are too small for arriving at any firm conclusion, in systems in which the slip flow governs, it appears that the power density increases only slightly with increased pressure at a given average vapor fraction. In any event, the power-density increase is not so large as would be predicted by scaling according to the pressure or h_{fg}/v_{fg}. There is evidence that the slip velocity decreases with increasing pressure but that it is still appreciable at 600 psi.[6] Experiments are being planned and apparatus is being designed for extending studies of the natural circulation system to higher pressures.

[6] E. Schmidt, P. Behringer, and W. Schurig, *VDI-Forschungsheft*, No. 365 (1934).

Part III

GENERAL HOMOGENEOUS REACTOR STUDIES

INTERMEDIATE-SCALE HOMOGENEOUS REACTOR DESIGN

R. B. Briggs, Section Chief

R. E. Aven
W. Terry
J. P. Sanders
R. Cheverton
C. L. Segaser
F. C. Zapp
R. H. Chapman
P. N. Haubenreich

AQUEOUS HOMOGENEOUS REACTORS FOR CENTRAL STATION POWER

The major effort of the ISHR Design Group has been devoted to the study of larger aqueous homogeneous reactors intended for the production of power from a central station. The results of this study will be published in ORNL-1642. The section of the report devoted to the study of thorium–U^{233}-fueled reactors has been completed, and a summary of that section is presented here.

BASIS FOR POWER STUDY

The basic power plant is one which will produce approximately 300 megawatts of electricity. The effect of reducing the power output to 100 megawatts or increasing it to 600 megawatts was examined also.. A study of thorium fuels and aqueous homogeneous reactor types resulted in the consideration of a two-region reactor with a dilute solution of uranyl sulfate flowing through the core and thorium oxide slurry in the blanket. A one-region reactor with a thorium oxide–uranium oxide slurry fuel was also considered.

TWO-REGION REACTOR STATION

The power plant based on two-region reactors contains three reactors, each operated at a power of 450 megawatts thermal with about 100 megawatts net electrical output. Each reactor consists of a 6-ft-dia spherical core, operated at a power of 320 megawatts (100 kw/liter), surrounded by a 2-ft-thick blanket which is operated at a power of 130 megawatts (11 kw/liter). Under equilibrium conditions at 250°C, the core solution contains 1.3 g of U^{233} and approximately 5 g of total uranium – U^{233}, U^{234}, U^{235}, and U^{236} – as uranyl sulfate dissolved in D_2O. A 50% increase in uranium concentration is required for operation at 300°C.

Uranyl sulfate solution is pumped through the core at a rate of 30,000 gpm. Liquid leaving the core is divided into two parallel circuits which lead into centrifugal gas separators in which the explosive mixture of deuterium and oxygen is separated from the liquid and diluted with a recirculated gas stream which contains oxygen, helium, and D_2O. The gas-free liquid circulates through heat exchangers and is returned to the core by canned-motor circulating pumps. In each circuit, 150 megawatts of heat is removed from 15,000 gpm of liquid.

The gas streams from the separators are combined and flow through a catalytic recombiner and a condenser which removes 20 megawatts of heat. D_2O removed from the gas by the condenser is returned to the reactor, and the diluent gases are recycled to the separators.

Similar gas and liquid recirculating systems are required for the blanket which, it is assumed, will consist of a slurry containing 500 to 1000 g/liter of thorium oxide in D_2O. The equipment has sufficient capacity to remove the 130 megawatts of heat generated in the blanket.

Both the core and the blanket systems are provided with low-pressure storage equipment that consists of dump tanks, condensers for removing the heat after shutdown, and catalytic D_2O recombiners. Gases which are let down from the high-pressure systems in the storage tanks pass through cold traps to remove D_2O and through fission-product adsorbers before they are exhausted to the atmosphere. Feed pumps, similar to the pulsafeeder pumps used in the HRE, or some acceptable substitute, are provided for introducing D_2O and fuel into the high-pressure system.

The D_2O inventory for each reactor system is estimated to be 40,000 liters. The average specific power in the system is 11.3 kw/liter. The specific power in the heat-removal and circulating systems is 20 kw/liter for the core solution and 14 kw/liter for the blanket slurry.

An arrangement of reactor cells and a power plant for a station that produces 1350 megawatts of heat is presented in Figs. 8, 9, and 10. Three large cells are provided for the reactors and

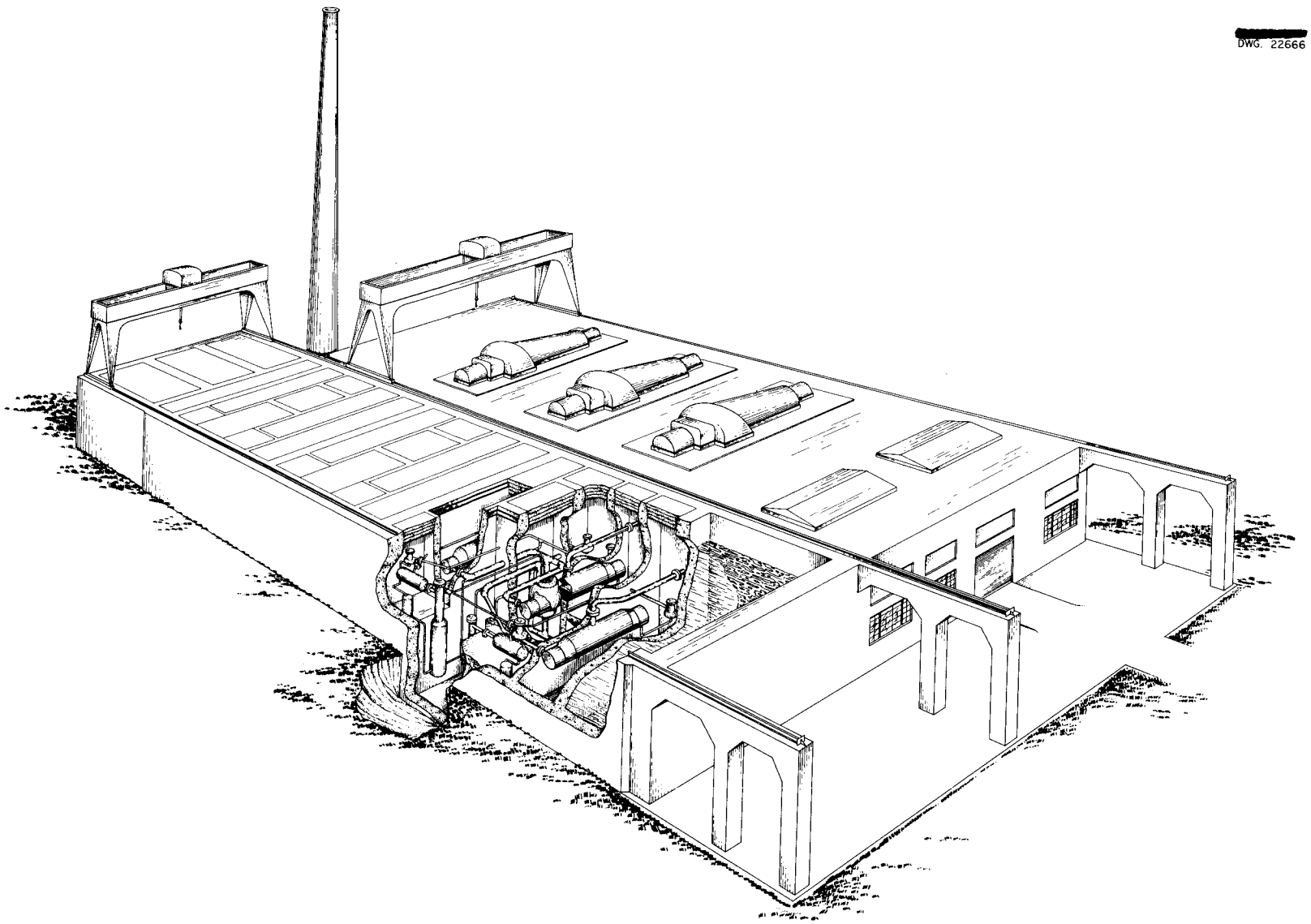

Fig. 8. Two-Region Reactor Station.

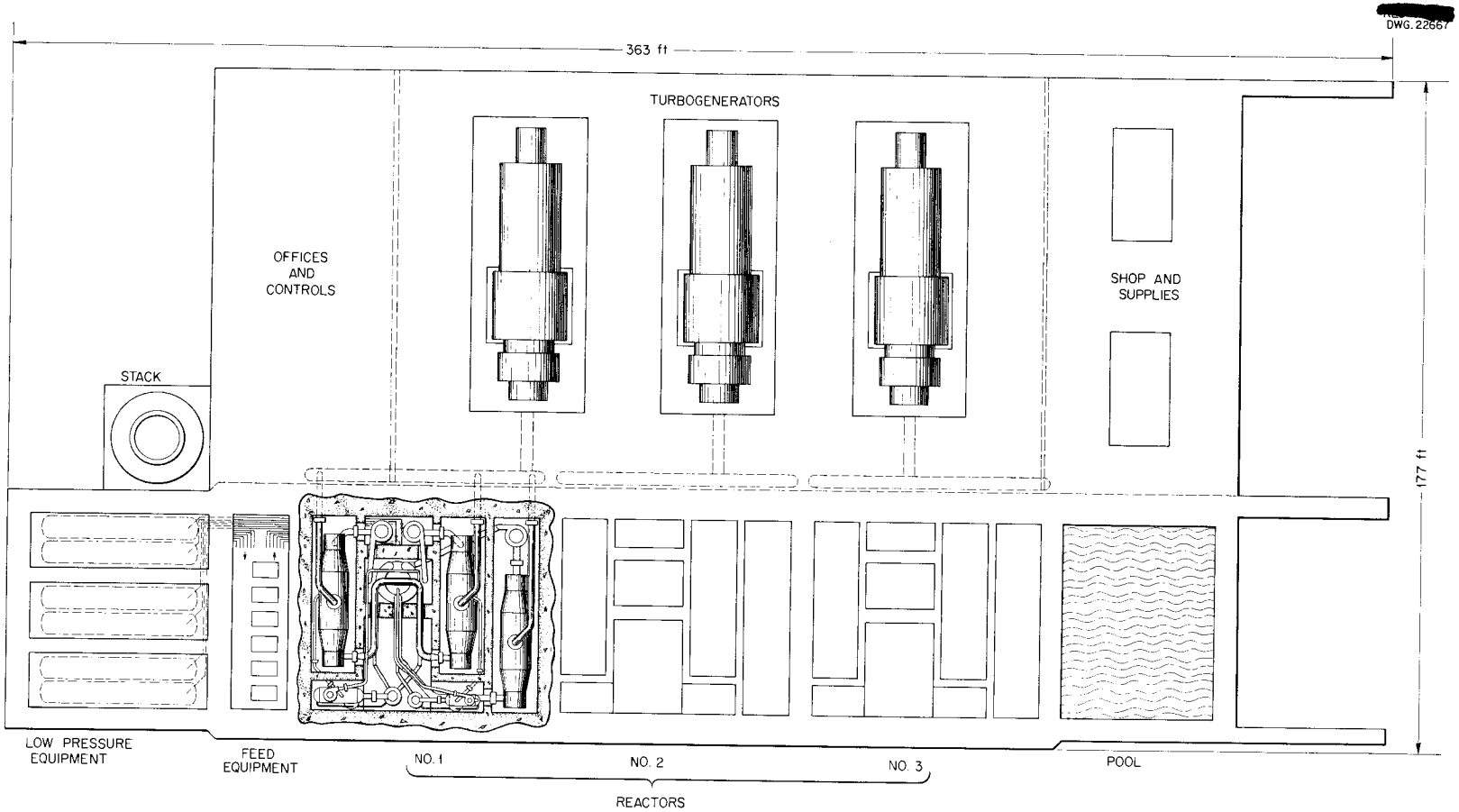

Fig. 9. Plan of Two-Region Reactor Station.

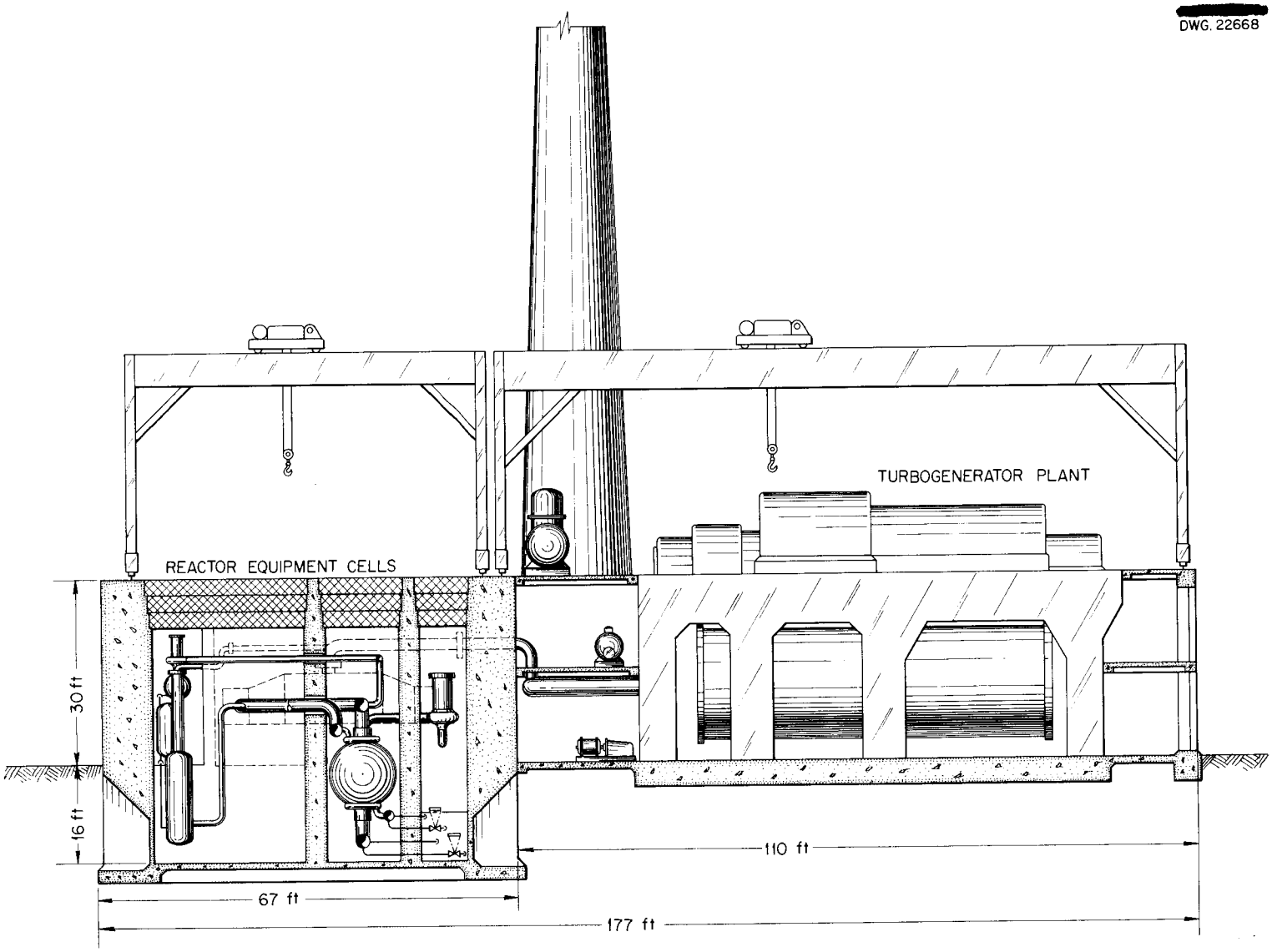

Fig. 10. Elevation of Two-Region Reactor Station.

associated high-pressure equipment, and four are provided for the dump tanks and low-pressure equipment. The shielded compartments which comprise the reactor building are serviced by a gantry crane. Coffins are provided for reducing the radioactivity to tolerable levels while radioactive materials are being transported from the cells to a pool for maintenance and repair.

Estimated costs (neglecting all development costs) and other related data for power plants containing two-region reactors operated at 250 and 300°C are presented in Table 4.

ONE-REGION REACTOR STATION

The one-region reactor station contains a single reactor operating at 1350 megawatts thermal to produce approximately 300 net megawatts of electricity. A thorium oxide–uranium oxide slurry containing 200 g of thorium per liter and 3.6 g of U^{233} per liter at 250°C and 3.9 g of U^{233} per liter at 300°C is pumped at a rate of 130,000 gpm through a 15-ft-dia spherical pressure vessel. The slurry is recirculated through the reactor, four large gas separators, and eight 160-megawatt heat exchangers by eight 16,000-gpm pumps. The decomposition gases which are removed from the gas separator by the recirculated diluent are recombined in four parallel high-pressure recombiner circuits which remove a total of 70 megawatts of heat. Low-pressure equipment is provided for fuel feed and storage, D_2O recovery, and disposal of fission product gases.

TABLE 4. OPERATING AND COST DATA FOR 1350-MEGAWATT REACTOR STATIONS

	TWO-REGION REACTORS		ONE-REGION REACTORS	
Reactor operating temperature, °C	250	300	250	300
Number of reactors per station	3	3	1	1
Total heat output, megawatts	1350	1350	1350	1350
Reactor pressure, psia	1000	2000	1000	2000
Total U^{233} inventory, kg	420	460	600	650
Total thorium inventory, metric tons	70	70	34	34
Total D_2O inventory, metric tons	135	135	153	153
Breeding gain,* $\frac{\text{atoms } U^{233} \text{ produced}}{\text{atoms } U^{233} \text{ consumed in core}} - 1$	0.12	0.10	0.02	0.00
Steam pressure, psia	215	560	215	560
Steam temperature, °F	388	478	388	478
Gross efficiency of turbine generator plant	0.264	0.307	0.264	0.307
Gross electrical capability, megawatts	356	415	356	415
Net station efficiency	0.234	0.274	0.234	0.274
Net electrical capability, megawatts	316	370	316	370
Reactor plant cost: millions of dollars	16	19	15	18
dollars/kw of net capacity	50	51	48	49
Power plant cost: millions of dollars	44	48	44	48
dollars/kw of gross capacity	123	116	123	116
dollars/kw of net capacity	139	130	139	130
Total plant cost: millions of dollars	60	67	59	66
dollars/kw of net capacity	189	181	187	179

*Poison fraction = 0.07.

The D_2O inventory in the reactor plant is 139,000 liters, equivalent to an average specific power of 9.7 kw/liter. The specific power in the external heat removal and circulating system is 16 kw/liter.

The one-region reactor power plant is shown in Figs. 11, 12, and 13. A 15-ft-dia reactor vessel is located in a central shield compartment, surrounded by compartments containing recombiner equipment, pumps, and heat exchangers. Equipment compartments are provided with only enough shielding to permit limited access when equipment is being repaired.

As compared with the two-region reactor plant, a different approach to the problem of disposal of radioactive equipment is suggested here. (Either approach is equally applicable to one-region or two-region reactor stations.) Equipment which has been disconnected from the circulating system can

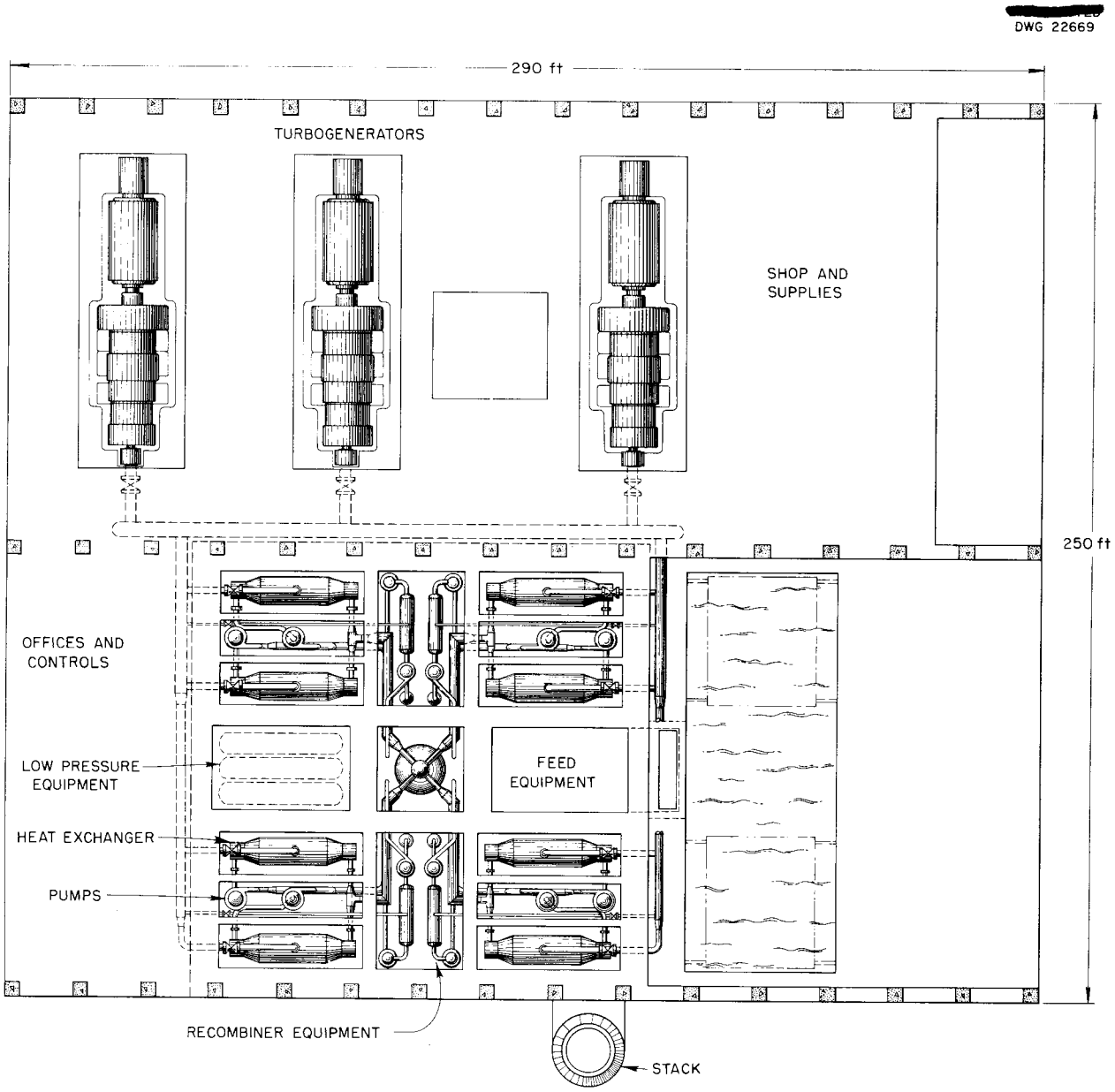

Fig. 11. Plan of One-Region Reactor Station.

[redacted]
DWG 22670

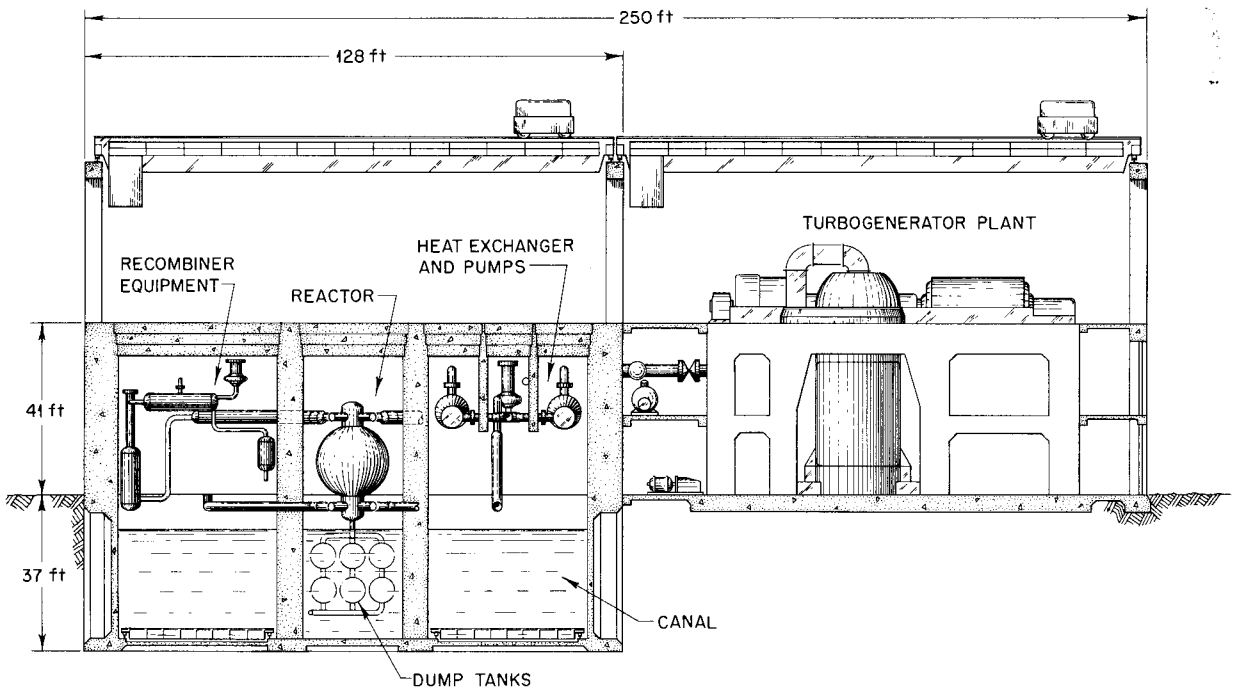

Fig. 12. Elevation of One-Region Reactor Station.

be lowered into a canal under the reactor and removed to a pool outside the shield to be repaired. No attempt has been made to provide valves for the isolation of defective equipment; it is assumed that the entire reactor will be shut down for replacements or repairs in the high-pressure system. If satisfactory valves can be developed, they should be included so that maintenance of some of the equipment will be permitted while the reactor is operating.

As in the two-region reactor station, the equipment cells comprise the reactor building, and the turbine generators are installed in the open. Only the shops, control rooms, stores, and other necessary facilities are housed.

Estimated costs and related data for the one-region reactor plant are contained in Table 4.

FUEL PROCESSING

Fission products are removed from the core of the two-region breeder reactor by two chemical processes. A calcium fluoride absorption process involving circulation of the heavy water solution of uranyl sulfate through a bed of calcium fluoride is used for removing the rare-earth fission products from the core solution. The remainder of the fission products is removed by Thorex processing.

The blanket of the two-region reactor is processed through Thorex for removal of U^{233}, Pa^{233}, and fission products. Examination of several designs for Thorex plants and for Purex plants resulted in the following relationship between processing costs and plant capacity:

$$C = \$5000 + \$3.00 \times W_{Th} + \$1.00 \times w_U ,$$

where C is the cost in dollars per day, W_{Th} is the kilograms of thorium processed per day, and w_U is the grams of fissionable uranium processed per day. In the one-region reactor processing, only the excess U^{233} produced is separated from the thorium and subject to the \$1.00/g charge for uranium processing.

The cost of calcium fluoride processing of the core solution is related to the capacity of processing by the equation:

$$C = \$400 + \$0.20 \times w_U .$$

Minimum core processing costs are realized when the ratio of the volume processed by calcium fluoride to the volume processed by Thorex is approximately 3.2.

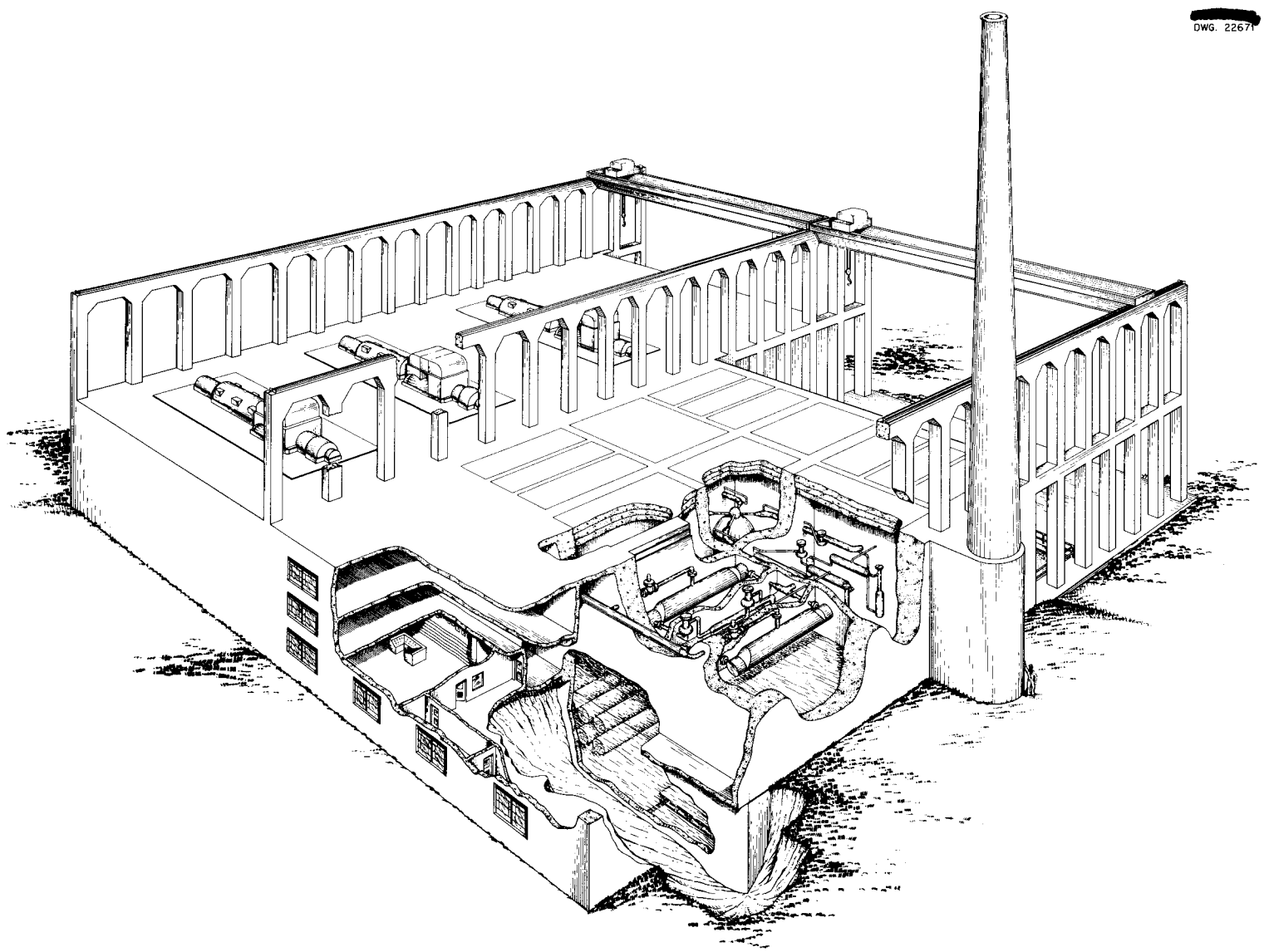

Fig. 13. One-Region Reactor Station.

COST OF POWER

Two-Region Reactor Stations

The components of the total cost of power are the fixed charges on the plant, the operating and maintenance costs, and the cost of fuel. The fixed charges on the plant were based upon a 15% annual charge on the investment in plant and an 0.8 plant-operating factor.

Operating costs were based upon similar costs for conventional power plants. Annual maintenance costs were assumed to be 1½% of the investment in plant, which is equivalent to 10% of the fixed charges. The fuel costs included inventory and consumption charges on thorium, uranium, and D_2O and the cost of chemical processing. Excess U^{233} produced in the breeder reactors was credited at the market value of U^{233}. Costs assumed in the analysis were \$20 and \$40 per gram for U^{233}, \$88 per kilogram for D_2O, and \$22 per kilogram for thorium.

Studies were made of the effect upon power costs of the concentrations of thorium and U^{233} in the blanket and of poison fraction in the core. Minimum power costs were obtained with a poison fraction of 0.07 and with a 1000-g/liter blanket containing approximately 4 g of U^{233} per kilogram of thorium. Total power costs and the distribution for the two-region breeder station are shown in Table 5. The total fuel costs for the reactors operating at 250°C was found to be 7.1 mills/kw-hr. Operation at 300°C reduced this cost to 6.6 mills/kw-hr. If the reactor station and chemical plant could be so completely integrated that the \$5000 per day fixed charge on the chemical plant would be eliminated, the total cost could be reduced to 6.4 mills/kw-hr at 250°C and to 6.0 mills/kw-hr at 300°C.

The cost of U^{233} has little effect upon the power cost because the value of the excess U^{233} produced is about equal to the inventory charge on U^{233}. Inventory charges on the D_2O constitute

TABLE 5. COST OF POWER

	TWO-REGION REACTORS		ONE-REGION REACTORS	
Reactor temperature, °C	250	300	250	300
Fixed charges, mills/kw-hr	4.1	3.9	4.1	3.9
Operating and maintenance, mills/kw-hr	0.8	0.7	0.8	0.7
Fuel cost, dollars/Mwd of heat				
CaF_2 processing of core	0.42	0.42		
Thorex processing of core	0.62	0.62	0.44	0.44
Thorex processing of blanket	1.45	1.45		
D_2O recovery	0.06	0.06	0.25	0.25
Thorium consumption and U^{233} processing losses	0.08	0.08	0.08	0.08
Uranium inventory*	2.50	2.75	3.60	3.95
Thorium inventory	0.45	0.45	0.22	0.22
D_2O inventory and losses	5.00	5.00	5.73	5.73
Value of excess U^{233}*	1.95	1.58	0.45	0.00
Fixed charge on chemical plant	4.15	4.15	3.85	3.85
Total fuel cost, mills/kw-hr				
Without fixed charge on chemical plants	1.5	1.4	1.7	1.6
With fixed charge on chemical plants	2.2	2.0	2.4	2.2
Total cost, mills/kw-hr				
Without fixed charge on chemical plants	6.4	6.0	6.6	6.2
With fixed charge on chemical plants	7.1	6.6	7.3	6.8

*Value of U^{233} assumed to be \$20 per gram.

the largest single item of fuel cost. Reducing the cost to $44 per kilogram would reduce the power cost by 0.4 mill/kw-hr. An almost equal reduction in cost might be achieved by an improved design that would reduce the volume of D_2O in the external equipment. By taking advantage of operation at 300°C, improved reactor design (but no reduction in D_2O cost), and construction of power plants in the range of 600 to 1000 megawatts of electricity, it appears possible to reduce the power costs to 5.5 mills/kw-hr for operation with an 0.8 plant factor.

One-Region Reactor Stations

Power costs were calculated for the one-region reactor on a basis similar to that for the two-region machines. Reactors were studied in sizes from 10 to 20 ft in diameter and with thorium concentrations of 100 to 400 g/liter. Minimum power costs were obtained with a 15-ft-dia reactor containing 200 g of thorium per liter, a poison fraction of 0.07, and having only a small breeding gain. Power costs for the one-region reactor are shown in Table 5 also. The total power cost was 7.3 mills/kw-hr for the reactor operating at 250°C and 6.8 mills/kw-hr for operation at 300°C. Elimination of the fixed charges on the chemical plant would reduce these costs to 6.6 mills/kw-hr at 250°C and 6.2 mills/kw-hr at 300°C. Because the breeding gain is small and the inventories of U^{233} and D_2O are large, the cost of power is very sensitive to the costs of U^{233} and D_2O. There appears to be no significant difference in the cost of power from one-region or two-region reactors or in the reduction in costs that might be achieved by improved technology if the electrical output of the plant is 300 to 600 megawatts. Two-region reactors have the advantage of smaller size and lower inventory at lower plant output. The multiplicity of reactors results in slightly higher costs for two-region reactors in larger power plants.

STRESS ANALYSIS OF CORE TANK

A theoretical stress analysis has been performed for the region around the outlet pipe on the ISHR core tank. The effects of differential expansion on the core tank were investigated, assuming a stainless steel core tank and carbon steel pressure vessel. The methods of Timoshenko[1] and of Malkin[2] were followed in the analysis of the stresses in a sphere that result from concentric ring load of P pounds per linear inch.

Denoting by a subscript ϕ the component in the direction of a meridian and by a subscript θ the component in the direction of a parallel circle, the normal forces are given by

$$N_\phi = \frac{2D\lambda^2}{a^2} e^{-\lambda\phi} \cot\phi \,(C_3 \sin\lambda\phi - C_4 \cos\lambda\phi) - \frac{P \sin a}{\sin^2\phi}$$

and

$$N_\theta = \frac{2D\lambda^3}{a^2} e^{-\lambda\phi} [C_3(\cos\lambda\phi - \sin\lambda\phi) + C_4(\cos\lambda\phi + \sin\lambda\phi)] + \frac{P \sin a}{\sin^2\phi} .$$

The bending moments are given by

$$M_\phi = \frac{D\lambda}{a} e^{-\lambda\phi} [C_3(\cos\lambda\phi + \sin\lambda\phi) + C_4(\sin\lambda\phi - \cos\lambda\phi)]$$

and

$$M_\theta = \nu M_\phi .$$

The constants are defined as

$$C_3 = P \frac{a^2(1+\nu)\sin\lambda a}{2D\lambda^2 e^{-\lambda a}(\lambda \sin a + \nu \cos a)}$$

and

$$C_4 = -C_3 \cot\lambda a .$$

The symbols used in the above equations are defined as follows:

N_ϕ = normal force on an element in the direction of a meridian at an angle ϕ measured from the vertical axis, lb/in.,

N_θ = normal force on an element perpendicular to N_ϕ, lb/in.,

M_ϕ = bending moment on an element in the direction of a meridian at an angle ϕ measured from the vertical axis, lb-in./in.,

[1] S. Timoshenko, *Theory of Plates and Shells*, Chapters 10 and 12, McGraw-Hill, New York, 1940.

[2] I. Malkin, *J. Franklin Inst.* 251, 247 (1951).

M_θ = bending moment on an element perpendicular to M_ϕ, lb-in./in.,
a = radius of sphere, in.,
D = flexural rigidity of a plate, $Eh^3/12(1-\nu^2)$, in which E = modulus of elasticity of the material, lb/in.^{2}, h = thickness of the plate, in., and ν = Poisson's ratio for the material,
λ = constant depending on material and proportions of the sphere, $[3(1-\nu^2)(a/h)^2]^{1/4}$,
α = angle defining the radius of the ring on which the load acts,
P = load acting on sphere, lb/in. of circumference,
ϕ = angle defining an element on which the forces and moments act, radians.

The stresses may be calculated by the usual equations and added algebraically. The stress equations may be written as

$$\sigma_{\phi,i} = \frac{N_\phi}{h} + \frac{6M_\phi}{h^2},$$

$$\sigma_{\phi,o} = \frac{N_\phi}{h} - \frac{6M_\phi}{h^2},$$

$$\sigma_{\theta,i} = \frac{N_\theta}{h} + \frac{6M_\theta}{h^2},$$

$$\sigma_{\theta,o} = \frac{N_\theta}{h} - \frac{6M_\theta}{h^2},$$

where the subscript i denotes inside surface and the subscript o denotes outside surface. Figure 14 shows the stress distribution for a portion of a sphere. The values used in calculating these stresses for the ISHR core tank are:

a = 24 in.,
h = $\frac{1}{8}$ in.,
ν = 0.38,
E = 26.5×10^6 psi,
α = 15 deg,
P = 1 lb/in.

The stresses for any other load applied at the same point will be proportional to the ones presented in the figure. It should be noted that the bending stress is relatively high at the weld joint and falls off rapidly as the angle ϕ increases. The weight of the shell and the effect of pressure were neglected in this analysis.

The significance of this analysis, if proved to be reasonably correct by experimental stress analysis, is to determine whether an expansion joint is required to absorb the differential expansion and thus decrease the stresses imposed on the core tank. Experimental work is needed to prove the reliability of the theoretical analysis, and this will be done on some scale models presently under construction.

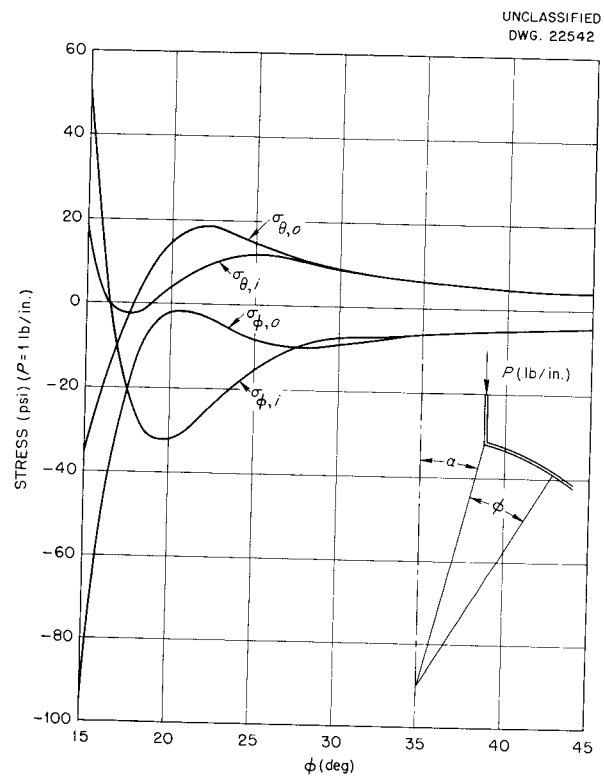

Fig. 14. Stresses in Sphere for Fixed Ring Load.

ENGINEERING DEVELOPMENT

C. B. Graham, Section Chief

J. M. Baker
W. D. Buchanan
J. S. Culver
L. F. Goode
R. Goodman
J. A. Hafford
R. J. Kedl
L. B. Lesem
R. Meza
W. L. Ross
I. Spiewak
R. E. Wascher
S. R. West
R. H. Wilson
C. D. Zerby

COMPONENTS FOR THE ISHR

Many of the following components for the ISHR have been described in previous reports: ORNL-1318, 1424, 1478, 1605, ORNL CF-53-10-107, 53-8-77, 53-7-198, and 53-8-53.

Full-Scale Core Model

Successful tests have been carried out in a full-scale core model (Fig. 15), which utilizes screens in the inlet to spread the flow evenly throughout the sphere. Low-pressure, cold water was pumped through the core at rates that varied from 1,000 to 16,000 gpm. The residence time was measured qualitatively by timing bursts of injected salt solution by means of conductivity probes which were connected to Brush recorders. No stagnation was observed, and the flow pattern conformed fairly well to the theoretical potential pattern.[1]

Heat removal from this type of core should be orderly, with a minimum of overheating. Gas bubbles traveled along the flow lines and were promptly removed from the core. The pressure drop (Fig. 16) was low and in good agreement with that predicted from 18-in. model tests.[2]

At a flow rate of 16,000 gpm, the first two screens pulled loose from the core wall; however, only about 20% of the screen wires had been welded to the wall. The ISHR design specifies 100% welding and a maximum flow of 5000 gpm; therefore it appears that the screens will have adequate strength.

Further details of the core test are presented in ORNL CF-53-10-107.[3]

Vaned Elbows

In order to provide good flow distribution to the ISHR core, a 90-deg vaned elbow, instead of a conventional elbow, will be installed in the inlet line. A steel vaned elbow was tested in the core-testing system and was found to perform satisfactorily. Pressure drop through the elbow was approximately that predicted from design considerations (0.24 velocity heads at 5000 gpm) and is plotted in Fig. 16.

Gas Separators

In the HRE, gas is removed from a vortex within the core itself; however, the straight-through ISHR core necessitates the use of an external gas separator. A full-scale "pipe line" gas separator will be tested during the next quarter.

During the past quarter, some small-scale tests were conducted in which the pressure drop in a system where gas and liquid flow concurrently was explored.[4] This two-phase pressure drop is of considerable importance in the gas-separator design. It was found that the Martinelli correlation[5] held quite well for straight horizontal and vertical runs of pipe. Two-phase pressure drop across 90-deg elbows was found to be about 35% higher than that expected from the "equivalent diameter" concept. The pressure drop across contractions was below expectations, but no general quantitative conclusions can be drawn.

High-Pressure Catalytic Recombiner

Components are currently being ordered for a small, high-pressure, test loop that will simulate the operation of the ISHR high-pressure recombiner system. It is anticipated that this loop will be put in operation in about ten months. In this

[1] D. H. Fax, W. Dashkin, S. C. Traugott, and G. F. Wislicenus, *Hydrodynamic Analysis of Flow Through Spherical Vessels*, Institute for Cooperative Research, Johns Hopkins University, June 1953.

[2] J. A. Hafford, L. B. Lesem, I. Spiewak, and R. H. Wilson, *HRP Quar. Prog. Rep. Jan. 1, 1953*, ORNL-1478, p. 45.

[3] L. B. Lesem to C. B. Graham, *Flow Test of Proposed ISHR Core*, ORNL CF-53-10-107 (Nov. 13, 1953).

[4] J. A. Hafford to C. B. Graham, *Two-Phase Flow in 90° Elbows*, October 7, 1953 (private communication).

[5] R. W. Lockhart and R. C. Martinelli, *Chem. Eng. Prog.* 45, 39 (1949).

[redacted]
DWG. 19538

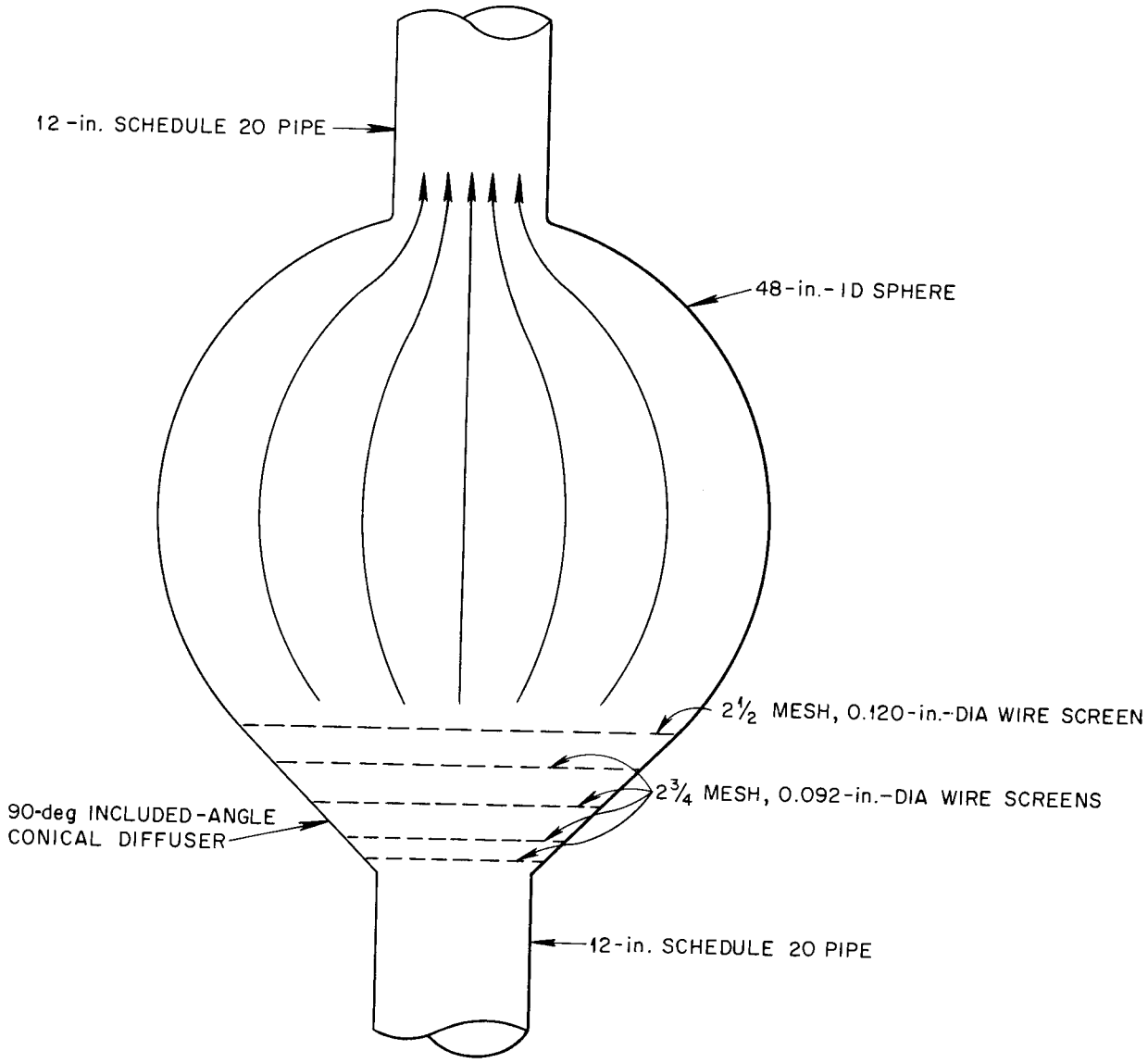

Fig. 15. ISHR Core.

system, steam and helium diluent is added to the hydrogen-oxygen mixture to make it nonexplosive, and the gases are later recombined in a catalytic recombiner (Fig. 17).

The four important points to be investigated are: the efficiency of a platinized alumina pellet catalyst at 1000 to 2000 psi and at temperatures of up to 500°C, the life of the catalyst, the ability of stainless steel to withstand operating conditions, and the safety and reliability considerations.

Entrainment Separators

In order to prevent the deposition of fissionable material in the ISHR gas system, a high-efficiency entrainment separator is required. Calculations indicate that a knitted-wire impingement separator

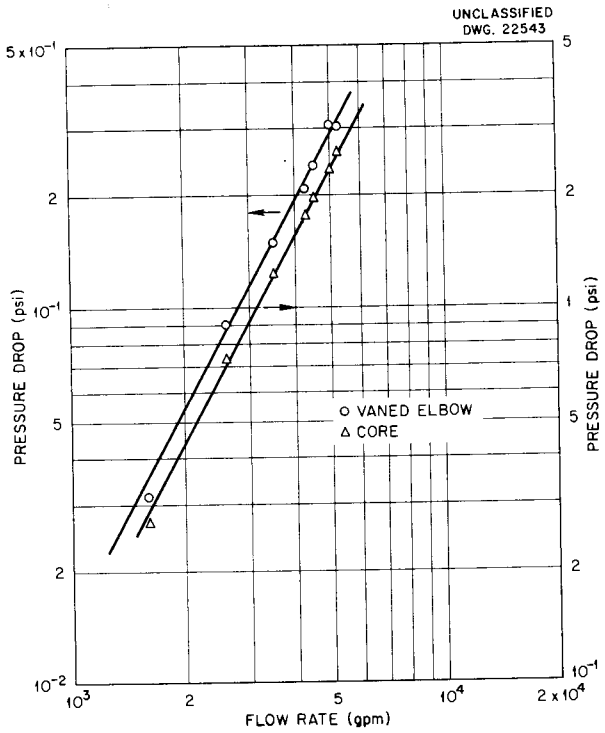

Fig. 16. Pressure Drop Through ISHR Core Model and Vaned Elbow.

of the type commonly used in the oil industry will accomplish the required separation with a very reasonable pressure drop.[6,7]

A small-scale prototype separator will be tested in a loop, parts of which are now on order. This loop will be completed in about six to ten months. The system, shown schematically in Fig. 18, simulates ISHR conditions on a smaller scale and operates at 250 to 300°C and 1000 to 2000 psia.

In the small-scale separator, uranyl sulfate solution is forced into a vapor stream by a 5-gpm ORNL pump. The two-phase mixture, simulating the gas separator product, enters a 6-in. schedule-120 pipe tangentially, and the very coarse droplets are removed. The stream then passes through 2 ft of coarse Yorkmesh and 1 ft of fine Yorkmesh. A 1-kw heater between the two types of packing simulates the reactor-gas radioactivity.[8] There is provision for continuous (or intermittent) washdown of the entrainment separator.

[6] J. A. Luker, *Determination of the Feasibility of Using a York Mesh Entrainment Separator in the I.S.H.R.*, ORNL CF-53-8-77 (Aug. 4, 1953).

[7] R. H. Wilson, *Pressure Drop Across Wire Mesh Packing*, ORNL CF-53-7-198 (July 30, 1953).

[8] I. Spiewak, *Radioactivity in the ISHR High Pressure Gas System*, ORNL CF-53-8-53 (Aug. 10, 1953).

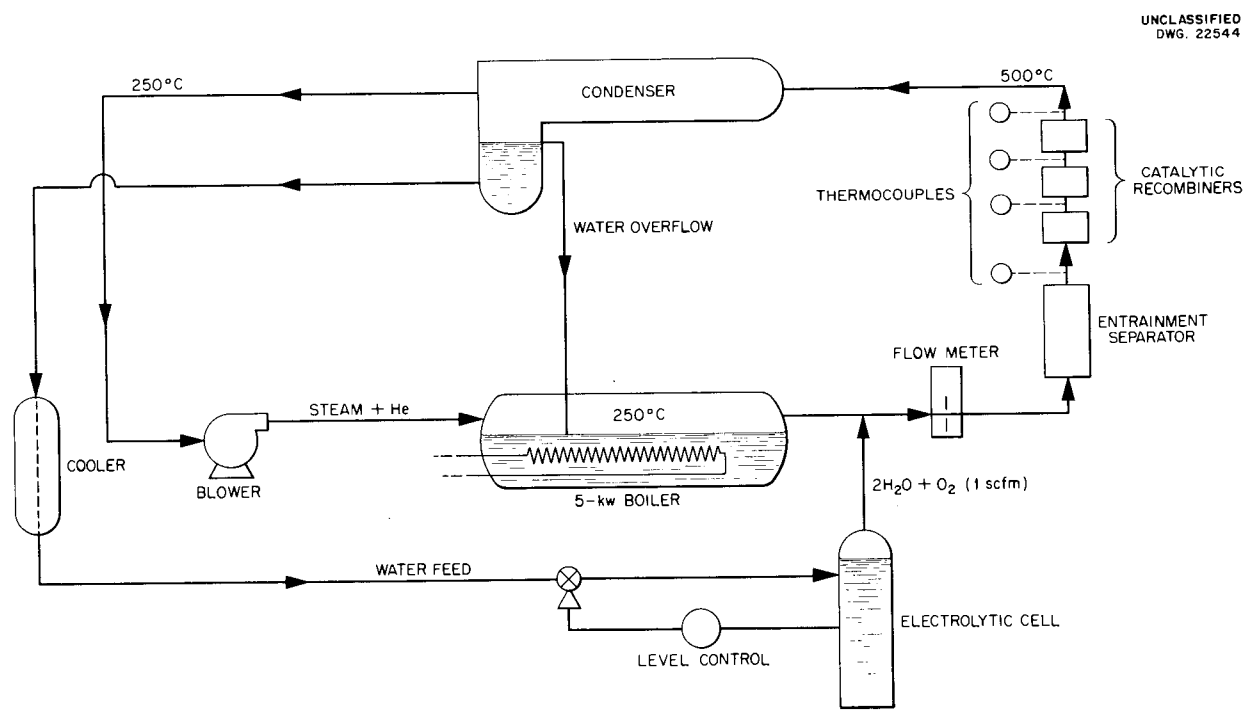

Fig. 17. 1000-psi Catalytic Recombiner Loop.

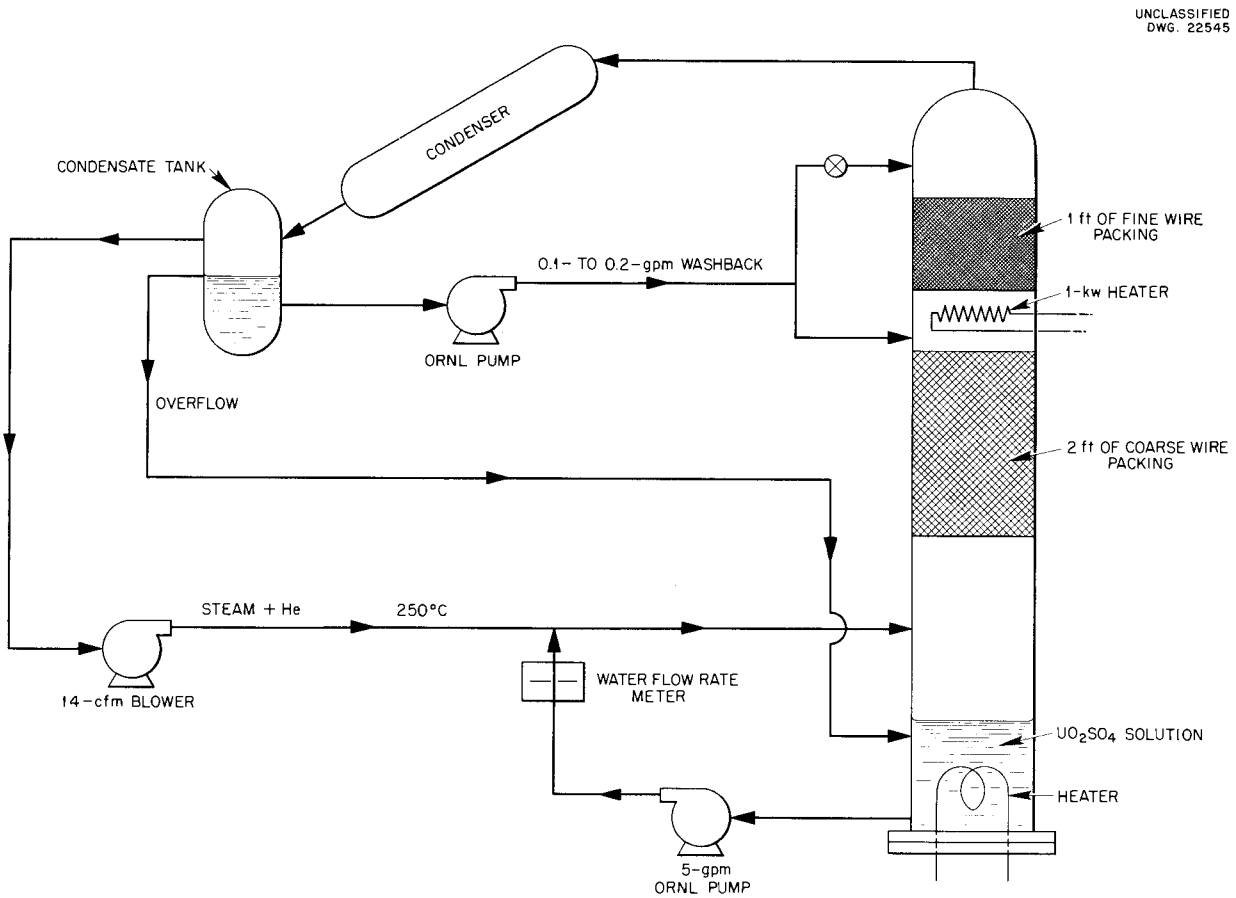

Fig. 18. Entrainment Separator Loop.

Other necessary auxiliaries in this system include a condenser for maintaining the desired temperature and a high-pressure blower for circulating the gas.

Bids for Large Components for the ISHR

Bids that cover the design, development, and fabrication of ISHR components have been received from various manufacturers. The bids were based on both 1000- and 2000-psi system pressure. The equipment involved consists of:

1. the main circulating pump[9] for 5000 gpm and 100-ft head (two bids),
2. the gas blower[10] for circulating gas through the recombiner system (four bids), and
3. the main heat exchanger[11] for the fuel system and the gas cooler[12] for the recombiner system (five bids).

MISCELLANEOUS DEVELOPMENT

4000-gpm Loop

All accessory equipment for the 4000-gpm loop is in place, and wiring of all components and instruments is complete. The placement of the 4000-gpm pump is awaiting installation of the flexible leads. The large pipe and fittings have been machined and some joints have been welded. The installation will be completed during the next quarter.

[9] W. L. Ross, *HRP Quar. Prog. Rep. July 31, 1953*, ORNL-1605, p. 56.

[10] W. L. Ross, *HRP Quar. Prog. Rep. July 31, 1953*, ORNL-1605, p. 56.

[11] L. F. Goode and W. L. Ross, *HRP Quar. Prog. Rep. July 31, 1953*, ORNL-1605, p. 58.

[12] R. B. Briggs *et al.*, *HRP Quar. Prog. Rep. July 31, 1953*, ORNL-1605, p. 42 and Fig. 20.

One of the principal reasons for building the 4000-gpm loop is to gain experience in fabricating large reactor components. In order to gain this experience, a welding program was initiated for perfecting methods and for training welders in the assembly of large piping systems. The piping in the loop is 6-, 8-, and 10-in., schedule 80, type 347 stainless steel. This piping is much larger than that encountered in the HRE and requires a new joint design and welding procedure. The weld design shown in Fig. 19 was selected after 18 different combinations were tried.

UNCLASSIFIED
DWG. 22546

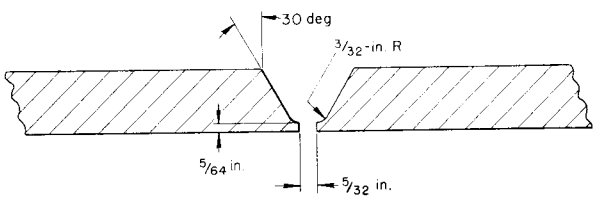

Fig. 19. Weld Design for 4000-gpm Loop Welds.

To date, sample joints have been all-heliarc welded by using a $\frac{3}{32}$-in., bare, type 347 stainless steel filler rod. An initial current of 45 amp is used for the root pass; then the current is increased as welding progresses. Currents as high as 145 amp have been used in later passes. For wall thicknesses up to $\frac{1}{2}$ in. (8-in., schedule 80), it is doubtful if filling the weld with coated rod after three or four heliarc passes is economical because of the extra cleaning required. Above $\frac{1}{2}$ in., it is planned to finish the weld with coated rod because of the much greater speed possible.

The inspection of the all-heliarc welds is limited to a final x-ray examination which must show no cracks, blowholes, or inclusions. If the weld is to be completed with coated rod, the first three heliarc passes are dye checked and x rayed to assure a perfect root weld. The completed weld will then be x rayed again.

Automatic Tube Welding

The Linde Air Products Company, Newark, New Jersey, has developed an automatic heliarc welding machine, based on a mechanically rotated arc, which appears to hold considerable promise for welding tubes to tube sheets such as those of the ISHR heat exchanger and gas condenser. Linde has agreed to make sample tube welds, in which type 347 stainless steel tubes ($\frac{3}{8}$-in. OD, 0.049-in. wall) and plate are to be used, for examination at ORNL. When fully developed, this machine may permit fully austenitic welds because of its ability to traverse the circumference of the tube at high speed. Also, a sigma-type welding head may be adapted to the machine, in the future, for adding controlled filler metal. Considerable additional development of the machine is required, but it is considered to be very promising at this time.

Worthington Corporation Pump Development

Preliminary operation of a bearing-test assembly has started at the Worthington plant. This assembly was fabricated to prove the feasibility of a 20,000-gpm pump[13,14] which utilizes a "pressure breakdown" and mechanical shaft seal. After 100 hr of operation at a bearing load of 50 psi, in which a Stellite journal and a Graphitar bearing were used, no damage was observed.

HRE Off-Gas Pump

Operation of the HRE off-gas system revealed the need for a small pump for reducing the pressure in the system and, at the same time, for overcoming the pressure drop in the charcoal absorber. This pump must be able to pump highly radioactive gas for long periods without any leakage and without maintenance.

A small $\frac{1}{4}$-hp vane pump manufactured by Lear, Incorporated was purchased and, because of its unique construction, appeared well adapted to the application. This pump, shown in Fig. 20, utilizes Graphitar vanes and end plates that require no lubrication. Rubber "O" rings both seal the end plates in the housing and supply sufficient force to maintain a seal at each end of the rotating parts. The pump end motor bearing is a sealed ball bearing and needs no lubrication. The other motor bearing is a bronze bushing which requires oiling only every 1000 hours.

The pump is not leak-free and must be enclosed in a gas-tight container to prevent the release of radioactive gases. Figure 21 shows the arrangement devised for this purpose. The motor and

[13] C. B. Graham *et al.*, *HRP Quar. Prog. Rep. July 1, 1952*, ORNL-1318, p. 112.

[14] C. B. Graham *et al.*, *HRP Quar. Prog. Rep. Oct. 1, 1952*, ORNL-1424, p. 65.

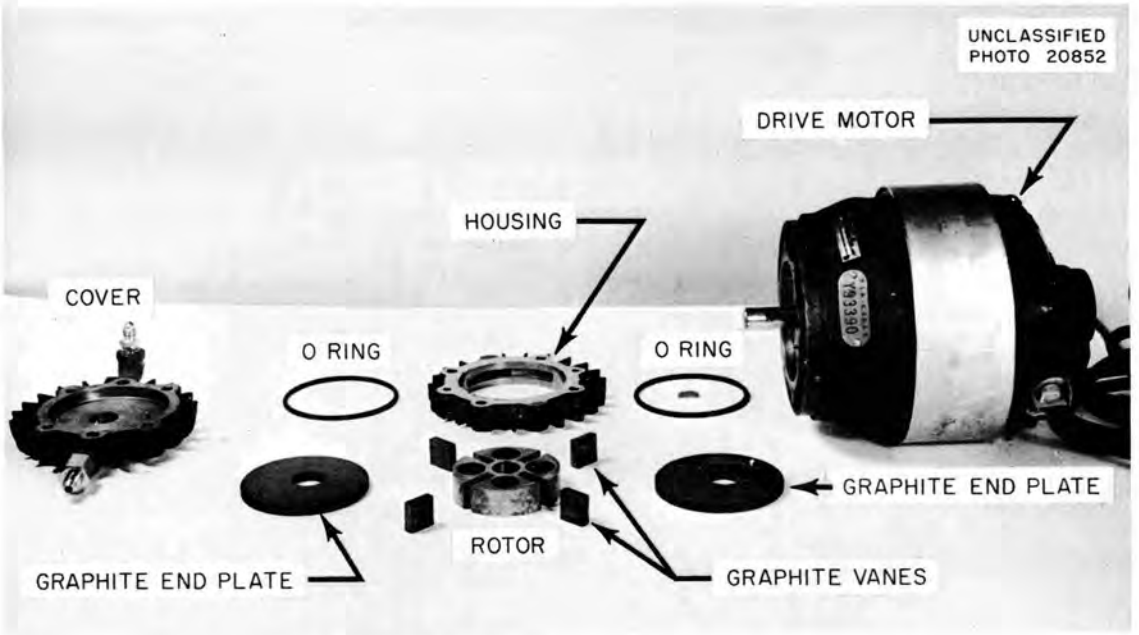

Fig. 20. Components of Lear Vane Pump.

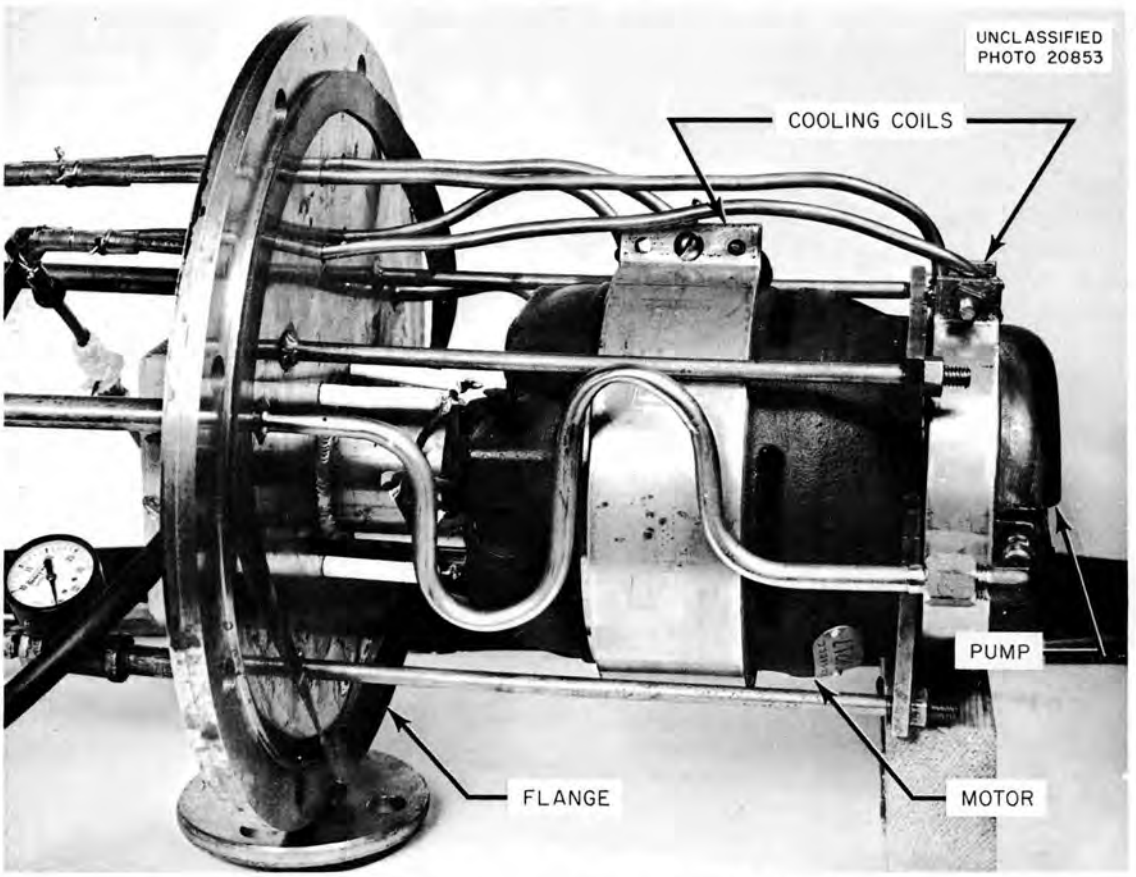

Fig. 21. Gas-Tight Container Arrangement for Lear Pump.

pump are mounted on a flange and are surrounded by water cooling coils that prevent overheating in the totally enclosed container. Since the off-gas stream is principally oxygen, the centrifugal starting switch was removed from the motor and replaced by a time-delay switch mounted outside the container. Electrical leads run through Kovar and glass seals in the flange.

As a result of measurements made on the equilibrium pressure in the container under various operating conditions, it is planned to pressurize the container with air at 7 psi, which is sufficient to assure in-leakage under all operating conditions.

Performance curves of the pump are shown in Figs. 22 and 23. Additional testing is in progress that will determine the effect of an oxygen atmosphere on the graphite parts.

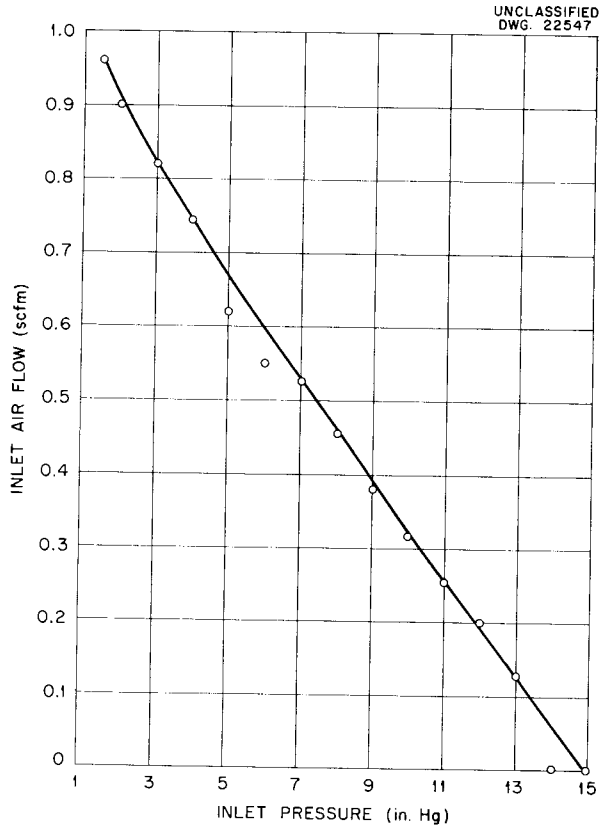

Fig. 22. Enclosed Lear Romec Pump – Capacity vs. Pressure. Discharging to atmosphere.

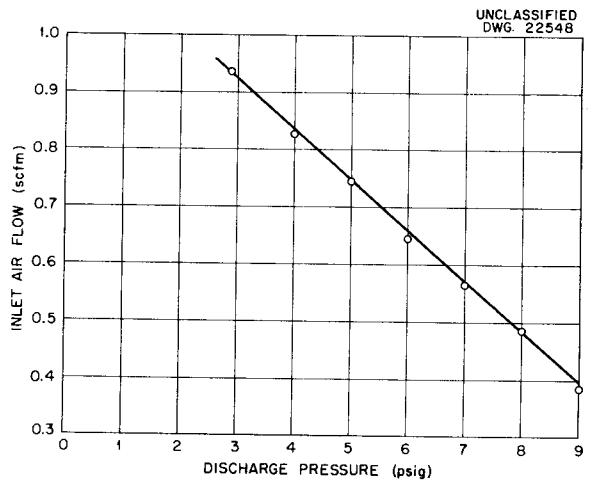

Fig. 23. Enclosed Lear Romec Pump – Capacity vs. Discharge Pressure. Suction atmospheric.

CONTROLS AND INSTRUMENTATION

J. N. Baird, Jr.
A. M. Billings
D. G. Davis
J. L. Redford
D. S. Toomb
W. P. Walker

IN-PILE CORROSION LOOP

At present, the instrumentation planned for the in-pile corrosion loop experiments will consist of three instrument boards: one for a development loop which will be operated on the mezzanine of Building 9204-1; a second for an out-of-pile loop to be operated in the loop area of the same building; and a third to be used in the LITR Building at X-10.

Identical process instrumentation is planned for each loop and will comprise eight strip-chart recorders, eight Simplytrol indicators and limiting devices, two Foxboro miniature strip-chart recorders, thirty commercial annunciator units, and a number of minor components. These instruments are either on hand or have been requisitioned. In order to maintain flexibility if process changes become necessary, the panel boards will be constructed from the standard modular panels and frames developed by the ORNL Instrument Department.

A separate 6-ft relay cabinet containing four single electrometers, a scintillation counter, and count-rate and radiation-alarm circuits will be provided for the in-pile loop. This equipment and the accompanying ion chambers are being built in the Circuit Construction Section of the ORNL Instrument Department.

Weston thermal converters are being used to measure the power consumed by the canned-rotor pump motor and one of the component heaters in each loop. The claimed accuracy for these devices is 1%, despite rather wide fluctuations in power factor and supply voltage. The converters supply millivoltage output which can be fed to simple indicating millivoltmeters or recording potentiometers containing numerous alarm switches.

The panel design is complete, and one set of panels has been constructed and delivered. Interlock and safety circuits have been completed, and relay chassis for two loops are under construction.

ALLIS-CHALMERS PUMP TEST LOOP

A loop has been constructed for determining operating characteristics of the in-pile loop design and for obtaining performance data on the Allis-Chalmers canned-rotor pump. The instrumentation provided adhered, as much as possible, to the present proposed design for in-pile experiments. A rather novel feature included on the panel board is an interlock panel. All protective interlock switch contacts which were provided to actuate alarms or shut-down equipment were wired to this panel and connected to jacks. A pilot light was installed between each pair of jacks to indicate the open or closed position of these contacts. If the operator needs to bypass any safety circuit temporarily, a "jumper" is plugged into the jacks corresponding to that interlock. The presence of the "jumper" is obvious at all times on the front of the panel board, and the pilot light indicates the position of the "jumpered" contacts.

ISHR CONTROL VALVES

Preliminary inquiries concerning construction of special control valves for the ISHR were sent to prospective manufacturers. Figure 24, illustrating the general type of construction visualized for these valves, was sent to the valve manufacturers, along with tentative requirements and specifications.

The following companies expressed a definite interest in the valve problem for the ISHR and will submit preliminary designs and approximate prices:

Hammel-Dahl Company
The Annin Company
Associated Valve and Engineering Company
Hoppe Engineering Company

CONDUCTIVITY TRANSIENT-MEASURING SYSTEM FOR FLOW STUDIES

A conductivity transient-measuring system utilizing probes fabricated into $\frac{1}{4}$-in. stainless steel tubing was designed and constructed for the hydrodynamics group as an instrument for indicating the pattern of flow in liquid systems.

The measuring scheme utilized the oscillator-amplifier-phase sensitive demodulator unit from a Foxboro Company dynalog recorder as the bridge supply source, signal amplifier, and unbalance detector. This unit was also self-powered.

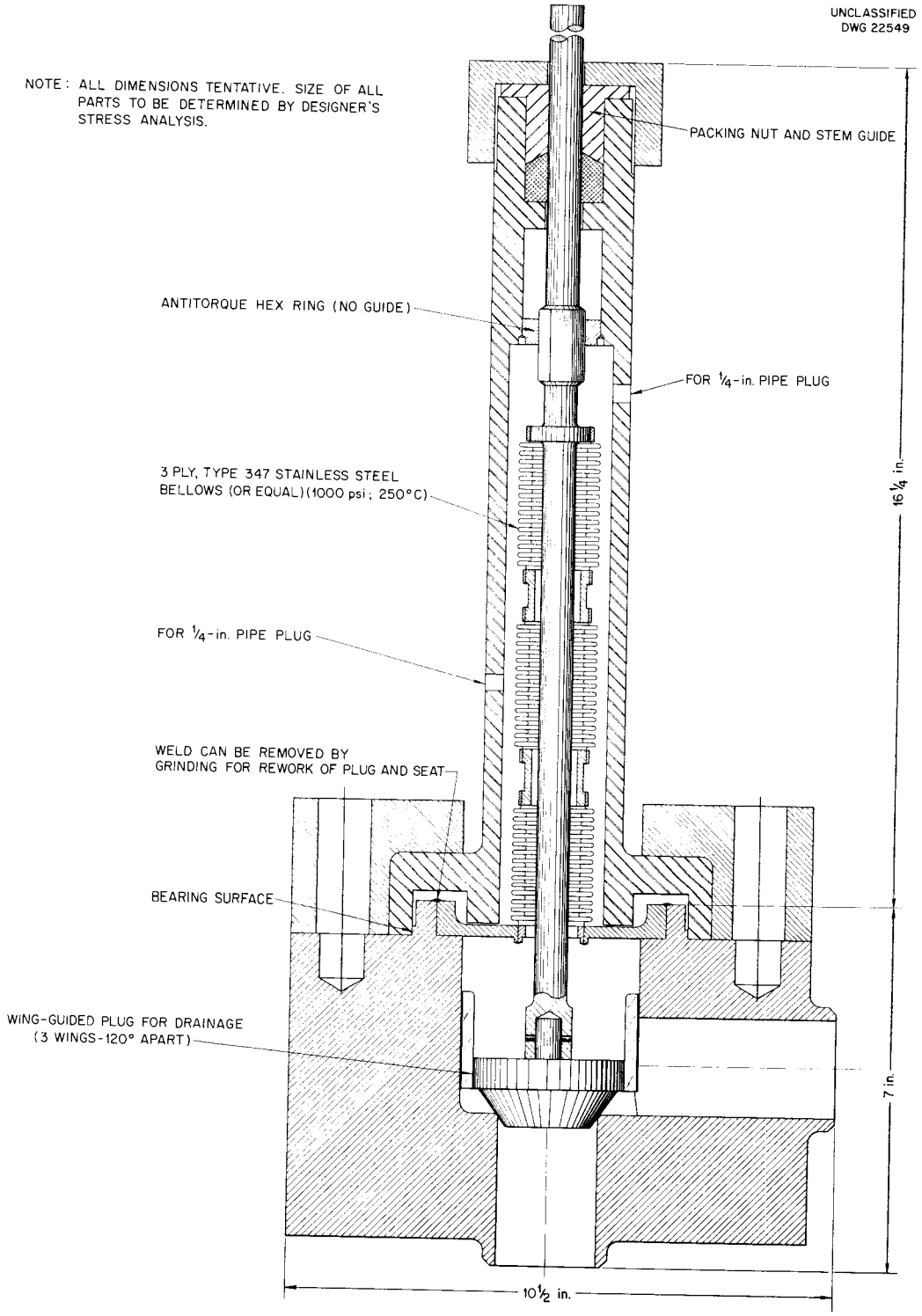

Fig. 24. ISHR Control Valve.

The conductivity probes were connected as one leg of a resistance bridge circuit; conductivity changes thus unbalanced the bridge and were detected by the Foxboro unit and recorded by a Brush oscillograph. Polarization effects were avoided by the use of low voltage, a high cell resistance, and a high frequency supply – 1000 cps – as supplied by the oscillator in the Foxboro chassis.

PRELIMINARY SALT LOOP MOCKUP INSTRUMENTATION

A flow-control unit mounted in a portable cabinet has been completed and is now in use with a preliminary salt loop mockup.

The function of the unit is to control and reverse the flow of liquid through corrosion samples that are inserted in a line connecting two similar containers of equal volume and extending the same depth into each. The control and reversal of the flow are accomplished pneumatically with air-pressure regulators, timers, and three-way solenoid valves.

EXPERIMENTAL STRESS ANALYSIS OF ISHR CORE TANK

Strain gages and Baldwin strain indicators have been provided for experimental stress analysis of the ISHR core tank. A special switch box has been constructed which permits either summing the stresses of tension and compression gages or reading the outputs of each gage separately with compensation.

CORROSION

E. G. Bohlmann, Section Chief

DYNAMIC CORROSION TESTS

Pump Loop Operation and Maintenance

H. C. Savage F. J. Walter
R. A. Lorenz

Thirteen dynamic-corrosion test loops are now in operation. In order to evaluate the effects of temperature, velocity, uranyl sulfate concentration, dissolved oxygen concentration, and time on the rate of corrosion, a large number of relatively short term (50- to 400-hr) runs are being made.

One long-term run in loop B was terminated after 4500 hr of continuous operation. The circulating solution in this run was uranyl sulfate solution containing 5 g of uranium per liter with 0.005 M sulfuric acid added for solution stability. The operating conditions were a temperature of 250°C, a pressure of 1000 psig, and an oxygen concentration that ranged from 500 to 2000 ppm. Loop B contained a number of welded connections and fabricated (forged) fittings that were intended for qualitative evaluation of corrosion damage in these areas of high turbulence. A visual inspection at several tees and bends showed no corrosion damage. The interior pipe surfaces had a thin, tightly adhering film similar to that in the previously described[1] loop K. The upper section of loop B, containing the welded connections and fabricated fittings, was removed and installed in loop K for additional operation under the same conditions as in loop B.

[1]H. C. Savage, R. A. Lorenz, and F. J. Walter, *HRP Quar. Prog. Rep. July 31, 1953*, ORNL-1605, p. 68 and Fig. 34.

Loop B has now been reworked in order to provide facilities for continuous-addition studies. Present plans are to add various substances at a controlled rate to the circulating solution via a Lapp CPS-1 pulsafeeder while the loop is at operating conditions and to attempt to follow the additive or its effect by sampling and specimen observation.

During this quarter, loop A was dismantled to make room for a loop in which higher temperature studies are projected. Loop A had been in operation for 5200 hr on a number of relatively short-term runs. The operating conditions for loop A are summarized in Table 6. The interior surfaces of the 1½-in., schedule 80, type 347 stainless steel pipe were found to be in good condition in spite of the relatively rigorous operating conditions. Even at sections of relatively high turbulence, such as tees, little serious damage was noted (see Figs. 25 and 26). The flow rate in the pipe sections varied between 10 and 20 fps.

Loop A has now been rebuilt to include three sample holders in a design similar to that of loop M.[2] This will allow simultaneous exposure of sample specimens to both high (~80 fps) and low (10 to 20 fps and below) flow rates. Loop A also has provisions for continuous addition of hydrogen and oxygen during operation. The loop is totally enclosed by a metal and plywood shield and will be used in studying the temperature range of 275 to 325°C.

[2]E. G. Bohlman *et al.*, *HRP Quar. Prog. Rep. March 15, 1952*, ORNL-1280, p. 45.

TABLE 6. OPERATING CONDITIONS FOR LOOP A

CIRCULATING SOLUTION	TIME (hr)	TEMPERATURE (°C)	DISSOLVED GAS
UO_2SO_4 – 300 g of uranium per liter	770	250	Oxygen + hydrogen
UO_2SO_4 – 40 g of uranium per liter	2400	250	Oxygen
	300	275	Oxygen
	520	300	Oxygen
UO_2SO_4 – 15 g of uranium per liter + 25 mole % H_2SO_4	770	250	Oxygen

UNCLASSIFIED
PHOTO 20858A

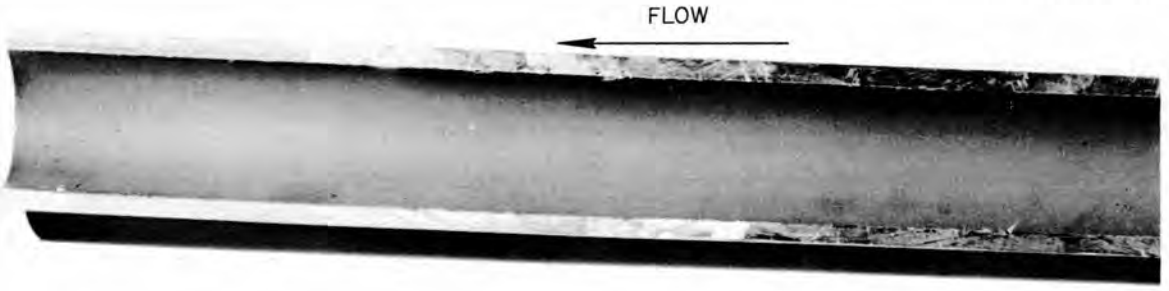

Fig. 25. Pipe Section, Loop A.

UNCLASSIFIED
PHOTO 20858B

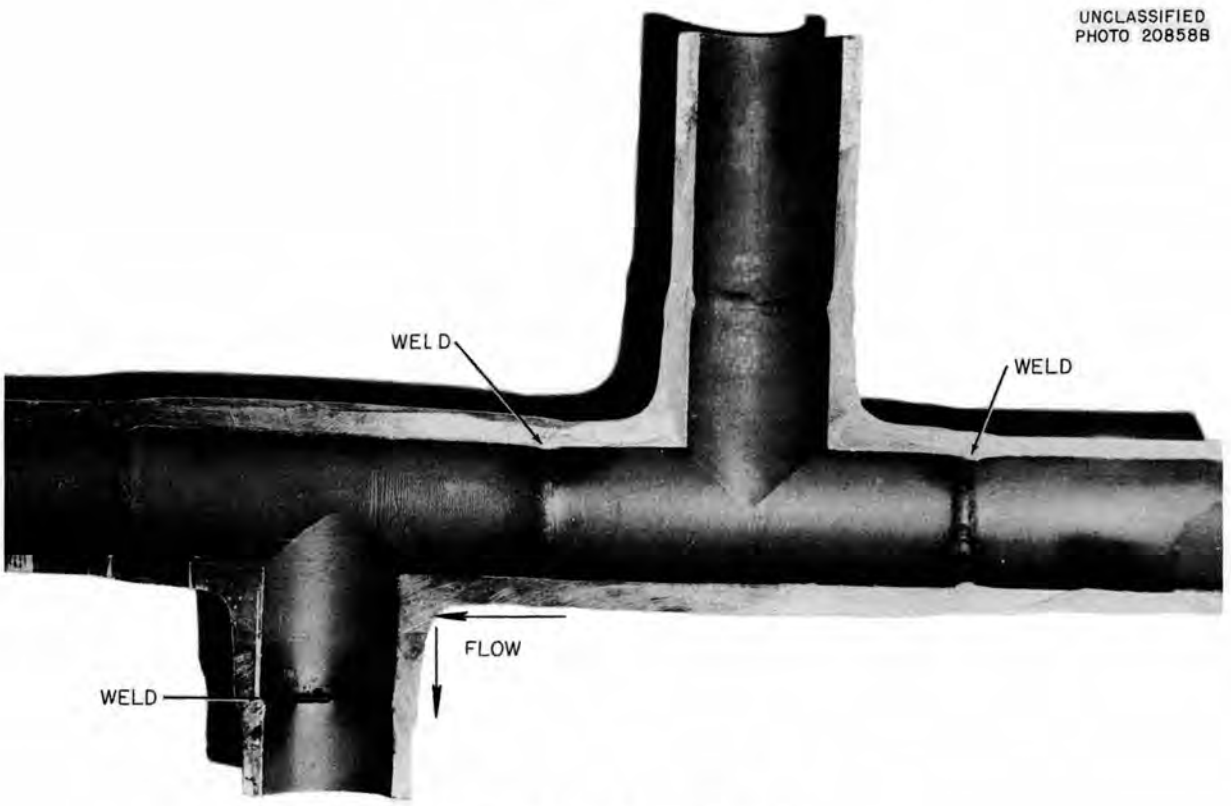

Fig. 26. Forged Tees, Loop A.

A new pressurizer that replaces the gas separating pressurizer which proved unsatisfactory was installed in loop F during this quarter. The new pressurizer is identical to those on all other loops. Operation of this loop has been confined to tests on the in-pile corrosion test units. The tests have been conducted at 250°C with uranyl sulfate solutions containing 40 g of uranium per liter with 0.01 *M* Cu^{++}. In each test, standard pin-type and tapered-coupon units have been installed in the

loop along with the in-pile units so that a direct comparison could be made. Results of these tests are given in the section "Loop Test Results."

Titanium Loop. The all-titanium loop, G, is now back in operation. The titanium impeller previously used in loop A was defilmed and installed when loop A was dismantled. Loop G is now operating at a temperature of 250°C, a pressure of 1000 psi of oxygen, and with a uranyl sulfate solution containing 5 g of uranium per liter with 0.005 M sulfuric acid. Pin-type corrosion specimens of Zircalloy II and titanium and Zircalloy II specimens machined for impact testing are included in the present run. Present plans are to terminate this run after 1000 hr of continuous operation.

HRE Mockup. A repaired remote pulsafeeder head was installed in the HRE mockup to replace the one in which a leak through the diaphragm had occurred, as was reported previously.[3] After approximately 300 additional hours of operation was accumulated, it was discovered that the remote pulsafeeder head was again leaking through the stainless steel diaphragm. When the head was removed and cut open, it was found that the 0.019-in.-thick stainless steel diaphragm had cracked; therefore a new diaphragm was installed and the remote head put back into the mockup.

On the startup of run M-15, it was observed that there was excessive leakage through the let-down valve. The leakage rate was about 0.5 gpm at less than 20 psig system pressure. At approximately 200 psig system pressure, the leakage through the let-down valve was equal to the output of the pulsafeeder (~1 gpm).

The valve seat and plug were removed, and it was found that a hole had been channeled around the seat in the fusion zone between the weld-deposited Stellite 6 seat and the type 347 stainless steel base metal; thus the valve seat was bypassed. A considerable amount of Stellite had been removed (see Fig. 27). Visually, the valve plug appeared to be in good condition (see Fig. 28). The trim in this valve was obtained from the Hammel-Dahl Valve Company. The plug is Stellite 6 with a Stellite-coated stainless steel guide stem. Visually, the Stellite 6 seat material appeared to be very porous, as did the Stellite coating on the guide stem, although the actual seating areas of the seat and plug were in good condition.

[3]H. C. Savage, R. A. Lorenz, and F. J. Walter, *HRP Quar. Prog. Rep. July 31, 1953*, ORNL-1605, p. 73.

Fig. 27. Seat Assembly of Let-Down Valve.

The operating history of the let-down valve is shown in Table 7. The temperature of the solution through the let-down valve varied between 80 and 85°C under all the operating conditions shown in Table 7. The pieces have been turned over to the Metallurgical Group for further examination.

New valve trim obtained from the Hammel-Dahl Valve Company has now been installed in the mockup let-down valve. This trim consists of a solid Stellite 12 seat and a Stellite 6 plug with Stellite 6 weld overlay on the guide stem. X-ray pictures and Rockwell hardness readings of this new trim were obtained before installation.

TABLE 7. OPERATING HISTORY OF LET-DOWN VALVE

TIME (hr)	SOLUTION IN MOCKUP	OPERATING TEMPERATURE (°C)
320	Water	100 to 250
25	3% Trisodium phosphate	150
7	5% Nitric acid	100
2000	Uranyl sulfate (20 to 40 g of uranium per liter)	200 to 250

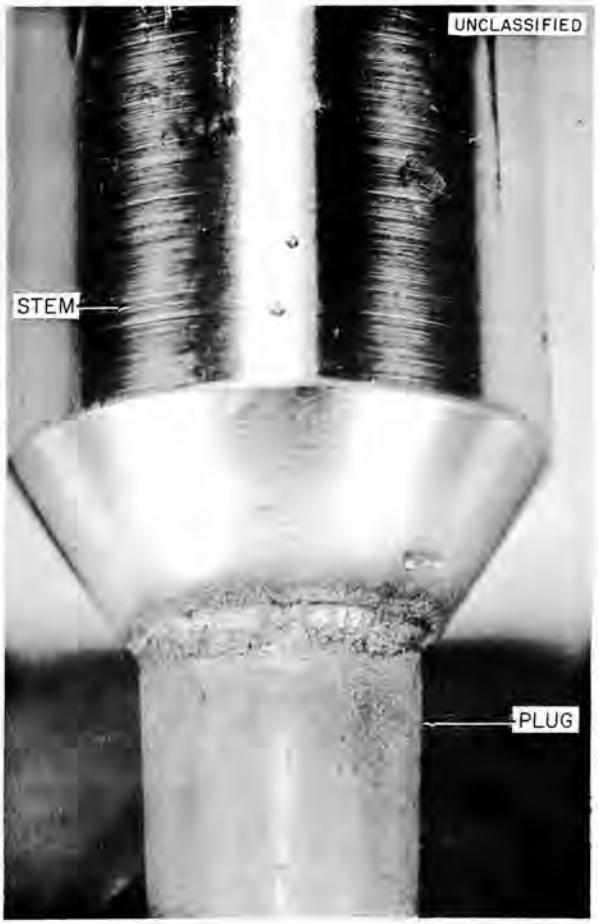

Fig. 28. Plug and Guide Stem of Let-Down Valve.

Westinghouse Model 100-A Pumps. The Westinghouse model 100-A pumps used in the dynamic test loops are now operating satisfactorily with no serious difficulties. A routine inspection of the bearings and a check of the hydraulic thrust balance[2] are made during periods of shutdown on individual loops. Installation of new bearings and/or adjustments of the hydraulic thrust balance are made when required.

Replacement impellers for the model 100-A pumps are now being made of titanium because of its increased corrosion resistance. To date two titanium impellers have been made and have been placed in service. Material for three additional impellers is now in the shop.

[4] J. C. Griess, J. M. Ruth, and R. E. Wacker, *HRP Quar. Prog. Rep. Jan. 1, 1953*, ORNL-1478, p. 63.

[5] J. C. Griess and R. E. Wacker, *HRP Quar. Prog. Rep. March 31, 1953*, ORNL-1554, p. 49.

Loop Test Results

J. C. Griess R. E. Wacker

Previous reports[4,5,6] have given information about the effect of several variables such as flow rates, uranium and oxygen concentrations, and time and temperature on the corrosion of austenitic stainless steels by uranyl sulfate solutions. During the past quarter, additional data have been collected which, among other things, show that at 200 and 225°C corrosion damage at all velocities can be quite high since an oxide coating which prevents further oxidation does not form. At temperatures in the range 250 to 300°C where a protective film forms, corrosion damage to austenitic steels is negligible at low velocities; but at high velocities, where the film is not stable, the corrosion rate is appreciably higher.

During the past quarter, a run in which dilute uranyl sulfate was circulated at 250°C was terminated after 4400 hr of uninterrupted operation. The extent of corrosion damage was very small, and the experiment has borne out previous data which showed that the corrosion rate is negligible after the first few hundred hours of operation. In addition, a number of other experiments have been completed during the past quarter, and these and all other data are reported in the sections which follow.

General Corrosion Rates. In the last three quarterly reports,[4,5,6] extensive tables were given which showed the results of the pins tested in the corrosion test loops. In this report, Table 8 shows the results obtained from the pin-type specimens during the past quarter. As in previous reports, the corrosion rates are given in mils per year (mpy) and are based on the weight of metal oxidized. The oxide scales formed during the corrosion process were removed before the final weighing of the pins. It is again pointed out that the corrosion rates as reported are average rates for the entire exposure time and that corrosion is not a constant-rate process at low flow rates. Hence discretion must be used in interpreting the data.

In addition to the pins listed in Table 8, a large number of metallurgically treated pins have been tested in the dynamic test loops. After test, these specimens were given to the HRP Metallurgy Group for examination, and the results of their study will be reported by that group.

[6] J. C. Griess and R. E. Wacker, *HRP Quar. Prog. Rep. July 31, 1953*, ORNL-1605, p. 74.

TABLE 8. SUMMATION OF CORROSION RESULTS OF PIN-TYPE SPECIMENS

RUN NO.	TEST CONDITIONS						PIN MATERIAL	NO. OF PINS	CORROSION RATE (mpy)		
	Solution	Uranium Concentration (g/l)	Temperature (°C)	Time (hr)	Additions	Flow Rate (fps ± 10%)			Minimum	Average	Maximum
A-53	UO_2SO_4	40	250	199	1000 to 2000 ppm O_2	2[a]	Type 304 ELC stainless steel	7	2.4	3.0	3.5
							Type 347 stainless steel	7	3.5	4.4	6.2
						55[a]	Type 304 ELC stainless steel	7	91	110	130
							Type 347 stainless steel	7	94	100	110
A-54	UO_2SO_4	40	275	106	1000 to 2000 ppm O_2	13	Type 304 ELC stainless steel	3	23	30	42
							Type 347 stainless steel	4	24	28	30
							Titanium, Ti-75A	1		0	
							Zirconium, crystal bar	2	0.3	0.4	0.5
							Zirconium–2.5% tin	1		0	
							Zircalloy II	2[b]		0.6	
						56	Type 304 ELC stainless steel	4	310	330	340
							Type 347 stainless steel	4	320	340	400
							Titanium, Ti-75A	1		0	
							Zirconium, crystal bar	2[b]		1.1	
							Zirconium–2.5% tin	1		0.5	
							Zircalloy II	2[b]		0.2	
A-55	UO_2SO_4	40	275	200	1000 to 2000 ppm O_2	13	Type 304 ELC stainless steel	4	13	14	16
							Type 347 stainless steel	4	4.3	12	16
							Platinum	1		0.2	
							Zirconium, crystal bar	2[b]		0.3	
							Zirconium–2.5% tin	1[b]			
							Zircalloy II	2[b]		0.1	
						70	Type 304 ELC stainless steel	4	350	400	530
							Type 347 stainless steel	4	350	480	530
							Platinum	1		2.1	
							Zirconium, crystal bar	2[b]		1.2	
							Zirconium–2.5% tin	1		0.8	
							Zircalloy II	2[b]		0.7	
A-56	UO_2SO_4	40	300	100	1000 to 2000 ppm O_2	14	Type 304 ELC stainless steel	4	7.3	9.2	13
							Type 347 stainless steel	4	7.5	9.8	12
							Plotinum	1		2.1	
							Titanium, RC-55	1		0.2	
							Zirconium, crystal bar	2	0	0	0
							Zircalloy II	2	0	0	0
						70	Type 304 ELC stainless steel	4	530	560[c]	600
							Type 347 stainless steel	4	570	580[c]	580
							Platinum	1		1.4	
							Titanium, RC-55	1		0.7	
							Zirconium, crystal bar	2	0	0	0
							Zircalloy II	2	0	0	0
A-57	UO_2SO_4	40	300	403	1000 to 2000 ppm O_2	14	Type 304 ELC stainless steel	4	2.4	2.8	3.5
							Type 347 stainless steel	4	1.4	2.8	3.6
							Titanium, RC-55	1		0.2	
							Zirconium, crystal bar	1[b]			
							Zirconium–2.5% tin	1[b]			
							Zircalloy II	3[b]			

TABLE 8. (continued)

RUN NO.	TEST CONDITIONS						PIN MATERIAL	NO. OF PINS	CORROSION RATE (mpy)		
	Solution	Uranium Concentration (g/l)	Temperature (°C)	Time (hr)	Additions	Flow Rate (fps ± 10%)			Minimum	Average	Maximum
A-57	UO_2SO_4	40	300	403	1000 to 2000 ppm O_2	71	Type 304 ELC stainless steel	4	65	84	100
							Type 347 stainless steel	4	52	130	180
							Titanium, RC-55	1		0.8	
							Zirconium, crystal bar	1		0.2	
							Zirconium–2.5% tin	1		0.3	
							Zircalloy II	3	0	0.2	0.3
B-26	UO_2SO_4	5	250	4404	1000 to 2000 ppm O_2, 0.005 M H_2SO_4	11 to 16	Type 304 ELC stainless steel	4	0.13	0.16	0.17
							Type 347 stainless steel	4	0.16	0.22	0.34
							Type 347 stainless steel[d]	2	0.14	0.17	0.20
							Type 347 stainless steel[e]	2	0.16	0.20	0.23
							Type 316 stainless steel	2	0.17	0.18	0.18
							Type 316 stainless steel[e]	2	0.17	0.21	0.24
							Type 316 ELC stainless steel	2	0.19	0.21	0.22
							Type 321 stainless steel	4	0.20	0.23	0.24
							Worthite[e]	2	1.5	1.5	1.5
							FA-20[e]	2	0.36	0.41	0.45
							Titanium, RC-70	2[b]			
							Zirconium–2.5% tin	2[b]			
B-28	UO_2SO_4	40	275	50	1000 to 2000 ppm O_2	13	Type 304 ELC stainless steel	6	17	29	40
							Type 347 stainless steel	5	20	37	45
							Platinum	1		0	
							Zirconium, crystal bar	1[b]			
							Zircalloy II	1[b]			
						75	Type 304 ELC stainless steel	6	250	270	290
							Type 347 stainless steel	5	260	270	280
							Platinum	1		0	
							Zirconium, crystal bar	1[b]			
							Zircalloy II	1[b]			
C-31	UO_2SO_4	5	250	200	1000 to 2000 ppm O_2, 50 ppm HF	9 to 13	Type 304 ELC stainless steel	4	0.51	0.70	0.94
							Type 347 stainless steel	4	0.68	0.96	1.4
							Titanium, RC-70	2	0	0	0
							Titanium, Ti-75A	2	0	0	0
							Titanium, Ti-100A	2	0	0	0
							Zirconium, crystal bar	4	0	0	0
							Zirconium–2.5% tin	4	0	0	0
							Zircalloy II	4	0	0	0
D-6	UO_2SO_4	10	250	100	1000 to 2000 ppm O_2, 0.006 M H_2SO_4	14	Type 304 ELC stainless steel	4	7.3	9.1	11
							Type 347 stainless steel	4	8.7	11	15
							Type 321 stainless steel	4	9.7	10	12
							Zirconium, crystal bar	1		0	
							Zirconium–2.5% tin	1		0	
						75	Type 304 ELC stainless steel	4	89	92	97
							Type 347 stainless steel	4	70	84	89
							Type 321 stainless steel	4	85	90	100
							Zirconium, crystal bar	1		1.6	
							Zirconium–2.5% tin	1		0.9	

TABLE 8. (continued)

RUN NO.	TEST CONDITIONS						PIN MATERIAL	NO. OF PINS	CORROSION RATE (mpy)		
	Solution	Uranium Concentration (g/l)	Temperature (°C)	Time (hr)	Additions	Flow Rate (fps ± 10%)			Minimum	Average	Maximum
D-7	UO_2SO_4	10	250	200	1000 to 2000 ppm O_2, 0.006 *M* H_2SO_4	14	Type 304 ELC stainless steel	4	6.3	7.0	7.7
							Type 347 stainless steel	4	7.7	8.7	9.6
							Type 321 stainless steel	4	3.8	7.5	9.5
							Zirconium, crystal bar	1		0	
							Zirconium–2.5% tin	1		0	
						75	Type 304 ELC stainless steel	4	84	85	86
							Type 347 stainless steel	4	86	87	90
							Type 321 stainless steel	4	78	82	87
							Zirconium, crystal bor	1		0	
							Zirconium–2.5% tin	1		0	
D-8	UO_2SO_4	10	250	51	1000 to 2000 ppm O_2, 0.006 *M* H_2SO_4	14	Type 304 ELC stainless steel	6	20	23	28
							Type 347 stainless steel	6	20	23	30
							Zirconium, crystal bar	1		0.3	
							Zirconium–2.5% tin	1		0.3	
						75	Type 304 ELC stainless steel	6	64	73	100
							Type 347 stainless steel	6	66	69	73
							Zirconium, crystal bar	1		0.7	
							Zirconium–2.5% tin	1		0.7	
D-9	UO_2SO_4	40	250	96	1000 to 2000 ppm O_2	39	Type 304 ELC stainless steel	3	140	140	140
							Type 347 stainless steel	3	79	96	110
						52	Type 304 ELC stainless steel	3	66	130	160
							Type 347 stainless steel	3	100	120	150
D-10	UO_2SO_4	40	250	24	1000 to 2000 ppm O_2, 40 ppm Zr, 14 ppm Nb, 0.04 *M* H_2SO_4	39	Type 304 ELC stainless steel	1		230	
							Type 347 stainless steel	2	240	320	390
						52	Type 304 ELC stainless steel	1		230	
							Type 347 stainless steel	2	270	320	360
D-11	0	0	85	4	200 psi He, 1.0 *M* HCl, 1.4 *M* H_2SO_4, 0.2 *M* H_2O_2, Inhibitor	39	Type 304 ELC stainless steel	2	2300	2500	2600
							Type 322W stainless steel[f]	1		4300	
							Type 17-4 PH stainless steel[f]	1		1700	
							Inconel X	1		1400	
							Stellite 6	1		510	
						52	Type 304 ELC stainless steel	2	2600	5700	8800
							Type 17-4 PH stainless steel[f]	1		2600	
							Inconel X	1		1600	
							Stellite 6	1		520	
							Stellite 98M2	1		580	
D-14	UO_2SO_4	10	250[g]	200	1000 to 2000 ppm O_2, 0.006 *M* H_2SO_4	17	Type 304 ELC stainless steel	5	1.6	1.8	2.0
							Type 347 stainless steel	5	1.9	2.2	2.6
							Type 321 stainless steel	1		2.0	
							Type 309 SCb stainless steel	1		2.1	
							Platinum	1		0.7	
							Zircalloy II			0	

TABLE 8. (continued)

RUN NO.	TEST CONDITIONS						PIN MATERIAL	NO. OF PINS	CORROSION RATE (mpy)		
	Solution	Uranium Concentration (g/l)	Temperature (°C)	Time (hr)	Additions	Flow Rate (fps ± 10%)			Minimum	Average	Maximum
D-14	UO_2SO_4	10	250[g]	200	1000 to 2000 ppm O_2, 0.006 M H_2SO_4	73	Type 304 ELC stainless steel	5	4.6	18	38
							Type 347 stainless steel	4	36	46	60
							Type 321 stainless steel	1		40	
							Type 309 SCb stainless steel	1		16	
							Platinum	1		0.9	
							Zircalloy II	1		0	
E-10	UO_2SO_4	5	250	100	1000 to 2000 ppm O_2, 0.005 M H_2SO_4	10 to 13	Type 304 ELC stainless steel	4	1.9	2.3	2.7
							Type 347 stainless steel	4	2.6	3.1	3.6
							Type 321 stainless steel	4	1.7	2.4	2.9
						77	Type 304 ELC stainless steel	2	3.9	6.2	8.5
							Type 347 stainless steel	2	30	32	34
							Type 321 stainless steel	2	28	30	31
E-11	UO_2SO_4	5	250	200	1000 to 2000 ppm O_2, 0.005 M H_2SO_4	10 to 13	Type 304 ELC stainless steel	4	0.51	0.83	1.1
							Type 347 stainless steel	4	0.68	0.88	1.0
							Type 321 stainless steel	4	0.51	0.99	1.4
						77	Type 304 ELC stainless steel	2	1.7	1.7	1.7
							Type 347 stainless steel	2	2.6	3.0	3.4
							Type 321 stainless steel	2	2.6	5.3	7.9
E-10 and E-11	UO_2SO_4	5	250	300	1000 to 2000 ppm O_2, 0.005 M H_2SO_4	10 to 13	Type 304 ELC stainless steel	4	0.62	0.74	0.80
							Type 347 stainless steel	4	1.0	1.0	1.1
							Type 321 stainless steel	4	1.0	1.1	1.3
							Titanium, RC-70	2	0.06	0.13	0.20
							Zirconium, crystal bor	2	0	0	0
						77	Type 304 ELC stainless steel	2	2.7	3.0	3.2
							Type 347 stainless steel	1		7.8	
							Type 321 stainless steel	2	13	17	21
							Titanium, RC-70	1		0.2	
							Zirconium–2.5% tin	1		0	
E-12	UO_2SO_4	5	250	102	1000 to 2000 ppm O_2, 0.01 M H_2SO_4	10 to 13	Type 304 ELC stainless steel	4	1.8	3.7	5.0
							Type 347 stainless steel	4	4.3	4.7	5.5
							Type 321 stainless steel	4	2.8	4.7	5.7
						77	Type 304 ELC stainless steel	2	18	21	33
							Type 347 stainless steel	2	14	37	60
							Type 321 stainless steel	2	58	63	67
E-13	UO_2SO_4	5	250	200	1000 to 2000 ppm O_2, 0.01 M H_2SO_4	10 to 13	Type 304 ELC stainless steel	4	1.8	3.5	4.2
							Type 347 stainless steel	4	2.6	3.9	5.4
							Type 321 stainless steel	4	2.1	3.5	4.8
						77	Type 304 ELC stainless steel	2	36	38	40
							Type 347 stainless steel	2	35	37	38
							Type 321 stoinless steel	2	46	57	68
E-12 and E-13	UO_2SO_4	5	250	302	1000 to 2000 ppm O_2, 0.01 M H_2SO_4	10 to 13	Type 304 ELC stainless steel	4	0.95	1.5	1.9
							Type 347 stainless steel	4	1.7	1.8	1.9
							Type 321 stainless steel	4	0.84	1.7	2.4
							Titanium, RC-70	2	0	0	0
							Zirconium, crystal bar	2	0	0	0

TABLE 8. (continued)

RUN NO.	TEST CONDITIONS						PIN MATERIAL	NO. OF PINS	CORROSION RATE (mpy)		
	Solution	Uranium Concentration (g/l)	Temperature (°C)	Time (hr)	Additions	Flow Rate (fps ± 10%)			Minimum	Average	Maximum
E-12 and E-13	UO_2SO_4	5	250	302	1000 to 2000 ppm O_2, 0.01 M H_2SO_4	77	Type 304 ELC stainless steel	2	6.5	8.3	10
							Type 347 stainless steel	2	14	16	17
							Type 321 stainless steel	1		35	
							Titanium, RC-70	1		0	
							Zirconium–2.5% tin	1		0	
E-14	UO_2SO_4	5	250	102	1000 to 2000 ppm O_2, 0.016 M H_2SO_4	14 to 16	Type 304 ELC stainless steel	4	11	12	13
							Type 347 stainless steel	4	11	12	15
							Type 321 stainless steel	4	13	14	15
						77	Type 304 ELC stainless steel	2	88	92	95
							Type 347 stainless steel	2	94	95	95
							Type 321 stainless steel	1		94	
E-15	UO_2SO_4	5	250	200	1000 to 2000 ppm O_2, 0.016 M H_2SO_4	14 to 16	Type 304 ELC stainless steel	4	1.8	3.4	5.1
							Type 347 stainless steel	4	4.2	5.3	6.1
							Type 321 stainless steel	4	4.5	5.1	5.6
						77	Type 304 ELC stainless steel	2	90	92	93
							Type 347 stainless steel	2	100	110	110
							Type 321 stainless steel	2	100	100	100
E-14 and E-15	UO_2SO_4	5	250	302	1000 to 2000 ppm O_2, 0.016 M H_2SO_4	14 to 16	Type 304 ELC stainless steel	4	2.2	4.0	4.7
							Type 347 stainless steel	4	3.5	3.7	4.0
							Type 321 stainless steel	4	4.2	4.6	5.0
							Titanium, RC-70	2	0	0	0
							Zirconium–2.5% tin	2	0	0	0
						77	Type 304 ELC stainless steel	2	34	35	35
							Type 347 stainless steel	2	32	37	42
							Type 321 stainless steel	2	63	69	74
							Titanium, RC-70	1		0.1	
							Zirconium–2.5% tin	1		0	
E-17	UO_2SO_4	5	250	103	1000 to 2000 ppm O_2, 0.021 M H_2SO_4	13 to 16	Type 304 ELC stainless steel	4	37	40	42
							Type 347 stainless steel	4	35	42	53
							Type 321 stainless steel	4	41	46	49
						77	Type 304 ELC stainless steel	2	100	110	120
							Type 347 stainless steel	2	150	160	160
							Type 321 stainless steel	2	130	140	150
E-18	UO_2SO_4	5	250	201	1000 to 2000 ppm O_2, 0.021 M H_2SO_4	13 to 16	Type 304 ELC stainless steel	4	310	330	360
							Type 347 stainless steel	4	160	180	210
							Type 321 stainless steel	4	210	220	240
						77	Type 304 ELC stainless steel	2	240	370	490
							Type 347 stainless steel	2	380	400	420
							Type 321 stainless steel	2	290	290	290
E-17 and E-18	UO_2SO_4	5	250	304	1000 to 2000 ppm O_2, 0.021 M H_2SO_4	13 to 16	Type 304 ELC stainless steel	4	12	14	15
							Type 347 stainless steel	4	13	14	14
							Type 321 stainless steel	4	13	15	17
							Titanium, RC-70	2	0.06	0.12	0.17
							Zirconium–2.5% tin	2	0	0	0

TABLE 8. (continued)

RUN NO.	TEST CONDITIONS						PIN MATERIAL	NO. OF PINS	CORROSION RATE (mpy)		
	Solution	Uranium Concentration (g/l)	Temperature (°C)	Time (hr)	Additions	Flow Rate (fps ± 10%)			Minimum	Average	Maximum
E-17 and E-18	UO_2SO_4	5	250	304	1000 to 2000 ppm O_2, 0.021 M H_2SO_4	77	Type 304 ELC stainless steel	2	180	200	210
							Type 347 stoinless steel	2	250	250	250
							Type 321 stainless steel	2	180	190	200
							Titanium, RC-70	1		0.06	
							Zirconium–2.5% tin	1		0	
E-19	UO_2SO_4	5	250	100	1000 to 2000 ppm O_2, 0.024 M H_2SO_4	13 to 17	Type 304 ELC stainless steel	4	11	30	51
							Type 347 stainless steel	3	24	31	45
							Type 321 stainless steel	4	56	60	64
						77	Type 304 ELC stainless steel	2	180	220	250
							Type 347 stainless steel	2	230	240	240
							Type 321 stainless steel	2	190	190	190
E-20	UO_2SO_4	5	250	200	1000 to 2000 ppm O_2, 0.024 M H_2SO_4	13 to 17	Type 304 ELC stainless steel	4	3.6	11	17
							Type 347 stainless steel	4	16	17	19
							Type 321 stainless steel	4	5.4	15	22
						77	Type 304 ELC stainless steel	2	170	210	250
							Type 347 stainless steel	2	170	190	200
							Type 321 stainless steel	2	190	240	280
E-19 and E-20	UO_2SO_4	5	250	300	1000 to 2000 ppm O_2, 0.024 M H_2SO_4	13 to 17	Type 304 ELC stainless steel	4	4.5	10	15
							Type 347 stainless steel	4	8.4	14	16
							Type 321 stainless steel	4	4.4	13	21
							Titanium, RC-70	2	0	0	0
							Zirconium, crystal bar	2	0	0.03	0.06
						77	Type 304 ELC stainless steel	2	190	200	200
							Type 347 stainless steel	2	200	210	210
							Type 321 stainless steel	2	190	200	200
							Titanium, Ti-75A	1		0	
							Zirconium–2.5% tin	1		0	
F-24[h]	UO_2SO_4	40	250	101	1000 to 2000 ppm O_2	14	Type 304 ELC stainless steel	2	12	14	15
							Type 304 stainless steel	2	14	15	15
							Type 347 stainless steel	4	14	15	16
							Type 321 stainless steel	3	17	19	23
							Type 309 SCb stainless steel	3	12	13	14
F-25	UO_2SO_4	40	250	199	1000 to 2000 ppm O_2, 0.01 M $CuSO_4$	12	Type 304 ELC stainless steel	7	11	13	16
							Type 347 stainless steel	7	9.6	14	16
F-26	UO_2SO_4	40	250	201	1000 to 2000 ppm O_2, 0.01 M $CuSO_4$	12	Type 304 ELC stainless steel	7	3.0	17	27
							Type 347 stainless steel	7	1.8	15	20
F-28	UO_2SO_4	40	250	201	1000 to 2000 ppm O_2, 0.001 M $CuSO_4$	12	Type 304 ELC stainless steel	7	17	19	23
							Type 347 stainless steel	7	15	17	19
H-21	UO_2SO_4	40	200	200	2000 to 3000 ppm O_2	15	Type 304 ELC stainless steel	7	21	27	33
							Type 347 stainless steel	7	25	27	29

TABLE 8. (continued)

RUN NO.	TEST CONDITIONS						PIN MATERIAL	NO. OF PINS	CORROSION RATE (mpy)		
	Solution	Uranium Concentration (g/l)	Temperature (°C)	Time (hr)	Additions	Flow Rate (fps ± 10%)			Minimum	Average	Maximum
H-21	UO_2SO_4	40	200	200	2000 to 3000 ppm O_2	77	Type 304 ELC stainless steel	7	33	41	47
							Type 347 stainless steel	7	38	47	48
H-22	UO_2SO_4	40	200	400	2000 to 3000 ppm O_2	17	Type 304 ELC stainless steel	7	17	20	24
							Type 347 stainless steel	7	14	15	18
						77	Type 304 ELC stainless steel	7	39	50	55
							Type 347 stainless steel	6	42	50	60
H-23	UO_2SO_4	40	200	880	2000 to 3000 ppm O_2	17	Type 304 ELC stainless steel	3	15	16	22
							Type 347 stainless steel	3	5.1	7.0	8.0
							Type 321 stainless steel	2	16	18	19
							Type 309 SCb stainless steel	2	10	10	10
						77	Type 304 ELC stainless steel	3	49	50	52
							Type 347 stainless steel	3	48	50	53
							Type 321 stainless steel	2	44	50	56
							Type 309 SCb stainless steel	2	51	54	56
H-24	UO_2SO_4	40	200	100	2000 to 3000 ppm O_2	17	Type 304 ELC stainless steel	5	25	26	29
							Type 347 stainless steel	5	26	31	39
							Type 321 stainless steel	2	12	16	20
							Type 309 SCb stainless steel	2	18	19	19
						77	Type 304 ELC stainless steel	5	42	44	47
							Type 347 stainless steel	5	43	47	52
							Type 321 stainless steel	2	23	27	30
							Type 309 SCb stoinless steel	2	27	27	27
J-27	UO_2SO_4	5	300	423	1000 to 2000 ppm O_2, 0.005 M H_2SO_4	17	Type 304 ELC stainless steel	4	0.80	0.86	0.89
							Type 347 stainless steel	4	0.60	0.81	0.89
							Type 321 stainless steel	3	1.4	1.4	1.4
							Titanium, RC-70	1		0.04	
							Zirconium, crystal bar	1		0	
							Zirconium–2.5% tin	1		0	
						77	Type 304 ELC stainless steel	3	0.85	0.94	1.0
							Type 347 stainless steel	4	0.93	1.1	1.3
							Type 321 stainless steel	3	0.80	0.91	1.0
							Titanium, RC-70	1		0.08	
							Zirconium, crystal bar	1		0	
							Zirconium–2.5% tin	1		0	
J-29[i]	UO_2SO_4	40	250	200	1000 to 2000 ppm O_2	16 fps for 100 hr;[i] 75 fps for 100 hr	Type 304 ELC stainless steel	4	14	31	54
							Type 347 stainless steel	4	12	18	22
							Type 321 stainless steel	3	32	77	110
							Type 309 SCb stainless steel	3	17	22	31
						75 fps for 100 hr; 16 fps for 100 hr	Type 304 ELC stainless steel	4	78	96	110
							Type 347 stainless steel	4	89	100	120
							Type 321 stainless steel	3	65	87	110
							Type 309 SCb stainless steel	3	88	96	110

TABLE 8. (continued)

RUN NO.	TEST CONDITIONS						PIN MATERIAL	NO. OF PINS	CORROSION RATE (mpy)		
	Solution	Uranium Concentration (g/l)	Temperature (°C)	Time (hr)	Additions	Flow Rate (fps ± 10%)			Minimum	Average	Maximum
J-30	UO_2SO_4	30	250	99	1000 to 2000 ppm O_2, 10 g of UO_3[k] per liter	13	Type 304 ELC stainless steel	3	26	41	64
							Type 347 stainless steel	3	31	32	33
							Type 321 stainless steel	3	20	43	64
							Type 322W stainless steel[f]	1		7.0	
							Titanium, Ti-75A	1		0	
							Zircalloy II	1		0	
						75	Type 304 ELC stainless steel	3	120	130	130
							Type 347 stainless steel	3	140	140	150
							Type 321 stainless steel	3	91	110	150
							Type 322W stainless steel[f]	1		170	
							Titanium, Ti-75A	1		0	
							Zircalloy II	1		0	
L-16	UO_2SO_4	5	250	781	1000 to 2000 ppm O_2, 0.005 *M* H_2SO_4	22 to 27[m]	Type 322W stainless steel[l]	1		5.8	
							Type 440C stainless steel	2	15	18	20
							Inconel X, age hardened	1		57	
							Incoloy	2	1.2	1.6	2.0
L-17	UO_2SO_4	40	250	400	1000 to 2000 ppm O_2, 0.04 *M* $CuSO_4$	13 to 25	Type 304 ELC stainless steel	7	3.2	7.8	18
							Type 304 stainless steel	2	3.4	5.8	8.1
							Type 347 stainless steel	5	10	13	18
							Type 321 stainless steel	3	4.7	6.3	6.8
							Type 17-4 PH stainless steel[f]	1		1.6	
							Type 17-4 PH stainless steel	1		1.8	
							Titanium, RC-70	1		0.21	
							Titanium, Ti-100A	1		0.43	
							Titanium, Ti-150A	1		0.81	
							Zirconium, crystal bar	1		0	
							Zirconium–2.5% tin	1		0	
							Zircalloy II	1		0	
							Misco A[n]	1		35	
							Misco B[n]	1		32	
							Misco C[n]	1		16	
							Miscro 4[n]	1		1.3	
L-18	UO_2SO_4	40	225	400	2500 to 5000 ppm O_2	14	Type 304 ELC stainless steel	3	53	59	69
							Type 347 stainless steel	3	16	18	22
							Type 321 stainless steel	2	35	45	55
							Type 309 SCb stainless steel	2	23	30	37
						75	Type 304 ELC stainless steel	3	140	160	180
							Type 347 stainless steel	3	140	170	220
							Type 321 stainless steel	2	100	120	140
							Type 309 SCb stainless steel	2	160	170	170
L-19	UO_2SO_4	40	225	200	2500 to 5000 ppm O_2	13	Type 304 ELC stainless steel	3	45	67	81
							Type 347 stainless steel	3	34	38	41
							Type 321 stainless steel	2	39	51	62
							Type 309 SCb stainless steel	2	46	51	55
						75	Type 304 ELC stainless steel	3	110	120	130
							Type 347 stainless steel	3	130	130	140
							Type 321 stainless steel	2	90	150	200
							Type 309 SCb stainless steel	2	130	140	140

TABLE 8. (continued)

RUN NO.	TEST CONDITIONS						PIN MATERIAL	NO. OF PINS	CORROSION RATE (mpy)		
	Solution	Uranium Concentration (g/l)	Temperature (°C)	Time (hr)	Additions	Flow Rate (fps ± 10%)			Minimum	Average	Maximum
L-20	UO_2SO_4	40	225	100	2500 to 5000 ppm O_2	14	Type 304 ELC stainless steel	3	63	76	86
							Type 347 stainless steel	3	53	63	69
							Type 321 stainless steel	2	67	69	71
							Type 309 SCb stainless steel	2	67	70	72
						75	Type 304 ELC stainless steel	3	130	140	150
							Type 347 stainless steel	3	130	150	160
							Type 321 stainless steel	2	90	120	140
							Type 309 SCb stainless steel	2	100	110	120
L-21	UO_2SO_4	40	225	200	700 to 800 ppm O_2	12	Type 304 ELC stainless steel	4	58	65	69
							Type 347 stainless steel	4	29	33	41
							Type 321 stainless steel	3	39	55	64
							Type 309 SCb stainless steel	3	36	44	57
						75	Type 304 ELC stainless steel	4	130	140	150
							Type 347 stainless steel	4	140	160	180
							Type 321 stainless steel	3	100	120	140
							Type 309 SCb stainless steel	3	140	160	180
M-4	UO_2SO_4	15	250	200	1000 to 2000 ppm O_2, 0.016 M H_2SO_4	15 to 16	Type 304 ELC stainless steel	8	2.7	5.4	13
							Type 304 stainless steel	5	2.6	5.0	12
							Type 347 stainless steel	7	4.2	8.9	22
							Type 321 stainless steel	5	2.7	3.7	6.9
							Type 309 SCb stainless steel	3	3.3	5.5	7.6
						36	Type 304 ELC stainless steel	4	7.6	27	82
							Type 347 stainless steel	4	14	36	86
							Type 321 stainless steel	3	2.7	57	100
						58	Type 304 ELC stainless steel	2	90	100	110
							Type 304 stainless steel	1		78	
							Type 347 stainless steel	2	75	79	83
							Type 321 stainless steel	2	81	90	100
							Type 309 SCb stainless steel	2	90	93	95
M-5	UO_2SO_4	15	250	100	1000 to 2000 ppm O_2, 0.016 M H_2SO_4	5	Type 304 ELC stainless steel	7	8.0	9.8	12
							Type 347 stainless steel	7	6.5	9.8	13
							Type 321 stainless steel	2	8.2	10	11
							Type 309 SCb stainless steel	2	8.7	11	13
							Type 322W stainless steel[f]	1		25	
							Type 17-4 PH stainless steel[f]	1		14	
							Misco A[n]	1		59	
							Misco B[n]	1		13	
							Misco C[n]	1		11	
							Miscro 4[n]	1		32	
							Titanium, RC-70	1		0	
							Zirconium, crystal bar	1		0	
							Zircalloy II	2	0	0	0
						11	Type 304 ELC stainless steel	3	10	11	12
							Type 347 stainless steel	3	11	13	15
							Type 321 stainless steel	1		12	
							Type 309 SCb stainless steel	1		15	
							Type 322W stainless steel[f]	1		24	
							Type 17-4 PH stainless steel[f]	1		37	
							Misco A[n]	1		40	
							Miscro 4[n]	1		67	

TABLE 8. (continued)

RUN NO.	TEST CONDITIONS						PIN MATERIAL	NO. OF PINS	CORROSION RATE (mpy)		
	Solution	Uranium Concentration (g/l)	Temperature (°C)	Time (hr)	Additions	Flow Rate (fps ± 10%)			Minimum	Average	Maximum
Mockup 13	UO_2SO_4	40	200	200	50 to 60 ppm O_2	16	Type 304 ELC stainless steel	6	10	12	14
							Type 347 stainless steel	6	11	14	16
							Stellite 98M2	1		600	
							Stellite 6	1		58	
Mockup 14	UO_2SO_4	40	200	100	50 to 60 ppm O_2	16	Type 304 ELC stainless steel	6	12	14	18
							Type 347 stainless steel	6	12	14	17
							Stellite 98M2	1		470	
							Stellite 6	1		50	
Mockup 15	UO_2SO_4	40	250°	100	200 to 350 ppm O_2	16	Type 304 ELC stainless steel	4	89	91	93
							Type 347 stainless steel	4	65	72	87
							Type 321 stainless steel	2	74	78	82
							Type 309 SCb stainless steel	2	84	90	95
							Miscro 4[n]	1		53	
							Zircalloy II	1		0	

[a]In this run, the specimens listed as having a flow rate of 2 fps were exposed to a flow rate of 2 fps for 100 hr and then exposed to a flow of 55 fps for the next 99 hours. The specimens listed under 55 fps were exposed to the same flow rates in the reverse order. The low flow rates were caused by the unintentional inclusion of two restrictors in the loop.

[b]In these cases, the pins not reported were given to A. Olsen for examination before the film was removed. In the "as-removed" condition, the pins showed weight gains and visual observation showed no signs of attack.

[c]The reported corrosion rate is based on weight loss. Only the lead edge of each pin was badly attacked, and hence on that portion of the pins the rate was considerably higher than the reported value.

[d]Centrifugally cast.

[e]Cast.

[f]Precipitation hardened.

[g]The temperature control was erratic during the early stages of the run and the temperature may have been as high as 275°C during the first 20 hours.

[h]Prior to this run, new sections were added to the loop. This fact may account for the low corrosion rates as explained in the last quarterly report.[6]

[i]This run was interrupted after 100 hr of operation to change the location of the pin holders.

[j]The pins were not defilmed; hence the actual corrosion rate would be somewhat higher.

[k]The UO_3 was added to determine what effect the circulation of UO_3 particles in uranyl sulfate solutions would have on corrosion. Two hours after startup, the UO_3 had collected between the sample units and the wall of the loop so that only solution was circulated for the remainder of the run. The pH was 3.3.

[l]Malcomized.

[m]This run also contained metallurgically treated specimens, the results of which will be reported elsewhere.

[n]These alloys were obtained from the Michigan Steel Casting Company and had the following composition (the balance being iron):

	COMPOSITION (%)			
	Ni	Cr	C	Si
Misco A	37.9	19.2	0.26	1.57
Misco B	13.3	25.4	0.36	1.45
Misco C	10.0	28.7	0.22	1.73
Miscro 4	0.15	13.1	0.07	1.41

[o]The run was stopped three times during the first 5 hr of operation due to a valve failure. The valve was then replaced and the system again brought to 250°C. The system was then dumped hot, allowed to cool, then pumped up and run for the remaining 90 hours.

Corrosion Testing with Dilute Uranyl Sulfate Solutions. The longest uninterrupted corrosion test that has been carried out in a loop during this investigation was completed during the past quarter. Run B-26, which contained 0.02 *M* uranyl sulfate (5 g of uranium per liter) solution containing 0.005 *M* sulfuric acid at 250°C, was terminated after 4400 hr of continuous operation. Throughout this run, aliquots of solution were withdrawn for analyses, and periodically, without the pump being stopped, both gas and solution were injected into the loop to replace the samples removed.

Chemical analyses showed that the oxygen concentration varied between 500 and 1500 ppm; the uranium and sulfate concentrations remained constant; both the nickel and the chromium concentrations increased uniformly to 54 ppm; and the pH varied between 2.10 and 2.25. The corrosion rate of the system as a whole, as calculated from the rate of nickel increase in the solution, was 0.05 mpy.

The data obtained from the alloys (pins) tested in the run can be seen in Table 8, run B-26, from which it is obvious that all the pins suffered very little corrosion damage. In fact, the weight loss of all the austenitic steel pins varied between 1.2 and 2.5 mg/cm^2. This weight loss is only very slightly higher than that observed after only 600 hr of operation under the same conditions (B-24) and rather clearly shows that specimens exposed to low-velocity streams of 0.02 *M* uranyl sulfate practically stop corroding after a relatively short period of operation. This same observation has been made at other concentrations of uranyl sulfate at 250°C, but the time had seldom exceeded 1000 hours.

Some welded pins were also included in run B-26 but are not shown in Table 8. The weight losses of these pins were the same as those of the wrought pins, and there was no evidence of selective attack on either the parent or weld metal.

A set of type 347 stainless steel coupons was also included in run B-26, and Fig. 29 shows a plot of the data. For comparison, the coupon data from run B-25, where the conditions were the same as in B-26 except that the duration of the run was only 1000 hr, are shown on the same graph. It is obvious that the coupons show the same trend as the pins, that is, very little weight loss between 1000 and 4400 hours. Note that the numerical values on the ordinate are very much lower than they were in cases where higher concentrations were used.

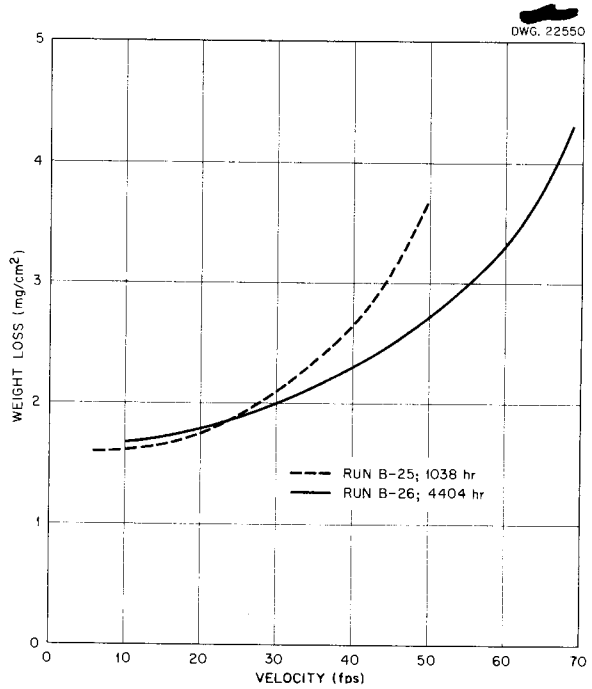

Fig. 29. Extent of Corrosion of Type 347 Stainless Steel in 0.02 *M* Uranyl Sulfate at 250°C as a Function of Velocity.

Inspection of the interior of the loop showed all parts to have a rather thin lustrous film with no evidence of localized attack. The stainless steel pump impeller showed neither weight nor appearance change during the run. It should be pointed out that this run was not terminated because of mechanical failure but because of a desire to inspect the corrosion specimens. The indications were that this loop could have been operated for an indefinite period before a shutdown would have been necessary.

At the time the last quarterly report was written, one run of short duration had been completed in which 0.02 *M* uranyl sulfate with 0.005 *M* sulfuric acid was used at 300°C. The data indicated that at 300°C corrosion was no greater, and was possibly less, than at 250°C. Since that time, one run (run J-27) of 400-hr duration has been completed which verified the results of the first run. In run J-27, the pins at low velocity lost approximately 1 mg/cm^2, and those at 77 fps lost the same amount. The weight losses of the coupons were in agreement with those of the pins, since all coupons

lost about 1 mg/cm^2. These weight losses are essentially the same as those observed at 250°C under the same conditions; hence it can be stated that the corrosion resistance of most austenitic stainless steels in 0.02 *M* uranyl sulfate containing 0.005 *M* sulfuric acid is as favorable at 300°C, and perhaps slightly more so, as it is at 250°C. Plans are now being made to test the same system at 325°C.

Effect of Acid on Corrosion by 0.02 *M* Uranyl Sulfate. It has previously been established that the addition of sulfuric acid to 0.02 *M* uranyl sulfate (5 g of uranium per liter) is necessary to prevent precipitation of uranium trioxide when the solution is circulated in a stainless steel loop at 250°C. If copper sulfate is to be added to the uranyl sulfate solution, additional sulfuric acid may have to be added to prevent the precipitation of a basic copper sulfate. Since the addition of small amounts of sulfuric acid is now routine and since in the future it may be necessary to add larger amounts than is normally done at present, it was desirable to determine how the extent and/or rate of corrosion varied with different amounts of sulfuric acid added to 0.02 *M* uranyl sulfate.

For this study, loop E was used and the following procedure was adopted. One pin holder and one coupon holder were placed in each of two bypass lines. In these lines, the solution flowed past the pins at a rate of 13 to 17 fps and past the coupons at a rate ranging from 10 to 75 fps. One pin holder was also placed in the main line where the solution flowed past the pins at a rate of 77 fps. A solution containing 0.02 *M* uranyl sulfate and 0.005 *M* sulfuric acid (25 mole %), pressurized with 200 psi of oxygen, was used for the first run. The solution was circulated at 250°C for 100 hr, after which half the pin-type specimens were removed from each holder and one complete set of coupons was similarly removed. The specimens that were removed were replaced by new ones, and the loop was again filled with a new solution of the same composition. The loop was then run at 250°C for 200 hours. At the completion of the second run, specimens had been exposed for 100-, 200-, and 300-hr periods, and the experiment at that given acid concentration was complete. The above procedure was then repeated with 0.02 *M* uranyl sulfate at the following sulfuric acid molarities: 0.011, 0.016, 0.021, and 0.024.

The pin data are shown in Fig. 30, where the log of the weight loss per square centimeter is plotted against the molarity of the added sulfuric acid. Since there appeared to be no consistent difference between the austenitic steels tested, the data have been plotted as a unit, with the symbols representing the average weight loss of all pins exposed under that particular set of conditions. The corrosion rates of the individual alloys can be seen in Table 8, runs E-10 through E-20. With the exception of the points at 0.021 *M* sulfuric acid, the points appear to lie on a reasonably straight line, the significance of which has not been determined. At low velocity (~15 fps) it should be noted that after 100 hr there appeared to be no further corrosion up to the maximum time tested. At higher flow rates, there appeared to be a constant corrosion rate for the 100- and 200-hr specimens, but the data from the 300-hr specimens are rather ambiguous. It may be that at the end of the 100-hr exposure the solution in the loop was at 250°C when the pump was stopped. After the circulation had stopped and while the solution was

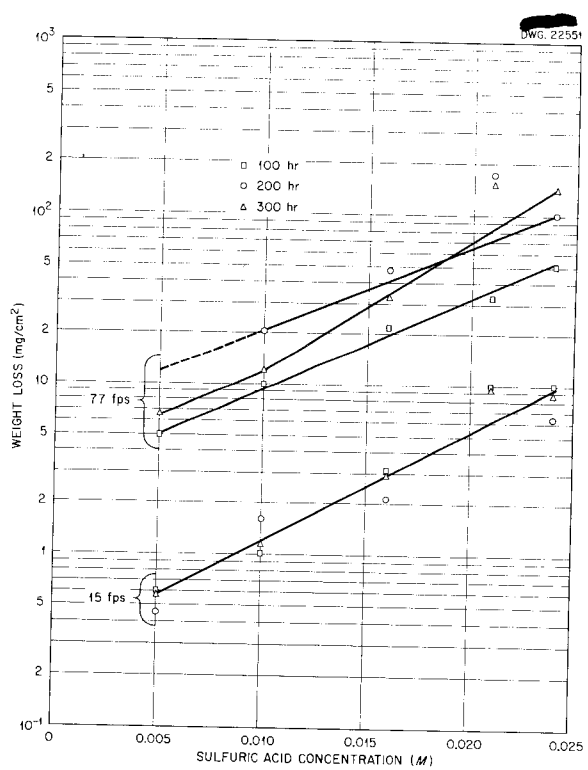

Fig. 30. Effect of Sulfuric Acid on the Corrosion of Stainless Steel by 0.02 *M* Uranyl Sulfate at 250°C.

cooling, some protective coating may have formed on the high-velocity specimens. This film would then offer partial protection to the underlying metal during the next 200-hr period at the lower acid concentrations. At the higher acid concentrations, this thin film would still be of some value, but its effectiveness would be diminished rapidly as the acid concentration was increased. If the above line of reasoning is correct, pins at high velocity should lose in 300 hr approximately three times the weight lost in 100 hr provided that the run was not interrupted. An experiment of this type will be run in the future. At low velocity, film builds up during the run, and the above effect would not be apparent.

The coupon data generally parallel the pin data. Figure 31 shows how corrosion (weight loss) varied with velocity at different acid concentrations during the first 100-hr runs. The curves obtained at the longer operating times were the same as those at 100 hr, except that at high flow rates the curves at the two highest acid concentrations were each about three times as high as those shown.

The coupon data differed in one respect from the pin data. Up to and including 0.016 M sulfuric acid, the weight-loss vs. velocity curves were the same, regardless of time at a given acid concentration. The high-velocity pins did not show this same result, in that there appeared to be a constant corrosion rate, at least for the 100- and 200-hr specimens.

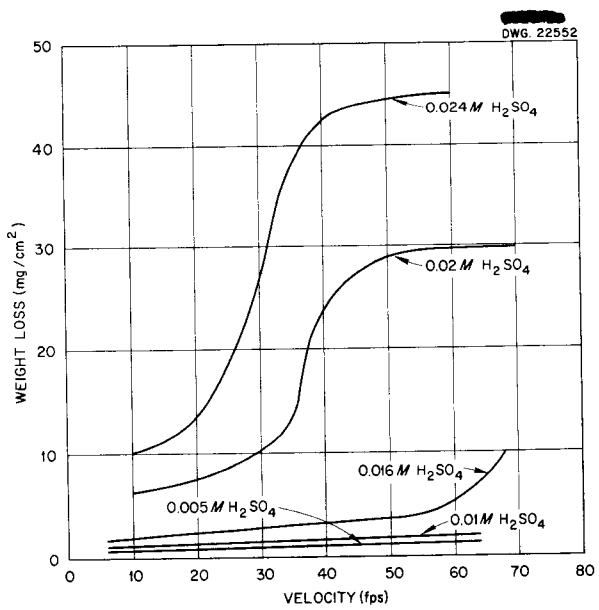

Fig. 31. Effect of Sulfuric Acid on Corrosion of Type 347 Stainless Steel by 0.02 M Uranyl Sulfate at 250°C. Exposure time: 100 hr.

Effect of Time, Velocity, and Uranium Concentration at 250°C. In the last quarterly report[6] data were presented on the corrosion rate of stainless steel in several different concentrations of uranyl sulfate at 250°C. Since that time, an additional concentration of 0.042 M uranyl sulfate (10 g of uranium per liter) containing 0.0063 M (15 mole %) sulfuric acid at 250°C has been investigated. The procedure was the same as that described in the last report, namely, exposing pins at both high and low velocity for different lengths of time and then determining the weight losses of the specimens. The general corrosion characteristics at this concentration were the same as those at higher uranium concentrations except that the corrosion rate was lower. At 15 fps, the pins lost about 3 mg/cm^2 before corrosion practically ceased. At high velocity, the pins corroded at a constant rate of 84 mpy. The coupons showed a velocity effect, that is, a rapid increase in corrosion with increased velocity at 30 to 40 fps. It should be noted that at this concentration of uranyl sulfate plus sulfuric acid a definite velocity effect was apparent, while at the 5 g level, even with a larger concentration of sulfuric acid, a significant velocity effect was not observed.

Up to this time, corrosion tests have been run by using several different concentrations of uranyl sulfate at 250°C, all of which contained about 1000 ppm of oxygen. At low flow rates (~15 fps) it was found that stainless steel corroded rapidly during the first 50 to 100 hr as a protective coating formed, and then corrosion practically ceased. Table 9 gives the average weight of metal attacked during this period at different solution compositions. It should be noted that the weight loss generally increased as the uranium concentration was increased, but there was no apparent correlation between the room-temperature pH of the solution and the weight loss.

At high velocities, protective films are generally not formed on stainless steel, and corrosion continues at a constant rate. From the data presented in previous quarterly reports[5,6] and from those given above, Fig. 32 has been constructed. The data show a linear relationship between the log of the uranium concentration and the corrosion rate when

TABLE 9. WEIGHT LOSS OF STAINLESS STEEL IN URANYL SULFATE SOLUTIONS DURING THE FIRST 50 TO 100 hr AT 250°C AT LOW FLOW RATES

MOLARITY OF URANYL SULFATE	MOLARITY OF SULFURIC ACID	ROOM-TEMPERATURE pH	WEIGHT LOSS (mg/cm^2)
0.02	0.005	2.1 to 2.2	2
0.04	0.006	2.0 to 2.1	3
0.06	0.016	1.6 to 1.7	6
0.11	0	2.6 to 2.7	5
0.17	0	2.4 to 2.5	12

the oxygen concentration was about 1000 ppm and the temperature was 250°C. The points at 10, 15, 25, and 40 g of uranium per liter represent the average of many pins exposed at high velocity (~75 fps). The points at 100 and 300 g of uranium per liter were based on the last coupon in only one holder in each case; hence they are not so reliable as the points at lower concentrations. The points at 10 and 15 g of uranium per liter were obtained from solutions containing added sulfuric acid, and these points do not appear to deviate from the line as drawn. Furthermore, two previously reported[5] runs, I-1 and I-3, were made in which 0.17 *M* uranyl sulfate containing 0.04 *M* sulfuric acid served as the corroding medium, and in each of these two runs, the last coupon in the holder corroded at a rate of 210 to 220 mpy, which agrees well with the point obtained with 40 g of uranium per liter without added acid. The results therefore indicate that the corrosion rate of stainless steel at high flow rates is independent of hydrogen and sulfate ion concentrations over the range investigated but is dependent on the uranium concentration and probably on the oxygen concentration (see section below). It is interesting to note that if the line is extrapolated to zero corrosion rate a value of about 5 g of uranium per liter is obtained. At this concentration, even with as much as 75 mole % added sulfuric acid, a constant high-velocity corrosion rate was not observable at the highest velocity obtainable.

Effect of Temperature and Oxygen Concentration. A number of experiments have recently been performed in which 0.17 *M* uranyl sulfate has been circulated at different temperatures and different oxygen concentrations. In the last quarterly

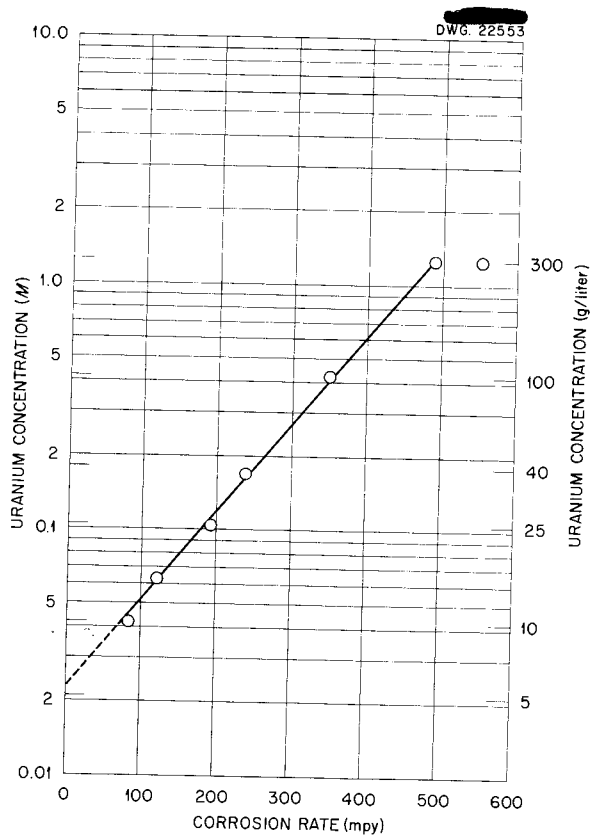

Fig. 32. Corrosion Rate of Stainless Steel at High Flow Rates as a Function of Uranyl Sulfate Concentration. Temperature: 250°C. Oxygen concentration: ~ 1000 ppm.

report,[6] it was shown that in mockup runs 10 and 12 there was a constant corrosion rate of 300 series stainless steels of about 25 mpy at 200°C in 0.17 *M* uranyl sulfate when the solution contained 200 ppm of oxygen. Since that time, other experiments have been completed at the same uranium concentration and temperature but at two different oxygen concentrations. Figure 33 shows the corrosion rate of type 347 stainless steel coupons in 0.17 *M* uranyl sulfate containing 50 ppm of oxygen at 200°C (mockup runs 13 and 14). The corrosion rate under these conditions was 15 mpy.

In loop H, runs H-21 through H-24, 0.17 *M* uranyl sulfate containing about 2500 ppm of oxygen was run at 200°C. In this series of runs, pins were exposed at two velocities, 17 and 77 fps, and type 347 stainless steel coupons were exposed over the range of 10 to 85 fps. Figure 34 shows the average

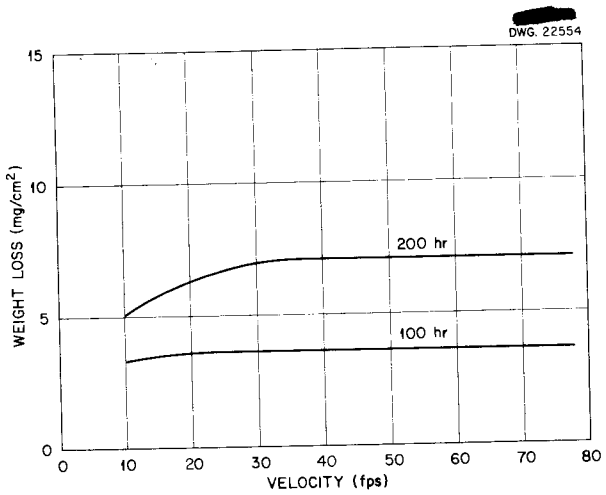

Fig. 33. Corrosion of Type 347 Stainless Steel in 0.17 M Uranyl Sulfate Containing 50 to 60 ppm of Oxygen at 200°C as a Function of Velocity.

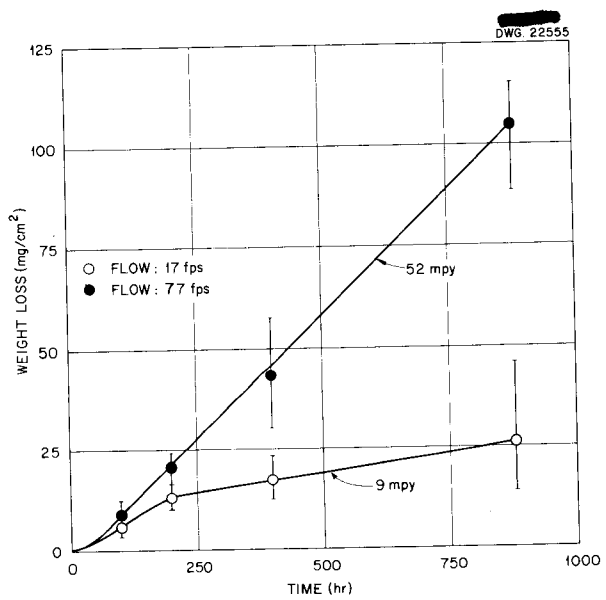

Fig. 34. Corrosion Rate of Stainless Steel Pins in 0.17 M Uranyl Sulfate Containing About 2500 ppm of Oxygen at 200°C.

pin weight loss as a function of time, and Fig. 35 gives the coupon weight loss as a function of velocity at different times. In Fig. 34, the symbols represent the average weight loss of the pins, and the line represents the maximum spread of all pins in the given holder. The corrosion rate under these conditions was 52 mpy at high velocity and 9 mpy

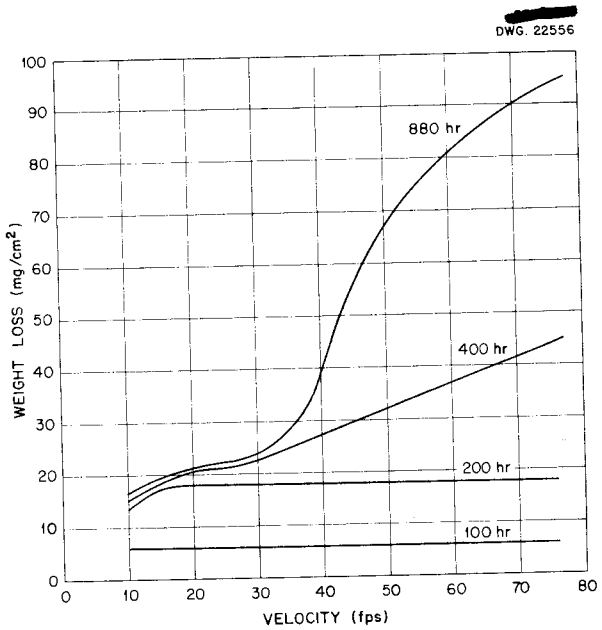

Fig. 35. Corrosion of Type 347 Stainless Steel in 0.17 M Uranyl Sulfate Containing About 2500 ppm of Oxygen at 200°C as a Function of Flow Rate.

at low velocity. It should be mentioned that at all oxygen concentrations at 200°C all specimens had films on them, even at the highest flow rate. The specimens at low flow rates had brownish-red coatings, and those at high flow rates had black films. The films formed at low velocity were heavy, and a large amount could be removed by rubbing with tissue. The data show that the film was not protective at any velocity or at any oxygen concentration. If the log of the oxygen concentration is plotted vs. the corrosion rate, the three points lie nearly on a straight line at high velocity. When this method is used to interpolate, a corrosion rate of about 40 mpy is obtained at 1000 ppm of oxygen, which is the normal amount used under most operating conditions.

A series of runs has been made at 225°C with 0.17 M uranyl sulfate containing about 2500 ppm of oxygen. The data for the pin-type specimens are shown in Fig. 36, and those for the coupons are given in Fig. 37. The curves show a corrosion rate of 29 mpy at the low velocity and a rate of 160 mpy at the high flow rates.

One additional run, L-21, was made at 225°C, and in this case, the oxygen concentration was 700 to 800 ppm. This run lasted for 200 hr, and

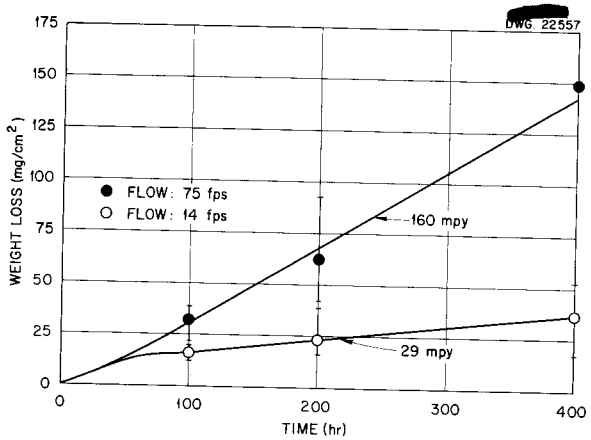

Fig. 36 Corrosion Rate of Stainless Steel in 0.17 M Uranyl Sulfate Containing About 2500 ppm of Oxygen at 225°C.

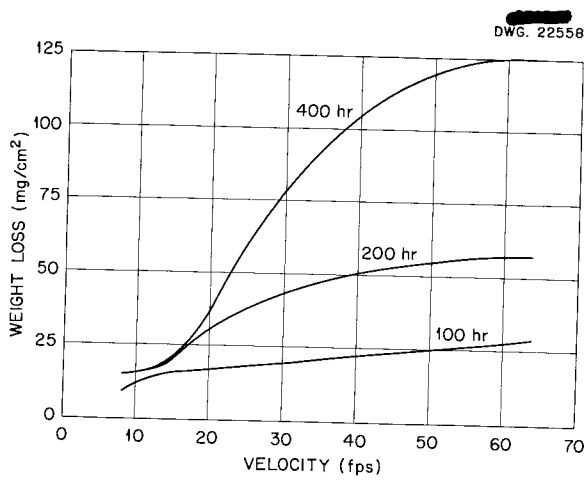

Fig. 37. Corrosion of Type 347 Stainless Steel in 0.17 M Uranyl Sulfate Containing About 2500 ppm of Oxygen at 225°C as a Function of Flow Rate.

the results agreed with those obtained at the higher oxygen concentrations. This indicates that there is no detectable oxygen effect in this oxygen concentration range.

It was interesting to note that at 225°C all specimens exposed at high velocity were free of film, as has been the case at 250°C. At low velocity, the film formed at 225°C appeared to be identical to that formed at 250°C, but its protective nature was definitely inferior to that formed at the higher temperature. At 225°C at low velocity, type 347 stainless steel appeared to be more corrosion resistant than the other steels tested, particularly at longer times (see Table 8, runs L-18 through L-21).

The last quarterly report[6] included data on the corrosion of stainless steel by 0.17 M uranyl sulfate containing about 1000 ppm of oxygen at 250°C. It was shown that the film-free steel corroded at a rate of 240 mpy and that the specimens tested at low flow rates lost about 12 mg/cm² before a protective film formed. To date, only the one oxygen concentration has been investigated at this uranium concentration at 250°C.

Three separate runs (A-54, A-55, and B-28) were made at 275°C with 0.17 M uranyl sulfate and 1000 ppm of oxygen. The pin data can be seen in Fig. 38, and the coupon data are shown in Fig. 39. The specimens exposed at low flow rates lostabout 6 mg/cm² before corrosion apparently stopped, whereas the specimens exposed at high flow rates corroded at a rate of 500 mpy. The coatings developed on all specimens did not differ in appearance from those formed at 250°C.

Two platinum pins were included in run A-55. Both pins developed black films; the one exposed at 13 fps had 4.4 mg of scale, and the one exposed at 75 fps had 5.1 mg. These scales were dissolved

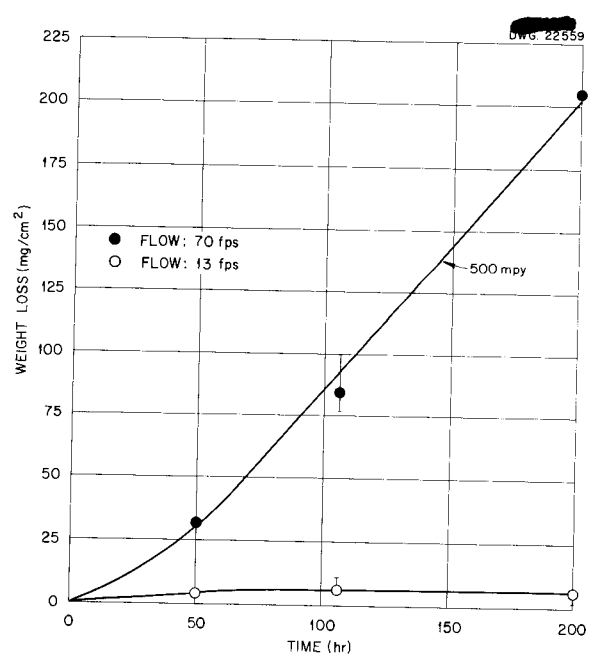

Fig. 38. Corrosion Rate of Stainless Steel in 0.17 M Uranyl Sulfate Containing About 1000 ppm of Oxygen at 275°C.

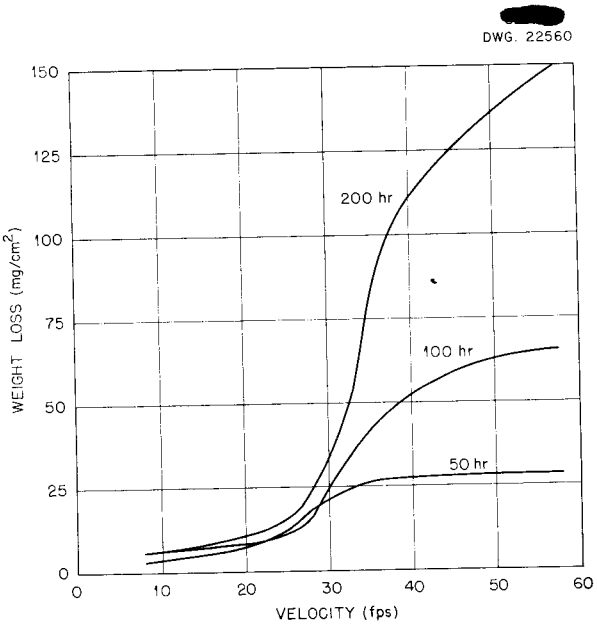

Fig. 39. Corrosion of Type 347 Stainless Steel in 0.17 M Uranyl Sulfate Containing About 1000 ppm of Oxygen at 275°C as a Function of Flow Rate.

from the pins with a mixture of perchloric and hydrofluoric acids, and the resulting solutions were analyzed. Table 10 shows the results of the analyses.

When the elements in Table 10 are converted to their oxides (Fe_2O_3, Cr_2O_3, and U_3O_8), 95% of the weight at 75 fps and 100% of the weight at 13 fps can be accounted for.

Two runs, A-56 and A-57, were made with 0.17 M uranyl sulfate containing 1000 ppm of oxygen at 300°C. The first run was of 100-hr duration, at the conclusion of which the specimens were examined. The pins exposed to high flow rates were film-free only on the surface on which the solution impinged. The back of each pin had a black film and showed no serious corrosion damage. The pins tested at low velocity had rather thin, black films and showed an average weight loss of only 2.2 mg/cm^2 after defilming. The coupons all had black coatings except for part of the one at the highest velocity, which was film-free and showed very heavy corrosion damage. When the depth of penetration on the part of the coupon that remained bare was approximated, a corrosion rate of 730 mpy was obtained. The same procedure on the high-velocity pins gave a corrosion rate of 1200 mpy on that part of the pin which remained free of film.

TABLE 10. COMPOSITION OF THE SCALE FORMED AT 275°C IN 0.17 M URANYL SULFATE

VELOCITY (fps)	COMPOSITION (%)			
	Fe	Cr	Ni	U
13	57	3.4	0.3	12.5
75	55	5.1	0.3	7.6

In run A-56, one platinum pin was exposed at each velocity. Neither pin developed a visible film, and each pin showed a slight weight loss. At both flow rates, the pins had an abraded or etched appearance on the lead edge of the pin, whereas the back side was undamaged.

The second run at 300°C (A-57) with 0.17 M uranyl sulfate lasted for 400 hr, during which the flow conditions were the same as in run A-56. An examination of the specimens at the conclusion of the run showed a black film on all specimens. As a result of this film, both pins and coupons exposed at high flow rates lost less weight than during the 100-hr run. The reason for this discrepancy is unknown. However, the specimens exposed at low velocity lost about the same weight as was lost during the 100-hr run. Hence it appears that at 300°C, as at 250 and 275°C, corrosion practically stops after a relatively short time at low flow rates.

The coupon data show that as the temperature is increased above 250°C the velocity effect does not become apparent until higher velocities are reached. Figure 40, which shows corrosion as function of velocity at 250, 275, and 300°C in 0.17 M uranyl sulfate, illustrates this point.

In summarizing the temperature study, at low flow rates (~15 fps) in 0.17 M uranyl sulfate containing about 1000 ppm of oxygen (except at 200°C), the following observations have been made: at 200°C (and 2500 ppm O_2), the corrosion rate is 9 mpy; at 225°C, the corrosion rate is 29 mpy; at 250°C, corrosion ceases after a weight loss of about 12 mg/cm^2; at 275°C, corrosion ceases after a weight loss of about 6 mg/cm^2; and at 300°C, there is no further corrosion after a weight loss of approximately 2.3 mg/cm^2.

The corrosion rate of stainless steel at high flow rates in 0.17 M uranyl sulfate containing 1000 ppm of oxygen can best be summarized by Fig. 41, where the log of the corrosion rate (mpy) is plotted against the reciprocal of the absolute temperature.

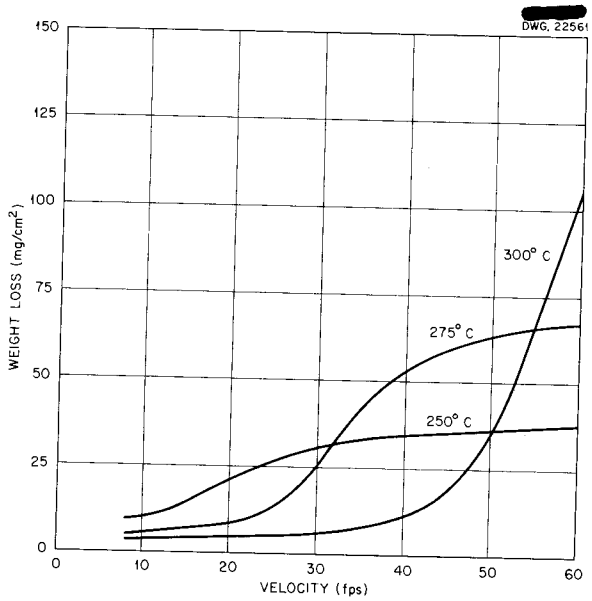

Fig. 40. Corrosion of Type 347 Stainless Steel in 0.17 *M* Uranyl Sulfate as a Function of Velocity at 250, 275, and 300°C.

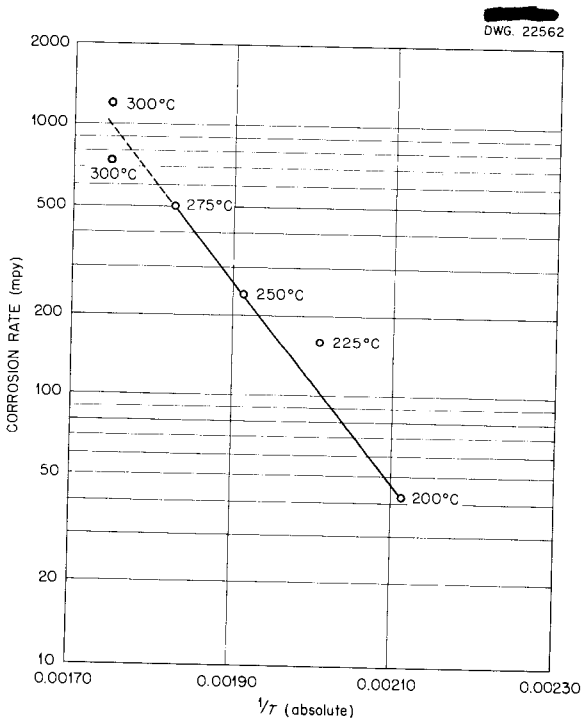

Fig. 41. Corrosion Rate of Film-Free Type 347 Stainless Steel in 0.17 *M* Uranyl Sulfate Containing About 1000 ppm of Oxygen.

Except for the two points at 300°C ($1/T$ = 0.00175) where one point is based on one coupon and the other is based on one pin, the points represent the average of a large number of pin-type specimens. It should be noted that in Figs. 34, 36, and 38 the extrapolations of the straight-line portions of the high-velocity curves do not intersect the origin of the graph. In Fig. 41, the log of the corrosion rate calculated from the slope of the straight-line portion of the curves is the value that has been plotted. The point at 225°C ($1/T$ = 0.00201) is definitely not on the line as drawn, and at present there is no explanation for this. From the slope of the line as drawn, an activation energy of about 17,000 cal can be calculated.

Other Experiments. A number of other experiments have been conducted during the past quarter.

Decontamination. In the last quarterly report,[6] a run was described in which the purpose was to descale the interior surface of the loop. During this quarter, a second such run has been made, but in this case the loop was first contaminated with zirconium and niobium activities and then descaled with a solution containing 1.0 *M* hydrochloric acid, 1.4 *M* sulfuric acid, 0.2 *M* hydrogen peroxide, and an inhibitor. The contaminating solution was 0.17 *M* uranyl sulfate to which had been added about 40 ppm of zirconium (active plus inactive) and 14 ppm of niobium (active and inactive). The contaminating solution was circulated in the loop for 24 hr at 250°C, but analysis of the solution showed that more than 95% of the activity had deposited, rather uniformly, on the interior loop surfaces by the time the loop temperature had reached 250°C. After 24 hr of operation, more than 99% of the activity had been removed from solution. The decontaminating solution which was circulated at 85°C for 4 hr was, in reality, a descaling solution in that it dissolved only a small amount of the zirconium or niobium activity. It did, however, loosen the scale, which contained the major part of the radioactivity, and the scale was then flushed from the loop. Radiation measurements made before and after the decontamination run showed that 97 to 99% of the activity deposited in the loop had been removed.

Scale Stability. It has already been shown that pins exposed to uranyl sulfate solution at 250°C (and higher) flowing at a rate of about 15 fps develop heavy, black films which very greatly retard further corrosion. At high velocity, a heavy

scale is not formed and corrosion proceeds at a high, constant rate. To determine the stability of the coating formed at low flow rates, the following experiment was performed. A normal run was made in loop J, run J-29, in which pins were placed in the main line (flow ~75 fps) and in a bypass line (flow ~15 fps); coupons were also included in the bypass line. The loop was filled with 0.17 M uranyl sulfate and operated at 250°C with 1000 ppm of oxygen for 100 hours. At the end of this time, the pin holders were reversed; that is, the pins that were in the main line were placed in the bypass line, and the pins in the bypass line were placed in the main line. The pins were not removed from the holders, but from the ends of the holders it could be seen that those exposed in the bypass line had black coatings and that those in the main line were film-free. After switching the pins, the run was continued for an additional 100 hr and then the specimens were examined. The pins that were first exposed to solution flowing at 75 fps and then to the lower velocity solution had black coatings and, after defilming, showed weight losses which were approximately the sum of the losses normally observed for 100 hr of operation at each velocity. The coupons which were not changed during the run showed weight losses similar to those usually observed for 200 hours. On the other hand, the pins first exposed at 15 fps and then at 75 fps were still largely covered with film, but all of them had some pits. Figure 42 shows an enlarged photograph of portions of two pins which represented

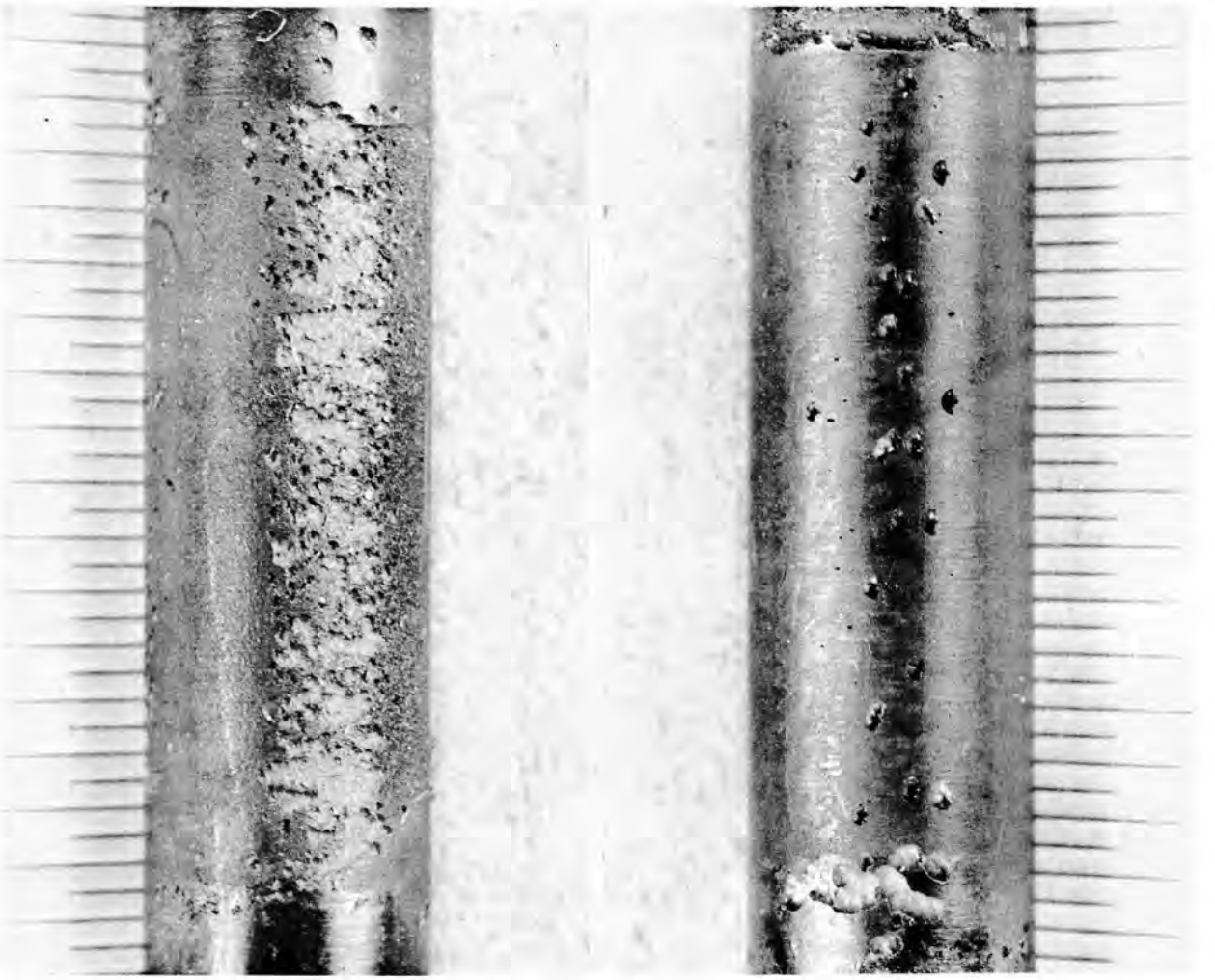

Fig. 42. Enlarged Photograph of Pins Exposed to 0.17 M Uranyl Sulfate at 250°C for 100 hr, Followed by 100-hr Exposure at 75 fps. Each division: 0.5 mm.

the two extremes. Note that in one case the film was nearly removed and that in the other case several pits had formed. In all cases it was the upstream side of the pin which had suffered the greatest corrosion damage. From this experiment it was clearly evident that coatings formed on pins at low velocity are not completely stable at high velocities and that after an undetermined time at high flow rates disintegration of the film occurs.

In-Pile Loop Corrosion Specimens. The corrosion specimens and holders to be used in the in-pile corrosion test loop are described elsewhere (see section by C. Zerby, this report); and it need only be mentioned that the specimens and their holders are considerably smaller than those used in the dynamic loop program and that the holders have been constructed on the venturi principle, which results in the specimens in the center of the holder being exposed to the highest flow rates. The conventional holder is tapered from end to end so that the coupon at one end of the holder is the one exposed to the highest flow rate. Since the geometry and size of the two types of holders are so different, it was of interest to compare the results obtained from the two holders. Loop F was used to make this comparison. An in-pile loop assembly, complete with two holders filled with type 347 stainless steel corrosion specimens, was flanged into the loop, and a conventional coupon holder containing type 347 stainless steel coupons was placed in a bypass in the same loop. The solution used was the same as that proposed for use in the in-pile loop, namely, 0.17 *M* uranyl sulfate, 0.01 *M* copper sulfate, and 1000 ppm of oxygen at 250°C. After two failures to obtain comparable corrosion results which were attributed to the loop pressurizer, the pressurizer was replaced and the data presented in Fig. 43 were obtained (see section by H. C. Savage and J. Walters, this report). In Fig. 43, the weight losses

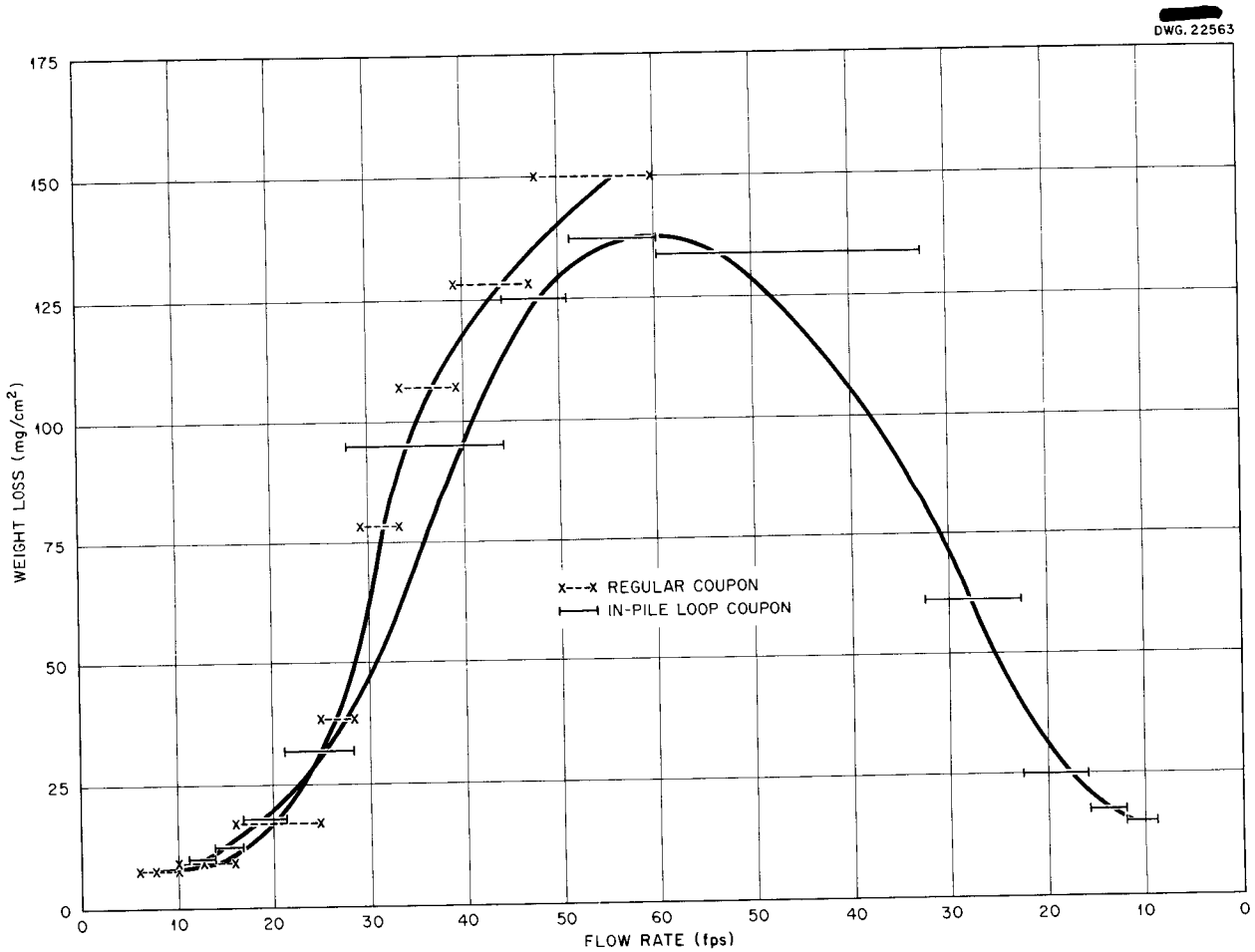

Fig. 43. Corrosion of Type 347 Stainless Steel Under In-Pile Conditions as a Function of Flow Rate.

of the individual coupons have been converted to weight loss per square centimeter of exposed surface area, and the horizontal lines represent the velocity range over the individual coupons. Three other in-pile sample holders, not shown in Fig. 43, were included in the same run. Within the limits of error, the three holders gave the same results as those shown in the figure. It is obvious that within experimental error the data from the two different holders yielded the same result. A complete mockup of the in-pile loop is being constructed, and its operation will allow further correlation of corrosion data from the two specimen setups.

It should be noted that the corrosion rate at the high velocity in this system was almost a factor of 2 greater than had been observed under the same conditions in the absence of copper sulfate. In run L-17 where the same conditions prevailed, except 0.04 *M* copper sulfate was added instead of 0.01 *M* copper sulfate, a corrosion rate about 2.5 times greater was also observed at the high flow rates. At low flow rates, the extent of corrosion was about the same with or without copper sulfate. It is hoped that future work will quantitatively define the effect of copper and other additives on the corrosion rate of stainless steel in uranyl sulfate solutions.

Discussion. The most dilute uranyl sulfate solution investigated to date has contained 5 g of uranium per liter. At this concentration with 0.005 *M* sulfuric acid (enough to prevent hydrolytic UO_3 precipitation) and at temperatures of 250 to 300°C, no serious corrosion damage has been encountered even at the highest velocities obtainable. Increasing the flow rate from 10 to 70 fps increased the weight loss per unit area by no more than a factor of 4, and even at the highest flow rates examined, a thin film ultimately formed which soon stifled further attack. Increasing the sulfuric acid concentration to as high as 0.015 *M* (75 mole %) increased the initial weight loss slightly, but even at velocities as high as 65 fps a film formed which minimized further attack. Further additions of acid increased the extent of corrosion at all velocities, and at high flow rates they inhibited the formation of a protective film, the absence of which resulted in a continuous, rapid corrosion rate. It is evident from Fig. 31 that the larger the amount of acid in the system, the lower the "critical velocity." The critical velocity has been defined as the flow rate in excess of which protective coatings do not form and below which films form which, after a relatively short exposure time, prevent further corrosion.

All systems investigated to this point, except for 5 g of uranium per liter with up to 75 mole % sulfuric acid, have shown a critical velocity at 250°C. Table 11 shows the systems investigated to date and the range of critical velocities in the different systems.

TABLE 11. CRITICAL VELOCITY RANGE OF URANYL SULFATE SYSTEMS AT 250°C WITH 1000 ppm OF OXYGEN

MOLARITY OF URANIUM	MOLARITY OF SULFURIC ACID	CRITICAL VELOCITY RANGE (fps)
0.42		10 to 20
0.17		15 to 25
0.17	0.04	10 to 20
0.11		30 to 40
0.06		50 to 60
0.06	0.015	25 to 35
0.04	0.006	30 to 40
0.02	0.005	>75
0.02	0.011	>75
0.02	0.016	>60
0.02	0.021	25 to 35
0.02	0.024	20 to 30

From Table 11 it is apparent that the main effect of adding acid or of increasing the uranium concentration is to lower the critical velocity.

Increasing the temperature of a system increases the critical velocity. For example, with 0.17 *M* uranyl sulfate at 250°C, a critical velocity range of 15 to 25 fps was observed; at 275°C, 25 to 35 fps; and at 300°C, 35 to 45 fps. The corrosion rates at these temperatures have already been given, and they demonstrate that at flow rates less than the critical velocity the extent of corrosion decreases with increasing temperature, while at flow rates greater than the critical velocity the rate of corrosion increases rapidly as the temperature increases.

At 225°C, no oxide coatings formed at velocities in excess of 20 fps. At lower velocities, black films were formed, but the nature of the film was such that it was not protective and corrosion proceeded at a rather high rate.

At 200°C, a film formed at all velocities, but obviously the film offered only limited protection. The specimens exposed at low flow rates were reddish-brown, while at higher flow rates the film was thinner and bluish-black in appearance. The curves shown in Fig. 35 indicate a "velocity effect" only at the longest exposure time, and here the effect appeared to be due only to the relative thickness of the film. At low velocity, the bulky film apparently kept the corrosion rate lower than it was at high velocity where the high rate of flow of the solution past the specimens kept the film thickness at a minimum.

Table 8 shows that a large number of different zirconium and titanium specimens have been tested during the last quarter. Generally, these specimens have not shown significant weight changes. In a few cases, both zirconium and titanium have shown weight losses, but these losses have never exceeded 0.5 mg/cm^2. It is interesting to note in this connection that even platinum showed weight losses as large as this and that in the case of platinum, at least, apparently erosive or abrasive forces were responsible. It seems reasonable to conclude that a similar explanation may be applicable in the cases of titanium and zirconium.

Very few corrosion tests on zirconium or titanium are contemplated at present, except for the operation of the titanium loop. A number of "notched-bar" specimens of both titanium and zirconium are being exposed at present. At the conclusion of the test, these specimens will be used by the Metallurgy Group to determine whether or not embrittlement of these two metals is a problem under dynamic loop conditions.

SMALL-SCALE DYNAMIC CORROSION PROGRAM

G. E. Moore

The small-scale dynamic corrosion program remains approximately as stated in the last quarterly report. The 20-toroid, DeRieux-McWherter toroid rotator I has been received, and preliminary checks on its performance have been undertaken. So far, the mechanism seems to be entirely satisfactory. Further testing will be carried out before it is used in corrosion studies. These tests are awaiting the toroids, which have been delayed in fabrication.

IN-PILE LOOP

G. H. Jenks

Operating Methods and Equipment

G. H. Jenks D. T. Jones
R. A. Lorenz

The general scheme for the operation of the in-pile loop was presented in the previous quarterly report.[7] Many of the methods and most of the equipment required in connection with the operation had been planned in detail at that time and were described. Methods and equipment which have been devised since are described here. The status of the engineering design and of the construction of the equipment is reported. Also included is a report of a determination of the thermal neutron flux in hole HB-4 of the LITR.

Neutron Shutter. As was mentioned in the previous report, the stoichiometric gas pressure in the in-pile loop must be determined at frequent intervals. To determine this pressure, it is necessary to reduce the neutron flux at the core to some known fraction of the normal value. Observations are then made of the resulting pressure drop in the loop. The pressure drop is a measure of the stoichiometric gas pressure prior to the reduction in flux. A flux depression of 40 to 50% will probably be necessary for these determinations.

The reduction in flux can be achieved by operating the pile at a fraction of the normal power during the measurements or by interposing a material black to neutrons between the core and the reactor. It will be undesirable to interfere with normal pile operation to the extent which would be necessary for these determinations. A neutron shutter is therefore indicated and is being planned.

Various schemes for obtaining a shutter action have been investigated. The scheme which appears to be most practical and which is being developed utilizes a cadmium foil held in a beryllium reflector piece in front of the hole. The beryllium is slotted so that the cadmium can be moved, in a vertical direction, in front of the hole or away from the hole. The position of the cadmium is controlled by means of a hydraulic cylinder mounted on the upper end of the beryllium. The cylinder is actuated by water pressure applied through small tubes which extend through the cover plate of the reactor.

The reflector pieces in the reactor are 3 in. wide. Some uncertainty exists as to whether a 3-in. width

[7] G. H. Jenks, D. T. Jones, and R. A. Rosenberg, *HRP Quar. Prog. Rep. July 31, 1953*, ORNL-1605, p. 100.

of absorber will reduce the flux in the hole by the desired 40 to 50%. Two adjacent pieces can be used if necessary, and the absorber can thus be made 6 in. wide. The use of two beryllium pieces would, of course, considerably increase the cost of the installation. Some measurements are now being made of the neutron flux along the axis of the hole with and without a cadmium foil at the end of the hole. The results of these measurements will be used in deciding whether one or two reflector pieces will be necessary.

Leak Detection. Provisions have been made in the design of the in-pile system for the detection of leaks of radioactive solution or gases during operation. These provisions are described below.

The interior of the loop is connected with equipment at the pile face through four tubes which are of capillary dimensions. The largest internal diameter is 50 mils and the smallest is 20 mils. These tubes are normally filled with inactive fuel solution or water. However, in case of a leak in the equipment which seals the tubes at the pile face, the tubes will become filled with active material from the loop. To detect leaks of this nature, each line at the pile face is passed in close proximity to one of four ionization chambers. The four chambers and lines are arranged so that, in case of a leak, the responsible tube can be identified.

Leaks from the loop into the loop jacket are also detected by radiation monitoring. Air is delivered continuously into the forward portion of the loop jacket during operation. The air passes back through the loop jacket, out through a duct in the rear of the jacket, and into the pile off-gas system. A section of the gas line between the jacket and the off-gas system is enlarged to a volume of 5 ml and filled with charcoal. Provisions are made for cooling the charcoal and gas to dry ice temperatures when desired. An external gamma detector of the scintillation type is used to monitor for radioactivity in the enlargement.

The rate of gas flow through the jacket will be adjusted at about 1 liter/second. For this flow rate, and with the charcoal at room temperature, the radiation monitor will reliably sense concentrations of activity in the gas stream which are developed by leaks of the order of 5×10^{-3} cc/sec or more. When the charcoal is at the low temperature, the sensitivity of leak detection will increase by a factor of 100 or more. The increased sensitivity will result from the holdup, by adsorption on the charcoal, of active xenon and, to a lesser extent, krypton.

In practice, the charcoal will be cooled at intervals of 10 to 12 hours. The long interval is permissible because the amount of material which might be lost during this time through undetected leaks would not seriously affect loop operation.

Solution Sampling. The method which has been adopted for withdrawing specimens of fuel solution from the loop is briefly the following. Solution from the loop is drawn through the drain line into a container. The volume of liquid which can be withdrawn at any one time is limited to the capacity of the container, about 3 milliliters. This volume is about one-half the capacity of the drain line between the loop and the container.

After the liquid is in the container, it is isolated from the drain line. The pressure on the liquid is adjusted, and the liquid is transferred to the fuel reservoir or to a removable sample bulb. In practice, the liquid comprising the first two fillings would be principally stagnant solution from the drain line, and these fillings would be discarded. The liquid in the third filling should be closely representative of that in the loop and would be transferred to the sample bulb.

The volume of solution removed from the loop in sampling is replaced with fresh solution immediately following completion of sampling. The fresh solution is added through the drain line so that active solution is flushed from it. The tube remains filled with fresh solution until the next sample is taken. Thermal expansion of liquid from a container of known volume is the method used to force the correct amount of fresh solution into the loop.

The apparatus required for sampling by this method is shown schematically in Fig. 44. The various parts and interconnections are evident from the sketch. The connection through which the sample bulb is joined to the system is of a special design which permits the connecting tubing and fillings to be freed of radioactive material. The essential feature of the design is a small tube which fits within the main tube as shown; wash solutions and gases are introduced into the system through this tube. The wash material enters at a point just below the seat of valve No. 10 and flows to the hot drain. It is believed that this design will make possible the removal of the sample bulb without the danger of contaminating the surroundings.

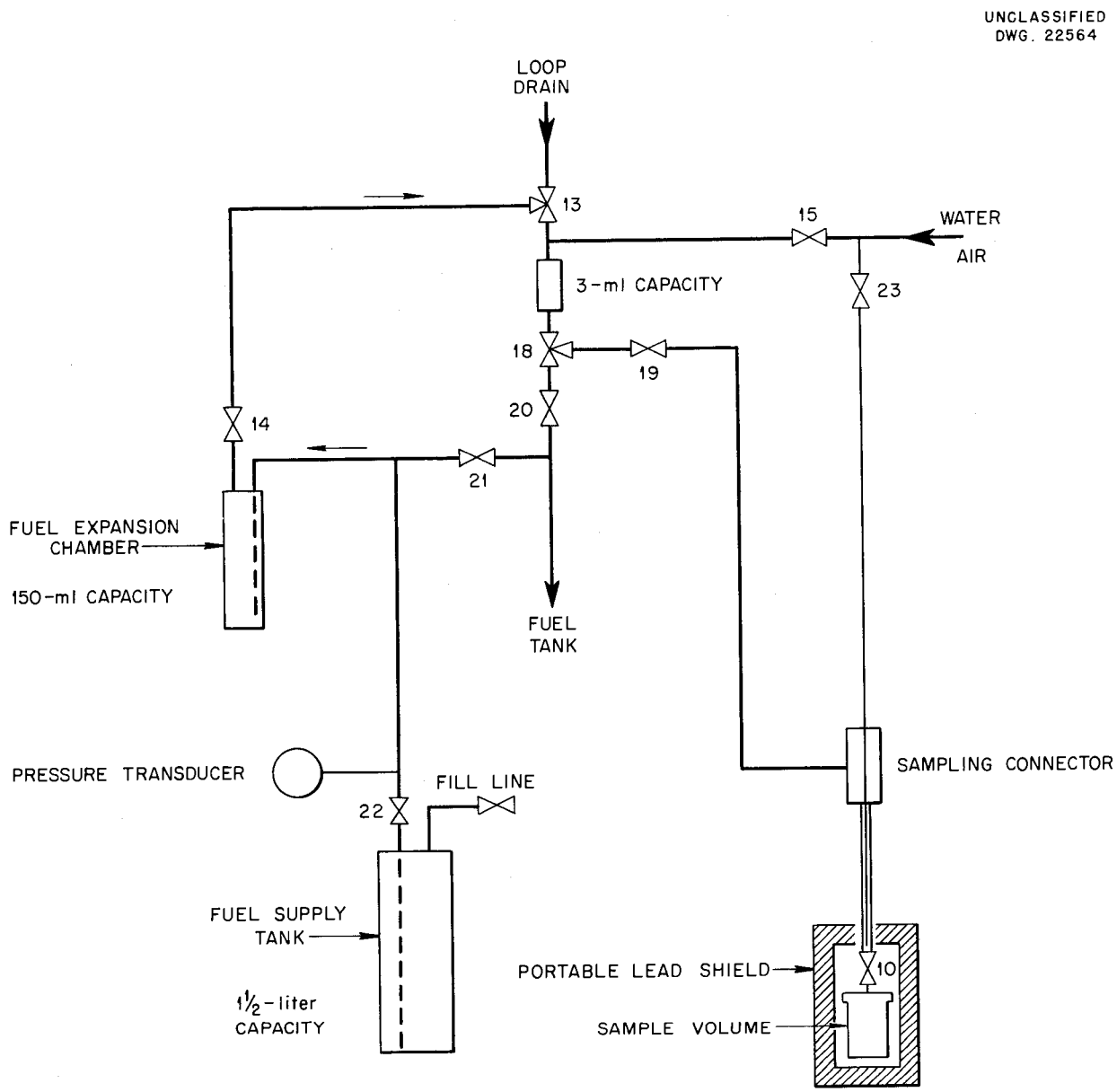

Fig. 44. Sampling System.

Tests of a preliminary nature have been made of the method and equipment, and the results indicate satisfactory performance. Final tests will be made in a mockup of the complete in-pile system.

Revision of Draining Equipment. The desire to simplify the drain equipment has prompted two changes in the previously reported design. The capacity of the fuel reservoir has been increased from 1.5 liters to 10 liters, and the 40-liter wash tank has been eliminated.

The added capacity of the fuel reservoir is now used for the recovery of uranium-rich wash solution. Formerly, the 40-liter tank was used for this purpose. Obviously, the volume of wash which can be collected is appreciably smaller than before; however, it is believed that the present capacity will permit the recovery of all the uranium which can be readily washed from the loop.

Neutron Flux in Hole HB-4. A determination has been made of the slow-neutron flux which will

prevail in the core solution and in the core corrosion specimens of the in-pile loop. The determination was carried out in the following manner. A duplicate was prepared of that portion of the loop assembly which fits within the tank of the reactor. Three small cobalt monitors were placed in the core section of the assembly. One of these monitors was located near the front of the core, another was near the rear, and the third was midway between the other two. All were on the axis of the core, and the distance between monitors was 7.5 cm. The assembly was exposed in the LITR hole, HB-4, for one week, during which time the reactor operated at 1900 kilowatts. Following exposure, the disintegration rate of each specimen was determined by means of a calibrated, 4π, gamma, ionization chamber.

The results of the measurements are summarized below in terms of the flux at each site for a reactor power of 3 megawatts. Values for the activation cross section and half life of cobalt were taken as 35 barns and 5.3 years, respectively.

CORE POSITION	FLUX (neutron/cm^2/sec)
Front	3.4×10^{12}
Middle	1.8×10^{12}
Rear	8.7×10^{11}

From these values, the power which will be developed from fission in the fuel solutions can be estimated. For solutions containing 40 g of 92%-enriched uranium per liter, the power developed in the forward position will be about 4.5 watts/milliliter. The power densities in the middle and rear positions will be, respectively, about one-half and one-fourth this value. The average power density will be about 2.8 watts/milliliter. Since the core will contain a total of 300 ml, the total power developed will be about 840 watts.

It should be noted that a change has been made in the reactor since the above data were obtained. Through an oversight, a magnesium reflector "L piece" was directly in front of a portion of the hole during the measurements. The magnesium has since been replaced with beryllium, and this change has probably resulted in an increase in the neutron flux in the hole.

Status of Design and Construction. Loop-accessory drawings are 80% complete. Final completion is scheduled for November 1, 1953, except for changes dictated by mockup operation. Wooden valve-box mockups will be completed and delivered to Y-12 by October 23, and a beam-hole liner which has been fitted to hole HB-4 will be ready shortly. All the accessory equipment for the two valve boxes will be ready for installation in the mockup boxes by late December.

The design of the loop disassembly equipment is about 80% complete, and construction is getting started. This equipment will all be installed by the time a mockup loop is ready for a test of the disassembly procedure.

Loop Package

Development and Design (C. D. Zerby, R. J. Kedl, T. H. Mauney, R. E. Wascher, W. L. Ross). Since much of the design of the basic circulating loop for the in-pile loop program has been completed, a general summary of the general features of the loop is given here.

The basic loop with all its major components is shown in Fig. 45. The loop liner indicated in the figure totally encloses the loop proper to confine the radioactive solution in the event of rupture of any component. A photograph of the first test model of the loop is shown in Fig. 46. The loop is designed to circulate an aqueous UO_2SO_4 solution containing 40 g of uranium per liter and with 0.01 M $CuSO_4$ as an internal, homogeneous catalyst for the recombination of the generated hydrogen and oxygen. The loop will operate at approximately 1000 psia pressure with a main loop temperature of 250°C and a pressurizer temperature of 280°C. The major portion of the loop will be constructed of type 347 stainless steel.

There will be two coupon sample holders in each loop. One coupon holder will be held in the center of the core, thus establishing it in the region of highest flux. It will also be arranged so that the solution leaving the core passes through the coupon holder, thus subjecting the corrosion specimens to the highest short-lived fission-product concentration. The other coupon holder will be placed in the circulating system removed from the high-flux region. Both coupon holders will be identical in every respect as far as the coupons are concerned. Considerable effort has been made to pattern the design of these coupon holders after the tapered ones now being used for the critical corrosion velocity investigations in the out-of-pile dynamic corrosion studies.

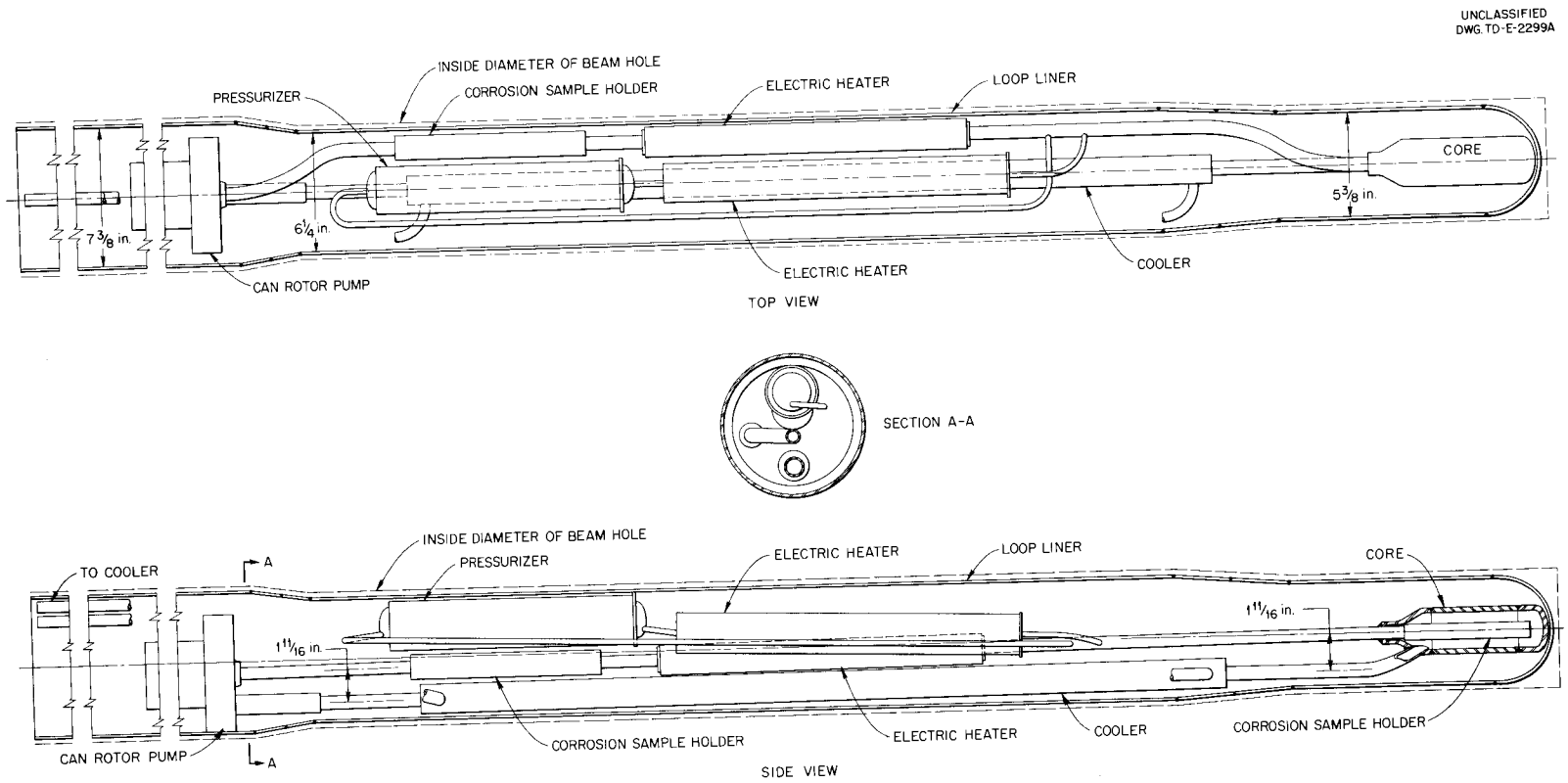

Fig. 45. Layout of In-Pile Loop.

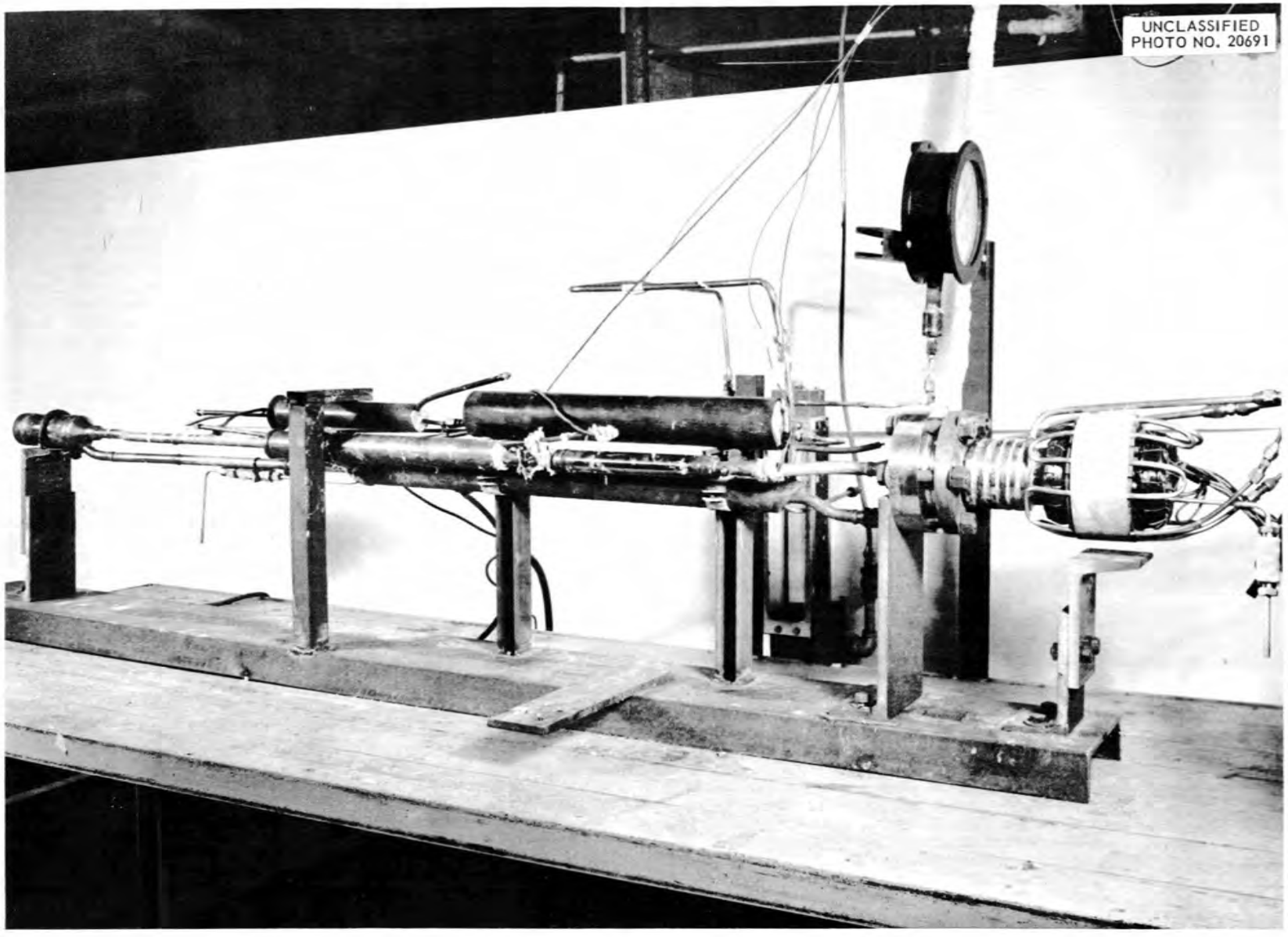

Fig. 46. Test Model of In-Pile Loop.

Figure 47 gives a view of the assembled coupon holder with coupons, and it also shows a velocity distribution curve. The coupon holder is designed in the form of a venturi in order to minimize the pressure drop, which, for a flow rate of 5.8 gpm, was measured to be 16.2 ft of water. Each coupon holder will have 12, 0.496 × 0.499 × 0.060 in. coupons. As can be seen from Fig. 47, the cross-sectional flow area is rectangular, and fluid flows on both sides of the coupons. The fluid enters the coupon holder at about 10 fps and reaches 36 fps at the end of the first tapered section. The second tapered section, which is about one-third as "steep" as the first tapered section, is necessary in order to distribute the higher velocities over two coupons. In this section, which is 1 in. long, the fluid velocity increases from 36 fps to 51 fps, giving an average velocity increase of 7.5 fps/coupon. The fluid velocity then decreases from 51 fps back down to pipe velocities in the outlet taper.

The coupon holder has been designed so that the coupons do not extend through the side of the holder. This design minimizes bypassing of the solution between the two halves of the holder. Recent exposure of the coupon holder and coupons in the solution under simulated operating conditions gave no indication of bypassing. The two halves of the coupon holder are held together by two type 347 stainless steel bands which are crimped into place to hold them secure. On the core coupon holder, part of the wall is machined away as indicated by the dotted line in Fig. 47. This was done to reduce the neutron absorption and to permit the highest possible flux to exist at the coupons.

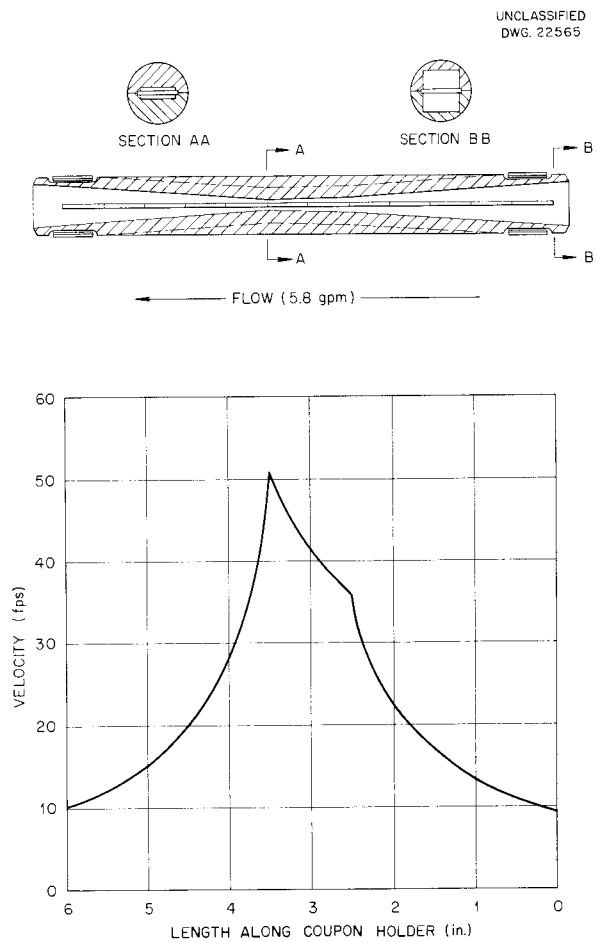

Fig. 47. Diagram of Coupon Holder for In-Pile Loop with Velocity Distribution.

Several design changes have had to be made on the core coupon holder of the in-pile loop as a result of exposing a model in the dynamic corrosion test loops to the solution expected to be used in the in-pile loop. In the higher velocity regions of the sample holder, the protective film is not formed; corrosion of the surfaces proceeds rapidly, which opens the flow passage and reduces the pressure drop. This corrosion results in a changed flow rate and a change in velocity past the corrosion coupons. This effect can be reduced by making the coupon holders of titanium or zirconium, which have very good corrosion resistance in the solution. Because of the low cross section, zirconium will be used in the in-pile studies; the titanium will be used in the out-of-pile studies. The design change was necessary in order to provide a means of holding the new coupon holders, since they cannot be welded to the type 347 stainless steel core as were the previous type 347 stainless steel holders.

The means for supporting eight, 5-in.-long, approximately ¼-in.-round or square, impact specimens in the core is also under consideration. Designs for this modification are essentially complete.

Results of building and operating the first test model of the in-pile loop showed that each item in the loop required modification. These changes have been made on all but the pressurizer and the heater on the line to the pressurizer. Design changes are now being made on the last two items. Testing of the changed components will be done in a development loop being constructed at this time.

Work is also in progress on the design of a fixture for fabricating the loops to the precise dimensional tolerances which are dictated by the limited confines of the beam hole. Designs are also being considered for the guides that are necessary to orient the finished loop within the loop liner can and to permit easy removal after irradiation in the pile.

A more complete model of the in-pile loop is now under construction as a development loop. This loop will consist of all the modified components of the basic loop, but it will be instrumented with identical instrumentation.

Some difficulties have developed in the thrust bearings for the ORNL small pump to be used in the in-pile loop. This is reviewed under "ORNL Small Pump" below.

ORNL Small Pump (C. D. Zerby, T. H. Mauney, C. B. Graham). The ORNL small pump has been under development in conjunction with the in-pile loop program.

One 200-hr run has been made at 250°C with a uranyl sulfate solution containing 40 g of uranium per liter with 0.01 *M* $CuSO_4$. Examination of the system after the run indicated that the uranium had partially precipitated during the run. Although the pump continued to operate satisfactorily during this test, there was excessive wear on the Graphitar thrust bearing. A comparison of the thrust faces of the bearings of the pump which had run on fuel and those of a pump that had run only in water showed similar characteristic wear. The trouble was attributed, at least partly, to an improperly located machine relief groove located at the edge of the thrust face. Excessive unit loading of the thrust bearing could also have been partly responsible for the wear. The groove at the edge of the thrust face has now been removed, and the thrust bearing has been enlarged to reduce the unit loading. Tests on the redesigned sections in water are under way.

In connection with the in-pile loop program, there is some concern as to the effect of wear on the Graphitar bearings. As the bearings wear, particles of the graphite get into the main fuel-circulating stream at 250°C, and the carbon is oxidized to carbon dioxide. This could result in unduly rapid oxygen consumption, particularly in a relatively small system. In the event that small but significant amounts of Graphitar bearing wear cannot be tolerated in the in-pile loop, all-metal bearings have been designed and are now under construction. The metal bearings consist of two $\frac{3}{4}$-in.-long Stellite 98M2 bearings, running on a Stellite 6 journal.

STATIC CORROSION STUDIES

J. L. English

Static corrosion studies are nearing completion on the corrosion of Inconel, Inconel X, Stellite 6, Stellite 98M2, tantalum, and type 347 stainless steel exposed in decontamination solutions at room temperature and at 85°C. The decontamination solutions under consideration are: 20% HNO_3–3% HF (by weight) and inhibited 1.2 *M* HCl–1.8 *M* H_2SO_4 containing approximately 0.05 *M* H_2O_2. Duplicate test specimens are removed at cumulative intervals of 1, 4, 24, 72, and 100 hours. A summary of these data will be included in the next quarterly progress report.

A test program was initiated during this past quarter for examining the corrosion behavior of type 347 stainless steel in thorium nitrate solutions as a function of thorium concentration and temperature. The thorium nitrate solutions are 2.07, 6.21, and 10.35 *M*, and the temperatures involved are 100, 150, 200, and 250°C. Corrosion tests are run for 100-hr periods at each temperature and solution concentration. All tests are operated with an oxygen partial pressure of approximately 150 psig.

Several miscellaneous corrosion tests were completed during the past quarter, and the results are summarized in the following sections.

Corrosion of Type V2B Stainless Steel

A specimen of hardened type V2B stainless steel was obtained from the Cooper Alloy Foundry Company and subjected to tests in uranyl sulfate solutions under various static conditions. Type V2B is a hardenable 18-8 stainless steel containing copper, molybdenum, silicon, and a small amount of beryllium. The combination of high strength, hardness, and nongalling characteristics possessed by the alloy makes it a desirable material for pump impellers, valve disks and trim, and other wearing parts. The corrosion resistance of type V2B stainless steel in the hardened condition in sulfuric, hydrochloric, and phosphoric acids is supposed to be superior to all other precipitation-hardenable alloys and even to that of type 316 stainless steel.

The test specimen was a machined disk 1.9 cm in diameter by 1.35 cm in length for an apparent

surface area of 13.7 cm^2. The measured hardness of the alloy was 56 Rockwell C.

The first two corrosion tests consisted of 100-hr runs at 100 ± 2°C in 0.42 *M* and 1.26 *M* uranyl sulfate solutions. The test solutions were neither aerated nor agitated in any manner. At the completion of each run, the specimen was weighed, electrolytically defilmed in inhibited 5% H_2SO_4, reweighed, and examined at a magnification of 30X for evidences of corrosion damage.

After 100 hr in the 0.42 *M* sulfate solution and after defilming, the specimen showed a weight gain of 0.1 mg/cm^2; other than the presence of small deposits of gray-colored and extremely adherent film, there were no indications of corrosion attack. The defilmed weight loss in the 1.26 *M* uranyl sulfate solution was slightly in excess of 0.2 mg/cm^2 for a corrosion rate of 1 mpy after 100 hours. No signs of corrosion damage were observed on the specimen.

The alloy was next exposed for 100 hr in 0.17 *M* uranyl sulfate solution contained in a stainless steel autoclave at 250°C with an oxygen partial pressure of approximately 150 psia. The specimen was electrically insulated from the autoclave by means of a quartz-rod hanger. Three attempts to run this test were unsuccessful; in all cases, the uranyl ion was reduced and precipitated as uranium oxides, and the specimen suffered severe corrosion damage. Defilmed weight losses on the specimen were in excess of 30 mg/cm^2 for each run.

On the basis of these preliminary tests, the behavior of the hardened V2B alloy looks fairly promising in 0.42 *M* and probably less concentrated uranyl sulfate solutions at 100°C, but its use at temperatures of 250°C in solutions containing 40 g of uranium per liter appears to be prohibited.

Corrosion of Colmonoy 6

In conjunction with the development of a suitable bearing surface for the ORNL 5-gpm pump, static corrosion studies were made with Colmonoy 6. Colmonoy 6 is a nickel-base, hard-facing alloy which contains 13 to 20% chromium, 2.75 to 4.75% boron, and a 10% maximum of iron, carbon, and silicon. The prepared specimens were tested at 95°C in air-aerated 0.17 *M* uranyl sulfate solutions, with and without 0.01 *M* $CuSO_4$ present.

The test specimens consisted of approximately 0.3-cm-thick deposited layers of Colmonoy 6 on 0.64-cm-thick pieces of type 347 stainless steel. The nominal surface area per specimen was 58 cm^2, of which nearly 30% was Colmonoy 6. After the hard facing operation, the deposited metal was given a medium-smooth grinding finish. Control specimens of type 347 stainless steel, prepared from the same material on which the Colmonoy 6 was deposited, were also run in each test.

The corrosion resistance of Colmonoy 6 was found to be extremely poor in the 0.17 *M* uranyl sulfate solutions, and the tests were stopped after 24 hours. Based on the weight losses attributable to corrosion on Colmonoy areas only, the hard-facing alloy exhibited nominal thickness losses of 1.3 and 1.6 mils, respectively, in aerated solutions without and with 0.01 *M* $CuSO_4$ present. Corrosion attack was generalized in nature with the surface assuming a dull black and heavily etched appearance. The type 347 stainless steel areas retained their original lustrous surface.

Thus, with weight losses of 8 to 10 mg/cm^2 in a 24-hr period, it is entirely reasonable to exclude Colmonoy 6 from further consideration as a bearing material for use in uranyl sulfate solutions.

Similar tests are now in operation with Stellite 12 hard-facing alloy.

METALLURGY

E. C. Miller, Section Chief

WELDING OF AUSTENITIC STAINLESS STEELS

W. J. Leonard

In an investigation of the metallurgical characteristics of weld-material combinations of type 347 stainless steel plate and weld rod considered for HRP work, selected materials were cast into 1-in.-dia buttons by vacuum-induction melting followed by slow cooling. The purpose was to produce a coarser segregation than normally occurs in welds and thus to facilitate metallographic examination of the phases formed in the solidification of welds, with a view to permitting identification and determination of the structural distribution of the phases. The cast buttons were sectioned along an axial plane which cut through the center of the shrinkage cavity and pipe.

Three different material types were melted: Oxweld 60 weld wire (a type 347 stainless steel rod with a composition balanced to give 6 to 10% ferrite) used in HRE welding; a commercial heat of ½-in., type 347 stainless steel plate with a relatively high silicon content that is within the range of the permissible ASTM specification; a commercial heat of ⅝-in., type 347 stainless steel plate with a silicon content that is on the low side of the permissible ASTM specification.

The microsections gave no indication of abnormal ferrite segregation in the area of the pipe, although some normal carbide segregation was observed. Metallographic etching techniques and Magne-gage examination of the buttons gave ferrite contents of 8 to 9% in the remelted weld wire, approximately 3% in the remelted high-silicon plate, and approximately 2% in the remelted low-silicon plate.

Because of the greater corrosion attack on some welds of high ferrite content compared with the attack on the initially austenitic base metal, when tested in certain dynamic corrosion tests (under conditions more severe than those contemplated for the present two-region power breeder reactor), several experimental heliarc welds were made as part of a study of the feasibility of producing suitable fully austenitic welds. Three types of welds were made in which excessively high heat inputs, 150 to 200 amp, were used: (1) Several single-pass welds were made by using a fusion pass in the root and no added filler wire. About half these welds cracked completely through immediately after the welding pass was finished or after subsequent cooling. Microscopic examination of one of the sound welds showed a fair amount of ferrite, and Magne-gage inspection indicated ½% ferrite. (2) Welds of the first type were completed by filling the grooves with Oxweld 28 filler rod (a type 347 stainless steel composition intended to give a fully austenitic weld). All welds were sound. Microscopic examination showed more ferrite than was present in the first type, and the ferrite content indicated by the Magne-gage ranged from 2% in the root of the weld, where some dilution by base metal occurred, to 4.4% in the top of the weld, where little or no dilution was involved. (3) All passes (one root and two filler) of the third type of weld were made by using Oxweld 28 filler rod. The ferrite content of the welds ranged from 3.2% where dilution occurred to 4.4% at the top of the weld – contents that were similar to those of the second type of weld. All welds of the third type were sound.

FRACTURE BEHAVIOR OF TITANIUM AND ZIRCONIUM

A. R. Olsen

A study of the notch susceptibility of titanium and of zirconium is being made in which a modification of the Kinzel notched-bar slow-bend test,[1] which has been used successfully in carbon steel investigations at Lehigh University, is used. The test consists in centrally loading a freely supported beam containing a notch in the center of the tension side and in obtaining a load-deflection curve through failure. The original plan was to use flat samples, 1⅜ × ½ × ⅛ in., with a machined notch; however, since a large number of corrosion pins 0.204 in. in diameter and 1⅜ in. long were available, it was decided to use them in a preliminary investigation of temperature effects. Because of the complicated notch effects on a round specimen, the procedure for making the notch was as simple and as reproducible as possible. A file notch, made by using a hardened

[1] A. B. Kinzel, *Trans. Am. Soc. Metals* 40, 27-82 (1948).

steel die for geometry control as suggested in a paper by Zapffe and Worden,[2] proved to be quick and economical and gave surprisingly good reproducibility. Shadowgraph and microscopic examinations of some 100 notches showed the angle to be 90 ± 1 deg, the maximum depth of the notch to be 0.043 ± 0.003 in., and the width of the root of the notch to be 0.005 ± 0.0005 inch.

Energy absorption, integrated from a curve of deflection-load, plotted against temperature has given the points which are shown in Fig. 48 and which compare remarkably well with the data of modified-Izod tests on the same material. The samples that were broken varied widely in previous history. All were taken from a single heat of each alloy, but some were in an as-machined condition, while others had been corrosion tested for different periods in different media. Within the rather broad scatter limits, it is difficult as yet to observe any recognizable effects of the corrosion testing.

The work to date is still very preliminary. It is planned to use other criteria[3] for evaluating ductile-to-brittle fracture transition in future tests so that a better understanding of the behavior of titanium and of zirconium and possibly the mechanism involved in this behavior can be obtained.

PROPERTIES OF TITANIUM AND ZIRCONIUM ALLOYS

W. J. Fretague

Commercial-Purity Titanium

Some differences in the microstructure of commercial-purity titanium (Ti-75A) have been observed after a one-month exposure to hydrogen at 250°C. Experiments are in progress that involve the vacuum-fusion analyses of material in the as-received condition, as well as following thermal treatments in a purified hydrogen atmosphere at 250°C, to determine whether the effect is simply a heat-treatment effect or whether it results from occlusion and diffusion of hydrogen, followed by precipitation of a hydride phase.

Zirconium-Aluminum System

Attempts to remelt the three previously described[4] zirconium alloys, which were calculated to approximate the composition of the peritectoid compound ZrAl, were unsuccessful in that all the melts cracked on cooling. Work is continuing in an effort to produce crack-free melts.

Zirconium-Tin Alloys

It is presently contemplated that Zircalloy II will be used for the construction of the core tank in the two-region thermal power-breeder homogeneous reactor. The suitability of this material or, in any event, the permissible design of the core tank will be determined in part by the notch sensitivity of the structural material and the welded joints, as affected by composition, metallurgical treatment, temperature of operation, and reaction to environment. The initial survey for studying these factors involves notch-bar impact testing of the material over a range of temperatures, both before and after exposure to simulated corrosion environments.

Impact tests were performed on four specimens of Zircalloy II that were machined from ¼-in.-thick plates of two heats (F-789 and F-909) received from WAPD. One specimen from each heat was machined to a rod that was 0.204 in. in diameter and 6¾ in. long and that had 45-deg circumferential V-notches spaced at 1-in. intervals along its length. The notch-root diameter was 0.164 in. and the root radius was 0.005 inch. The remaining specimen from each heat was 0.200 in. square and 6¾ in. long and had 0.040-in.-deep, 45-deg, V-notches located perpendicular to the rolling plane of the plate at 1-in. intervals along the length of the specimen. Table 12 lists the data obtained, and Fig. 49 is a graphical representation of the results.

Specimens of Zircalloy II were obtained from ⅜-in.-dia rods which were swaged to 0.217-in. dia, sand blasted, pickled, vacuum annealed at 750°C for 2 hr, and furnace cooled, prior to machining. Sixteen, 10¾-in.-long specimens were prepared and submitted to the Dynamic Corrosion Group for testing. Impact tests have been performed on four of these specimens that were exposed to a UO_2SO_4 solution containing 40 g of uranium per liter. The exposure was for 400 hr at 300°C with a 100-psi O_2 overpressure (run A-57). The results of the impact tests are listed in Table

[2] C. A. Zapffe and C. O. Worden, *Welding Research Supplement*, p. 47S-54S (Jan. 1949).

[3] C. J. Osborn, A. F. Scotchbrook, R. D. Stout, and B. G. Johnston, *Welding Research Supplement*, p. 24S-33S (Jan. 1949).

[4] W. J. Fretague and E. C. Miller, *HRP Quar. Prog. Rep. July 31, 1953*, ORNL-1605, p. 118.

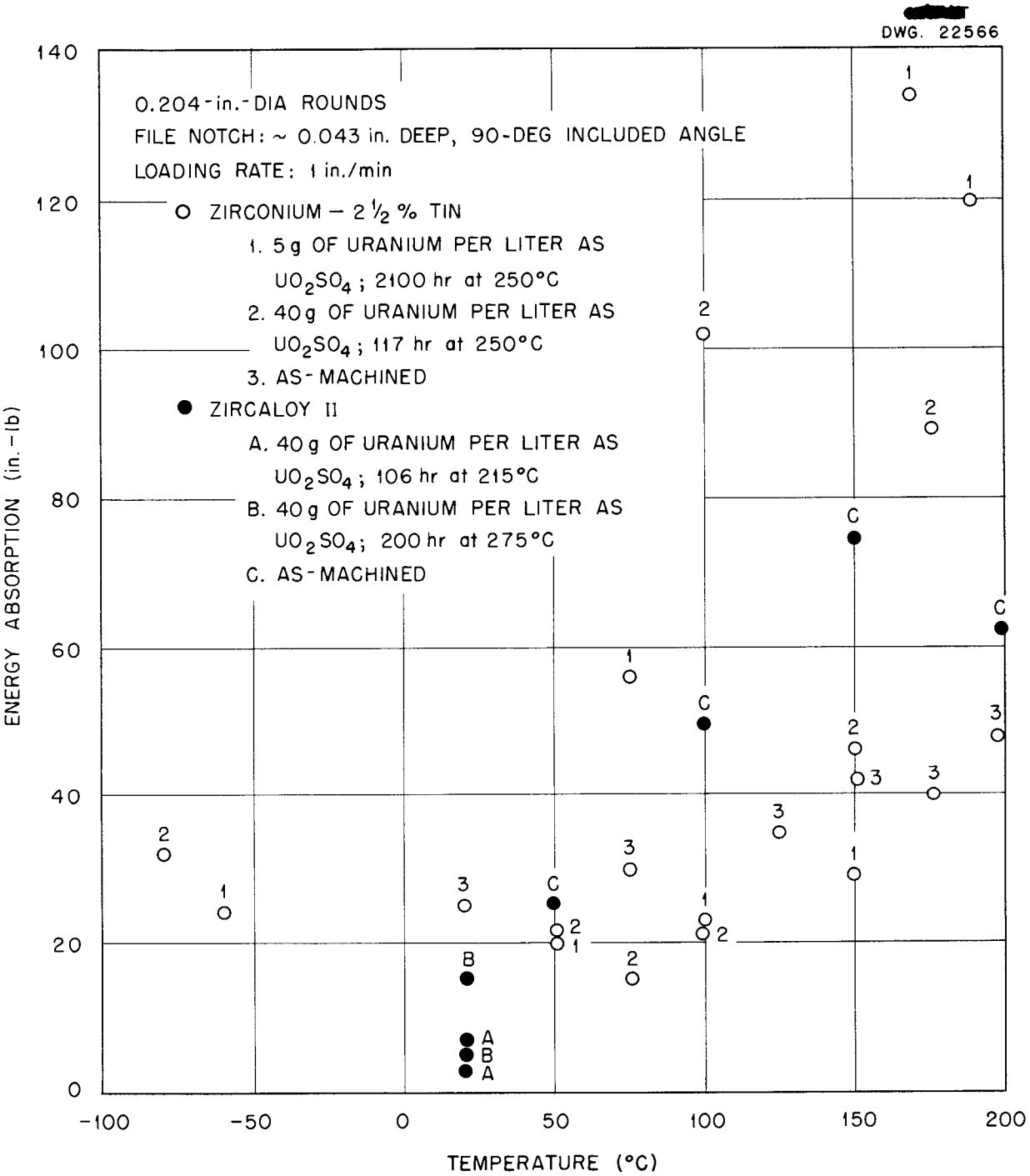

Fig. 48. Notch Slow-Bend Tests of Zirconium – 2½% Tin and Zircalloy II Alloys.

13 and are presented graphically in Fig. 50. Representative samples of the swaged, vacuum-annealed, Zircalloy II, impact specimens before and after corrosion testing have been submitted for O_2, N_2, and H_2 analysis by the vacuum-fusion method.

The Zircalloy II rods from which the corrosion impact specimens were machined were analyzed by J. Edgerton of the Chemistry Division. The results of the analyses are presented in Table 14.

SELECTIVE OXIDATION OF AUSTENITIC STAINLESS STEELS

W. O. Harms T. W. Fulton

Selective oxidation by pretreatment in moist hydrogen, as a means for improving the corrosion resistance of austenitic stainless steels in HRP loop environments, was discussed in the previous quarterly report.[5] During this quarter, additional pretreated specimens were subjected to dynamic corrosion tests, and the oxide films formed under certain conditions of pretreatment were studied by electron diffraction, electron microscopy, x-ray diffraction, and chemical analysis.

Corrosion Tests

A series of pins and coupons was pretreated at 1000°F for 24 hr in hydrogen containing 6 vol % moisture. The pins, which included AISI types

[5] W. O. Harms, T. W. Fulton, and E. C. Miller, *HRP Quar. Prog. Rep. July 31, 1953*, ORNL-1605, p. 115.

TABLE 12. IMPACT ENERGY vs. TEMPERATURE FOR ROUND AND SQUARE SPECIMENS MACHINED FROM ZIRCALLOY II PLATES*

SPECIMEN NUMBER	NOTCH NUMBER	SCALE USED (in.-lb)	TEMPERATURE (°C)	IMPACT ENERGY (in.-lb)
F-879R (Round)	1	0 to 100	35	4
	2	0 to 100	−195.6	<1
	3	0 to 100	−100	1
	4	0 to 100	60	4.5
	5	0 to 100	120	0.9
	6	0 to 100	200	28.5
F-909R (Round)	1	0 to 100	35	11
	2	0 to 100	−195.6	4
	3	0 to 100	−100	4.5
	4	0 to 100	60	9
	5	0 to 100	120	11
	6	0 to 100	200	36.5
F-879S (Square)	1	0 to 25	30	15.25
	2	0 to 50	60	15.5
	3	0 to 50	−195.6	3
	4	0 to 50	−100	3.5
	5	0 to 50	120	27
	6	0 to 50	200	64.5
F-909S (Square)	1	0 to 25	30	17.5
	2	0 to 50	60	Pendulum hit thermocouple
	3	0 to 50	−195.6	4
	4	0 to 50	−100	6
	5	0 to 50	120	34
	6	0 to 100	200	62

*Specimens machined from ¼-in. plate of heats F-879 and F-909.

TABLE 13. TEMPERATURE DEPENDENCE OF IMPACT BEHAVIOR OF ZIRCALLOY II SPECIMENS AFTER CORROSION EXPOSURE*

SPECIMEN NUMBER	NOTCH NUMBER	SCALE USED (in.-lb)	TEMPERATURE (°C)	IMPACT ENERGY (in.-lb)
Z 2-9	1	0 to 100	27	15.5
	2	0 to 100	0	11.0
	3	0 to 100	−40	10.0
	4	0 to 25	−80	11.0
	5	0 to 25	−120	9.5
	6	0 to 25	−195.6	6.0
	7	0 to 50	50	12.0
	8	0 to 50	70	17.0
	9	0 to 100	280	79.5**
	10	0 to 100	300	81.5**
Z 2-12	1	0 to 50	40	14.5
	2	0 to 50	60	15.5
	3	0 to 50	80	18.0
	4	0 to 50	100	18.5
	5	0 to 50	120	22.5
	6	0 to 50	140	25.5
	7	0 to 50	160	31.5
	8	0 to 50	180	38.5**
	9	0 to 100	200	47.0**
	10	0 to 100	220	58.5**
Z 2-14	1	0 to 50	100	21.5
	2	0 to 50	130	24.5
	3	0 to 50	150	29.0
	4	0 to 50	170	33.0
	5	0 to 100	190	41.5**
	6	0 to 100	210	51.0**
	7	0 to 100	240	75.0**
	8	0 to 100	260	73.2**
	9	0 to 50	90	21.5
	10	0 to 50	110	28.5
Z 2-15	1	0 to 100	20	***
	2	0 to 50	40	15.0
	3	0 to 50	70	15.0
	4	0 to 50	90	18.5
	5	0 to 50	110	21.0
	6	0 to 50	130	32.0
	7	0 to 100	230	56.0**
	8	0 to 100	250	59.0**
	9	0 to 100	270	71.0**
	10	0 to 100	290	75.5**

*Specimens machined from swaged and vacuum-annealed rod and exposed in UO_2SO_4 solution containing 40 g of uranium per liter at 300°C for 400 hr prior to impact testing.

**Specimen did not break.

***Missed reading.

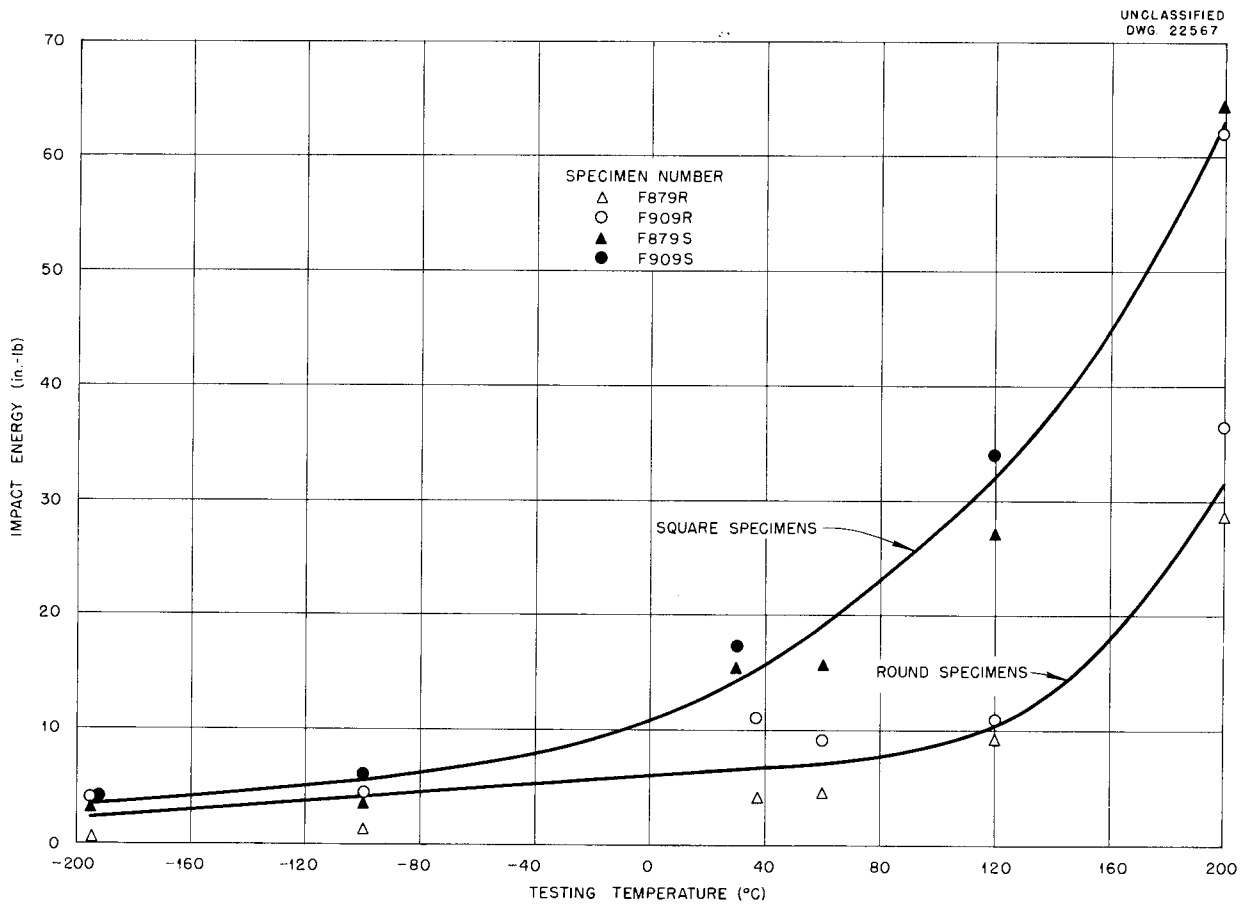

Fig. 49. Impact Energy vs. Temperature for Round and Square Specimens Machined from Zircalloy II Plates.

TABLE 14. CHEMICAL ANALYSIS OF ZIRCALLOY II ROD USED FOR CORROSION IMPACT SPECIMENS*

ALLOYING ELEMENTS	TYPICAL COMPOSITION (wt%)	ACTUAL ANALYSIS (wt%)
Sn	1.3 to 1.6	1.1
Fe	0.07 to 0.20	0.20
Cr	0.05 to 0.16	0.034
Ni	0.03 to 0.08	0.044
N	0.006 max	<0.001
C	<0.01	0.055

*Sample number N 1271

304, 304L, 347, 321, and 309 SCb stainless steel, were loop tested in oxygen-pressurized 0.06 M UO_2SO_4 (15 g of uranium per liter) plus 0.015 M H_2SO_4 for 200 hr at 250°C and at flow rates of 15 to 16, 36, and 58 fps. The coupon specimens were of type 304L stainless steel and were tested in a tapered-bore specimen holder in the same run over a range of flow rates from 9 to 81 fps.

Results of the pin tests are shown in Fig. 51, where pretreated specimens are compared with as-machined specimens tested in the same run. Included in this plot are data for six pins of type 304L stainless steel, pretreated at temperatures other than 1000°F, and tested at 36 fps. Pretreatment temperatures and defilmed weight-change data for these specimens are given in Table 15.

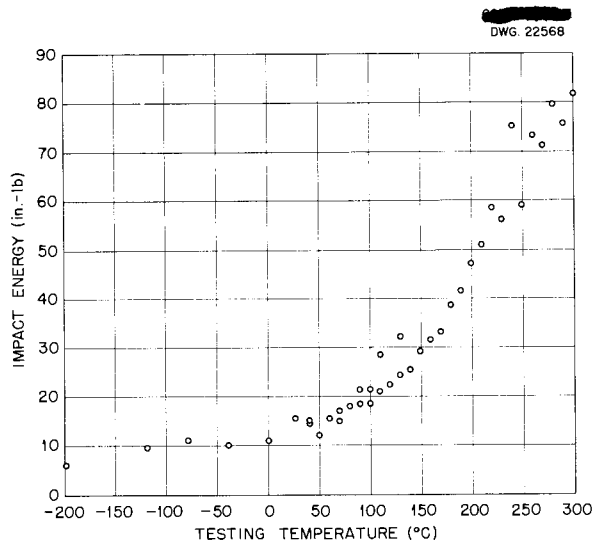

Fig. 50. Temperature Dependence of Impact Behavior of Zircalloy II Specimens After Corrosion Exposure. Specimens swaged from ⅜-in.-dia rod to 0.217-in.-dia rod; sand blasted, pickled, vacuum annealed at 750°C for 2 hr, and furnace cooled; and exposed to solution of 40 g of uranium per liter as UO_2SO_4 at 300°C for 400 hr prior to impact testing.

TABLE 15. EFFECT OF PRETREATMENT TEMPERATURE ON CORROSION RESISTANCE OF TYPE 304L STAINLESS STEEL PIN SPECIMENS*

PRETREATMENT TEMPERATURE (°F)	DEFILMED WEIGHT CHANGE (mg)
900	−1.3
1150	−0.4
1300	−0.4
1500	+2.6**
1850	−0.8
1950	−14.3

*Pretreated 24 hr in hydrogen containing 6 vol % H_2O and loop tested in 0.06 M UO_2SO_4 plus 0.015 M H_2SO_4 for 200 hr at 250°C and 36 fps.

**Film not removed by standard defilming technique.

Coupon data are shown in Fig. 52, along with data for as-machined coupons from loop run A-44 in which test conditions were the same.

Film Studies

The oxide films on pin specimens of type 304L stainless steel pretreated in hydrogen containing 6 vol % moisture for 24 hr and at temperatures of 900, 1000, 1150, 1300, 1500, 1850, and 1950°F were studied by electron diffraction, electron microscopy, x-ray diffraction, and chemical analysis. The results of these studies are given in Table 16.

Electron micrographs of stripped films showed that in all cases the oxides formed by pretreatment consist of at least two layers, the total thickness varying from approximately 200 Å to more than 1000 Å at 1950°F. Electron transmission diffraction data indicate that the substrate layers are rich in a spinel phase and that they sometimes show traces of Cr_2O_3. X-ray diffraction patterns, which reveal the structures in the entire films, show, in addition, a double-halo effect similar to that found in "diffraction" patterns of amorphous silica.

The films were analyzed spectrographically for iron, chromium, manganese, and nickel. In Table 16 it is seen that, with the exception of specimen No. 2, the effect of increasing pretreatment temperature on the composition of the film is to decrease the iron and nickel contents and to increase the chromium content. Manganese does not behave in any consistent fashion, being lowest in specimen No. 2 and highest in No. 5. The film from specimen No. 3 could not be dissolved in a suitable condition for spectrographic analysis, and the material left from specimen No. 7 after film had been removed for electron-diffraction studies was not analyzed because it did not appear to be representative of the oxide layers in their original form.

Discussion

The corrosion tests indicate that if the pretreatment film, produced under the conditions described, fails, it may be wholly ineffective but that if it forms in a continuous and uniform manner it may retain its protective ability even at fairly high flow rates. This behavior is most pronounced at a flow

[redacted]
DWG. 21811A

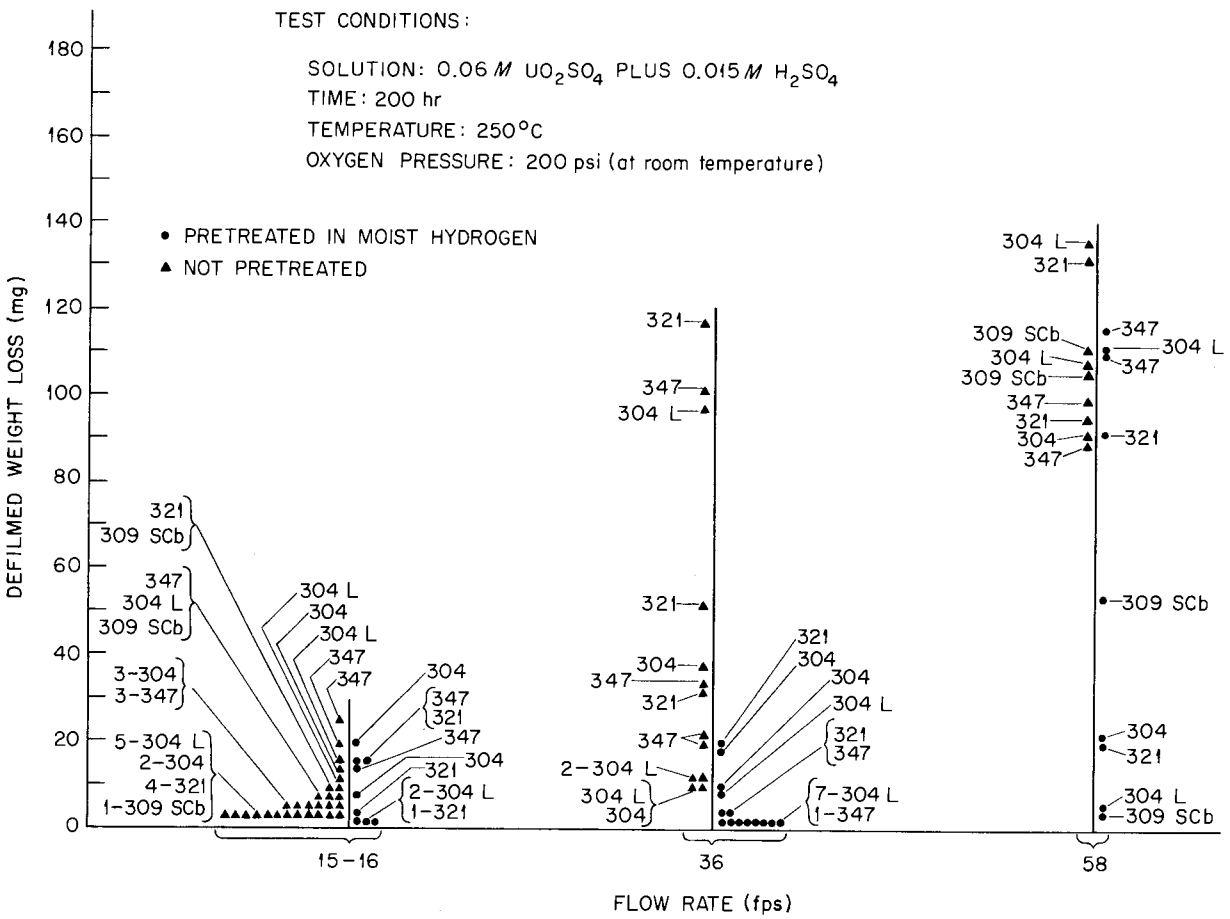

Fig. 51. Effect of Moist Hydrogen Pretreatment of Austenitic Stainless Steel on Corrosion Resistance in Dynamic Loop Tests.

rate of 58 fps (see Fig. 51). The coupon-test data show that although the particular treatment used may raise the threshold velocity below which the oxide film is stable, considerable damage may occur at higher flow rates. It should be emphasized that, except for the six pins mentioned previously, these corrosion data are representative of one set of pretreatment conditions only. Corrosion tests and film studies on specimens pretreated at higher temperatures indicate that optimum conditions of pretreatment time, temperature, and moisture content were not achieved in the experiments described here. Present efforts are directed toward determining such optimum conditions.

Film studies indicate that on the basis of the limited corrosion tests performed the most protective films are high in chromium and manganese and low in iron and nickel contents, contain spinels of high lattice parameter, and may contain considerable amounts of silica, although evidence of this is only indirect at present. The significance of the lattice parameters of many of the spinels found is difficult to evaluate, since spinels containing iron, chromium, nickel, and manganese of a wide range of compositions are known to have unit cell dimensions of 8.36 to 8.39 kX units (kX × 1.00202 = 1 Å). However, an interesting correlation exists between x-ray diffraction and chemical analysis data in the case of low- and

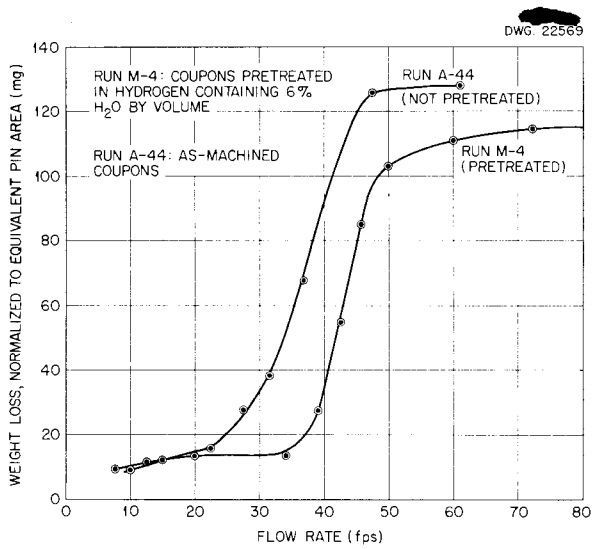

Fig. 52. Effect of Moist-Hydrogen Pretreatment on Corrosion Resistance of Type 304L Stainless Steel Coupons. Test conditions for both runs: 0.06 *M* UO_2SO_4 plus 25 mole % excess H_2SO_4 for 200 hr at 250°C and at an O_2 pressure of 200 psi.

high-parameter spinels: low-parameter spinels are often associated with the presence of Ni^{++} (the lattice parameter of $NiO{\cdot}Cr_2O_3$, for instance, is 8.32 kX units) and were observed in the low-temperature runs where chemical analysis showed relatively high nickel contents; the accepted parameter for $MnO{\cdot}Cr_2O_3$ is 8.43 kX units, exactly as found for specimen No. 5 of Table 16, which showed the highest manganese content and very high chromium content. The less continuous scale formed at 1950°F is apparently less protective than are the uniform films formed at lower temperatures.

STRESS CORROSION CRACKING OF TYPE 347 STAINLESS STEEL

W. O. Harms T. W. Fulton

Preliminary experiments have been performed in the study of the effects of plastic deformation and subsequent heat treatment on the stress-corrosion cracking of austenitic stainless steels. Such effects, if found to be significant, would require consideration in the development of specifications for composition, forming, and heat treatment of heat exchanger tubes and tube sheets.

Three-inch lengths of annealed, type 347 stainless steel, ¼-in. tubing having a 1/32-in. wall thickness were crimped at the ends, twisted through 90 deg, and bent through 95 to 100 deg at the midpoint at temperatures of –320, 75, 212, and 400°F. All specimens were tested in the as-worked condition, and, in addition, the subzero worked specimens were tested after partial stress relief and full annealing at 750 and 1900°F, respectively. Two of the subzero worked and heat-treated specimens were elastically stressed by a stud-and-nut arrangement through the crimped ends of the specimens.

The corrosion tests were performed by the HRP Static Corrosion Group in boiling 42% magnesium chloride solutions under conditions of total reflux. Specimens were removed every ½ hr and examined microscopically at 30X for evidence of cracks. The results are summarized in Table 17.

The severely stressed specimens (No. 5 and No. 6) showed the best stress-corrosion resistance under the test conditions employed, and those worked at room temperature and higher (No. 7 through No. 14) were the least resistant. The specimens worked at –320°F (in liquid nitrogen) were strongly magnetic at the ends and in the bend. Specimens heated to 750°F remained magnetic; however, those which were fully annealed and those which were deformed at room temperature and higher without subsequent heat treatment were not magnetic. The observed magnetism is believed to be due to the presence of pseudo-martensitic ferrite formed during plastic deformation and subzero cooling; this is being checked metallographically and will be reported later.

Specimen No. 2, which was subzero worked, fully annealed, and elastically stressed, showed less stress-corrosion resistance than did specimen No. 1, which was treated similarly but tested in the absence of elastic stress. Comparison of specimens Nos. 3 and 4, however, indicates that the effect of elastic stress may be less significant in material which is subzero worked and subsequently stress-relieved at 750°F. The elastically stressed specimens cracked at the bend, while the as-heat-treated specimens cracked at the crimped ends. Future plans include closer study of the effects of elastic stress.

Prior to the tests in boiling 42% magnesium chloride solutions, several subzero worked specimens, with and without elastic stress, were tested

TABLE 16. FILM STUDIES ON PIN SPECIMENS PRETREATED IN MOIST HYDROGEN[a]

SPECIMEN NUMBER	PRETREATMENT TEMPERATURE (°F)	RESULTS OF DIFFRACTION STUDIES		SPECTROGRAPHIC ANALYSIS[c]			
		X ray[b]	Electron Transmission	Fe	Cr	Mn	Ni
1	900	Spinel (8.39 kX), s; Cr_2O_3, vw; halo	Spinel (8.33 to 8.36 kX), Cr_2O_3	31.8	47.8	13.6	6.8
2	1000	Spinel (8.39 kX), s; halo	Spinel (8.39 kX)	65.3	24.8	1.9	8.0
3	1150	Spinel (8.39 kX), s; Cr_2O_3, vvw; halo	Spinel (8.39 kX), Cr_2O_3; unidentified lines				
4	1300		Spinel (8.39 to 8.41 kX), unidentified lines	16.8	67.6	10.4	5.2
5	1500	Spinel (8.43 kX), s; Cr_2O_3; halo plus unidentified lines	Spinel (8.39 kX)	7.1	73.5	16.3	3.1
6	1850		Spinel,[d] Cr_2O_3	2.0	85.0	12.3	0.7
7	1950		Spinel,[d] Cr_2O_3				

[a]Specimens pretreated in H_2 containing 6 vol % moisture for 24 hours.

[b]Numbers in parentheses are lattice parameters in kX units. (kX × 1.00202 = 1 Å); s, vw, vvw correspond to strong, very weak, and very, very weak, respectively.

[c]Each element reported as per cent of total weight of Fe, Cr, Mn, and Ni. Traces of Al, Ca, Cu, and Ti were also detected.

[d]Lattice parameter not determined.

in the less severe media of 3% sodium chloride solutions with either 1.5 or 0.15% sodium dichromate, and they showed no cracking after periods as long as 384 hours.

The results of these preliminary tests indicate that the relation between plastic deformation and subsequent heat treatment on the one hand, and stress-corrosion cracking on the other, may not be a simple one, and it therefore warrants further investigation.

A jig for forming specimens which, when elastically stressed, will have a constant bending moment over a large area is now being fabricated. Plans for future work also include a more intensive study of the effects of martensite and martensite-forming susceptibility on stress-corrosion resistance. Specimens are being designed so that the amount of martensitic-type phase present in the structure can be estimated by Magne-gage measurements.

TABLE 17. EFFECT OF COLD-WORKING TEMPERATURE AND SUBSEQUENT HEAT TREATMENT ON THE STRESS-CORROSION CRACKING OF TYPE 347 STAINLESS STEEL TUBING IN BOILING 42% $MgCl_2$ SOLUTIONS

SPECIMEN NUMBER	COLD-WORKING TEMPERATURE (°F)	REHEATING TEMPERATURE (°F)	ELASTIC STRESS	FIRST CRACK	
				Time (hr ± ½ hr)	Location
1	–320	1900	No	18	Crimped end
2	–320	1900	Yes	5	Bend
3	–320	750	No	5	Crimped end
4	–320	750	Yes	5	Bend
5	–320		No	25	Bend
6	–320		No	30	Bend
7	75		No	2	Bend
8	75		No	2	Bend
9	75		No	2½	Bend
10	75		No	2	Bend
11	212		No	2	Bend
12	212		No	2	Bend
13	400		No	2	Bend
14	400		No	2	Bend

AQUEOUS SOLUTION AND RADIATION CHEMISTRY

THE SYSTEM UO_3-NiO-SO_3-H_2O

C. H. Secoy E. V. Jones
J. S. Gill D. M. Richardson

Certain portions of the phase diagram for the four-component system, UO_3-NiO-SO_3-H_2O, are of interest in understanding the behavior of uranyl sulfate fuel solutions contained in stainless steel. Much exploratory work has been reported earlier concerning these regions of importance in which approximate boundary or limiting data rather than definitive data were obtained. No attention was given to the identification of solid phases, and compositions were frequently expressed on a volumetric basis and, therefore, were not useful for the graphic representation of the phase relationships.

During the last few months, a longer-range and more systematic approach has been adopted. The immediate objectives were to describe completely the UO_3-rich portion of the UO_3-SO_3-H_2O system, the NiO-rich portion of the NiO-SO_3-H_2O system, and the UO_2SO_4-$NiSO_4$-H_2O system at 25, 100, 175, and 250°C. This work was to be followed by a thorough study of the UO_3-NiO-SO_3-H_2O system at uranium concentrations of less than 15 g of uranium per liter. Completion of this program and completion of the studies of the two-liquid-phase region of the UO_3-SO_3-H_2O system (300 to 400°C) described elsewhere in this report should provide an adequate picture of the phase relationships in proposed reactor-fuel systems and should provide a basis for further studies of the effect of additional components.

Experimental methods have involved saturating a solution with an excess of a solid, stirring for a period of time (usually about two weeks), and sampling and chemically analyzing the liquid phase and the wet solid residue. In many cases, the solid phases have been examined by the x-ray spectrometer.[1] The data are summarized in Tables 18 through 22. Careful plotting of the data indicates considerably more scatter to the points than can be attributed to analytical error, and this scatter may result from one or more factors. First, the UO_3-rich solutions give some indications of the presence of colloidal material. If this is the case, error would be introduced by failure to effect complete phase separations. Second, the solid material used in saturating the solutions was frequently not the true equilibrium solid phase. Thus a solid-solid transition was necessary, and the time allowed for the establishment of equilibrium was probably insufficient for the completion of such a transition. The x-ray diffraction patterns were not indicative of pure solid phases in many cases. It is expected that the quantitative character of the data can be improved by proper changes in technique designed to eliminate these uncertainties.

In spite of these factors, a schematic representation of the phase diagram is possible. Such diagrams for the different isotherms are shown in Figs. 53, 54, 55, 56, and 57. As indicated on the figures, the identity of several of the solid phases remains uncertain. In particular, the exact compositions of the K and G basic salts in the tables are not certain, and at least three undefined solid phases appear in the UO_2SO_4-$NiSO_4$-H_2O system. The evidence to date indicates that none of the latter are double salts, acidic salts, or basic salts. Therefore it is most likely that they are all lower hydrates of uranyl sulfate and nickel sulfate.

The 250°C isotherm (Fig. 56) is of special interest because the solubility curve crosses the stoichiometric line. The cross-over occurs at very

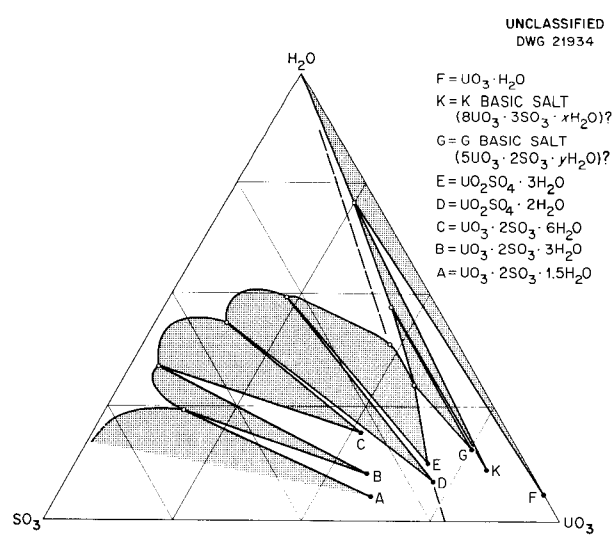

Fig. 53. The System UO_3-SO_3-H_2O at 25°C.

[1] Preparation and interpretation of the x-ray diffraction patterns have been the work of R. D. Ellison of the Chemistry Division, whose help is gratefully acknowledged.

TABLE 18. THE SYSTEM UO_3-SO_3-H_2O AT 25°C

SAMPLE NUMBER	LIQUID PHASE			WET SOLID		X-RAY IDENTIFICATION OF SOLID
	UO_3 (wt %)	SO_3 (wt %)	Mole Ratio UO_3/SO_3	UO_3 (wt %)	SO_3 (wt %)	
K - 1	0.119	0.021	1.59			
K - 2	0.225	0.041	1.54			
K - 3b	0.853	0.163	1.46			
K - 3a	0.865	0.161	1.50			
K - 4a	2.43	0.465	1.46			
K - 4b	3.07	0.464	1.25			
K - 5b	3.77	0.537	1.96			
K - 5a	3.79	0.779	1.36			
G -18	5.10	0.94	1.52			
G -17	5.12	0.93	1.54			
J - 1	5.23	0.93	1.57			
K - 6	7.72	1.77	1.22			
G -12	9.32	1.96	1.33			
G -13	9.36	1.83	1.43			α-$UO_3 \cdot H_2O$
O - 1	10.03	1.73	1.62	88.99	0.42	α-$UO_3 \cdot H_2O$
K - 7	15.16	3.08	1.38			
G -15	16.34	3.14	1.46			
G -16	16.46	3.16	1.46			
J - 2	16.68	2.98	1.57			
M - 2	17.39	3.06	1.59	78.59	1.17	α-$UO_3 \cdot H_2O$
G -14	22.94	4.19	1.53			
K - 7a	23.10	4.74	1.36			
G -10	23.19	4.48	1.45			
O - 2	24.84	4.34	1.60	79.79	1.25	α-$UO_3 \cdot H_2O$ + K basic salt
K_2- 7b	30.67	5.95	1.44	54.25	3.90	K basic salt
G - 5	33.04	6.43	1.44			
O - 3	33.16	6.33	1.47	67.17	4.00	K basic salt
G -11	33.76	6.45	1.46			α-$UO_3 \cdot H_2O$
M - 3	34.35	6.19	1.55	79.07	2.25	α-$UO_3 \cdot H_2O$
K_2- 8	34.41	6.85	1.41	58.88	7.92	
J - 3	34.75	6.22	1.56			
K - 7b	35.06	6.48	1.51			G basic salt
K_2- 9	37.49	9.23	1.14	59.60	8.79	

TABLE 18. (continued)

SAMPLE NUMBER	LIQUID PHASE			WET SOLID		X-RAY IDENTIFICATION OF SOLID
	UO_3 (wt %)	SO_3 (wt %)	Mole Ratio UO_3/SO_3	UO_3 (wt %)	SO_3 (wt %)	
K -13	40.88	9.01	1.27			G basic salt
K_2-13	41.64	8.79	1.33	55.86	8.66	G basic salt
G - 4a	42.37	8.76	1.35			
G - 3a	42.90	8.92	1.35			
K_2-10	44.11	11.11	1.11	58.40	9.92	
O - 4	44.71	8.78	1.43	75.58	8.83	G basic salt
O - 5a	45.16	9.38	1.35	64.17	8.08	G basic salt
M - 4	45.40	9.49	1.34	62.36	8.92	Unknown
G - 6	45.54	9.58	1.33			
G - 8	45.54	9.58	1.33			G basic salt
K -12	45.65	10.35	1.23			G basic salt
J - 4	46.54	9.64	1.35	76.23	10.04	
O - 5	47.04	9.90	1.33	76.06	9.67	G basic salt
K_2-12	47.51	10.38	1.28	58.13	9.73	
G - 7	50.35	11.00	1.28			G basic salt
G - 9	50.35	11.08	1.27	76.42	9.92	G basic salt
M - 5	50.79	11.47	1.24	62.60	9.92	Unknown
J - 5	50.91	10.81	1.32	75.66	10.48	
K -11	51.61	11.43	1.26			
O - 6a	52.74	11.74	1.26	65.13	9.17	G basic salt
K_2-11	53.27	12.49	1.19	61.70	11.28	
U - 1	55.81	12.68	1.23	63.80	11.25	G + unknown lines
U - X	56.91	12.95	1.23	65.97	13.08	G + K + unknown
U - Y	57.30	12.90	1.24	64.89	11.08	G + unknown
U - Z	57.76	13.38	1.21	66.93	15.67	G + unknown

nearly 0.6 wt % UO_3, which corresponds almost exactly to 5 g of uranium per liter.

Further insight into the phase relationships of the UO_3-SO_3-H_2O system can be obtained by reference to Fig. 58. In this figure, temperature is plotted against the percentage of UO_3. Lines are drawn through points of constant SO_3 composition. The graph is intended to show two things: the approximate temperature and composition ranges for the regions in which the different solid phases are stable and the increase or decrease of the solubility of the stable solid with temperature, which is indicated by the slope of the lines. Points *B* and *E*, whose exact positions are unknown, represent invariant points at which three solid phases can coexist in equilibrium with saturated solution and vapor.

TABLE 19. THE SYSTEM UO_3-SO_3-H_2O AT 100°C

SAMPLE NUMBER	LIQUID PHASE			WET SOLID		X-RAY IDENTIFICATION OF SOLID
	UO_3 (wt %)	SO_3 (wt %)	Mole Ratio UO_3/SO_3	UO_3 (wt %)	SO_3 (wt %)	
H-1	2.19	0.50	1.23			
H-2	4.28	0.94	1.27			
H-3	8.12	1.76	1.29			
L-1	8.40	1.70	1.38			
I-1	8.43	1.57	1.50			
H-4	15.56	3.11	1.40			
I-2	21.47	4.45	1.35			
L-2	21.90	4.29	1.43	88.20	2.17	α-$UO_3 \cdot H_2O$
H-5	22.01	4.61	1.34			
H-6	31.55	6.60	1.34			
L-3	31.65	6.27	1.41	81.83	3.08	α-$UO_3 \cdot H_2O$
I-3	33.78	6.39	1.48			
I-4a	43.18	8.78	1.38			
H-7b	43.23	9.06	1.34			
L-4	43.23	8.64	1.40	89.04	3.25	
L-5	45.58	9.24	1.38	86.58	3.17	
N-1	46.46	9.07	1.43	80.99	2.17	α-$UO_3 \cdot H_2O$ + G basic salt
I-8a	46.96	9.61	1.37			
H-8b	47.01	9.94	1.32			
L-6	47.51	9.30	1.43	85.07	4.08	
I-5a	47.64	9.74	1.37			
N-2	50.98	9.63	1.48	77.50	4.67	α-$UO_3 \cdot H_2O$ + G basic salt
H-9c	52.30	10.65	1.37			
H-9b	52.83	10.64	1.39	67.17	10.25	
I-6a	53.03	11.06	1.34			
L-7	53.19	11.05	1.35	66.81	11.92	
I-6	53.47	11.11	1.35			

THE SYSTEM UO_3-SO_3-H_2O ABOVE 300°C

D. W. Sherwood C. H. Secoy

Consideration of the need for further data in the two-liquid-phase region of uranyl sulfate solutions has led to the formulation of a plan of attack involving a large pressure vessel with windows that is designed to contain a sealed quartz solution vessel. This quartz vessel is equipped with a spiral quartz capillary gage which is to be used as a null-point instrument by balancing the internal pressure (vapor pressure of the system) with an external inert-gas pressure. By means of the

TABLE 20. THE SYSTEM UO_3-SO_3-H_2O AT 175°C

SAMPLE NUMBER	LIQUID PHASE			WET RESIDUE		X-RAY IDENTIFICATION OF SOLID
	UO_3 (wt %)	SO_3 (wt %)	Mole Ratio UO_3/SO_3	UO_3 (wt %)	SO_3 (wt %)	
U-30	0.13	0.031	1.17	94.93	<0.1	
U-36	0.81	0.21	1.08	86.40	<0.1	
U-51a	1.34	0.34	1.10	87.12	<0.1	
U-79a	1.93	0.45	1.20	86.03	0.93	
U-88a	2.11	0.49	1.21	87.24	<0.1	
U-80a	4.43	0.98	1.27	85.43	0.83	α-$UO_3 \cdot H_2O$
U-81a	9.61	2.02	1.33	86.15	0.42	α-$UO_3 \cdot H_2O$
U-82a	14.63	3.15	1.30	84.23	1.08	
U-83a	20.38	4.50	1.27	85.91	1.20	α-$UO_3 \cdot H_2O$
U-84a	29.74	6.25	1.33	91.20	1.42	α-$UO_3 \cdot H_2O$ + β-$UO_3 \cdot H_2O$
U-85a	39.17	8.71	1.26	87.36	1.50	
U-40	45.11	9.66	1.31	74.14	3.33	
U-86a	46.45	9.92	1.31	86.27	2.25	α-$UO_3 \cdot H_2O$ + G basic salt
U-39a	49.23	10.87	1.27	84.35	4.83	
U-87a	54.41	11.15	1.37	81.11	5.08	α-$UO_3 \cdot H_2O$ + G basic salt

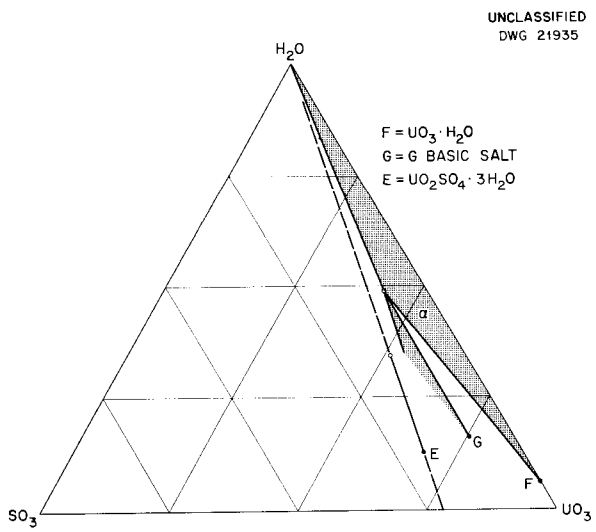

Fig. 54. The System UO_3-SO_3-H_2O at 100°C.

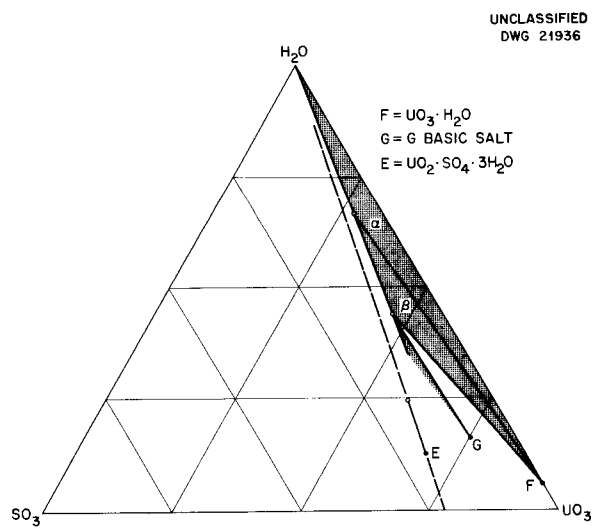

Fig. 55. The System UO_3-SO_3-H_2O at 175°C.

TABLE 21. THE SYSTEM UO_3-SO_3-H_2O AT 250°C

SAMPLE NUMBER	LIQUID PHASE			X-RAY IDENTIFICATION OF SOLID
	UO_3 (wt %)	SO_3 (wt %)	Mole Ratio UO_3/SO_3	
S-1	0.0386	0.0122^5	0.882	
98-a	0.0412^5	0.0158^5	0.728	
S-2	0.0678	0.0220	0.862	
97-a	0.1112	0.0382	0.814	
93-a	0.1140	0.0366	0.871	β-$UO_3 \cdot H_2O$
S-3	0.130	0.038	0.956	
S-4	0.152	0.040	1.066	
96-a	0.158	0.051	0.86	
92-a	0.171	0.054	0.89	β-$UO_3 \cdot H_2O$
95-a	0.291	0.094	0.87	
S-5	0.458	0.125	1.03	
91-a	0.500	0.143	0.98	β-$UO_3 \cdot H_2O$
S-7	0.572	0.159	1.01	
101-a	0.736	0.200	1.03	
S-8	1.273	0.314	1.14	

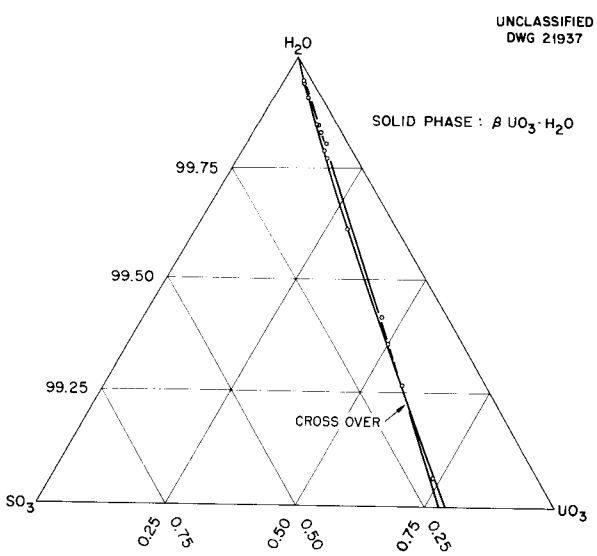

Fig. 56. The System UO_3-SO_3-H_2O at 250°C.

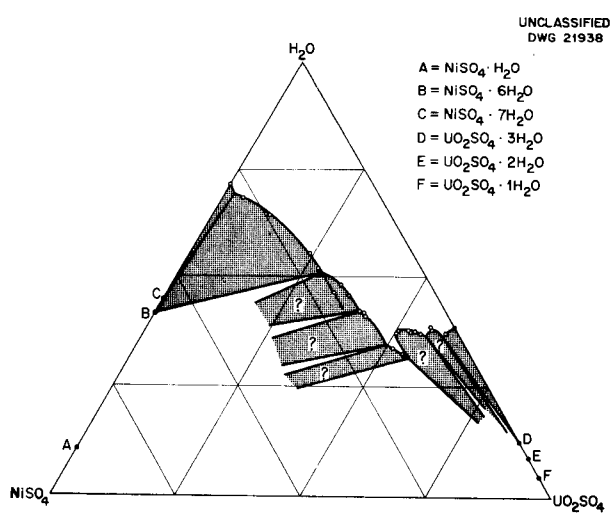

Fig. 57. The System UO_2SO_4-$NiSO_4$-H_2O at 25°C.

TABLE 22. THE SYSTEM UO_2SO_4-$NiSO_4$-H_2O AT 25°C

SAMPLE NUMBER	LIQUID PHASE		WET RESIDUE		X-RAY IDENTIFICATION OF SOLID
	UO_2SO_4 (wt %)	$NiSO_4$ (wt %)	UO_2SO_4 (wt %)	$NiSO_4$ (wt %)	
	61.18	0.00			$UO_2SO_4 \cdot 3H_2O$
21	60.28	2.42	77.0	0.87	
65	57.1	4.96	79.7	1.62	Unknown A
17	56.6	4.85	76.4	1.41	
67	55.2	7.59	78.3	2.51	Unknown A + unknown
53	54.3	8.33	75.8	2.74	$UO_2SO_4 \cdot 3H_2O$ + unknown
15	54.3	8.08	75.2	1.70	
13	54.0	8.31	74.7	2.34	
51	53.1	9.39	73.1	3.56	$UO_2SO_4 \cdot 3H_2O$ + unknown
11	52.3	9.49	75.5	4.08	Unknown
57	50.4	11.45	75.6	3.99	Unknown A
47	50.4	12.20	75.0	4.50	
49	51.5	14.8	27.0	37.1	Unknown
63	54.0	13.4	21.8	41.2	$UO_2SO_4 \cdot 3H_2O$ + unknown
31	42.3	16.56	22.92	38.5	Unknown
59	41.7	16.5	5.49	53.5	$NiSO_4$ hydrate mixture (7-6-1)
61	40.7	17.15	12.3	46.1	Unknown
33	36.8	17.72	19.93	36.82	
35	34.0	17.90	5.98	53.7	
37	33.5	20.06	7.30	50.2	
41	24.0	20.62	2.30	54.7	α-$NiSO_4 \cdot 6H_2O$
39	27.5	20.70	9.61	46.0	
43	11.51	24.20	0.80	56.0	α-$NiSO_4 \cdot 6H_2O$
45	4.07	27.60	0.35	57.8	
	0.00	28.51			$NiSO_4 \cdot 7H_2O$

windows, the relative volumes of the three phases present may be determined simultaneously with the vapor-pressure determination. Concentrations of each of the components in each of the phases may be calculated from these data.

It is planned to mount the observation windows of the pressure vessel in a way which is new for windows of the proposed size. To this end, experimental work has been under way in testing such a window mounting in type 347 stainless steel. To date, tests at room temperature have been satisfactory, and high-temperature testing is in progress.

PRELIMINARY EXPLORATION OF THE $Th(NO_3)_4$-HNO_3-H_2O SYSTEM AT ELEVATED TEMPERATURE

W. L. Marshall C. H. Secoy

Some experimental data have been obtained previously[2] for the hydrolytic phase stability of $Th(NO_3)_4$ in H_2O at temperatures above 100°C in which the vapor-to-liquid ratio was unity. These data indicated that a maximum temperature, before

[2]W. L. Marshall, J. S. Gill, and C. H. Secoy, *HRE Quar. Prog. Rep. Nov. 30, 1950*, ORNL-925, p. 279.

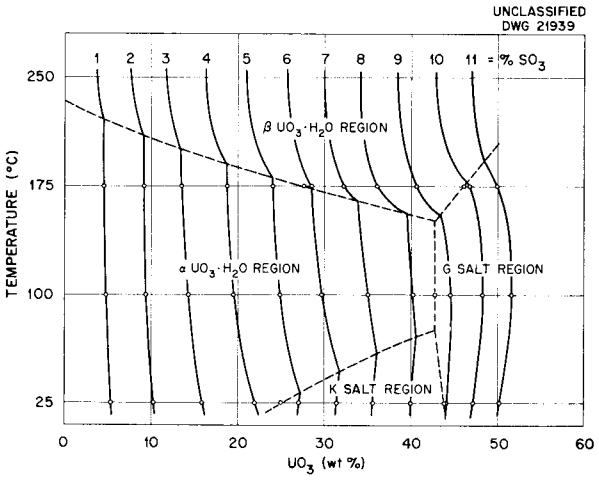

Fig. 58. Schematic Representation of the System UO_3-SO_3-H_2O.

precipitation, could be obtained at about 400 g of thorium per liter. The purpose of the present investigation was to estimate the amount of excess HNO_3 necessary to prevent hydrolytic precipitation at higher temperatures than could be obtained with stoichiometric $Th(NO_3)_4$.

Solutions with nitrate-to-thorium ratios of 3.95, 5.47, and 6.65 were prepared in concentrations that varied from 20 to 400 g of thorium per liter. Capillary tubes containing these various solutions in a 1:1 vapor-to-liquid ratio were run in the semimicro phase-study apparatus described previously.[3] The temperature was raised rapidly (about 8°C/min), and the point at which precipitation occurred was determined. An experiment over a slow period (temperature raised ½°C/min) and also some static runs over three to four days were compared with the rapid experiments in order to decide what correction in temperature should be made to these latter values. The data are given in Table 23, together with some observations on the solid and vapor phases. In Figs. 59 and 60, curves are drawn to represent the best estimate, from these data, of the equilibrium temperatures at which precipitation will occur.

It is significant to note that the first mole of excess nitrate causes the biggest elevation in precipitation temperature, that the vapor-phase coloration is much greater per unit change of nitrate after the initial four moles are added to the thorium, and that crystalline solids appear in concentrated regions, the compositions of which might correspond to acid salts. These latter crystalline compounds are reversible in solubility over the time of the experiments as compared with the apparent irreversibility of the hydrolysis product(s).

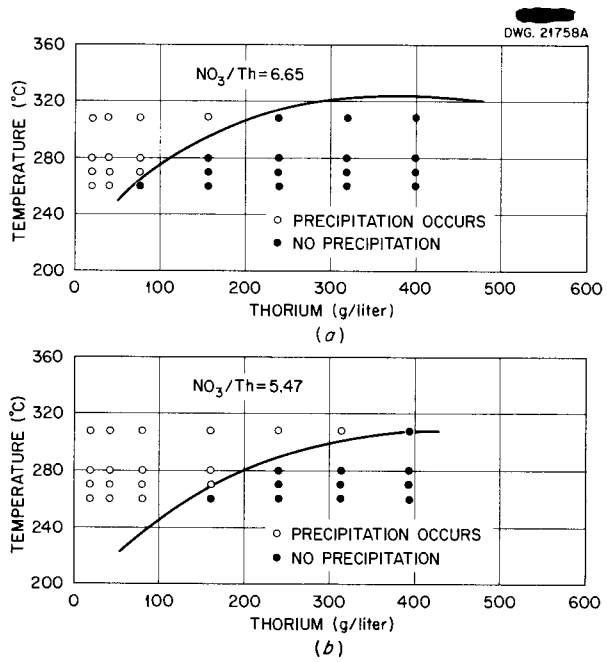

Fig. 59. Estimate of Phase Stability of the System $Th(NO_3)_4$-HNO_3-H_2O.

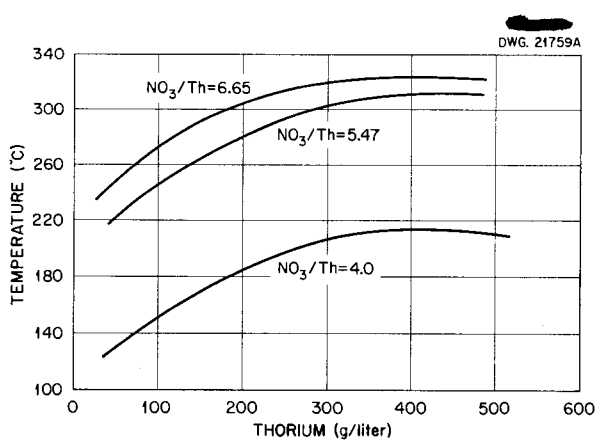

Fig. 60. Estimate of Phase Stability as a Function of Mole Ratio, NO_3/Th, of the System $Th(NO_3)_4$-HNO_3-H_2O.

[3] H. W. Wright and W. L. Marshall, *HRP Quar. Prog. Rep. Oct. 1, 1952*, ORNL-1424, p. 108.

TABLE 23. EXPLORATION OF HYDROLYTIC PHASE STABILITY FOR THE SYSTEM $Th(NO_3)_4$-HNO_3-H_2O

MOLE RATIO NO_3/Th	THORIUM CONCENTRATION (g/l)	RATE OF TEMPERATURE RISE (°C/min)	PRECIPITATION TEMPERATURE (°C)	SOLID PHASE APPEARANCE*	VAPOR PHASE COLORATION**
		Dynamic Experiments			
3.95	19.9	8	185	Amorphous (?)	None
	39.9	8	200	Amorphous (?)	None
	79.8	8	220	Amorphous (?)	None
	159.5	8	255	Amorphous (?)	None
	239.3	8	268	Amorphous (?)	None
	319.0	8	280	Amorphous (?)	Slight
	398.8	8	272	Crystalline	Yes
5.47	19.7	8	230	Amorphous (?)	None
	39.4	8	274	Amorphous (?)	None
	78.8	8	298	Amorphous (?)	Yes, 285°C
	157.6	8	318	Amorphous (?)	Yes, 285°C
	236.5	8	316	Crystalline	Yes, 285°C
	315.3	8	332	Crystalline	Yes, below 285°C
	394.1	8	300 to 314	Crystalline	Yes, below 250°C
6.65	20.2	8	265	Amorphous (?)	
	40.3	8	302	Amorphous (?)	Yes, 295°C
	80.5	8	308	Crystalline	
	161.1	8	310	Crystalline	Yes, below 280°C
	241.6	8	340	Crystalline	Yes, 260°C
	322.2	8	336	Crystalline	
	402.7	8	332	Crystalline	Yes, 220°C
3.95	398.8	½	225	Crystalline	
		Static Experiments A			
		TIME AT TEMPERATURE			
5.47	394.1	60 hr at 305°C	305	Slight crystalline precipitation	
3.95	398.8	17 hr at 250°C		Crystalline precipitation	
5.47	394.1	17 hr at 250°C		No precipitation	
6.65	402.7	17 hr at 250°C		No precipitation	

*Use of 20X microscope.

**To precipitation temperature.

TABLE 23 (continued)

MOLE RATIO NO_3/Th	THORIUM CONCENTRATION (g/l)	PRECIPITATION OF SOLID PHASE			
		At 260°C for 3 hr	At 270°C for 60 hr	At 280°C for 18 hr	At 308°C for 18 hr
Static Experiments B					
5.47	19.7	Yes	Yes	Yes	Yes
	39.4	Yes	Yes	Yes	Yes
	78.8	Yes	Yes	Yes	Yes
	157.6	No	Yes	Yes	Yes
	236.5	No	No	No	Yes
	315.3	No	No	No	Yes
	394.1	No	No	No	No
6.65	20.2	Yes	Yes	Yes	Yes
	40.3	Yes	Yes	Yes	Yes
	80.5	No	Yes	Yes	Yes
	161.1	No	No	No	Yes
	241.6	No	No	No	No
	322.2	No	No	No	No
	402.7	No	No	No	No

It is not to be implied from these data that valid extrapolations or interpolations to other compositions can be made without considering the possibility that additional solid phases not indicated by these data may appear at lower temperatures.

SOLUBILITY OF TUNGSTIC ACID IN UO_2SO_4 AND UO_2F_2 – CORROSION INHIBITION

C. E. Coffey W. L. Marshall
G. H. Cartledge

Sodium tungstate has been known to be an inhibitor of the corrosion of carbon steel at room temperature, but recent experiments in this laboratory[4] showed that the inhibition also extends to higher temperatures. In view of the possibility that the oxide or acid might function in solutions of interest in reactors, an investigation was made of the solubility of tungstic acid, H_2WO_4, in aqueous uranyl sulfate and uranyl fluoride at various temperatures and concentrations.

Baker's c.p. H_2WO_4 instead of an alkali tungstate was used in this investigation because aqueous UO_2SO_4 and UO_2F_2 are strongly acidic at room temperature and a tungstate would be converted to tungstic acid. Runs were conducted on a large shaker at room temperature, in a water bath at 50°C, in a dibutyl phthalate bath at 100 and 150°C, in titanium filter bombs[5] from 150 to 300°C, and in sealed glass tubes from room temperature to 300°C.

Little confidence can be placed in the results from the run at 150°C because the sampling method was poor. The sealed-tube method was satisfactory for solutions in which the solubility was approximately 1 g per liter or more. Quantitative results from the sealed-tube method were impossible in the case of the solution containing 30 g of uranium per liter as UO_2SO_4, and the results were only approximate in the case of the solution containing 300 g of uranium per liter as UO_2F_2. The filter bombs furnished the most reliable results, but even with them, there was often reduction of the

[4] G. H. Cartledge and R. P. Yaffe, *Chem. Semiannual Prog. Rep. June 20, 1953*, ORNL-1587, p. 17.

[5] J. S. Gill, E. V. Jones, and W. L. Marshall, *HRP Quar. Prog. Rep. March 31, 1953*, ORNL-1554, p. 99.

uranium. When reduction was detected, the runs were discarded. Analytical determination of the small amounts of tungsten in the presence of uranium was difficult, and duplicate checks on the same sample usually differed by about 5%. In some cases (low concentration of tungsten), the error was of the order of 50%.

The results in 1.26 M UO_2SO_4 are scattered (Table 24 and Fig. 61), but a curve which splits the values from the filter bombs and also agrees with the sealed tube results can be drawn through the points.

The solubility of tungsten in 0.126 M UO_2SO_4 is very low compared with that in 1.26 M UO_2SO_4, and the sealed tubes gave only approximate results. These sealed-tube results, however, did indicate a decrease in solubility that corresponded to the break in the curve at about 120°C (Table 24 and Fig. 62) and an increase in solubility that corresponded to an apparent break at 260°C. Equilibrium was reached rather slowly above 120°C, probably because a slow solid-solid transformation took place. At constant temperature (200 or 250°C), a plot of solubility vs. time indicated that the equilibrium value was reached in about 115 hours. The solubility curve is better than indicated by the scattered points, since the runs with times less than the maximum at any temperature are discarded. It seems that supersaturation of the liquid with respect to the low-temperature solid phase can occur readily.

The solubility values in 1.26 M UO_2F_2 obtained in glass tubes were used in drawing an approximate curve (Table 25 and Fig. 63). Filter-bomb data were discarded because of the corrosive nature of UO_2F_2 on titanium. There is a very voluminous precipitate formed in the sealed tubes between 150 and 200°C. The solubility of H_2WO_4 in solutions containing 30 g of uranium per liter as UO_2F_2 is less than that in solutions containing 300 g of uranium per liter as UO_2F_2.

Corrosion Tests. Since it was believed that the corrosion tests would be more significant if run under dynamic conditions, it was decided to construct a dynamic corrosion tester. A corrosion testing apparatus patterned after a unit designed

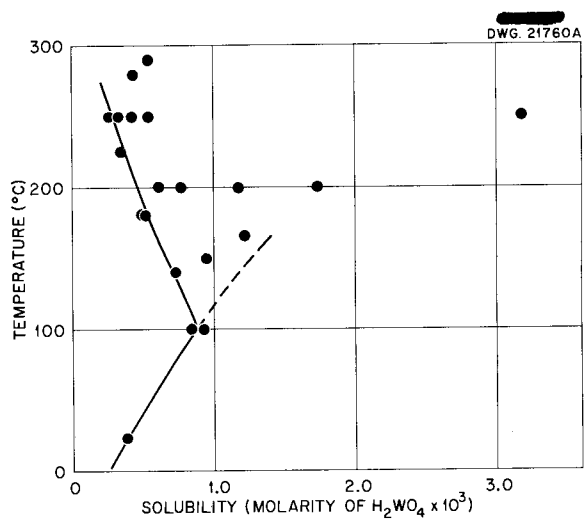

Fig. 62. Solubility of H_2WO_4 in 0.126 M UO_2SO_4.

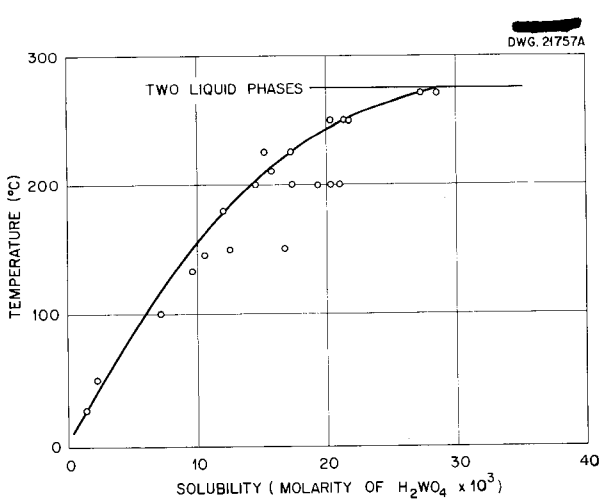

Fig. 61. Solubility of H_2WO_4 in 1.26 M UO_2SO_4.

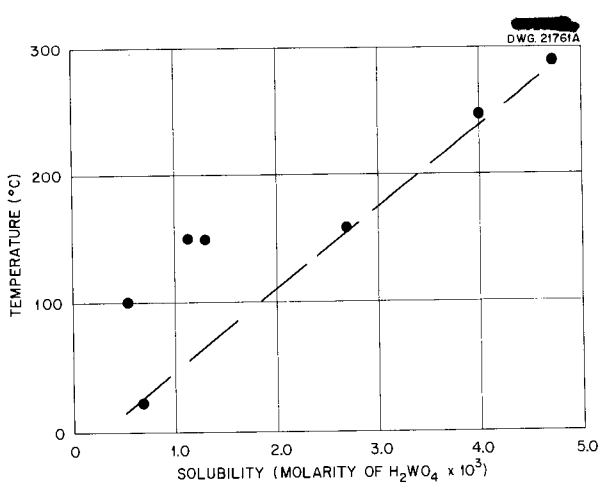

Fig. 63. Solubility of H_2WO_4 in 1.26 M UO_2F_2.

TABLE 24. SOLUBILITY OF H_2WO_4 IN AQUEOUS UO_2SO_4

TEMPERATURE (°C)	EXPERIMENT TYPE	TIME OF RUN (hr)	SOLUBILITY OF H_2WO_4 AT 23° C ($M \times 10^3$)
Molarity of UO_2SO_4 at 23° C: 0.126			
23	Glass tube		0.37
100	Filter bomb	Under 95	0.832
100	Filter bomb	Under 95	0.913
140	Glass tube		0.734
150	Filter bomb	100	0.946
166	Glass tube		1.21
181	Filter bomb	140	0.489
181	Filter bomb	140	0.516
200	Filter bomb	30	1.74
200	Filter bomb	50	1.18
200	Filter bomb	95	0.788
200	Filter bomb	95	0.609
226	Filter bomb	112	0.35
250	Filter bomb		3.18
250	Filter bomb	24	0.54
250	Filter bomb	40	0.424
250	Filter bomb	40	0.34
250	Filter bomb	119	0.27
278	Filter bomb	Under 95	0.44
290	Glass tube		0.54
Molarity of UO_2SO_4 at 23° C: 1.26			
23	Filter bomb	Under 95	1.4
50	Filter bomb	Under 95	2.1
100	Filter bomb	Under 95	7.07
134	Glass tube		9.51
145	Glass tube		10.6
150	Filter bomb	Over 95	16.8
150	Filter bomb	Over 95	12.5
180	Filter bomb	Over 95	12.0
200	Filter bomb	Over 95	21.0
200	Filter bomb	Over 95	20.3
200	Filter bomb	Under 95	19.3
200	Filter bomb	Under 95	17.3
200	Glass tube		14.5
210	Glass tube		15.8
225	Filter bomb	Over 95	17.4
225	Filter bomb	Over 95	15.2
250	Glass tube		21.7
250	Filter bomb	Over 95	21.5
250	Filter bomb	Over 95	20.4
276	Filter bomb	Over 95	27.2
280	Filter bomb	Under 95	28.5
285			Two liquid phases

TABLE 25. SOLUBILITY OF H_2WO_4 IN AQUEOUS 1.26 *M* UO_2F_2*

TEMPERATURE (°C)	EXPERIMENT TYPE	SOLUBILITY OF H_2WO_4 AT 23°C ($M \times 10^3$)
23	Analytical	0.71
100	Analytical	0.54
150	Analytical	1.3
150	Analytical	1.1
158	Glass tube	2.7
245	Glass tube	4.0
290	Glass tube	4.9

*Molarity at 23°C.

by H. F. McDuffie *et al.* [6] was constructed, but it included some modifications to fit the particular need. An "Air Speed" pneumatically operated saw and file gun is used to shake four bombs that are mounted in a carriage which is connected to the chuck of the gun. The carriage is constructed of aluminum alloy and holds four of the small pressure bombs described previously.[7] The carriage weighs 230 g when fully loaded and is arranged to vibrate vertically in a cylindrical furnace. The temperature can be raised to 250°C in less than 45 minutes. This temperature is at the center of the carriage. By controlling the rate of air flow to the shaker, the vibration can be held at 11.7 to 20 cps. At 20 cps and with a ½-in. throw, this corresponds to a flow rate of 1.7 fps. This rate is slow compared with the large pump loops but is much better than that obtained in static tests.

Preliminary static corrosion tests were inconclusive. The presence of tungsten usually decreased the total amount of corrosion by a factor of 2 or 3, but the attack was often localized with subsequent pitting.

The dynamic corrosion tests seemed to be much better than static tests. The films formed were more regular in spite of (or because of) the shaking. All these runs were made on the small shaker at 250°C with excess oxygen pressure supplied by the use of 30% H_2O_2. The samples were mounted in Teflon that was screwed into the cap of the bomb.

The results of two runs are given in Table 26. Nickel was found to be 10 to 15 times less in 0.126 *M* UO_2SO_4 and 3 to 4 times less in 1.26 *M* UO_2SO_4 at 250°C, both solutions saturated with H_2WO_4, than in corresponding control runs. These differences are appreciable and might well indicate that further dynamic corrosion evaluation is in order at the higher temperatures. The weight changes do not indicate these differences; however, after a consideration of the small sample weight involved, the emphasis should be placed on the nickel results.

In summary, the solubility of H_2WO_4 at 250°C has been found to be approximately 0.00028 *M* in 0.126 *M* UO_2SO_4, 0.02 *M* in 1.26 *M* UO_2SO_4, and 0.004 *M* in 1.26 *M* UO_2F_2. Exploratory corrosion tests at 250°C indicate that H_2WO_4 does act as a corrosion inhibitor.

ESTIMATION OF ACTIVITY COEFFICIENTS OF UO_2SO_4 SOLUTIONS FROM VAPOR-PRESSURE MEASUREMENTS

H. O. Day, Jr. C. H. Secoy

During recent months, a considerable amount of data has been obtained on the vapor-pressure depression of water in UO_2SO_4 solutions. Since the vapor pressure of an aqueous solution of a nonvolatile solute is a measure of the activity of the water, the activity of the solute may be computed by means of the Gibbs-Duhem relationship.

The fundamental equation expressing the activity coefficient of a solute as a function of the vapor pressure may be written as

$$d \ln \gamma_{\pm} = -\frac{1}{m} d\left[m(1 - \phi)\right] ,$$

which on integration gives

$$\ln \gamma_{\pm} = -(1 - \phi) - \int_0^m \frac{1 - \phi}{m} dm .$$

In these equations, $\gamma_{\pm}$ is the stoichiometric mean ionic molal activity coefficient and is usually called the practical activity coefficient, m is the molality of the UO_2SO_4 solution, and ϕ is the osmotic coefficient. The ϕ is a direct function of the vapor pressure of a solution and is defined thusly:

$$\phi = -\frac{1000}{\nu m M_1} \ln \frac{P}{P_0} ,$$

[6] H. F. McDuffie, *Small Scale Dynamic Corrosion Tests*, ORNL CF-53-9-39 (Sept. 4, 1953).

[7] W. L. Marshall, *HRP Quar. Prog. Rep. March 31, 1953*, ORNL-1554, p. 106.

TABLE 26. CORROSION OF TYPE 347 STAINLESS STEEL WITH H_2WO_4 AS AN INHIBITOR

GRAMS OF SAMPLE OF TYPE 347 STAINLESS STEEL	TOTAL SOLUTION (cc)	MOLARITY OF UO_2SO_4	H_2WO_4	WEIGHT OF TYPE 347 STAINLESS STEEL LOST (g/cm^2)	NICKEL IN SOLUTION (ppm)	SAMPLE AREA (cm^2)
Series A: 32 hr at 250°C						
0.16744	2	0.126	Excess	0.00082	4.8	0.7
0.13994	2	0.126	None	0.00220	79	0.7
0.16582	2	1.26	Excess	0.00425	93	0.7
0.15982	2	1.26	None	0.059	350	0.7
Series B: 40 hr at 250°C						
0.21662	2	0.126	Excess	0.00116	5	1.0
0.18868	2	0.126	None	0.00111	45	1.0
0.20950	2	1.26	Excess	0.00488	165	1.0
0.21064	2	1.26	None	0.00934	492	1.0

where P is the vapor pressure of the solution at some temperature, P_0 is the vapor pressure of the pure solvent at the same temperature, m is the molality, M_1 is the molecular weight of the solvent, and ν is the stoichiometric number of ions produced when the solute is dissolved in the solvent. For UO_2SO_4, ν is equal to 2.

From this equation, activity coefficients have been calculated from 0.1 to 6.0 m at temperatures from 30 to 100°C. The exact details of the calculation will be described in an ORNL report that will complete this particular investigation. The calculated activity coefficients are given in Table 27.

DECOMPOSITION OF PEROXIDE IN URANYL SALT SOLUTIONS

M. D. Silverman C. H. Secoy

Kinetic studies of the decomposition of peroxide in the system

$$(1) \quad UO_2^{++} + H_2O_2 \rightleftharpoons UO_4 + 2H^+$$

in uranyl sulfate solutions, with special application to reactor conditions, have been reported in previous HRP quarterly reports and summarized in a recent publication.[8] A more complete and fundamental study of the equilibrium postulated above, as well as an investigation of the mechanism of peroxide decomposition in this system, has been more recently undertaken.

Grieger *et al.*[9] have reported equilibrium data for systems containing solid uranyl peroxide in uranyl sulfate solution. Evidence that the equilibrium indicated by Eq. 1 exists has been independently confirmed.[10] If an equilibrium exists even in the absence of solid uranyl peroxide, then the addition of excess hydrogen ion should shift this equilibrium to the left. Furthermore, if the rate of decomposition of peroxide changes markedly because of this addition (of hydrogen ion), it would indicate that two different modes of decomposition of peroxide are possible or that two different species are being decomposed.

No attempt was made in previous work[8] to elucidate the mechanism whereby peroxide is decomposed in these uranium systems at 100°C.

[8] M. D. Silverman, G. M. Watson, and H. F. McDuffie, TID-2010, p. 43 (Sept. 1953).

[9] P. F. Grieger, E. W. Christopherson, and J. W. Gates, Jr., *Tuballoy Peroxide, Part I.*, CD-4021; P. F. Grieger, E. W. Christopherson, R. Oringer, and J. W. Gates, Jr., *Tuballoy Peroxide, Part II.*, CD-4016; P. F. Grieger and J. W. Gates, Jr., *Tuballoy Peroxide, Part III.*, CD-4023.

[10] Private communication from H. H. Willard; also verified by this author.

TABLE 27. VALUES OF THE ACTIVITY COEFFICIENT, $\gamma_{\pm}$

MOLALITY	TEMPERATURE (°C)															
	25	30	35	40	45	50	55	60	65	70	75	80	85	90	95	100
0.1	0.150	0.147_8	0.145_5	0.143_2	0.140_9	0.138_5	0.136_0	0.133_6	0.131_1	0.128_6	0.126_0	0.123_4	0.1207	0.118_0	0.115_2	0.112_4
0.2	0.102	0.100_6	0.0987	0.0969	0.0950	0.0931	0.0911	0.0892	0.0872	0.0852	0.0831	0.0811	0.0791	0.0770	0.0748	0.0727
0.3	0.0807	0.0795	0.0781	0.0766	0.0752	0.0736	0.0720	0.0704	0.0687	0.0670	0.0652	0.0634	0.0614	0.0596	0.0576	0.0557
0.5	0.0611	0.0602	0.0590	0.0579	0.0566	0.0553	0.0538	0.0524	0.0509	0.0494	0.0477	0.0461	0.0444	0.0428	0.0410	0.0393
0.7	0.0515	0.0507	0.0496	0.0484	0.0472	0.0459	0.0446	0.0432	0.0417	0.0403	0.0387	0.0373	0.0357	0.0342	0.0327	0.0312
1.0	0.0439	0.0428	0.0417	0.0404	0.0392	0.0379	0.0366	0.0353	0.0339	0.0325	0.0311	0.0298	0.0284	0.0271	0.0258	0.0245
1.5	0.0385	0.0371	0.0358	0.0344	0.0332	0.0319	0.0305	0.0292	0.0278	0.0266	0.0252	0.0240	0.0227	0.0214	0.0202	0.0190
2.0	0.0367	0.0354	0.0340	0.0326	0.0311	0.0298	0.0283	0.0269	0.0255	0.0242	0.0228	0.0214	0.0201	0.0189	0.0177	0.0165
2.5	0.0370	0.0355	0.0338	0.0323	0.0307	0.0291	0.0275	0.0260	0.0245	0.0231	0.0217	0.0203	0.0189	0.0176	0.0164	0.0152
3.0	0.0383	0.0366	0.0346	0.0329	0.0310	0.0293	0.0275	0.0259	0.0242	0.0227	0.0212	0.0197	0.0183	0.0170	0.0157	0.0145
3.5	0.0401	0.0383	0.0361	0.0340	0.0319	0.0300	0.0280	0.0262	0.0244	0.0227	0.0211	0.0196	0.0181	0.0167	0.0154	0.0142
4.0	0.0433	0.0405	0.0380	0.0356	0.0332	0.0311	0.0288	0.0268	0.0248	0.0230	0.0213	0.0197	0.0181	0.0167	0.0153	0.0141
4.5	0.0465	0.0434	0.0403	0.0374	0.0348	0.0323	0.0299	0.0277	0.0255	0.0236	0.0217	0.0200	0.0183	0.0168	0.0154	0.0141
5.0	0.0500	0.0464	0.0429	0.0397	0.0367	0.0339	0.0312	0.0287	0.0264	0.0243	0.0222	0.0204	0.0187	0.0171	0.0156	0.0143
5.5	0.0536	0.0497	0.0459	0.0422	0.0389	0.0357	0.0329	0.0300	0.0274	0.0251	0.0229	0.0210	0.0191	0.0175	0.0160	0.0145
6.0	0.0571	0.0531	0.0489	0.0449	0.0412	0.0377	0.0344	0.0314	0.0286	0.0261	0.0238	0.0217	0.0197	0.0179	0.0164	0.0149

However, two alternative modes of decomposition were suggested:

$$(2)\quad \begin{aligned} UO_4 + 2H^+ &\longrightarrow UO_2^{++} + H_2O_2 \\ H_2O_2 &\longrightarrow H_2O + \tfrac{1}{2}O_2 \end{aligned}$$

$$(3)\quad \begin{aligned} UO_4 &\longrightarrow UO_3 + \tfrac{1}{2}O_2 \\ UO_3 + 2H^+ &\longrightarrow UO_2^{++} + H_2O \end{aligned}$$

Previous work[8] indicated that the rate-determining step in each of the modes presented above does not involve hydrogen ion.

Data presented below indicate that in the solutions previously employed[8] the decomposition proceeds through mode (3) and not through (2). However, in the presence of a large excess of hydrogen ion, the rate of decomposition is markedly decreased and the mode of decomposition is that given in (2).

When solid uranyl peroxide is present, the concentrations of only the other three species have to be determined in order to obtain an equilibrium constant for the reaction given in Eq. 1. Grieger *et al.*[9] neglected the concentration of uranium and peroxide present as dissolved uranyl peroxide and analyzed only for total uranium and total peroxide in the presence of a large excess of uranium and hydrogen peroxide. However, in the absence of any solid uranyl peroxide, the concentration of both the hydrogen peroxide and uranyl peroxide would have to be known in order to obtain an equilibrium constant for the reaction. This appears to be extremely difficult analytically at 100°C, if not impossible. A study of the rate constants over a wide range of hydrogen ion concentration offers a possible method for determining the concentration of these two species. The rate of decomposition of peroxide in the absence of any uranyl peroxide (pure hydrogen peroxide in acid) is very slow, and the rate in the presence of uranyl peroxide with no added acid is quite fast. Intermediate rates of decomposition are obtained by adjusting the hydrogen ion concentration. By using the rate constants k_3 (from these intermediate runs) and by knowing the rate constants k_1 and k_2 for the decomposition of the species UO_4 and H_2O_2 at either end of the "range," it is possible to calculate the concentration of both the uranyl peroxide and hydrogen peroxide present from the equation

$$k_3 a = k_1 x + k_2(a - x) ,$$

where a is the known amount of hydrogen peroxide added, x is the concentration of uranyl peroxide, and $(a - x)$ is the concentration of unreacted hydrogen peroxide. It is assumed that the rate of decomposition in the absence of excess hydrogen ion is due practically entirely to the uranyl peroxide species. By this method, values have been obtained for the concentration of uranyl peroxide and hydrogen peroxide in these solutions, and preliminary equilibrium constants have been calculated.

Since the rate of decomposition of peroxide in these solutions appears to be directly proportional to the concentration of dissolved uranyl peroxide and since the concentration of dissolved uranyl peroxide is directly proportional to the uranyl ion concentration, then it is conceivable that this method of rates of decomposition could be pushed a step further so that a measure of the complexing of uranyl ion by different anionic species could be obtained. Early work indicates that this method holds definite promise.

Experimental

The experimental apparatus, techniques, and procedure are largely the same as those reported previously[8] for the chemical method. Again, the ceric sulfate–ferrous ammonium sulfate titration in which orthophenanthroline is used as the indicator was employed.

The uranyl perchlorate solution was prepared by adding a weighed amount of a previously analyzed UO_3 preparation to concentrated perchloric acid and diluting to a convenient concentration. The final solution was analyzed to confirm the stoichiometric ratio of uranium to perchlorate.

Discussion and Results

The data are summarized in Tables 28, 29, and 30. In Table 28 are listed the exploratory data obtained in uranyl sulfate solution. These experiments indicate that in the presence of a large excess of hydrogen ion the decomposition of peroxide proceeds through mode (2) given above and that when no excess hydrogen ion is present the decomposition proceeds through (3). No serious attempt was made to fix the ionic strength of the solutions used in these preliminary experiments.

In Table 29 are listed exploratory data obtained in perchlorate systems wherein two different preparations of uranyl perchlorate were used.

TABLE 28. DECOMPOSITION OF PEROXIDE IN URANYL SULFATE SOLUTIONS

TOTAL URANIUM CONCENTRATION (M)	TOTAL H^+ CONCENTRATION* (M)	IONIC STRENGTH,** μ	OBSERVED RATE CONSTANT, $k_3 \times 10^3$ (min^{-1})	CALCULATED CONCENTRATION ($M \times 10^4$)		EQUILIBRIUM CONSTANT, K_c
				UO_4	H_2O_2	
0	2.3	2.3	0.815 (k_2)			
0.034	0.004	2.0	86.6 (k_1)			
0.030	0.32	2.2	55.0	12.64	7.36	5.9
0.023	1.01	2.2	8.94	1.89	18.11	4.7
0.034	2.0	2.6	5.1	1.00	19.0	6.2
0.63	0.015	1.9	129 (k_1)			
0.56	1.16	2.9	79.3	15.35	9.65	3.8
0.63	2.32	4.2	38.5	7.43	17.57	3.6

*Excess acidity added as $HClO_4$.
**Adjusted by adding $NaClO_4$.

TABLE 29. EXPLORATORY EXPERIMENTS ON THE DECOMPOSITION OF PEROXIDE IN URANYL PERCHLORATE SOLUTIONS

TOTAL URANIUM CONCENTRATION (M)	TOTAL H^+ CONCENTRATION* (M)	IONIC STRENGTH,** μ	OBSERVED RATE CONSTANT, $k_3 \times 10^3$ (min^{-1})	CALCULATED CONCENTRATION ($M \times 10^4$)		EQUILIBRIUM CONSTANT, K_c
				UO_4	H_2O_2	
0	2.0	2.0	0.815 (k_2)			
0.034	0.022	2.0	206 (k_1)	21.0	0	
0.092	0.15	2.3	136	13.2	6.80	0.11
0.089	0.50	2.2	26.3	2.48	17.5	0.17
0.081	1.00	2.2	11.6	1.05	18.9	0.31
0.062	2.00	2.3	4.75	0.384	19.6	0.58
0.60	0.054	4.4	169 (k_1)	20.0	0	
0.59	0.50	4.1	123	14.6	5.42	1.1
0.565	0.99	3.9	57.3	6.71	13.3	0.9
0.60	2.0	3.8	30.1	3.48	16.5	1.4

*Excess acidity added as $HClO_4$.
**Adjusted by adding $NaClO_4$.

The data listed in Table 30 were obtained on the purer uranyl perchlorate preparation. The ionic strength was fixed for each series of experiments, and the precautions taken to avoid impurities were greater than those taken in earlier runs.

Values for the equilibrium constant, K_c, are given for both the sulfate and perchlorate systems in Tables 28 and in 29 and 30, respectively. The average values are $K_c(SO_4^{--}) = 4.7$, and $K_c(ClO_4^-) = 0.60$. Although these values differ for the same

TABLE 30. DECOMPOSITION OF PEROXIDE IN URANYL PERCHLORATE SOLUTIONS

TOTAL URANIUM CONCENTRATION (M)	TOTAL H^+ CONCENTRATION* (M)	IONIC STRENGTH,** μ	OBSERVED RATE CONSTANT, $k_3 \times 10^3$ (min^{-1})	CALCULATED CONCENTRATION ($M \times 10^4$)		EQUILIBRIUM CONSTANT, K_c
				UO_4	H_2O_2	
0	2.0	2.12	0.95 (k_2)		19	
0.04	~0.0008	2.12	78.2 (k_1)	16.5	0	
0.038	0.101	2.11	25.5	6.60	14.1	0.13
0.038	0.101	2.11	24.8	6.04	13.2	0.12
0.04	0.50	2.12	5.0	1.04	18.5	0.35
0.04	1.00	2.12	3.5	0.66	19.3	0.85
0.12	0.001	2.36	144.4 (k_1)	10.0	0	
0.114	0.103	2.34	100.2	13.1	5.86	0.21
0.120	0.50	2.36	12.1	1.11	13.2	0.18
0.120	1.00	2.36	6.9	1.06	24.4	0.36
0.120	2.00	2.36	4.85	1.94	69.6	0.93
0.120	0.001	2.36	113	15.1	0	
0.114	0.106	2.34	83.2	29.7	10.8	0.27
0.30	0.01	2.9	123.0 (k_1)	25.0	0	
0.30	0.50	2.9	34.4	11.2	29.8	0.32
0.30	1.00	2.9	13.3	4.44	39.3	0.38
0.30	2.00	2.9	10.8	3.12	35.5	1.10
0.60	0.05	3.8	185.0 (k_1)	17.9	0	
0.60	0.50	3.8	129.0	15.2	6.7	0.96
0.60	1.00	3.8	65.6	7.2	13.3	0.91
0.58	1.92	3.7	37.3	5.5	22.1	1.5

*Excess acidity added as $HClO_4$.
**Adjusted by adding $NaClO_4$.

equilibrium, the differences are probably due to total concentrations having been employed in place of activities.

Intensive efforts have been made to calculate, or rather to approximate, activity coefficients for H^+ and UO_2^{++} in the perchlorate system (assuming the activity coefficient ratio for UO_4 to H_2O_2 is constant throughout these experiments). Too many extrapolations and assumptions have to be made in order to obtain activity coefficients for these ions in a mixed system, especially at 100°C. A reasonable explanation for the shift in K_c with both concentration and ionic strength can be made on the basis of the known activity coefficients at 25°C of the pure species, uranyl perchlorate, perchloric acid, and sodium perchlorate.

MECHANISM OF THE HYDROGEN-OXYGEN RECOMBINATION REACTION IN SOLUTIONS

H. F. McDuffie L. F. Woo
C. H. Secoy

An extension of the studies discussed in a previous quarterly report[11] has been concentrated on the firmer establishment of the dependence of the reaction rate on copper concentration and temperature, and it has included preliminary studies of the rate of the reaction with deuterium instead of hydrogen.

Dependence on Copper Concentration

The reaction rate at 250°C has been confirmed as first order in copper concentration for solutions of copper sulfate in uranyl sulfate (0.17 *M* at room temperature). Table 31 and Fig. 64 show that the first-order behavior has been extended down to solutions which are 10^{-4} *M* in copper. It will be recalled that in-pile experiments have indicated first-order behavior up to 0.05 *M* copper; thus a 500-fold range of concentration has been spanned.

TABLE 31. EFFECT OF COPPER SULFATE CONCENTRATION UPON RECOMBINATION RATE AT 250°C IN 0.166 *M* URANYL SULFATE SOLUTION

RUN NUMBER	COPPER CONCENTRATION AT 250°C (moles/liter)	k_{sol}
B-202	0.000125	0.75
B-207	0.000125	0.85
B-203	0.00021	1.29
B-205	0.00021	1.23
B-204	0.00042	2.56
B-206	0.00042	2.49
A-216	0.0023	13.0
A-217	0.0022	12.8
A-221	0.0023	12.5
A-277	0.0020	9.3
A-297	0.0021	11.3
A-210	0.0021	11.4
A-213	0.0021	10.5

[11] H. F. McDuffie and L. F. Woo, *HRP Quar. Prog. Rep. March 31, 1953*, ORNL-1554, p. 89-96.

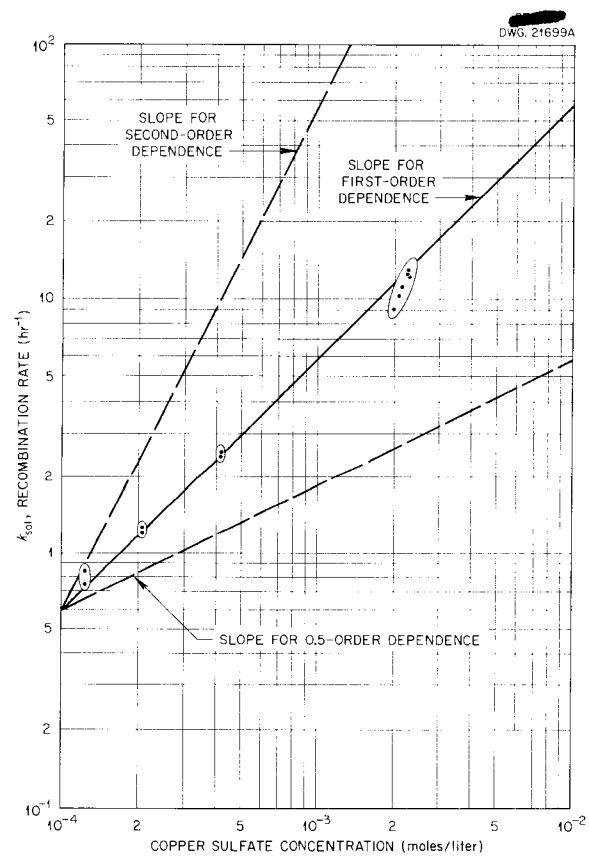

Fig. 64. Effect of Copper Sulfate Concentration Upon Recombination Rate at 250°C in 0.166 *M* UO_2SO_4 Solutions.

The reaction rate at 250°C has likewise been demonstrated to be first order for solutions of copper sulfate in 0.005 M sulfuric acid over the tenfold concentration range of 10^{-4} to 10^{-3} M copper. Table 32 and Fig. 65 illustrate the clean first-order behavior observed.

It was noted that, although first-order behavior was observed in both cases, the actual rates were different. This is believed to be due to the difference in the environment, which affects the copper. One possibility is that the active species changes from Cu^{++} or $Cu(OH)_2$ in perchlorate solutions to the more active $(CuHSO_4)^+$ or $Cu(OH)(HSO_4)$ in dilute sulfuric acid solutions and that it finally is pushed toward the less active $Cu(HSO_4)_2$ in more concentrated sulfuric acid or uranyl sulfate solutions. Changing the anionic constituents would be expected to change the relative catalytic effectiveness, that is, chloride, bromide, nitrate, acetate, and phosphate might be expected to behave differently from sulfate. Attempts will be made to obtain information through this approach.

TABLE 32. EFFECT OF COPPER SULFATE CONCENTRATION UPON RECOMBINATION RATE AT 250°C IN 0.005 M SULFURIC ACID SOLUTIONS

RUN NUMBER	COPPER CONCENTRATION (moles/liter)	k_{sol}
B-214	0.00010	17.2[a]
B-222	0.00010	1.76
B-223	0.00010	1.38
B-215	0.00025	26.7[a]
B-219	0.00025	8.3[a]
B-221	0.00025	3.97
B-225	0.00025	3.09
B-226	0.00025	2.89
B-216	0.00060	36.3[a]
B-218	0.00060	7.7
B-220	0.00060	7.1
B-224	0.00060	7.6
B-217	0.0010	11.6
B-227	0.00010	1.45[b]
B-228	0.00010	1.39[c]

[a]Data excluded because of contamination from previous runs.

[b]Sulfuric acid concentration 0.0010 M.

[c]Sulfuric acid concentration 0.0030 M.

Temperature Coefficient of the Reaction

Table 33 presents data for the reaction rate at several different temperatures. The starting solutions were the same at room temperature (0.166 M uranyl sulfate, 0.0025 M copper sulfate), and, therefore, the compositions were not precisely the same at the reaction temperature. Corrections for this small difference in composition have been applied to give the observed values for k_{Cu}. The experimentally observed activation energy for the 190 to 250°C values is 24 ± 4 kcal.

Rate of Reaction with Deuterium

Since operating reactors of the homogeneous type may well use heavy-water solutions instead of light water, the decomposition gases would be deuterium and oxygen instead of hydrogen and

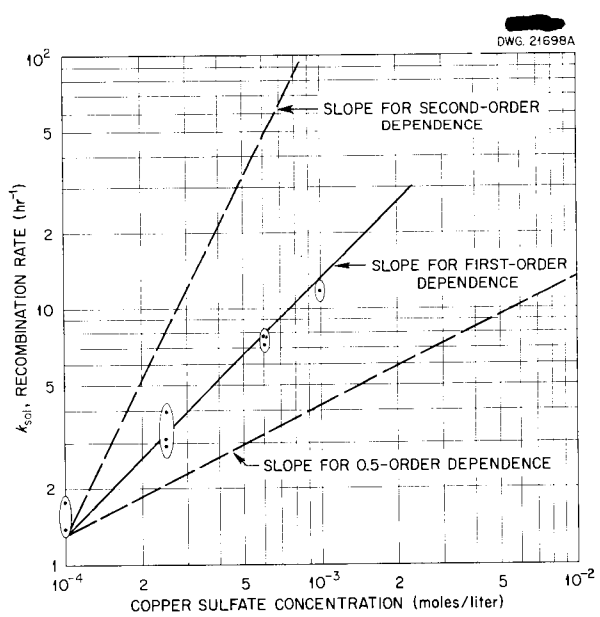

Fig. 65. Effect of Copper Sulfate Concentration Upon Recombination Rate at 250°C in 0.005 M Sulfuric Acid Solutions.

TABLE 33. TEMPERATURE DEPENDENCE OF RECOMBINATION IN 0.166 *M* URANYL SULFATE–0.0025 *M* COPPER SULFATE SOLUTIONS

RUN NUMBER	TEMPERATURE (°C)	k_{sol}	HOT COPPER CONCENTRATION (moles/liter)	$k_{Cu} \times 10^{-3}$
A-236	190	0.64	0.0022	0.29
A-237	190	0.58	0.0022	0.26
A-243	190	0.53	0.0022	0.24
				0.26 Avg.
A-233	220	10.3	0.0023	4.55*
A-234	220	3.29	0.0022	1.52
A-240	220	3.01	0.0022	1.40
A-241	220	3.42	0.0022	1.59
				1.50 Avg.
B-208	220	3.69	0.0022	1.71
B-209	220	3.70	0.0022	1.70
B-210	220	3.50	0.0022	1.61
				1.67 Avg.
A-216	250	13.0	0.0023	5.72
A-217	250	12.8	0.0022	5.70
A-221	250	12.5	0.0023	5.51
A-277	250	9.3	0.0020	4.63
A-297	250	11.3	0.0021	5.36
A-210	250	11.4	0.0021	5.43
A-213	250	10.5	0.0021	5.07
				5.35 Avg.

*Discarded – obviously erroneous.

oxygen. The reaction of deuterium with the catalyst might be expected to be somewhat slower than the reaction of hydrogen. Accordingly, three experiments at different ratios of liquid to gas phase were conducted in which deuterium gas was substituted for hydrogen gas (ultimately the reaction will be checked by using heavy water solutions and deuterium). The solution was one for which considerable data with hydrogen gas were available (0.005 *M* sulfuric acid and 0.001 *M* copper sulfate). Results are presented in Table 34. A least-squares line for the relationship[12] between V_g/V_l and $1/k_\pi$ gave the following values:

$$k_{sol} = 2.2$$

$$a = 1.7 \times 10^3 \text{ psi/mole·liter}$$

$$\frac{a}{k_{sol}} = 760$$

Comparison of this value of a/k_{sol} with that for hydrogen, using the same solution (433), indicates that the reaction is about 60% as fast with deuterium as with hydrogen at the same pressure. The solubility of deuterium is indicated as being slightly greater than that of hydrogen in light water, but the number of experiments is too small to permit any strong conclusion. At least the solubilities do not differ substantially.

[12] C. E. Ronneberg, *HRP Quar. Prog. Report March 31, 1953*, ORNL-1554, p. 96.

TABLE 34. RECOMBINATION OF DEUTERIUM AND OXYGEN IN LIGHT-WATER SOLUTIONS CONTAINING 0.005 M SULFURIC ACID AND 0.001 M COPPER SULFATE

RUN NUMBER	V_g/V_l	$1/k_\pi$
B-233	6.05	7.75
B-234	0.60	1.08
B-235	1.87	2.91

Plans for Next Quarter

Because of the increasing interest in low concentrations of uranyl sulfate and temperatures higher than 250°C, a more intensive study will be made of recombination at 250 to 300°C in uranyl sulfate solutions containing 1 to 10 g of uranium per liter.

The reaction rate will also be checked by using deuterium gas with heavy water solutions of the catalyst.

As indicated above, variation in the anionic constituent associated with the copper will be attempted in an effort to establish how the anion affects the activity of the copper.

HOMOGENEOUS REACTOR SOLUTIONS UNDER IRRADIATION

C. H. Secoy
H. O. Day
B. O. Heston
Q. V. Larson
F. H. Sweeton
W. C. Yee

During the last quarter, more studies of the corrosion of metals by homogeneous reactor solutions under reactor radiation have been carried out; for comparison purposes, some out-of-pile studies have also been made. During this time, the instrumentation of hole HB-6 in the Low-Intensity Test Reactor has been finished, and this new facility has been put into use. The new facility is superior to the older one in HB-5 in that a bomb can be rotated manually while it is in the hole and the reactor is operating. Bombs irradiated in this new hole are normally kept horizontal during the test in order to obtain quicker equilibrium between the oxygen in the vapor phase and that dissolved in the liquid phase. Tests during the quarter have involved type 347 stainless steel and also titanium.

As before, the change in oxygen partial pressure in a bomb has been used to calculate the corrosion penetration by assuming that corrosion occurs only on the bomb surface wetted by the test solution, that the corrosion is uniform over that surface, and that there is no selective oxidation of any particular component of the stainless steel.

Stainless Steel

Several out-of-pile tests with stainless steel have been completed during the quarter.

Test H-16A. This test was made by using a special 38-ml bomb that contained an appreciable quantity of stainless steel turnings; therefore the surface-to-volume ratio was larger by a factor of 3 than that of the bombs used in reactor. Most of the data for the test are included in Fig. 66. As usual, oxygen was added to the bomb in the form of hydrogen peroxide, which later decomposed on heating. The oxygen partial pressure was about 95 psi at the start, and it decreased gradually to about zero during the test. An analysis of the residual gas in the bomb after the test was stopped showed that actually about 5 psi of oxygen was present and, in addition, about 7 psi of hydrogen. When the bomb was opened, all the uranium was found to be precipitated.

The results of the test can be best discussed by breaking the curve of Fig. 66 into three parts. The first part, in which the rate of corrosion is apparently increasing, has not been observed previously in

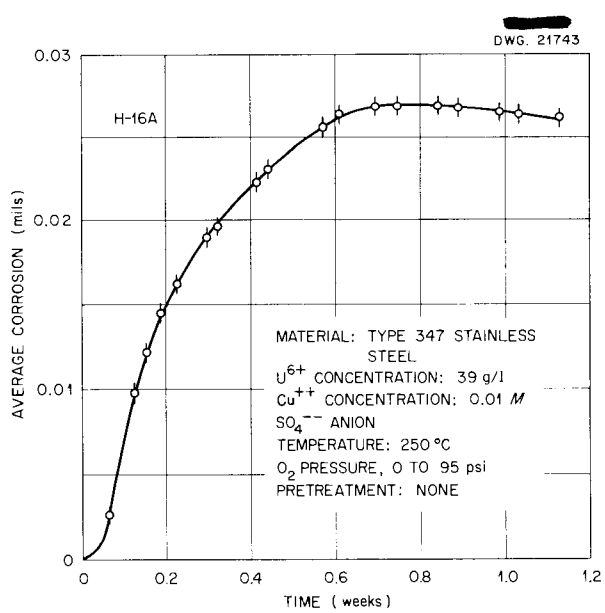

Fig. 66. Out-of-Pile Corrosion of Stainless Steel by Homogeneous Reactor Solution.

this series of experiments. It may be due to the slow rate of oxygen diffusion from the vapor phase down into the solution where it is being depleted by corrosion. The middle portion of the curve between 0.16 and 0.6 week is quite regular, and it appears to be the more or less normal effect of corrosion on the oxygen pressure. In this region, the corrosion appears to progress as the square root of time. The negative slope of the last portion of the curve probably is not real. As usual, the plotted corrosion is that calculated by assuming (1) that all changes in total pressure are due to oxygen being absorbed in the corrosion process and (2) that no other oxidizing agent is acting on the steel. If stainless steel is oxidized by either uranium (with the precipitation of reduced uranium) or water (with the liberation of hydrogen), the calculated corrosion shown in the graph will be erroneously low. This is believed to be true in this case, since both precipitated uranium and hydrogen gas were found when the bomb was opened.

Test H-16B. Another out-of-pile test was later performed with the same bomb. However, the pressure decreased so fast that the bomb appeared to be leaking. Oxygen gas was then added and no further apparent leaking occurred, but the rate of change in pressure was erratic in that it dropped significantly more during one period of less than 4 hr than either before or after the 4-hr period. It is concluded that the data of this test are not reliable, because either the surface of the bomb was not equivalent to a new one or the treatment of the bomb when a leak was suspected affected its corrosion curve.

Test H-16. The results of another out-of-pile test are shown in Fig. 67. This test was essentially similar to test H-16A except that a bomb of normal size (~9 ml) was used and no turnings were present in the bomb to increase the surface. The corrosion rate decreased throughout the test. The average rate for the last three weeks was 0.1 mpy. The corrosion during the first 0.6 week agreed in general with that of test H-16A within a factor of 2, which is reasonably close when the uncertainty of the microscopic surface area is considered.

Test H-11. This was the first in-pile radiation completed this quarter. As can be seen in Fig. 68, test H-11 was essentially the same as tests H-16 and H-16A, except for its fission density and its somewhat higher oxygen partial pressure. This experiment was terminated in order to make room

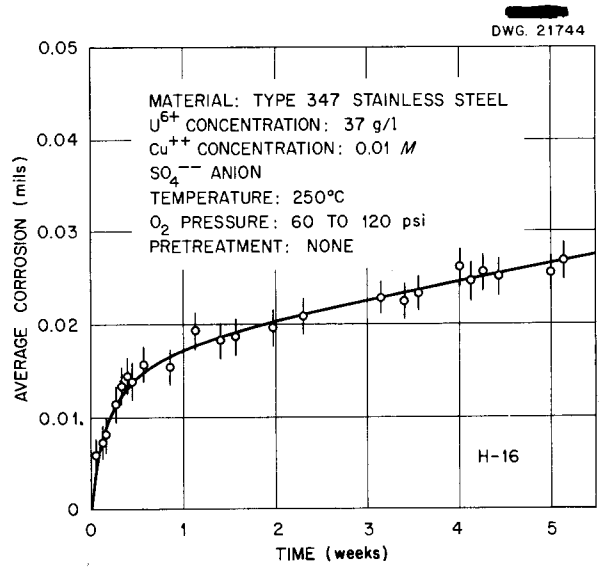

Fig. 67. Out-of-Pile Corrosion of Stainless Steel by Homogeneous Reactor Solution.

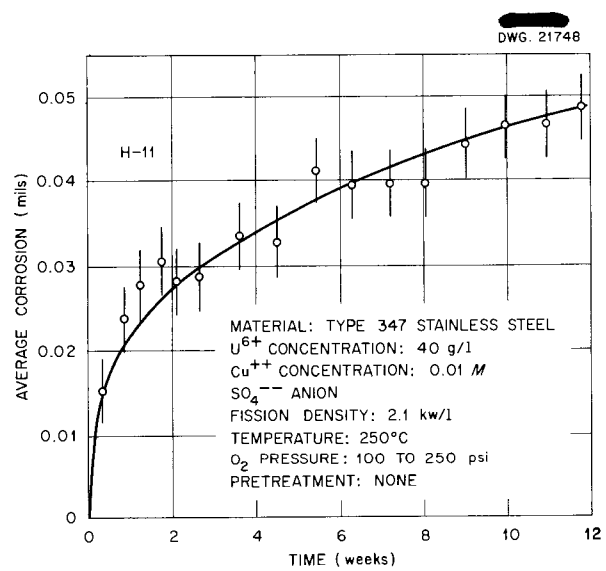

Fig. 68. In-Pile Corrosion of Stainless Steel by Homogeneous Reactor Solution.

for other experiments. As can be seen on the graph, the rate of corrosion continued to decrease; it averaged about 0.1 mpy from the fourth week on to the end. Comparison of the test with tests H-16 and H-16A indicates no appreciable difference in corrosion and also suggests that at this fission density (2.1 kw/liter) radiation may not be affecting the corrosion.

Test H-12. This test, described in Fig. 69, was supposedly the same as two tests reported last quarter, tests H-7 and H-10, except that (1) this bomb had been put through an electropolishing process and (2) the test was made at 290°C instead of 250°C. Only four experimental points were obtained before the loss of excess oxygen made it necessary to terminate the test in order to avoid precipitation of uranium. These points are in poor agreement; however, they seem to indicate that the corrosion under these conditions is roughly the same as that at 250°C. There is a possibility that geometry may have made electropolishing unsuccessful and may have affected the corrosion rate. Another test at elevated temperature with a mechanically polished bomb will probably be tried.

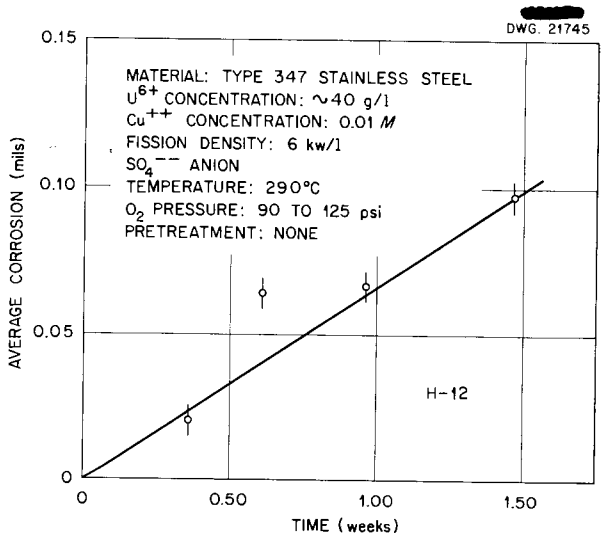

Fig. 69. In-Pile Corrosion of Stainless Steel by Homogeneous Reactor Solution.

Test H-13. This test was made at an intermediate power density, and as can be seen in Fig. 70, it showed the high corrosion found at a density of 6 kw/liter. The corrosion was so rapid that the experiment had to be terminated after one week, after only two corrosion points had been obtained. The corrosion appeared to average about 6 mpy during this one week. However, this bomb, like that of test H-12, was put through an electropolishing process which may have adversely affected its surface. A repetition of this test with a mechanically polished bomb is desirable.

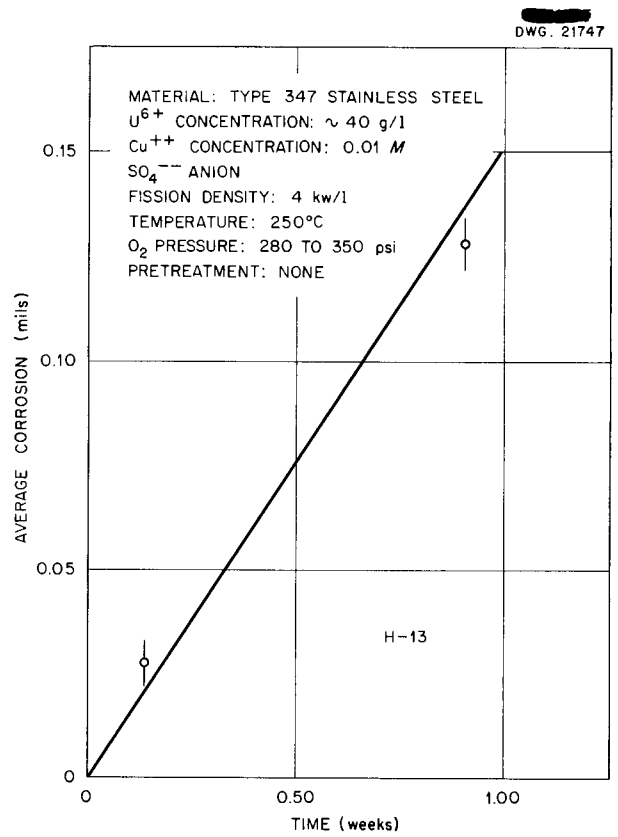

Fig. 70. In-Pile Corrosion of Stainless Steel by Homogeneous Reactor Solution.

Titanium

Tests H-14 and H-15. These tests were made with titanium bombs, and the results are combined in Fig. 71. The two tests were essentially the same except for fission density and a small difference in copper concentration. The corrosion data are strikingly different. The out-of-pile test, H-15, gave high initial corrosion followed by an essentially complete passivation. The in-pile test H-14, however, had a much lower initial rate, but it never approached a passivated state. The change in fission density during the test was due to a stepping up of the reactor operating power. There is a slight indication that the corrosion rate may have been decreasing at the lower fission densities, but at the final power level the corrosion appeared to be proceeding at the linear rate of about 1.3 mpy.

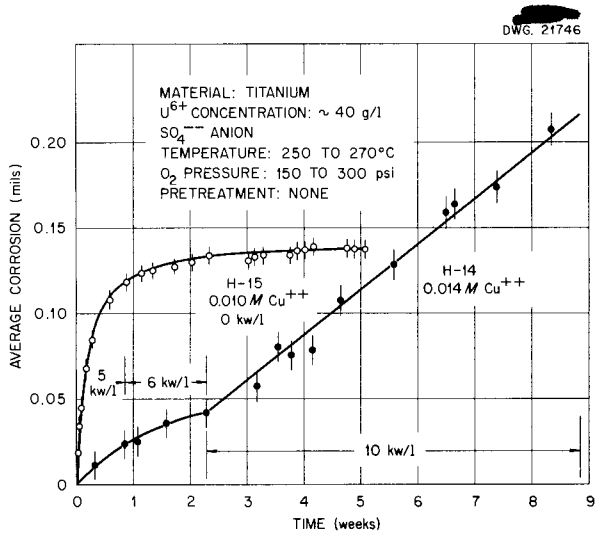

Fig. 71. Corrosion of Titanium by Homogeneous Reactor Solution.

Future Work

Both in-pile and out-of-pile tests will be continued during the next quarter. It is hoped that some of these will be made with Zircalloy II. The out-of-pile testing equipment is being modified to allow shaking and thus to remove diffusion as a possible cause of error in these experiments. T. E. Willmarth, of the Analytical Division, will make microscopic examination of the surface of out-of-pile bombs, and M. J. Feldman, of the Solid State Division, will similarly examine the in-pile bombs. It is planned to make use of test pins in bombs to provide an independent check on the amount of corrosion and to furnish surface films for microscopic studies.

RELATED CHEMISTRY RESEARCH

CHEMISTRY OF CORROSION

G. H. Cartledge

A brief study was made of the effect of welding upon the chemical activity of stainless steel, type 347. The deposition of a beta ray emitting material (presumably technetium dioxide) from a solution of potassium pertechnetate was used as a measure of the relative chemical activity of the metal surface.[1] The experiments showed that the unpolished weld surface and adjacent area were excessively active, being anodic to polished or machined surfaces in the same neighborhood. The excess activity extended over a 2-cm distance at the weld, with inconclusive evidence of a secondary increase near the ends of a 15-cm bar which had the weld in the middle. When a specimen bar was electropolished on three sides and ground on the fourth, the ground surface picked up 80% of the activity, although it had only 25% of the total geometrical surface. Autoradiograms of weld areas disclosed clearly the contours of the weld zone in both a fusion weld and one made with filler rod.

Further study of the inhibition of corrosion by potassium pertechnetate has shown that, in distilled water at 100°C, 5 ppm of technetium gives complete protection of the carbon steel used in these experiments.

[1] G. H. Cartledge and R. P. Yaffe, *Chem. Semiannual Prog. Rep. June 20, 1953*, ORNL-1587, p. 17.

BLANKET SYSTEMS

THORIUM OXIDE CHEMISTRY

D. E. Ferguson, Assistant Section Chief
J. P. McBride R. G. Mansfield
L. E. Morse W. L. Pattison

Thermal Decomposition of Thorium Oxalate

In the preparation of thorium oxide by the thermal decomposition of thorium oxalate at 500°C, carbon monoxide, which is evolved as one of the reaction products, is capable of the following reactions:

$$2CO \longrightarrow CO_2 + C \text{ (disproportionation)}$$

$$CO + \tfrac{1}{2}O_2 \longrightarrow CO_2 \text{ (oxidation)}$$

Both reactions are accompanied by the evolution of considerable amounts of heat.

Because it has been demonstrated that the physical properties of thorium oxide prepared by thermal decomposition of thorium oxalate are closely related to the temperature of calcination, it is important, especially in the preparation of large quantities of thorium oxide, to know whether or not overheating occurs within the oxide bed.

Three experiments were performed that involved the decomposition of thorium oxalate at 500°C in a muffle furnace in which the temperature changes occurring in the oxide bed were followed continuously by means of a thermocouple placed in the bed and connected to a Brown recorder. Typical heating curves are shown in Fig. 72. Curves A and C were obtained by using the same Alundum thimble with 60.8 and 48.7 g of thorium oxalate. The temperature rise above 500°C increased with the amount of thorium oxalate decomposed. The volumes of material were about the same, however, since the material used for curve C was a more bulky preparation.

Curve *B* was obtained by using 60.7 g of thorium oxalate and a porcelain crucible that was flatter and wider than the Alundum thimble, and the temperature rise was about 15°C higher than that obtained for the same amount of material in the Alundum thimble. This higher temperature may be due to a greater access of air and will be discussed later.

The plateaus in all three curves in the region of 250°C are probably associated with the reaction:

$$Th(C_2O_4)_2 \cdot 2H_2O \longrightarrow Th(C_2O_4)_2 + 2H_2O$$

The decomposition of thorium oxalate appears to start at about 350°C, and while the exact mechanism is still a matter of discussion, it has been established that CO is liberated. It may be surmised, then, that the subsequent behavior of CO will influence the temperature effects. For example, if CO should be engaged in exothermic reactions before it is able to diffuse away from the site of liberation, heat would be developed in the immediate region of the ThO_2 product, whereas if most of the CO were to diffuse away before reacting, less or no heating effect would be observed.

In preliminary experiments in which thorium oxalate was decomposed in an open container in a muffle furnace at 500°C, temperature excursions were noticed. However, when the same decomposition was accomplished in a covered container, the temperature did not exceed that of the furnace even though some heat was produced. This would indicate that the principal source of heat production is the oxidation of CO to CO_2, a reaction which would be hindered by the limited access of air in experiment C. This also may explain why more heat was observed in the experiment performed in the porcelain crucible whose dimensions allowed for greater access of air.

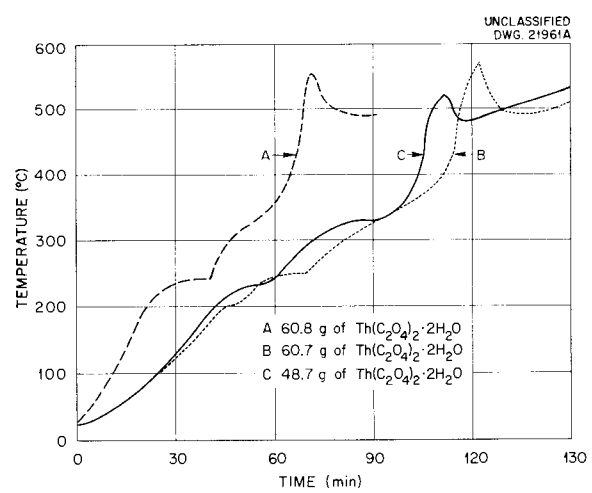

Fig. 72. Decomposition of Thorium Oxalate Heating Curves.

Deposition of carbon on the ThO_2 in all these experiments indicated that some disproportionation of CO also occurred.

In the preparation of thorium oxide, the effects of temperature excursion might be minimized or entirely avoided by holding the furnace in the region of the decomposition temperature of thorium oxalate, about 350°C, until the reaction is complete and then raising the product to the desired final temperature. Difficulties due to temperature excursions during preparation have been noted by the Ames Laboratory,[1] where large quantities of the oxide are produced by calcining thorium oxalate at 650°C in a forced air draft.

Reaction Between Thorium Oxide and Water at 250°C

The possibility that there is a reaction at 250°C that leads to the binding of water by thorium oxide in the slurry blanket is of interest. The principal difficulty encountered in attacking the problem is the selection of a method for distinguishing between the bound and unbound water in thorium oxide.

[1]G. L. Bridger, K. G. Shaw, and M. E. Whatley, *I. Process for Production of Pure Thorium and Uranium from Monazite*; H. A. Wilhelm, W. D. Tucker, R. H. Griffin, and R. W. Fisher, *II. Purification of Thorium Nitrate and the Subsequent Production of Thorium Oxide*, ISC-134, p. 32 (Jan. 15, 1951).

In a study of the dehydration of hydrous thorium oxide,[2] it was proposed that the water retained by the sample after it was dried at 250°C for 3 hr but lost when the sample was ignited to 900°C for 2 hr represented water bound to the ThO_2. About 4 to 5 wt % of water was involved, and the manner in which the water was bound was not clearly specified.

In the present study, the method pursued was to heat a sample of the oxide in water at 250°C and then analyze it for bound water by determining the weight loss on heating at 900°C after first drying for 3 hr at 250°C. Three different thorium oxide preparations were examined in this manner (Table 35).

In no case did the amount of bound water approach 4 to 5 wt % when thorium oxide went from the hydrated to the dehydrated state.

The amount of water retained by the oxides at 250°C decreased as the calcination temperature at which the oxide was prepared increased; this decrease is probably associated with the surface areas of the thorium oxides, which also decrease with increasing calcination temperature.

An interesting relationship between water content and surface area may be obtained by comparing surface areas calculated on the basis that

[2]O. Glemser, *Z. Electrochem.* 45, 820 (1939).

TABLE 35. REACTION BETWEEN THORIUM OXIDE AND WATER AT 250°C

OXIDE	HEATING TIME IN WATER AT 250°C (hr)	WATER ASSOCIATED WITH ThO_2 DRIED AT 250°C (%)	SURFACE AREAS (m^2/g)	
			From N_2 Adsorption or Calculated From Particle Size	Calculated From Water Content of Solid Dried at 250°C
Thorium oxide prepared by decomposing thorium oxycarbonate at 375°C	48	1.31	39 (N_2 adsorption)	46
Thorium oxide prepared by decomposing thorium oxalate at 500°C	96	1.04	37 (N_2 adsorption)	35
Ames thorium oxide prepared by decomposing thorium oxalate at 650°C and sieving through 325-mesh screen	39 103 219	0.76 0.52 0.61 Avg. 0.63	32 (Calculated from an average particle size of 0.02 μ)	22

the adsorbed water, which has a cross-sectional area of 10.6 $Å^2$ per molecule, is held as a monomolecular film on the ThO_2, with the surface areas obtained by the N_2-adsorption method or calculated from the average particle size (see Table 35). The agreement between the two methods is fairly good.

The results obtained show that if hydrates of a definite composition are formed from the three oxides in water at 250°C they are not identical and that the amount of water remaining with the oxides on drying at 250°C is accountable for on the basis of a surface adsorption of the water. This does not imply that water is actually present as adsorbed water, but the coincidence is demonstrated.

Hydrolytic Decomposition of Thorium Oxalate

A method of oxide preparation which seems to hold some promise is the pyrohydrolysis of thorium oxalate in water at 250°C. Initial attempts to prepare the compound in steel autoclaves resulted in a slurry product that was considerably contaminated with iron. The use of an aluminum liner gave a bulky white nonabrasive slurry containing only 216 ppm of aluminum.

The material has a very small average particle size (~0.1 μ) and settles to only 600 g of thorium per liter. Experiments for determining the effect of prolonged heating in water at 250°C on the properties of this material are in progress.

[3]W. W. Floyd, J. P. McBride, L. E. Morse, and W. L. Pattison, *HRP Quar. Prog. Rep. July 31, 1953*, ORNL-1605, p. 35.

LABORATORY STUDIES OF THE PROPERTIES OF THORIUM OXIDE PREPARATIONS

Chemical Purity

Table 36 gives the analytical data for oxide residues prepared by the calcination at 300, 500, 700, and 900°C of thorium oxalate prepared in the usual manner by precipitation from a thorium nitrate solution at 50 to 70°C.[3] The second column lists the heating period. Essentially complete decarbonization was obtained in all experiments. The low thorium contents are believed to be representative of relative affinity for water, rather than the result of a failure to attain complete decomposition of the oxalate. The high nitrate contents shown for the material prepared at 700 and 900°C are probably the result of incomplete washing of the oxalate precipitate.

Physical Properties

The oxide residues from the oxalate decompositions described above were examined for particle size (optical microscope), crystallinity, total surface area, density, and relative abrasiveness. Table 37 gives the data obtained.

The photomicrograph used for the particle-size measurements showed the oxide residues to be composed of well-formed crystallites of rather large average size (2 to 5 μ). This fact makes the relatively broad x-ray diffraction pattern and large surface areas obtained with the low-burned materials surprising.

The x-ray diffraction patterns are seen to become sharper with increasing calcination temperature, and this is indicative either of crystallite growth or of annealing in the crystal. The surface

TABLE 36. ANALYSIS OF RESIDUES FROM THORIUM OXALATE DECOMPOSITION

CALCINATION TEMPERATURE (°C)	CALCINATION TIME	COMPOSITION (%)		
		Th*	C	NO_3
300	38 days	83.3	0.08	<0.01
500	120 hr	84.1	0.18	<0.01
700	6 hr	85.3	0.07	0.6
900	3 hr	86.0	0.01	0.6

*Per cent thorium in ThO_2: 87.8.

TABLE 37. PROPERTIES OF OXIDE RESIDUES FROM THORIUM OXALATE DECOMPOSITION

CALCINATION TEMPERATURE (°C)	AVERAGE PARTICLE SIZE (μ)	X-RAY* DIFFRACTION LINE WIDTH (deg)	SURFACE** AREA (m^2/g)	DENSITY (g/cc)		RELATIVE ABRASIVENESS
				Water	Toluene	
300	2	1.7	43.87	8.07	7.94	Slight
500	4	1	37.14	8.49	8.32	Slight
700	5	0.7	7.33	9.00	8.62	Moderate
900	5	0.3	1.83	9.64	9.50	High

*Background line width was 0.2 deg; measurements by R. D. Ellison, Chemistry Division.

**N_2 adsorption; measurements by J. A. Westbrook, K-25.

area decreases with temperature of calcination, again the result of either crystallite growth or a sintering of a porous material, or both. The most profound change occurs between 500 and 700°C.

The density measurements were made in both water and toluene by using a pycnometer. The measurements were made in duplicate, and the agreement was better than 0.8% in all cases. The densities obtained in both solvents show a regular increase with temperature of calcination. The slightly lower densities obtained with toluene are believed to indicate that the toluene molecule failed to fill the pores of the material as readily as did the water. The largest difference is observed with the 700°C material. Hence, as in the surface area measurements, there is indication that an annealing or sintering takes place in this temperature region.

An increase in abrasiveness with temperature of calcination parallels the changes in physical properties that have been described above, and this increase will be explained in more detail below.

The physical measurements that have been described supplement and are in agreement with the concept of the thermal decomposition presented by Beckett and Winfield.[4] From electron micrographs of the oxide residues, these investigators concluded that the initial oxalate crystal imposes on the residual oxide crystals a mosaic structure of thin, spongy, microcrystalline laminae all oriented in very nearly the same direction. As indicated above, an increase in the temperature of calcination produces three results: an annealing and sintering process that results in sharpening of the x-ray pattern, a decrease in surface area, and an increase in abrasive hardness. The low abrasiveness exhibited by the material prepared at 500°C may be attributed to the more ready breaking apart of the microcrystalline units of the mosaic which anneal into a hard, compact crystal at higher temperatures.

Abrasive Properties

Since the initial pumping studies indicated that abrasion in high-velocity flow regions might be a serious problem in the practical utilization of a thorium oxide slurry, considerable attention was paid to the effect of the method of preparation and of the treatment on the abrasive properties of the oxide slurries. The accelerated laboratory abrasion test, described in the last quarterly report,[5] has been used to obtain the data discussed in the following section. In this test, a jet of slurry is impinged against a steel test plate 1.0 mil thick, and the time of penetration is noted.

Abrasive Properties of Calcined Thorium Oxide. Values of the relative abrasiveness of the Ames oxide and of oxide residues obtained by calcining oxalate at various temperatures were determined after treatment with water at both room temperature and 250°C. Table 38 summarizes the results obtained.

[4] R. Beckett and M. E. Winfield, *Australian J. Sci. Research* 4, 644 (1951).

[5] J. P. McBride and W. L. Pattison, *HRP Quar. Prog. Rep. July 31, 1953*, ORNL-1605, p. 139.

TABLE 38. ABRASIVE PROPERTIES OF CALCINED THORIUM OXIDE

CALCINATION TEMPERATURE (°C)	AVERAGE PARTICLE SIZE (μ)	PENETRATION TIME AFTER TREATMENT WITH WATER (min)			
		At Room Temperature	At 250°C		
		for 4 days	for 4.5 days	for 300 hr	for 600 hr
300	2		None*		
500	4	None*	None*	None*	None*
650 (Ames)	0.02	30	55	None*	None*
700	5	None*	36.5		
900	5	2.5	2.5		

*After 60 minutes.

The abrasiveness was found not only to increase with calcination temperature but also, in some cases, to be affected by treatment with water at 250°C. The 500°C material shows no appreciable change in abrasiveness on extended heating in water at 250°C. The Ames material, on the other hand, is visibly softened. The 700°C material becomes harder after a relatively short time of heating at 250°C.

Abrasive Properties of Fluorinated Oxides. During the last quarter, two experiments in which thorium fluoride was added to the 500°C oxide and autoclaved in water at 250°C were found to yield highly abrasive slurries.[6] Another method of adding the fluoride was investigated this quarter, and the results were similar. In this preparation, thorium hydroxide was dissolved in excess of ammonium carbonate. Hydrofluoric acid was then added in a hydrofluoric acid-to-thorium mole ratio of 2, and the resulting solution was boiled to precipitate a compound that was stoichiometrically thorium oxyfluoride ($ThOF_2$) but that exhibited a weak ThO_2 x-ray diffraction pattern. This material was autoclaved in water at 250°C for 16 hours. An abrasion test showed it to be more abrasive than the 500°C oxide or thorium fluoride which had been subjected to similar autoclavings. Table 39 gives the abrasion results for the fluorinated materials.

TABLE 39. ABRASIVE PROPERTIES OF FLUORINATED THORIUM OXIDE*

MATERIAL	F-to-Th RATIO	TIME OF PENETRATION (min)
500°C ThO_2	0	None**
ThO_2-ThF_4	0.5	3
ThO_2-$NaThF_5$	0.9	6
$ThOF_2$	2.0	19
ThF_4	4.0	None**

*Conditions: autoclaved in water at 250°C; 250 g of thorium per liter.

**After 60 minutes.

Abrasion and Particle Size. Although no specific study has been made on the effect of particle size on relative abrasiveness, the results of optical and electron microscope particle-size measurements of some of the thorium oxide slurry preparation used in the laboratory abrasion tests support the conclusion that relative crystallinity and past history of a slurry preparation are probably more important than particle size in determining its abrasiveness. This conclusion is dictated by the following: 1. Ames oxide, which has an average particle size of 0.02 μ, shows no change in particle size on 4 days shaking in water at room temperature or at 250°C; however, it is only one-half as abrasive after the high-temperature treatment, as compared with the room

[6] W. W. Floyd, J. P. McBride, L. E. Morse, and W. L. Pattison, *HRP Quar. Prog. Rep. July 31, 1953*, ORNL-1605, p. 141.

temperature hydrolysis. 2. Oxide prepared by the 900°C calcination of thorium oxalate (particle size, 5 μ) is still extremely abrasive, although to a lesser extent, even after the particles have been degraded to the order of 0.1 μ or less by extended impingement at high velocity against a steel plate (penetration time, 7 min; initial penetration time, 2.5 min). 3. Oxide from the 500°C calcination of thorium oxalate shows but little abrasive effect even though the average particle size of the material changes from an initial average value of 4 μ to a final value of 0.02 μ during a 60-min abrasion test.

ENGINEERING STUDIES OF CIRCULATING THORIUM OXIDE SLURRIES

R. N. Lyon, Section Chief
A. S. Kitzes W. Q. Hullings
P. R. Crowley C. A. Gifford
R. B. Gallaher

Pumping Studies at Room Temperature

A loop, constructed of ½-in. stainless steel piping and originally fabricated for use with uranium oxide slurries, was equipped with a Roth turbine pump operating at 3400 rpm and the necessary instrumentation for measuring flow rate and the pressure drop over a 12-ft straight section of pipe. There were also provisions for heating and cooling. The pump, although not suitable for handling abrasive slurries, was originally selected because of its low capacity and high head.

Erosion was measured by means of stainless steel test pieces in the pump casing and in the 90-deg elbows, as well as in a straight pipe section. The system was maintained at room temperature by cooling the slurry in the heat exchanger.

The first run (L-1) was made by using Ames ThO_2 in a slurry containing 270 g of Th per liter. Three liters of slurry was circulated for a total of 15 hr, at which time the operation was terminated due to excessive leakage of the slurry through the pump packing. The data obtained in this run are summarized in Table 40 which, for comparison, also includes data obtained from similar water pumping experiments. Standard engineering calculations were employed.

The test piece in the pump, which was a region of very high turbulence, had an erosion rate equivalent to 19 mpy. Microscopic examination revealed that the surface was generally roughened and contained many pit marks. The pump rotor sustained a weight loss of 0.02%, but the elbow test pieces were unaffected. Continuous introduction of fresh water into the back end of the pump (around the canned rotor) would prevent abrasion of the rotor can by the slurry particles.

Because the study of the physical behavior of slurries is now under way in the high-temperature loops at Y-12, it was decided that continued effort on the loop could serve no further purpose at this time, and the work was terminated.

Pumping Studies at Elevated Temperatures

In order to determine the behavior of thorium oxide slurries at 250°C, several runs were made in which between 100 and 300 g/liter of the oxide

TABLE 40. ENGINEERING DATA FOR PUMP EXPERIMENT – RUN L-1

	WITH WATER	WITH THORIUM OXIDE SLURRY CONTAINING 270 g OF THORIUM PER LITER
Time		15 hr
Temperature	40°C	28°C
Pump power	2.73 kw	3.33 kw
Flow	4.7 gpm	5.0 gpm
Velocity	20.1 fps	12.7 fps
Viscosity	0.58 centipoise at 40°C (standard value at 40°C = 0.66 centipoise)	2.45 centipoise at 28°C (H_2O at 28°C = 0.85)

was circulated in dynamic corrosion testing loop T with a Westinghouse 100A pump. In these runs, the Graphitar bearings were continually lubricated with water that was supplied by condensing steam from the pressurizer, and they showed essentially no wear. Table 41 summarizes the results of these runs.

Several general conclusions can be drawn from these data.

1. Although thorium oxide slurries are abrasive, the results of the runs at 250°C can be viewed optimistically. The components most severely attacked were the pump and the flow restrictor. The straight runs of pipe and the reducers showed no effect, while the elbows and tees showed evidence of only mild abrasion.

Figures 73 and 74 are photographs of the pump impeller before and after pumping a slurry containing 100 to 300 g of thorium oxide per liter at 250°C for 500 hr of accumulated time. Approximately two-thirds of all the iron, nickel, and chromium accumulated by the slurry can be accounted for by the weight loss of the pump impeller, which, at 3450 rpm, has a circumferential speed of 120 fps. The outer surface of the impeller appears to be abraded at radii greater than about two-thirds the distance from the axis to the edge; this implies that most of the abrasion occurred at velocities of 80 fps or greater. As can be seen in Fig. 74, the inner two-thirds of the impeller is apparently undamaged except for the formation of a shiny black film. The hub showed some abrasion at points adjacent to the wear rings. Since the liquid is moving under a 250-ft head at this point, the velocity, although undetermined, is assumed to be high. Interestingly, the wear rings, which are tantalum, showed no wear when measured with a micrometer (±0.001 in.) after the 500 hr of operation.

Figures 75 and 76 are photographs of the upstream face of the orifice (flow restrictor) before and after 255 hr of accumulated time on test in the 250°C loop. Again it is seen that obvious

Fig. 73. Impeller Before Circulation of ThO_2 Slurries at 250°C.

Fig. 74. Pump Impeller After Circulation of ThO_2 Slurries at 250°C for an Accumulated Time of 500 Hours.

TABLE 41. CIRCULATION OF ThO_2 SLURRIES AT 250°C WITH WESTINGHOUSE 100A PUMP USING A STANDARD IMPELLER*

SAMPLE NO.	CIRCULATION TIME (hr)	SOLIDS, BASED ON TOTAL SLURRY					FILTRATE						PUMP REQUIREMENTS		
		Th (g/l)	Fe (ppm)	Ni (ppm)	Cr (ppm)	NO_3 (ppm)	Th (ppm)	pH	Fe (ppm)	Ni (ppm)	Cr (ppm)	NO_3 (ppm)	Power (kw)	Current (amp)	Thorium Concentration (g/l)
T-13-1	2	206	291	22	52		<1	5.95	<1	8	<1				
T-13-2**	5.3	163**	248**	4**	6**		<1	5.14	<1	6	<1	<1			
T-13-3	21.6	189	586	32	198		<1	4.95							
T-13-4	28.0	206	646	20	153		<1	6.60		6					
T-13-5	46.0	203	812	17	214		<1	5.25		4					
T-13-6	52.3	190	798	17	210		<1	5.20		4					
T-13-7	70.4	180	886	23	219		<1	5.18		4					
T-13-8	139	181	1800	223	470		<1	5.12		3					
T-14-0	0	193	21	7	4				2						
T-14-1	1.3	210	78	17	12		2	5.15	2	<1	<1				
T-14-2	22.7	76	90	23	8	20	<1	8.20	2	7		6			
T-14-3	27.0	77	81	6	6		<1	7.65		<1					
T-14-4	94.4	97	546	78	111		<1	7.40		<1					
T-15-0	0	268	<1	1	3		<1	5.6	<1	<1					
T-15-1	1	263	145	21	31		<1	5.0	2	5	<1		14.9	60	272
T-15-2	17.5	241	391	18	79		<1	4.9	2	4	1		14.9	60	272
T-15-3	89.6	222	885	9	223		<1	5.9		3			14.7	59	237
T-15-4	114.1	157	753	13	231		<1	5.4		3			14.7	59	237
T-15-5	135.1	189	772	43	259		<1	5.4		4			14.4	58	206
T-15-6	159.1	187	840	49	266		<1	5.3		3			14.5	58	206
T-15-7	183.1	175	895	52	295		<1	5.2		2			14.4	58	206
T-15-8	255.1	167	1160	92	350		<1	5.1		3			14.3	58	192

*T-13 – Ames oxide: particle size, 44 μ or less.

T-14 – Oxide prepared by calcining oxalate at 500°C for 48 hr and subsequently autoclaving at 250°C for four days.

T-15 – Ames oxide: particle size, 44 μ or less; material autoclaved four days at 250°C.

**Sample lost – approximate analysis only.

Fig. 75. Flow Restrictor as Initially Installed.

Fig. 76. Upstream Face of Flow Restrictor Illustrating Abrasion and Corrosion by ThO_2 Slurries. Opening, $\frac{3}{4}$ inch. Run T-15.

abrasion occurred only in the high-velocity region. A heavy black film formed on this face and less film formed on the downstream face, which is shown in Fig. 77. It appears also that a mild polishing action occurred near the opening on the downstream face. The velocity through the opening is estimated to have been about 90 fps.

2. Slurries of Ames thorium oxide, prepared by calcining the oxalate at temperatures above 650°C, can be pumped at 250°C without evidence of sedimentation or caking. The solids appear to be easily redispersed after shutdown, and any agglomerations appear to be broken up into smaller individual particles during circulation. Figures 78 and 79 are electron micrographs of the particles at the beginning and at the end of 140 hr of circulation at 250°C. A number of small rods will be noticed in Fig. 79; however, their nature has not yet been determined. A gradual reduction in the concentration of circulating solid was observed in these tests. This reduction is found to be due largely to a slow net flow into the pressurizer because of distillation of water for injection into the back of the pump. Such a gradual accumulation probably would not occur in the S loop for which thorium tests are now planned.

3. A slurry of low-burned thoria did not show the expected favorable properties, but the presence of impurities suggests that a re-evaluation might be of value. The low-burned material, used in run T-14, was prepared by calcining thorium oxalate at 500°C for 48 hr and, subsequently, autoclaving with water at 250°C for four days. The resulting solid was recovered by decantation and reslurried in fresh water. (In laboratory tests with the jet-impingement method, this material appeared to be substantially less abrasive than Ames oxide.) Prior to loading into the loop, the excess water was again decanted from the slurry,

Fig. 77. Downstream Face of Flow Restrictor Showing Dark Film Around Hole. Opening, $\frac{3}{4}$ inch. Run T-15.

and the ThO_2 concentration was adjusted to about 200 g of thorium per liter at pH 5.15. After 21 hr of circulation, the pump power requirements decreased (usually indicating the loss of solids in circulation). This was confirmed by a radiological survey of the loop, which indicated that the solids were moving along the bottom of the piping. Analysis of a slurry sample showed that the thorium content in suspension had fallen to 76 g/liter and that the pH had increased to 8.2. The concentration of suspended thorium remained unchanged after 27 hr, but the pH had decreased to 7.65. The run was concluded after 94.4 hr, when the thorium concentration still remained low and the pH showed a further decrease to 7.40.

During the course of the run, the amount of iron, nickel, and chromium associated with the solid phase increased steadily. The concentrations of soluble thorium, iron, nickel, and chromium were less than 2 ppm.

Chemical analysis of the slurry material before the start of the pumping study showed it to contain 200 ppm of nitrate. At the end of 22 hr of operation, the suspended solids, representing about 40% of the original charge, were found to contain only 20 ppm of nitrate. After termination of the run, the bulk of the material was recovered and was found to contain more than 1400 ppm of nitrate.

Examination of the loop after dismantling disclosed some evidence of erosion. The impeller lost 1.5 g in weight, and the front and back bearings of the impeller shaft showed signs of wear. The orifice also showed signs of abrasive action but not nearly so severe as in run T-13, which was made with Ames ThO_2. Further, the formation of a tightly adherent deposit of ThO_2 during the run made the cleanup of the loop a difficult operation.

X-ray diffraction patterns of the oxide were obtained before and after it was heated in water for four days at 250°C and after it had been circulated in the loop. Both before and after heating in water at 250°C, the oxide exhibited the characteristic diffuse x-ray diffraction pattern associated with the oxides produced by low-temperature calcination. Upon the termination of the pumping study, however, the oxide was found to have a sharp diffraction pattern that was similar to the patterns obtained with the 900°C material, thus indicating that recrystallization had taken place.

Whether the above results are characteristic of the method of preparation of the 500°C oxide can be established only by a repetition of the loop experiment. It may be significant, however, that four days of heating of the oxide in water at 250°C prior to the loop experiment gave no evidence of particle growth or of recrystallization. The presence of a significant increase in the nitrate impurity found at the end of the run and the preferential concentration of nitrate in the material which failed to suspend suggest that the unfavorable results of particle growth, recrystallization, oxide deposition on the walls, and corrosion-erosion may be attributable in whole or in part to the nitrate impurity.

4. Under the conditions of the tests, a black oxide film formed on components of the system in low-velocity regions such as the thermal spacer of the pump, areas in the pump volute, and both

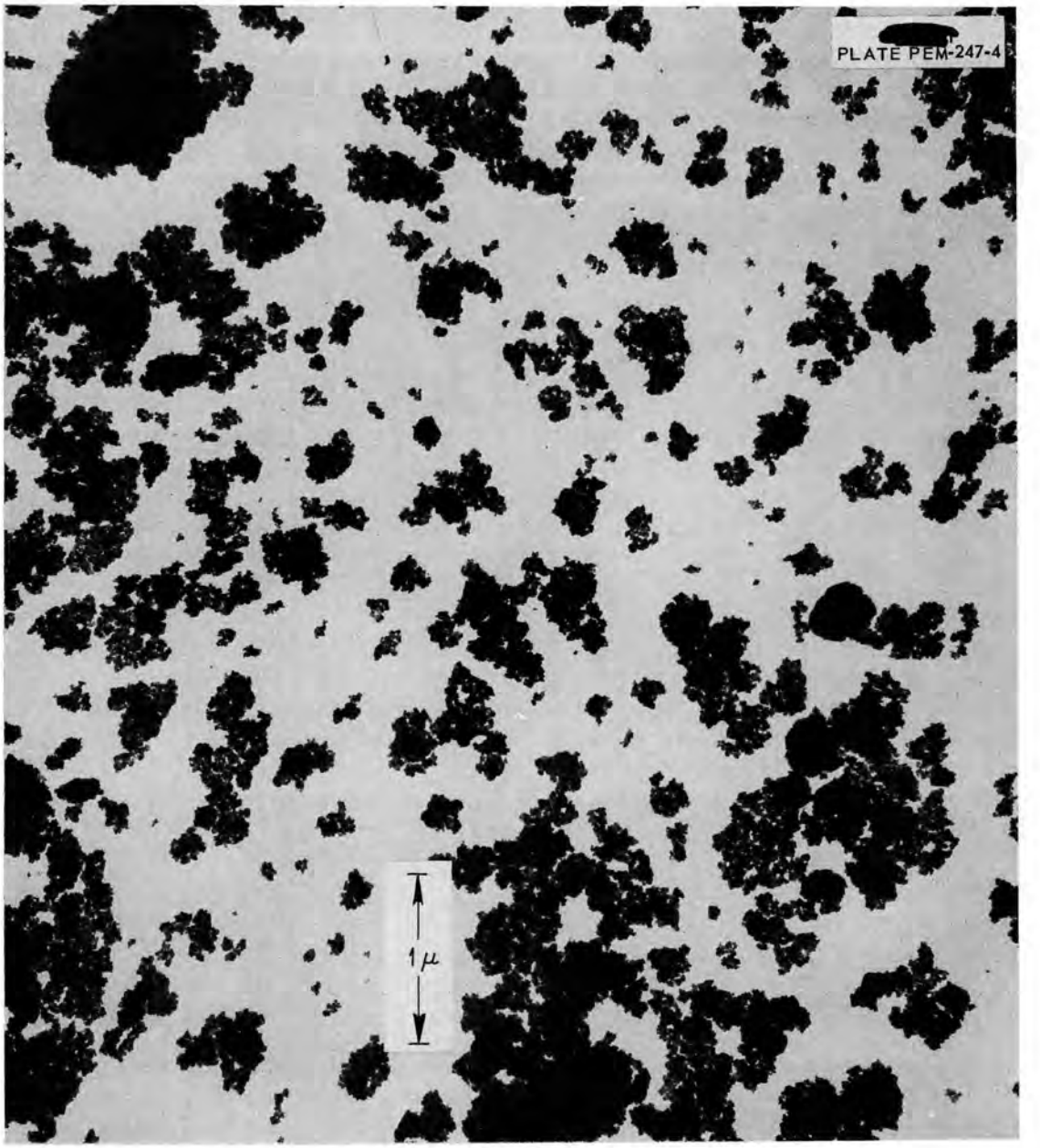

Fig. 78. Electron Micrograph of Ames ThO_2 Before Circulation.

upstream and downstream faces of the flow restrictor. This film did not form to an appreciable extent on the pipe walls. The nature of the film is still under investigation. Friable black flakes were found in the circulated material and may be the form in which most of the iron, nickel, and chromium occurs in the slurry.

5. From the limited data available, it is difficult to determine the effect that autoclaving at 250°C for four days has on the hardness of Ames oxide. The autoclaved material appears to be less abrasive than the regular Ames oxide. However, the data so far are too meager to permit a full analysis of the question.

6. Circulation of 1000 g of thorium per liter as Ames oxide gave no more difficulty than the lower concentrations, except that the diameter of the pump impeller had to be reduced to prevent over-

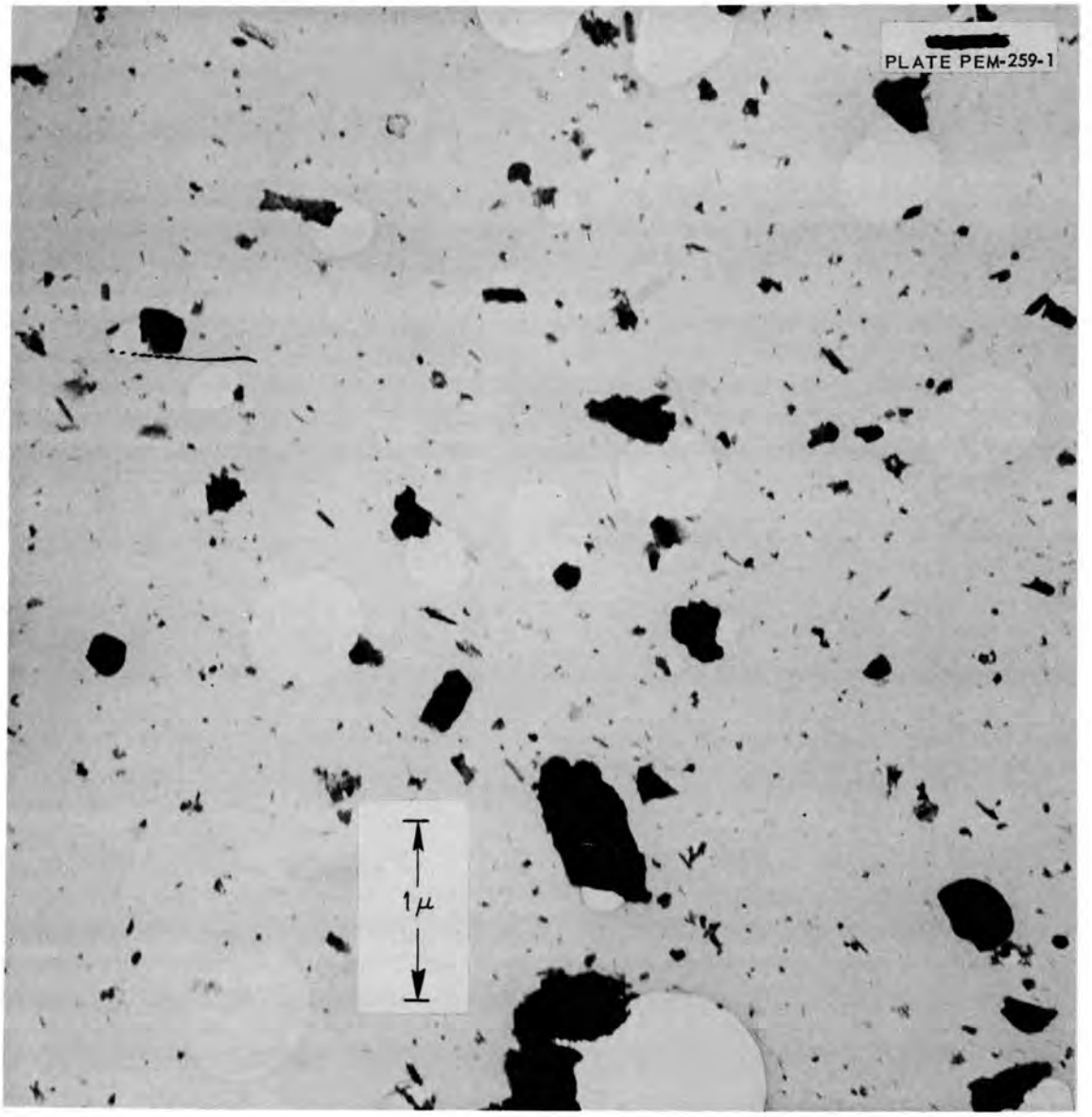

Fig. 79. Electron Micrograph of Ames ThO_2 After Circulation in T Loop for 140 hr at 250°C.

loading the pump motor. In addition, 1000 g/liter is approximately the settled density of Ames thorium oxide after autoclaving; hence the slurry is essentially nonsettling. It is still fluid enough to be easily pumped, but in some cases it may be impossible to obtain the desired higher concentrations by settling alone.

BOILING SLURRIES

In connection with studies of power removal from homogeneous boiling reactors, a recent report of the analysis of experimental work on power removal is somewhat discouraging.[7] Optimistic assumptions for pressure effects in a 10-ft-dia reactor with a 10-ft boiling height lead to only 3 or 4 kw/liter for allowable power densities. At present it is contemplated that power densities in a thorium blanket will go up to 8 kw/liter as the uranium content of the blanket builds up with

[7] R. V. Bailey, *Progress Report on Power Removal from Homogeneous Boiling Reactors*, ORNL CF-53-11-65 (Nov. 4, 1953).

time. The report suggests that the hope for homogeneous boiling reactors for power production (and thus for power removal from boiling slurries) centers on a controlled natural-circulation type with vapor separators to reduce recirculation entrainment. It is considered that the development of vapor separators is more difficult for slurries than for solutions.

FLUIDIZED SOLID BLANKET BED

During the past quarter, an investigation of the possibilities of a fluidized ThO_2 blanket has been initiated. Preliminary calculations were made in order to obtain a general picture of this type of blanket. The calculations included approximate particle sizes of pellets, densities of ThO_2, and porosities of the bed. A program[8] has been started to determine the characteristics of fluidized beds that would be met under blanket conditions.

The initial phase of the program will be concerned with obtaining working equations for predicting the effect of porosity, particle diameter, particle shape, etc. of fluidization velocity. A literature search is under way, and some experimental apparatus has been constructed.

A more detailed description of this program was presented in a memorandum[9] discussing the feasibility of a fluidized thorium oxide blanket.

Test of Thoria Pellets in Fluidized Bed

A fluidized thoria breeder blanket appears to be a promising alternate to slurries for reactor applications. The apparatus shown in Fig. 80 is being set up for studying attrition rates and abrasion of fluidized thoria, of various types, in metallic containers. Although the test will operate at room temperature, it is believed that the results will apply qualitatively to high-temperature operation. This test will be started during the next quarter.

[8] Joint effort of REED and the Engineering Research and Engineering Development Sections.

[9] P. R. Crowley and A. S. Kitzes, *Feasibility of a Fluidized Thorium Oxide Blanket*, ORNL CF-53-9-94 (Sept. 2, 1953).

UNCLASSIFIED
DWG. 22791

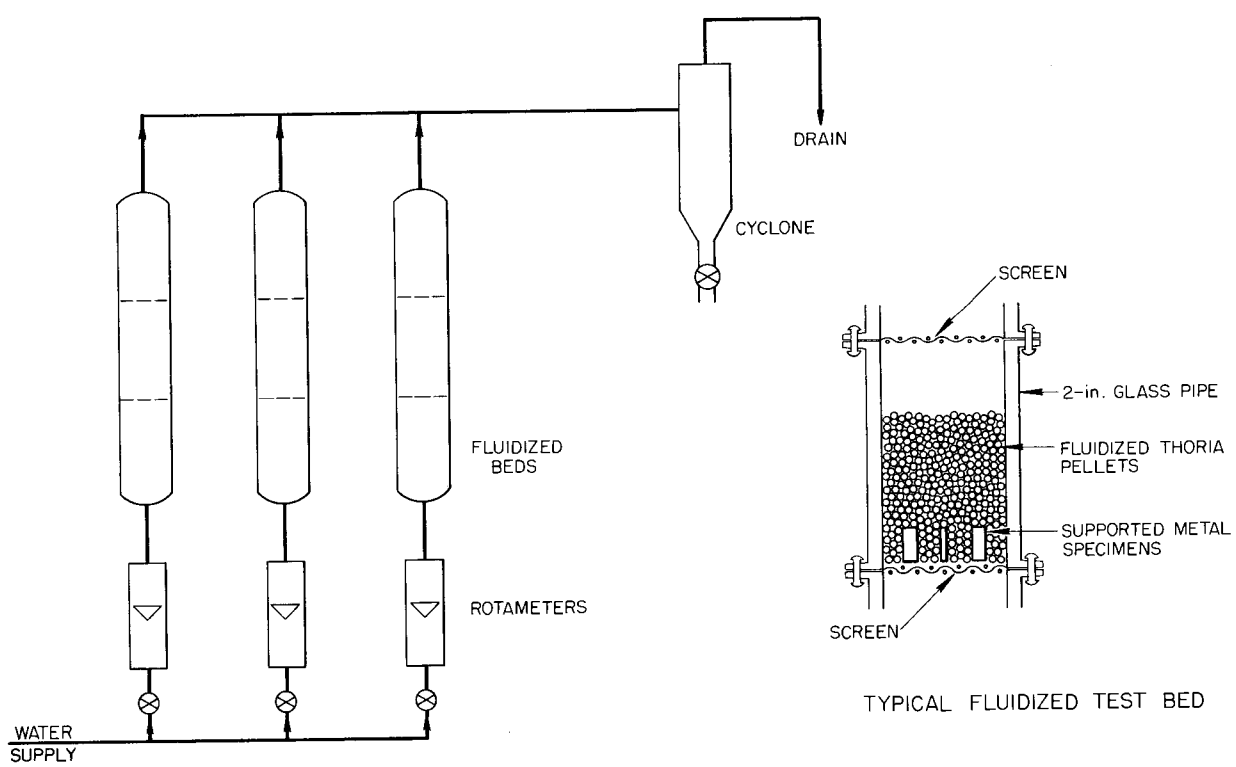

Fig. 80. Fluidized Bed Erosion Test.

THORIUM NITRATE SOLUTIONS

As discussed in the previous HRP quarterly report,[10] thorium nitrate appears to furnish the only possible material for a blanket solution operating at elevated temperatures. Characteristics of thorium nitrate solutions are discussed in the "Aqueous Solution and Radiation Chemistry" section of this report.

To round out investigation of this material, studies of the stability of thorium nitrate solutions under exposure to reactor radiation have been initiated during the quarter.

In any case, the probable high cost of separating and using N^{15} will discourage use of thorium nitrate except under circumstances that are otherwise extremely favorable to the solution.

PRESENT PROGRAM

Primary emphasis is being given to studies of circulating thorium oxide slurries. Currently, a three-phase program is under way that is directed toward developing softer slurries, more resistant materials of construction, and more favorable mechanical conditions.

The Chemical Technology Division, the Analytical Chemistry Division, and REED are cooperating on the development of softer thorium-bearing slurries. This work includes studies on the effect of the method of preparation of thorium oxide, methods of treating thorium oxide, and preparation of other thorium compounds.

A number of metals, which may be more resistant to abrasion than is stainless steel, are being tested. In this connection, the exact mechanism of metal removal is in some doubt – it is not clear whether the particles actually gouge out pieces of the base metal or whether they merely scrape off the protective oxide layer and expose the base metal to corrosive attack by the water and its dissolved oxygen. Microscopic examination of the orifice and impeller makes it appear that the gouging mechanism predominates, but appearance alone is not conclusive, and the presence of black flakes indicates that at least part of the abrasion products were at one time an oxide film. In order to test these materials, a composite orifice plate has been designed and fabricated. In this plate, a variety of metals can be arranged around the orifice opening so that their relative abrasion resistance can be determined in the 250°C circulating loops.

It may be unnecessary to have fast-moving components or high velocities in a thorium oxide slurry blanket. The third phase of the current program will consist of a determination of the abrasion experienced in slower systems and, in cooperation with the Design and Engineering Development Sections, the minimum velocities permissible in a practical reactor blanket system.

The program discussed above will furnish information, useful to the Design Group, concerning heat transfer, pressure drops, viscosity characteristics, etc. for slurries at various concentrations and temperatures.

Study of the effects of radiation upon thorium oxide systems is being initiated by the Radiation Chemistry Group of the Chemistry Division (small-scale tests in glass or silica ampoules) and by the Slurry Group of the Chemical Technology Division (small-scale tests in stainless steel bombs at elevated temperatures in which dash-pot stirring is used). Use will be made of irradiated slurries, formed in these studies, by the group interested in processing and repreparing slurries from hot, processed material.

Plans for in-pile dynamic tests will be based on the results of this preliminary radiation work, on the experience in pumping slurries at elevated temperatures, and on the experience of the group developing the in-pile loop for testing fuel solutions.

As noted above, the programs under way are being directed toward evaluation of boiling slurries, fluidized solid bed blankets, and thorium nitrate solutions.

[10] P. A. Agron *et al.*, *HRP Quar. Prog. Rep. July 31, 1953*, ORNL-1605, p. 128.

PHYSICAL STUDIES OF URANIUM SLURRIES

R. N. Lyon, Section Chief
A. S. Kitzes R. B. Gallaher
P. R. Crowley W. Q. Hullings
C. A. Gifford

Two methods have been found for reducing the caking tendency of $UO_3 \cdot H_2O$ slurries in circulation systems at 250°C. One method involves a modification of the circulating system itself, while the other involves the addition of $(UO_2)_3(PO_4)_2$ to the slurry.

In order to determine the types of circulating systems in which $UO_3 \cdot H_2O$ would not cake out, T loop was altered several times. In the past, the caking has been found in those parts of the system where linear flow did not predominate – for example, when a vortex is permitted to develop in the pressurizer (see Fig. 81), this vortex continues in the loop piping back to the pump and caking occurs throughout this part of the system. When vertical baffles are provided in the pressurizer to prevent formation of a vortex, caking does not occur in the main circulating system but does occur in the pressurizer itself just above the flow inlet.

The best system found so far is shown in Fig. 82. In this system, the pressurizer is not an integral part of the loop. It is isolated and connected to the circulating stream only by means of a trap and an S-shaped stainless steel tube to minimize formation of a vortex. Originally, the trap was omitted from the system, but it was added when the results of chemical analyses showed that solids were being lost from the circulating system.

To prevent accumulation of solids in the trap and plugging of the line to the trap, about 15 gpm of slurry is circulated to the trap and back to the loop. The stream enters and leaves from the

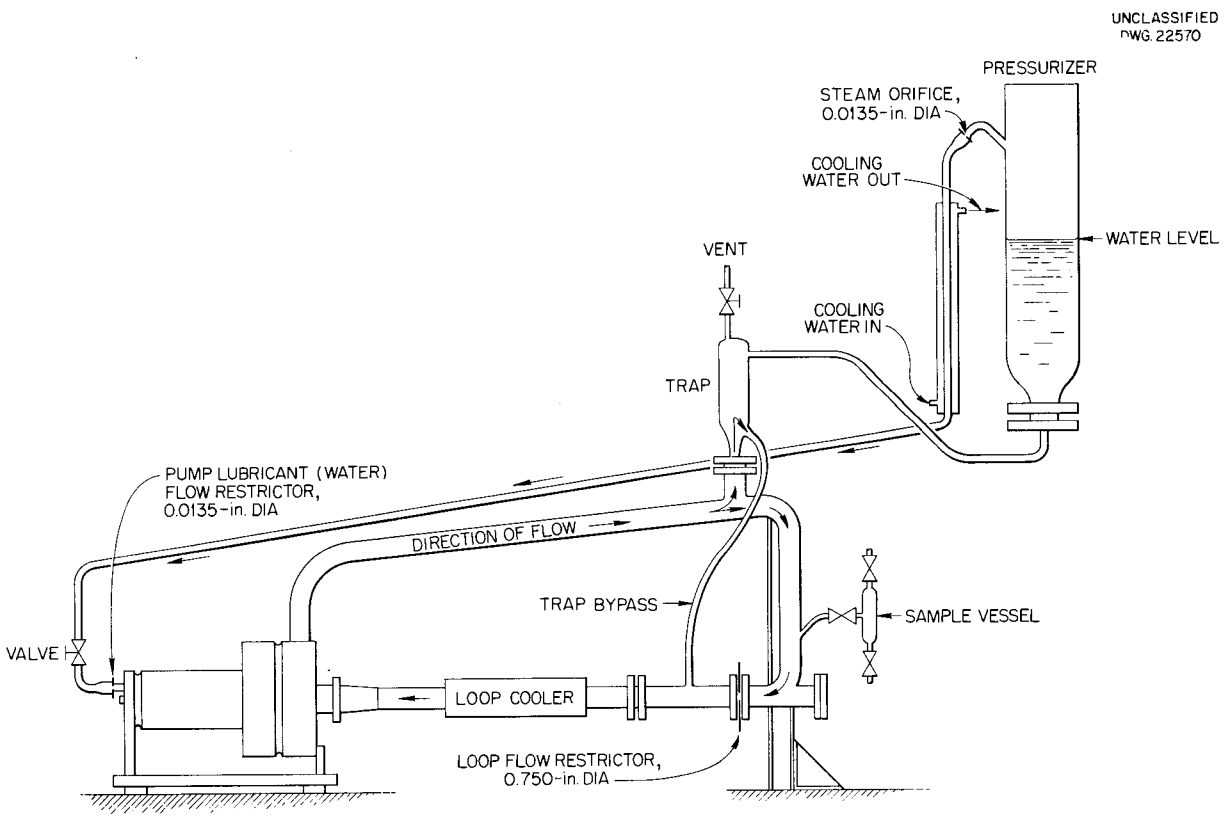

Fig. 81. Schematic Flow Sheet for T Loop.

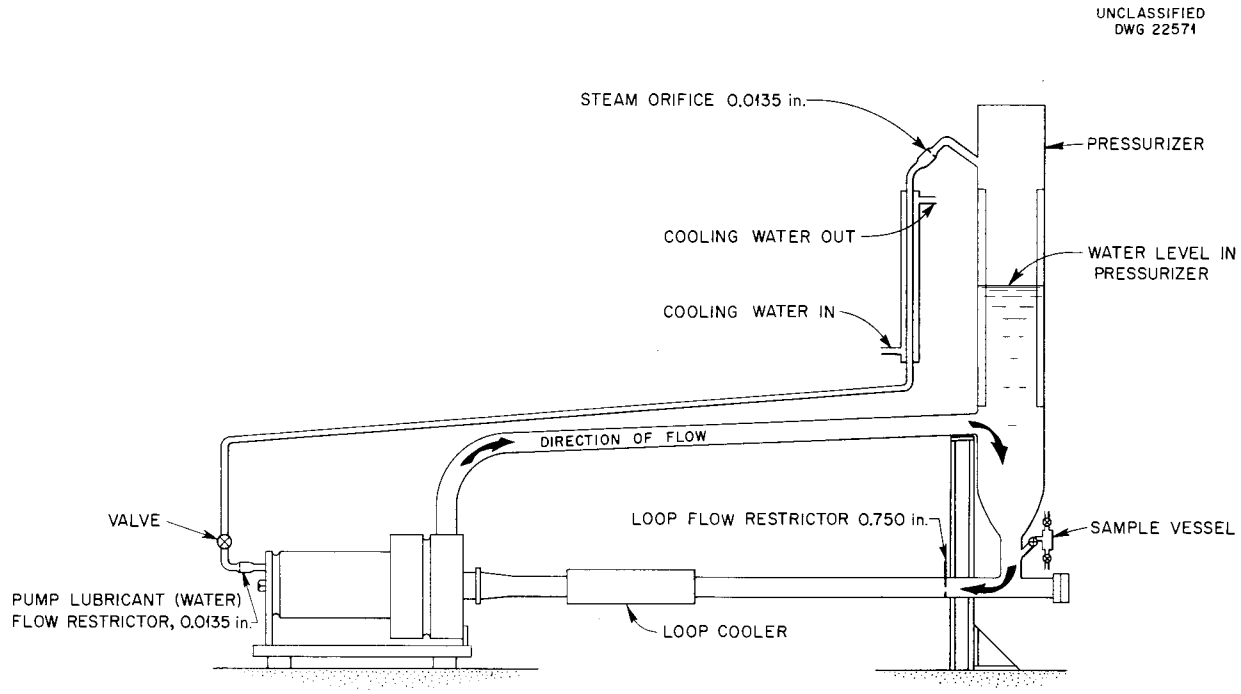

Fig. 82. Schematic Flow Sheet for S Loop.

bottom of the trap to allow the solids to settle out of the upper part of the trap where the pressurizer is connected. Since the trap has the same diameter as the pressurizer, it appears probable that merely passing a small flow through the bottom of the pressurizer may accomplish the same purpose. This possibility will be tested.

There is a net vertical flow of about 1 liter/hr in the trap and pressurizer as a result of the removal of steam from the top of the pressurizer. The steam is condensed and fed into the back of the pump to keep the motor and bearings flushed free of solids. The flow of 1 liter/hr corresponds to an average velocity of about 2 mm/min in the 4-in.-dia trap and pressurizer. This can be compared with the hindered settling rate of about 5 mm/min for the slurry.

The results of a typical test are shown in Table 42. In studying these data it is well to bear in mind that the volume of the entire circulating system is only 5 liters, and hence the entire solids charge was only about 1 kg. The initial concentration was somewhat above the 200 g/liter, probably because the solids had not become well mixed.

Within the first 100 hr, the concentration dropped to 100 g/liter and stayed there, with some variation, for the next 240 hours. The pH of the slurry remained constant except for two samples for which the value increased to 6.30. Soluble uranium content for these two samples was about 10 ppm, compared with an average value of 75 ppm for the other samples. There was no evidence of erosion or corrosion; the iron, nickel, and chromium contents of the solids remained unchanged.

Inspection of the pump casing, impeller, and loop walls again showed no evidence of erosion. The pump impeller did not change in weight as compared with its weight when originally installed.

Although solids were lost from the circulation portion of the loop, there was no accumulation of solids in the pressurizer or trap. There was no evidence of caking of solids on the pipe walls; however, there was an apparent crystal growth indicated by the gradual darkening of the crystals to an orange-yellow color.

The assumption of crystal growth and subsequent settling out of the solids would account for the decrease in solids concentration. A comparison of the concentration values as determined by chemical analysis of samples drawn periodically from the loop with those estimated from the pump requirements to circulate the slurry at a rate of 125 gpm shows that the desired concentration was not being

TABLE 42. CIRCULATION OF $UO_3 \cdot H_2O$ SLURRY CONTAINING 250 g OF URANIUM PER LITER AT 250°C BY USING A WESTINGHOUSE 100A PUMP WITH A STANDARD IMPELLER: CHEMICAL ANALYSES AND POWER REQUIREMENTS

SAMPLE NUMBER	CIRCULATION TIME (hr)	SOLIDS					LIQUID			PUMP REQUIREMENTS		TOTAL URANIUM CONCENTRATION IN LOOP AS ESTIMATED FROM PUMP INPUT CURRENT (g/l)
		Total U (g/l)	U(IV) (ppm)	Fe (ppm)	Ni (ppm)	Cr (ppm)	pH	Total U (ppm)	NO_3 (ppm)	(kw)	(amp)	
T-12-0	0.7	235	25	26	3	5	5.50	160	14	15	60	258
T-12-1	17.5	198	25	28	3	3	5.55	47	4	14.4	58	195
T-12-2	108.5	92	25	36	9	6	5.55	75		13.0	55	73
T-12-3	153.8	114	30	37		3	6.30	14		13.5	57	115
T-12-4	275.0	160	0	65	4	9	5.60	75		14.1	58	161
T-12-5	341.0	104	0	50	1	6	6.35	9		13.1	55	73

pumped. To check the possibility that the solids are settling out of the stream and to determine the cause, it is planned to survey the loop periodically with a G-M tube at fixed points around the loop. At present, a portable scintillation-counter type of survey meter is used to check the homogeneity of the circulating stream.

ALTERNATIVE URANIUM SLURRIES

Because of the difficulty encountered in maintaining the concentrations of $UO_3 \cdot H_2O$ slurries during circulation at 250°C, other uranium compounds such as uranyl phosphate are being tested. Normal uranyl phosphate slurries are of interest because they are nonabrasive, non- or only mildly corrosive, and have acceptable neutron economy. In addition, the normal phosphate acts as a deflocculating agent for dispersing UO_3 in water. This is consistent with the fact that phosphates in general are efficient deflocculating and dispersing agents. During this quarter, a number of uranyl phosphate slurries have been circulated in loop S. The phosphate was prepared according to the procedure described by Ryon and Kuhn.[1]

URANYL PHOSPHATE, $(UO_2)_3(PO_4)_2 \cdot 4H_2O$

In the last quarterly report,[2] it was reported that uranyl phosphate slurry was circulated in loop S at 250°C for 140 hours. During the course of the run, the concentration varied somewhat. The concentration remained at 100 g of uranium per liter for the first 74 hr of operation and then dropped to an average concentration of 61 g/liter and remained constant to within ±10% for the remainder of the run. The drop in concentration from 100 to 61 g/liter was accounted for by assuming that solids had accumulated in the various stagnant areas of the loop.

Because of the promising results obtained with uranyl phosphate slurries, duplicate runs were made as follows in loop S:

Run No. 36 – Uranyl phosphate; no condensate flow through the back of the pump.

Run No. 38 – A mixture of uranyl phosphate and $UO_3 \cdot H_2O$ in the ratio of 2 parts of phosphate to 1 part of oxide-water; condensate flow through back of pump.

Run No. 39 – A mixture of 10% by weight of uranyl phosphate and 90% by weight of $UO_3 \cdot H_2O$; condensate flow through back of pump.

Data for these runs are tabulated in Table 43.

[1] A. D. Ryon and D. W. Kuhn, *Solubility of Uranyl Ammonium Phosphate in Nitric Acid and Ammonium Nitrate Solutions as a Function of Temperature*, Y-315 (Jan. 10, 1948).

[2] A. S. Kitzes *et al.*, *HRP Quar. Prog. Rep. July 31, 1953*, ORNL-1605, p. 147-154.

TABLE 43. CIRCULATION OF URANYL PHOSPHATE AND URANYL PHOSPHATE–URANIUM OXIDE SLURRIES AT 250°C BY USING A WESTINGHOUSE 100A PUMP WITH A STANDARD IMPELLER: CHEMICAL ANALYSES AND PUMP REQUIREMENTS

SAMPLE NUMBER*	CIRCULATION TIME (hr)	SOLIDS						LIQUID				PUMP REQUIREMENTS	ESTIMATED CONCENTRATION FROM PUMP REQUIREMENTS (g/l)
		Total U (g/l)	U(IV) (ppm)	PO_4 (g/l)	Fe (ppm)	Ni (ppm)	Cr (ppm)	pH	U (ppm)	PO_4 (ppm)	NO_3 (ppm)	(amp)	
S-36-0	1	168	320	43	11	2	2	3.2	3	34	4	56	166
S-36-1	19	108	340	28	35	4	4	3.1	12	49	6	56.5	193
S-36-2	138	75	220	20	89	4	4	3.8	20	17		56.6	198
S-36-3	186	76	350	20	136	16	6	3.2	20	29		56.0	183
S-36-4	399	100	220	26	78	18	8	3.7	10	<1		55.0	149
S-38-0	2	198	390	36	90	90	11	5.6	2	1	14	58	228
S-38-1	27	146	420	27	84	145	13	4.2	9	3		59	262
S-38-2	171	112	500	22	88	23	13	5.4	6	<1		58	253
S-38-3	312	129	1900	24.5	120	81	19	5.6	5	<1		58	243
S-38-4	433	120	620	22	125	113	28	5.5	4	4		58	243
S-39-0	2.5	365	4	12.5	117	53	13	5.1	103	<1	5		
S-39-1	21.6	344	23	11.9	143	44	11	7.8	31	<1			
S-39-2	43.1	267	40	10.8	187	53	11	5.0	32	<1			
S-39-3	97.4	224	8	7.8	136	50	9	6.0	24	<1			
S-39-4	149.2	163		5.5	46	2	1	6.1	67	<1			
S-39-5	170	157	15	5.1	29	10	1	6.0	59	<1			
S-39-7	257	139	12	4.9	17	5	9	7.3	<1	<1			
S-39-8	327	120	<30	3.87	46	15	7	5.1	165	<1			
S-39-10**	577	144		8.74	60	9.5	12	5.95	22	<1			

*Run S-36 – 100 g of uranium per liter as uranyl phosphate.
Run S-38 – 150 g of uranium per liter as a mixture of 2 parts uranyl phosphate and 1 part $UO_3 \cdot H_2O$.
Run S-39 – Mixture of 10 wt% of uranyl phosphate and 90 wt% of $UO_3 \cdot H_2O$.

**Run still in progress as of 10/23/53; accumulated time. 800 hours.

DISCUSSION OF RUN S-36

A slurry containing 100 g of uranium (as the phosphate) per liter was circulated in loop S at 250°C for 424 hr with no flow of water through the back of the pump to lubricate the Graphitar bearings (Fig. 82). The run was stopped because of difficulties with the cooling oil pump, which necessitated shutting down the loop. It was impossible to restart the pump, and upon examination, it was found that the slurry had settled in both the front and back bearings and had caused the pump to freeze.

Inspection of the pump casing, the impeller, and the pipe walls showed no evidence of erosion, although the visible oxide film on these parts had been removed. The removal of the film probably accounts for the increase in the iron, nickel, and chromium contents of the solids. The pump impeller lost 2 g in weight as compared with its weight when originally installed.

The pump required more current than would ordinarily be predicted from the density of the slurry. From this fact it is concluded that uranyl phosphate slurries are more viscous than are the oxide slurries and cause higher drag on the outside of the impeller.

DISCUSSION OF RUN S-38

Run S-38 was similar to Run 36, except that the slurry initially contained 150 g of uranium per liter as 2 parts of uranyl phosphate to 1 part of uranium oxide monohydrate. The slurry was circulated in loop S for 532 hr with water flow through the back of

the pump for 170 hr before both jets became plugged with solids and the flow was cut off. For the remainder of the run, the bearings were not lubricated with water. The run was stopped because the stator windings of the Westinghouse Model 100A pump shorted out. The pump failure is not attributed to the fact that slurry was being pumped.

Again there was no evidence of erosion by visual inspection of the various loop components. The pump impeller did not change weight and was shiny. The iron, nickel, and chromium contents of the solids did not change appreciably. The uranium and phosphate content of the supernate was below 10 ppm during the entire course of the run. Apparently, the oxide was preventing hydrolysis of the phosphate. The pH of this slurry averaged 5.5 as compared with the pH of 3.1 to 3.8 for a slurry of pure uranyl phosphate. The phosphate, on the other hand, prevented the dissolution of the UO_3 in water and also greatly reduced the caking of the oxide on the system walls.

Again in this run, more current was drawn by the pump motor than would be predicted from the density of the slurry.

DISCUSSION OF RUN S-39

Run S-39 is still in progress in loop S after 800 hr of accumulated circulation time, and apparently the concentration is being maintained. During the first 100 hr of operation, it was necessary to withdraw 4 liters of the slurry and to substitute water to prevent the pump from being overloaded. No withdrawals of slurry except for sampling were made after the concentration reached 150 g of uranium per liter. The loop was operated at this concentration for 480 hr; in order to decrease the soluble uranium content of the filtrate, the phosphate content was then increased by the addition of 300 g of $(UO_2)_3(PO_4)_2 \cdot 4H_2O$. After an additional 170 hr of operation, 300 g of uranyl phosphate was again added to further reduce the soluble uranium content.

The Graphitar bearings are continually being flushed with water by condensing steam from the pressurizer. There is no indication of wear on the bearings.

The run will be terminated after 1000 hr of accumulated circulation time. The various possible wear points such as pump parts, flow restrictor, elbows, etc. will then be visually inspected for abrasion. X-ray diffraction and electron-microscope studies will be made to determine any crystal changes or any change in the average particle size.

CHEMICAL PROCESSING

D. E. Ferguson, Assistant Section Chief
W. B. Howerton A. M. Rom
R. A. McNees O. K. Tallent
W. E. Tomlin

CALCIUM FLUORIDE PROCESSING FOR TWO-REGION BREEDER REACTOR

An adsorption process capable of continuously removing rare-earth fission products from the fuel solution of a two-region, aqueous homogeneous thermal breeder reactor will reduce the amount of fuel that must be completely reprocessed by a factor of 5 to 10. Such a process must be capable of operating with a cooling period of less than one day, must not add impurities to the fuel solution which will interfere with reactor operation, and must not remove a significant amount of uranium from the fuel solution.

Of the inorganic adsorbents tested to date, calcium fluoride appears to be the most attractive for removing the rare earths from a dilute heavy-water solution of uranyl sulfate. One gram of calcium fluoride is capable of removing 90% of the rare earths from at least 0.8 liter of fuel solution. However, in a packed bed, the process probably would not be run to the point of completely exhausting the calcium fluoride, and a working capacity of 0.5 liter of solution per gram of calcium fluoride seems to be reasonable. This is the basis of the schematic chemical flowsheet given in Fig. 83.

In passing through a calcium fluoride bed at 100°C, the fuel solution picks up about 400 ppm of fluoride and 300 ppm of calcium. The calcium, if precipitated inside the reactor as calcium sulfate, would be detrimental to heat-transfer surfaces, and the fluoride might accelerate corrosion of the zirconium core tank. Therefore, provisions are made in the proposed process for reducing the fluoride concentration by adding soluble $Th(SO_4)_2$ to precipitate ThF_4 and by removing the calcium as calcium sulfate in a column packed with solid calcium sulfate and operated at 270 to 300°C.

Capacity of Calcium Fluoride

When used as an adsorbent for rare-earth fission products, calcium fluoride acts as a fluoride source which supplies a controlled amount of fluoride to the solution passing through the bed. At 100°C,

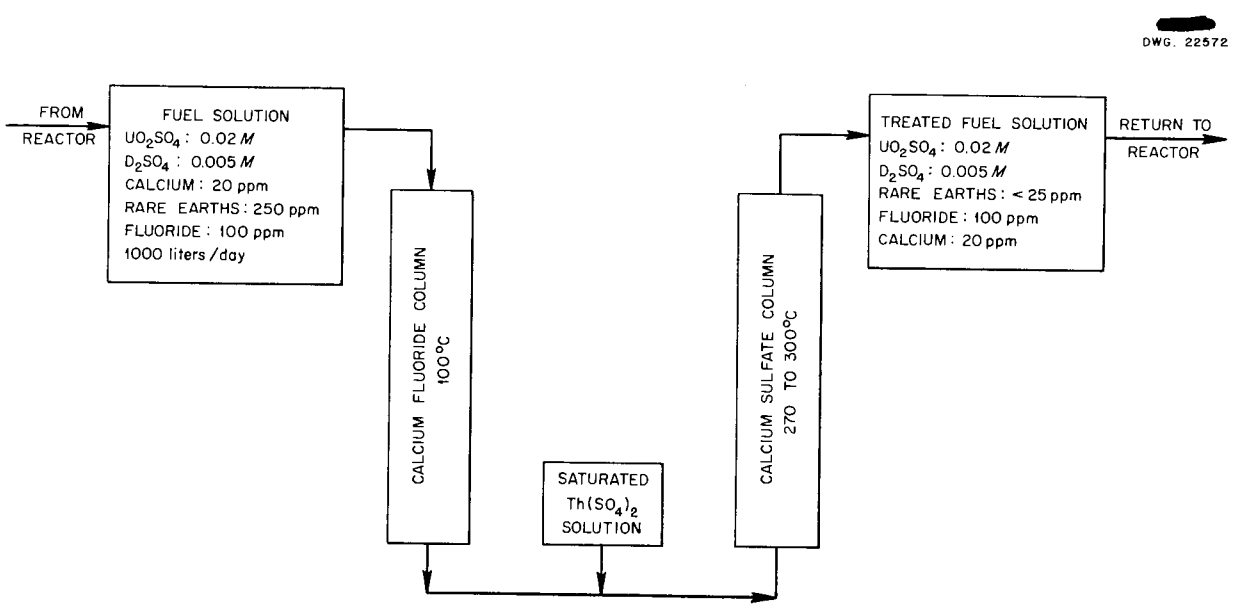

Fig. 83. CaF_2 Adsorption Process. Basis: 320-megawatt reactor core operating at 250°C.

a fluoride concentration of 250 to 300 ppm is required to precipitate 90% of the rare earths from 0.02 M UO_2SO_4–0.005 M H_2SO_4 solution. At equilibrium, the calcium fluoride maintains a concentration of 400 ppm of fluoride in solution which precipitates rare-earth fluorides back on the solid CaF_2.

It was found that a column 9 cm long and packed with 15 g of granular CaF_2 removed more than 90% of the rare earths from 12 liters of simulated fuel solution (0.02 M UO_2SO_4–0.005 M H_2SO_4) which originally contained 0.25 g of mixed rare earths per liter. The bed removed 70% of the rare earths from the thirteenth liter, and the removal of rare earths dropped to zero on the sixteenth liter of solution (see Fig. 84). At this point, the bed was exhausted of CaF_2 and contained only about one-third of its original volume of solids. The solids were rare-earth fluorides and $CaSO_4$. Based on this result, 1 g of CaF_2 will process 0.8 liter of fuel for more than 90% removal of rare-earth fission products. However, in an actual process, 1 g of CaF_2 for 0.5 liter of solution seems to be a good working capacity.

The amount of uranium held up on the calcium fluoride column after one water wash amounted to less than 10^{-4}% of the 80 g of uranium processed by the column.

Control of $CaSO_4$ Concentration

The solubility of calcium, as $CaSO_4$, in 0.02 M UO_2SO_4–0.005 M H_2SO_4 at 100°C is 375 ppm (see Fig. 85). This is approximately the concentration of calcium that is observed in the effluent from a calcium fluoride column operating at 100°C.

Until recently, the maximum design temperature in the reactor fuel system was 250°C. At this temperature the solubility of calcium in the fuel solution is only 30 ppm. Therefore, if the effluent

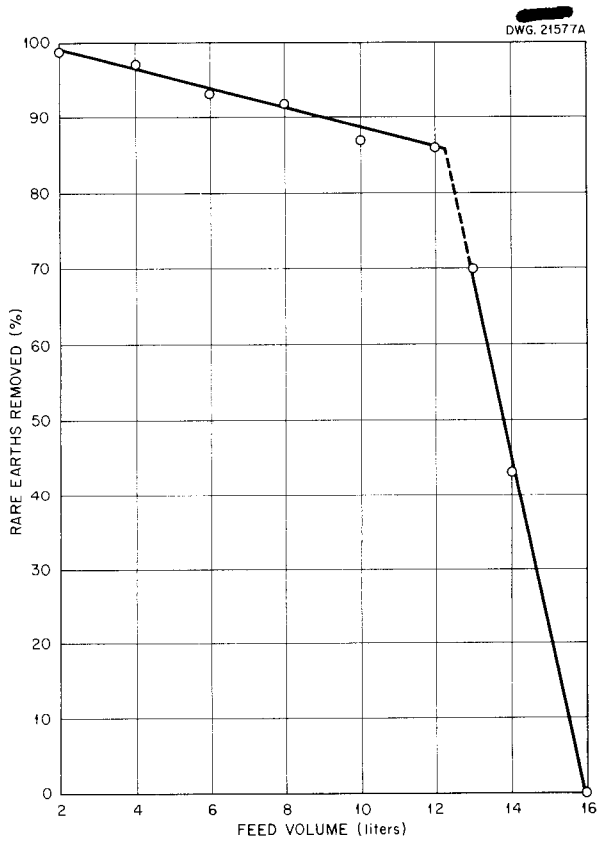

Fig. 84. Adsorption of Rare Earths by CaF_2. Feed: 0.02 M UO_2SO_4, 0.005 M H_2SO_4, and 0.25 g/l of rare earths. CaF_2 bed: 10 × 0.5 cm – 15 g of CaF_2. Temperature: 97°C.

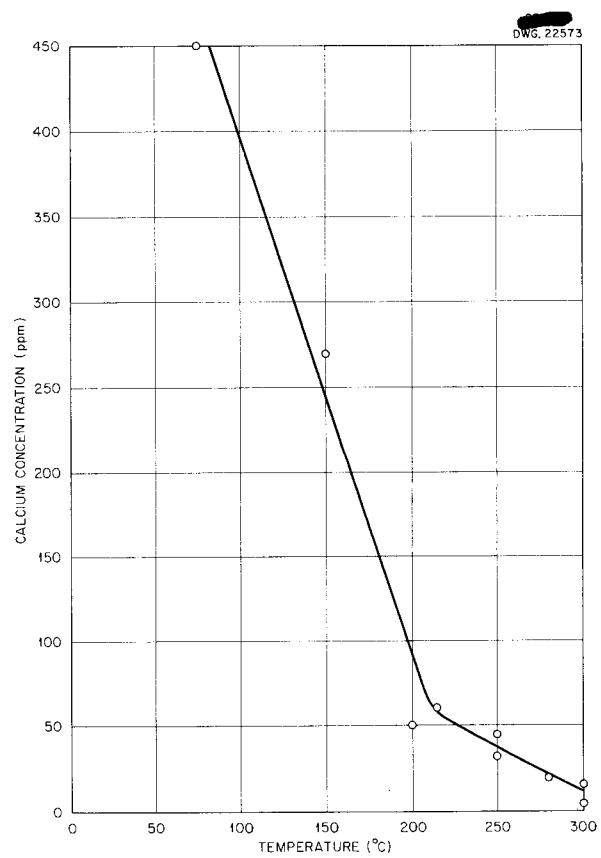

Fig. 85. Solubility of $CaSO_4$ in 0.02 M UO_2SO_4–0.005 M H_2SO_4 Solution.

from a calcium fluoride bed was returned directly to the reactor, precipitation of calcium sulfate would occur inside the reactor. This can be avoided by passing the effluent from the CaF_2 column through a column packed with granules of $CaSO_4$ and at a temperature above the maximum reactor temperature. Vitro Corporation was able to reduce the calcium concentration in CaF_2-treated fuel solution to 20 ppm in this way by operating the $CaSO_4$ column at 270°C.

The operating temperature of the reactor has now been raised to 300°C, and the $CaSO_4$ column temperature must be raised accordingly.

Removal of Fluoride from Calcium Fluoride-Treated Uranyl Sulfate Solutions

The fluoride present in the effluent from a calcium fluoride bed may exist in at least three forms: fluoride ions, molecular hydrofluoric acid, and uranyl fluoride complexes. Based on available mass-action data, it is estimated that in an effluent containing 300 ppm total fluoride, at room temperature, only 1 ppm would exist as fluoride ion. Hydrofluoric acid accounts for about 15 ppm, with the remainder of the fluoride being tied up as very stable uranyl fluoride complexes. The corrosion rate of zirconium by such a solution is not known; so it has been assumed that the residual fluoride concentration must be minimized before the solution is returned to the reactor. In order to remove such a tightly complexed fluoride, reagents capable of forming either very insoluble fluoride precipitates or more stable complexes which can be removed from solution must be used.

The most promising reagents tried so far are thorium dioxide and silica. Analytical difficulties prevent an accurate evaluation of these reagents at this time, but in one test with thorium dioxide about 50% of the fluoride was removed from a solution originally containing 450 ppm of fluoride per liter. Silica gel removed some fluoride from solution and seemed to be more effective at low temperatures than at 100°C. Zirconium dioxide was ineffective at room temperature and at 100°C.

Process Equipment Design

Preliminary design studies are being made to assist in the development of an adsorption process for continuously removing fission products from the fuel solution of a two-region breeder reactor. Although based on the CaF_2 process, these studies will apply equally well to any adsorption type of process used for homogeneous reactor processing. The preliminary design of an adsorption unit is primarily concerned with the following considerations:

1. removing heat, due to fission product decay, from the adsorption unit,
2. removing the used adsorbent from the unit,
3. minimizing losses of D_2O and U^{233} during adsorbent change.

It is expected that this study will result in a better determination of the large-scale feasibility of an adsorption process and will provide data for economic comparison with other methods of processing.

The design efforts are based on a unit capable of processing fuel from a 320-megawatt power breeder reactor, with a core volume of 3200 liters and a total reactor fuel volume of 19,000 liters containing 28 kg of U^{233}. In these preliminary studies the following assumptions have been made: average chemical cycle, 20 days; average cooling time, 12 hr; maximum reactor poison fraction, 5%.

Using the above assumptions and the equations in a memorandum by Ferguson and Sanders,[1] the most economical processing rate for core solution through the CaF_2 process was determined to be 878 liters/day. Assuming that 90% of the fission products is absorbed on the CaF_2, 630 g of CaF_2 would be consumed, and 475 g of insoluble fission product fluorides would be formed per day. Heat generation estimates of the fission products so absorbed indicate that about 40,000 Btu/hr would be liberated after one day of operation.

Several types of adsorption units are now being studied, and one or more will be built for unit-operation evaluation. Features which are desired in such a unit include complete recovery of D_2O from adsorbent, simplicity, a minimum of maintenance, and a minimum of operational attention. The following types of design units are now being studied:

1. package CaF_2 units which may be removed by remote disconnects,
2. CaF_2 beds which may be removed by gravity flushing, by backwashing into a receiver tank, or by dissolving the bed by H_2SO_4,

[1] D. E. Ferguson and J. P. Sanders, *Economics of Chemical Processing for a Uranium-233 Breeder*, ORNL CF-53-6-173 (June 18, 1953).

3. a circulating-type bed.

At this point in the study, the second type of installation appears to be the most attractive.

SUMMARY OF CHEMICAL PROCESS DEVELOPMENT BY THE VITRO CORPORATION OF AMERICA[2]

Natural garnet was found to be a specific adsorbent for cerium and does not remove a significant quantity of other rare-earth fission products from dilute uranyl sulfate solution. Calcium fluoride removes both Y^{91}-tagged rare earths or Ce^{144}-tagged cerium.

Batch tests have shown that the optimum temperature for CaF_2 adsorption of rare earths is about 100°C. Above 100°C, more fluoride goes into solution than is necessary to remove the rare earths, and at lower temperatures the efficiency of rare-earth removal drops off.

In a batch test at 100°C, calcium fluoride-impregnated Alundum pellets removed 98% of the rare earths from simulated fuel solution; however, column tests with this material were not successful.

The calcium concentration of the effluent from a CaF_2 adsorption column was reduced to 20 ppm by heating to 270 to 300°C and contacting with solid calcium sulfate to precipitate calcium sulfate. The fluoride concentration was reduced to 90 ppm by adding a 10% excess of soluble thorium nitrate to precipitate the thorium tetrafluoride.

Other adsorbents tested included titanite, which removed most of either cerium- or yttrium-tagged rare earths from solution at 250°C but also removed an unspecified amount of uranium. Additional tests are necessary to determine whether the uranium removal is due to impurities in the titanite mineral. Magnesium fluoride at 100°C did not remove yttrium-tagged rare earths from a uranyl sulfate solution.

Batch precipitation tests were made by adding potassium fluoride to cerous sulfate, mixed rare-earth sulfates, and yttrium sulfate solutions at room temperature. In order to get complete precipitation of the cations, the largest excess of fluoride was needed for the yttrium solution, while the cerium solution required the smallest excess.

---

[2] *HR Fuel Reprocessing Quar. Prog. Rep. July 1 to Sept. 30, 1953*, KLX-1704.